2025

The role of Fbxo42 in Ataxin-2-mediated regulation of Xbp1 signalling

Cristiana C. Santos

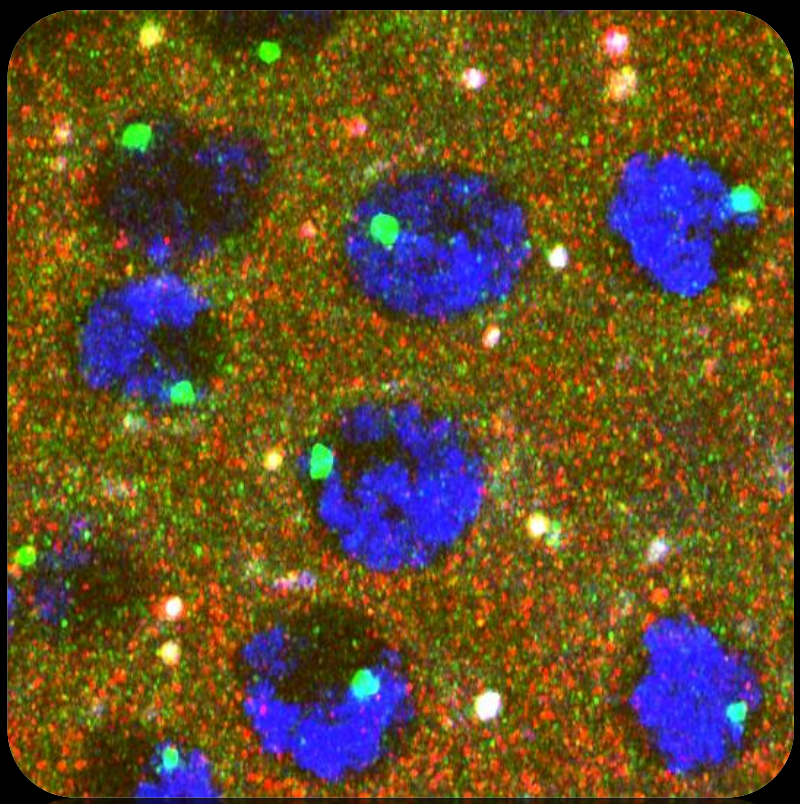

Dissertation presented to obtain the

Ph.D degree in Molecular Biosciences

Speciality Biochemistry

Oeiras, June, 2025

INSTITUTO DE TECNOLOGIA QUÍMICA E BIOLÓGICA ANTÓNIO XAVIER | UNIVERSIDADE NOVA DE LISBOA

ITQB NOVA, Avenida da República, 2780-157 Oeiras, Portugal | Tel +351 214 469 100 | itqb.unl.pt

The role of Fbxo42 in Ataxin-2-mediated regulation of Xbp1 signalling

Cristiana C. Santos

Dissertation presented to obtain the PhD degree in Molecular Biosciences

Instituto de Tecnologia Química e Biológica António Xavier | Universidade Nova de Lisboa

Oeiras, June, 2025

Research was coordinated by:

Cover figure: Image obtained by confocal microscopy of ring gland cells of *Drosophila melanogaster* third instar larva. Co-localization between Ataxin-2 protein (in red) and Xbp1 mRNA (in green).

Immunofluorescence and RNA FISH of ring gland cells, treated with 5 mM DTT for 4 hours. Endogenous Ataxin-2 is marked by anti-Ataxin-2 (red), Xbp1 mRNA is detected using Stellaris FISH probes against Xbp1, labelled with Quasar 670 dye (green), and DAPI marks the nuclei (blue).

Table of Contents

Declaration i
Declaração ii
Summary iii
Sumário vi
Acknowledgments ix
List of publications x
List of abbreviations xi
CHAPTER I:General Introduction 1
1.1 The endoplasmic reticulum 2
Protein synthesis and folding in the ER 3
1.2 ER-associated degradation (ERAD) 7
1.3 ER stress and UPR 9
IRE1 signalling 11
PERK signalling 12
ATF6 signalling 13
1.4 Chronic ER stress and Apoptosis 14
1.5 Ubiquitylation 18
Types of substrate ubiquitylation 22
Deubiquitylases (DUBs) 25
Proteasome 26
E3 ubiquitin ligases 28
F-box proteins 30
The Fbxo42 protein 31
1.6 Ataxin-2 34
Molecular domains of Ataxin-2 34
Molecular functions of Ataxin-2 36

Expression of the Ataxin-2 protein 43

1.7 The Drosophila eye 43

1.8 The GAL4/UAS system 48

1.9 The Flippase/FRT system 50

1.10 Scope of this thesis 52

1.11 References 53

CHAPTER II:Fbxo42 mediates the ubiquitylation of the RNA-binding protein Ataxin-2 in adult fly eyes and in *Drosophila* S2 cells .68

2.1 Abstract 69

2.2 Introduction 70

2.3 Methods 73

2.4 Results 91

Overexpression of the Xbp1s in the *Drosophila* adult eye induces the “glossy” eye phenotype 91

Loss-of-function mutations in *Fbxo42* suppress the “glossy” eye phenotype induced by Xbp1s 95

Rescue of the mosaic suppression of the Xbp1s-induced “glossy” eye phenotype by Fbxo42 constructs 100

Production of a polyclonal antibody against Fbxo42 104

Fbxo42 expression levels in different fly tissues 110

Fbxo42 protein co-immunoprecipitates with SkpA 111

Identification of the Fbxo42 protein binders by using Mass Spectrometry in HEK cell extracts 112

Identification of the Fbxo42 substrates using the ^{bio}Ub approach 120

Ataxin-2 RNAi abrogates the suppression of the “glossy” eye phenotype (Xbp1s-induced) caused by *Fbxo42* mutations 129

2.5 Discussion 130

2.6 Acknowledgments 134
2.7 References 134
CHAPTER III: Fbxo42 promotes the proteasomal degradation of Ataxin-2 139
3.1 Abstract 140
3.2 Introduction 141
Drosophila ring gland 141
Drosophila ovary 142
3.4 Results 151
Fbxo42 co-immunoprecipitates with Ataxin-2-GFP in S2 *Drosophila* cells 151
Fbxo42 co-immunoprecipitates with Ataxin-2-GFP in *Drosophila* eyes 153
Fbxo42 localizes in close proximity to Ataxin-2 in the ring gland cells of *Drosophila* larvae, under ER stress conditions 154
Analysis of Ataxin-2-GFP protein stability using cycloheximide (CHX) chase assays 160
MG132, a proteosome inhibitor, increases the stability of Ataxin-2-GFP 160
Fbxo42 overexpression/depletion affects the stability of Ataxin-2-GFP 161
Fbxo42 ubiquitylates Ataxin-2-GFP on cysteine 244 164
Ataxin-2^{C244A}-GFP does not present DTT-sensitive Ataxin-2-GFP/ubiquitin conjugates 166
AlphaFold prediction of the Ataxin-2/Fbxo42/Cullin-1/Skp-1/Rbx1/E2/Ub complex 168
3.5 Discussion 170
3.6 Acknowledgments 174
3.7 References 174

CHAPTER IV: Ataxin-2 stabilizes Xbp1 mRNA and protects it from degradation under ER stress conditions 177

4.1 Abstract 178

4.2 Introduction 179

ER stress and UPR activation 180

4.3 Methods 182

4.4 Results 194

Ataxin-2 co-localizes with Xbp1 mRNA during UPR activation in ring gland cells 194

Ataxin-2 co-localizes with Xbp1 mRNA during UPR activation in human (HeLa) cells 197

Ataxin-2 binds to Xbp1 mRNA during UPR activation in S2 *Drosophila* cells 198

Ataxin-2 regulates Xbp1 mRNA stability during UPR activation in S2 *Drosophila* cells 202

Ataxin-2 regulates Xbp1 mRNA translation during UPR activation in S2 *Drosophila* cells 203

Fbxo42 regulates Xbp1 mRNA translation during UPR activation in S2 *Drosophila* cells and in eye imaginal discs 204

4.5 Discussion 206

4.6 Acknowledgements 210

4.7 References 210

CHAPTER V:General Discussion and Future Perspectives . 213

5.1 Fbxo42 protein 214

5.2 Ataxin-2 is a substrate of Fbxo42 215

5.3 Fbxo42 interacts with Ataxin-2 protein 216

5.4 Ataxin-2 binds to Xbp1 mRNA in Ataxin-2 granules, during UPR activation 218

Concluding remarks 223

Future perspectives..... 224
References 225
Appendix 227

Declaration

I, Cristiana Catarina Dias Santos, declare that this dissertation and the data presented are the result of my own research, developed between 2016 and 2025 in the laboratory of Dr. Pedro Domingos at the Instituto de Tecnologia Química e Biológica António Xavier (ITQB-NOVA), in Oeiras. Author contributions are mentioned at the beginning of each chapter and in each acknowledgements section. Personal financial support was granted by the Fundação para a Ciência e Tecnologia (FCT, SFRH/BD/130817/2017) and by the fellowship with the reference 031/BI/2022, which is part of the project FCT AGA-KHAN/541141368/2019 (FCT and Aga Khan Foundation). The laboratory was funded by MOSTMICRO-ITQB, with references UIDB/04612/2020 and UIDP/04612/2020. Additionally, the laboratory received funding from the grants LCF/PR/HR17/52150018 (“la Caixa” Foundation) and FCT AGA-KHAN/541141368/2019.

Declaração

Eu, Cristiana Catarina Dias Santos, declaro que esta dissertação e os dados apresentados são o resultado da minha investigação, desenvolvida entre 2016 e 2025 no laboratório do Doutor Pedro Domingos, no instituto de Tecnologia Química e Biológica António Xavier (ITQB-NOVA), em Oeiras. As contribuições dos autores são mencionadas no início de cada capítulo e em cada secção de agradecimentos. O meu financiamento foi concedido pela Fundação para a Ciência e Tecnologia (FCT, SFRH/BD/130817/2017) e pela bolsa com a referência 031/BI/2022, que faz parte do projeto KHAN/541141368/2019 (FCT e Fundação Aga Khan). O laboratório foi financiado pelo MOSTMICRO-ITQB, com as referências UIDB/04612/2020 e UIDP/04612/2020. Adicionalmente, o laboratório recebeu financiamento dos projetos com as referências LCF/PR/HR17/52150018 (da Fundação “la Caixa”) e FCT AGA-KHAN/541141368/2019.

Summary

The accumulation of misfolded/unfolded proteins in the endoplasmic reticulum (ER) leads to a cellular condition known as “ER stress”. To alleviate this stress and restore cellular homeostasis, cells activate a signalling pathway collectively referred to as the Unfolded Protein Response (UPR). As a result, the ER sensor protein IRE1 is activated and mediates the splicing of XBP1 mRNA. Xbp1 spliced (Xbp1s) is an effective transcription factor and promotes the transcription of UPR-target genes, helping to reduce ER stress levels. However, when stress is prolonged or severe, it can lead to cell death by apoptosis.

Previous work in our lab showed that overexpression of Xbp1 spliced causes cell death and retinal degeneration in the *Drosophila* adult eye, leading to the “glossy” eye phenotype. We performed a genetic screen, to find mutations that could rescue the “glossy” eye phenotype. Through this screen, we identified different loss-of-function mutations in *Fbxo42* gene.

To understand how *Fbxo42* mutants could rescue Xbp1s-induced retinal degeneration, we began by generating an antibody against Fbxo42. This antibody allowed us to detect the expression of Fbxo42 protein in various larval tissues, including the brain, eye imaginal discs and ring gland, as well as in the adult brain, ovary and testis (Chapter II).

Fbxo42 encodes an F-box protein, whose function is not yet fully understood. F-box proteins form complexes with Skp-1, Cullin-1 and Rbx (SCF complexes) to mediate the ubiquitylation of specific

substrates. In Chapter II, we present the identification of substrates for this F-box protein by performing two different proteomic approaches: one using HEK-293 cell lysates and another using fly extracts. The proteomic approach with HEK cell extracts allowed us to identify Lamin-B as an interactor of Fbxo42. Regarding the proteomic approach with fly extracts, based on a ^{bio}Ub strategy, enabled us to identify the RNA-binding protein Ataxin-2 as a substrate of Fbxo42. In this Chapter, we also present ubiquitylation assays showing that Fbxo42 mediates the formation of DTT-sensitive Ataxin-2/ubiquitin conjugates.

In Chapter III, we further confirm the interaction between Fbxo42 and Ataxin-2 through immunoprecipitation assays and immunofluorescence experiments using ring gland cells. We show the formation of Ataxin-2 granules, upon ER stress induction. Also, in Chapter III, we present assays that address whether Fbxo42 mediates the activity of Ataxin-2 or promotes its degradation. Specifically, we present cycloheximide (CHX)-chase assays, demonstrating that Fbxo42 mediates the proteasomal degradation of Ataxin-2. Moreover, in this Chapter, we show that cysteine 244 is the Ataxin-2 residue that is ubiquitylated by Fbxo42.

Finally, in Chapter IV, we investigate the role of Ataxin-2 in the regulation of stability and translation of Xbp1 mRNA. We show the co-localization of Xbp1 mRNA with cytoplasmic Ataxin-2 granules in ring gland cells, upon ER stress induction. In addition, we demonstrate that human Xbp1 mRNA also accumulates in Ataxin-2 granules in human HeLa cells, under ER stress conditions. Through iCLIP experiments, we show that Ataxin-2 binds to Xbp-1

mRNA. Moreover, in this Chapter, we present stability assays demonstrating that Ataxin-2 regulates Xbp1 mRNA stability and translation. Our final experiment shows that the protein levels of Fbxo42 also influence Xbp1 mRNA translation.

Through this work, we provide further insights into the biological function of Fbxo42. Importantly, we uncover a novel mechanism in which, during the early phase of UPR activation, Xbp1 mRNA is stabilized within Ataxin-2 granules, by Ataxin-2-binding, being protected from degradation. During the late phase of UPR activation, Fbxo42 is recruited to the Ataxin-2 granules, promoting the ubiquitylation of Ataxin-2 and its proteasomal degradation. This process ultimately leads to the degradation of these granules, allowing Xbp1 mRNA to be release and translated. Notably, under high levels of ER stress and UPR activation, Xbp1 spliced protein can promote cell death, as observed in the “glossy” eye phenotype induced by Xbp1s-overexpression.

Sumário

A acumulação de proteínas “misfolded/unfolded” no retículo endoplasmático (RE) origina uma condição celular, conhecida por “stress no RE”. Para aliviar o stress no RE, e restaurar a homeostasia celular, as células ativam um mecanismo de sinalização, que é designado de “Unfolded Protein Response” (UPR). Como resultado, a proteína “sensor” do RE, IRE1, é ativada e medeia o splicing do mRNA de Xbp1. A proteína Xbp1 “spliced” (XBp1s) é um fator de transcrição eficaz e promove a transcrição de genes-alvo da UPR, ajudando a reduzir os níveis de stress no RE. No entanto, se o stress for muito longo ou forte pode levar à morte celular.

Um trabalho realizado anteriormente no nosso laboratório mostrou que a sobre-expressão de Xbp1s causava morte celular e degeneração da retina do olho da *Drosophila*, originando o fenótipo de olho “glossy”. No nosso laboratório realizámos um screen genético para encontrar mutações que pudessem resgatar este fenótipo. Através deste screen, identificámos diferentes mutações de perda de função do gene *Fbxo42*.

Para compreender como mutantes de *Fbxo42* poderiam resgatar a degeneração da retina, induzida por sobre-expressão de Xbp1s, começámos por gerar um anticorpo contra Fbxo42. Este anticorpo permitiu-nos detetar a expressão da proteína Fbxo42 em vários tecidos da larva, incluindo o cérebro, os discos imaginais do

olho e a glândula anelar, assim como no cérebro, ovários e testículos da mosca adulta (Capítulo II).

O gene *Fbxo42* codifica uma proteína F-box, cuja função ainda não é totalmente conhecida. As proteínas F-box formam complexos com Skp-1, Cullin-1 e Rbx (complexos SCF) para mediar a ubiquitilação de substratos específicos. No Capítulo II, apresentamos a identificação de substratos para esta proteína F-box, através de duas abordagens proteómicas distintas: uma delas utilizando lisados de células HEK-293 e a outra usando extratos de mosca. A abordagem proteómica com lisados de células HEK, permitiu-nos identificar Lamin-B como um interator de Fbxo42. Através da abordagem proteómica com extratos de mosca, baseada numa estratégia de ^{bio}Ub, identificámos a proteína de ligação ao RNA Ataxin-2. No Capítulo II, apresentamos também ensaios de ubiquitilação, que mostram que Fbxo42 medeia a formação de conjugados de Ataxin-2/ubiquitina, que são sensíveis ao DTT.

No Capítulo III, confirmamos a interação entre Fbxo42 e Ataxin-2 através de ensaios de imunoprecipitação e experiências de imunofluorescência, utilizando células da glândula anelar. Nas células da glândula anelar, mostramos a formação de grânulos de Ataxin-2, após a indução de stress no retículo endoplasmático. Além disso, no Capítulo III, apresentamos ensaios que abordam se Fbxo42 regula a atividade de Ataxin-2 ou promove a sua degradação. Especificamente, apresentamos ensaios com ciclohexamida, que demonstram que Fbxo42 medeia a degradação proteossomal de Ataxin-2. Adicionalmente, neste Capítulo,

mostramos que a cisteína 244 é o resíduo de Ataxin-2 que é ubiquitilado por Fbxo42.

Finalmente, no Capítulo IV, investigamos o papel de Ataxin-2 na regulação da estabilidade e tradução do mRNA de Xbp1. Mostramos a co-localização do mRNA de Xbp1 com grânulos citoplasmáticos de Ataxin-2 em células da glândula anelar, após a indução de stress no RE. Além disso, demonstramos que o mRNA de Xbp1 também acumula nos grânulos de Ataxin-2 em células HeLa, em condições de stress no RE. Através de experiências de iCLIP, mostramos que Ataxin-2 se liga ao mRNA de Xbp1. Para além disso, neste Capítulo, apresentamos ensaios de estabilidade, que demonstram que Ataxin-2 regula a estabilidade e tradução do mRNA de Xbp1. A nossa experiência final mostra que os níveis de Fbxo42 também influenciam a tradução do mRNA de Xbp1.

Com este trabalho, fornecemos novas informações sobre a função biológica de Fbxo42. De realçar que, descobrimos um novo mecanismo em que, durante a fase inicial de ativação da UPR, o mRNA de Xbp1 é estabilizado em grânulos de Ataxin-2, através da ligação a Ataxin-2, sendo protegido da degradação. Durante a fase tardia da ativação da UPR, a proteína Fbxo42 é recrutada para os grânulos de Ataxin-2 promovendo a ubiquitilação de Ataxin-2 e a sua degradação. Este processo resulta, em última instância na degradação dos grânulos de Ataxin-2, permitindo desta forma que o mRNA de Xbp1 seja libertado e traduzido. De notar que, sob níveis elevados de stress no RE e ativação da UPR, o Xbp1s pode promover a morte celular, como observado no fenótipo de olho “glossy”, induzido pela sobre-expressão de Xbp1s.

Acknowledgments

I would like to acknowledge all the people who have helped me over the past years of my PhD. It has been a long journey with highs and lows, but in the end, all the effort pays off. I have learned a lot over the years, at all levels. It took me a while to get here, because I was very stubborn and resilient at the same time, always thinking, “I have to do one more experiment, just one more…” but in the end, our work is always unfinished, and that is part of the process.

First, I would like to thank my supervisor, Pedro Domingos, for choosing me for this project, for believing in my abilities and for his guidance over the years. I would also like to thank my lab colleagues, both former and current: Catarina, Fátima, Gonçalo, Lígia, João, Joana, Yolanda, Érika and Miguel, for helping me with the lab work and for sharing some funny moments with me.

Throughout this journey, I have always had the support of my dearest family and friends. I would like to thank my parents for always believing in me. My mother, for calling me and calming me when an experiment goes wrong.

I would like to acknowledge my friends, Catarina, my dearest friend since I can remember, and my godchild Tiago – you are both an inspiration. My friends Patrícia and Ana, I always miss you. I would like to thank Maria for your friendship and for sharing the best hiking trails with me.

I have finished this journey certain that I have done my best, and I hope the future brings more equally challenging adventures.

List of publications

This dissertation contains sections of the following publication:

Santos CC, Schweizer N, Cairrão F, Ramirez J, Osinalde N, Yang M, Gaspar CJ, Rasheva VI, Hensel Z, Adrain C, Tiago N, Voigt F, Gameiro PA, Mayor U & Domingos PM (2024). **Fbxo42 promotes the degradation of Ataxin-2 granules to trigger terminal Xbp1 signaling.** *bioRxiv*1–28.
doi: https://doi.org/10.1101/2024.12.22.629979.

Currently "in revision" in Nature Communications.

List of abbreviations

2R: Right arm of the second chromosome
3' UTR: Three prime untranslated region
A2BP1: Ataxin-2 binding protein 1
aa: Amino acid
ACAT2: Acyl-CoA:cholesterol acyltransferase 2
ACC: Acetyl-coenzyme A
ActD: Actinomycin D
AD: Alzheimer's disease
ADP: Adenosine diphosphate
Ago1: Argonaute 1
ALS: Amyotrophic lateral sclerosis
AREs: AU-rich elements
Ask1: Apoptosis signal-regulating kinase 1
AT: Adenine/Thymine
ATF4: Activating transcription factor 4
ATF6: Activating transcription factor-6
Atg8a: Autophagy-related protein 8a
Ato: Atonal
ATP: Adenosine-5'-triphosphate
Atx-2 or Atx2: Ataxin-2
ATXN2: Ataxin-2
ATXN2-L: Ataxin-2-like
Aβ: Amyloid-β
^{bio}Ub: Biotinylated ubiquitin
BiP: Binding immunoglobulin protein
BirA: Biotin ligase
BMP: Bone Morphogenic Protein
bp: base pairs
bZIP: Basic leucine zipper
CaMKII: Ca2+/calmodulin-dependent protein kinase II
CASH: Carbohydrate-interacting
CCT: Chaperonin containing TCP-1
CCT3: Chaperonin containing T-complex protein-1 subunit 3
CCT4: Chaperonin containing T-complex protein-1 subunit 4
cDNA: Complementary DNA
CHIP: C-terminal of Hsp70 interacting protein
CHOP:C/EBP homologous protein
CHX: Cycloheximide
CNX: Calnexin
co-IP: Co-immunoprecipitation

COP1: Constitutive photomorphogenic 1
CRT: Calreticulin
CST: Cell Signalling Technology
C-terminus: Carboxyl-terminus
Cul1: Cullin-1
Cyo: Curly of Oster
Cys: Cysteine
DAPI: 4',6-diamidino-2-phenylindole
DDX6: DEAD-Box Helicase 6
DGRC: *Drosophila* Genomics Resource Center
DIAP-1: *Drosophila* inhibitor of apoptosis 1
Dl: Delta
DNA: Deoxyribonucleic acid
Dpp: Decapentaplegic
DR: Death receptor
DSHB: Developmental Studies Hybridoma Bank
dsRNA: double-stranded RNA
DTT: Dithiothreitol
DUBs: Deubiquitinases
E6-AP: E6-associated protein
EDTA: Ethylenediaminetetraacetic acid
EGFR: Epidermal Growth Factor Receptor
eIF2α: Eukaryotic translation initiation factor 2 subunit alpha
eIF4G: Eukaryotic translation initiation factor 4G
ELAV: Embryonic lethal abnormal visual system
EMC: ER membrane protein complex
EMS: Ethyl methanesulfonate
ER: Endoplasmic Reticulum
ERAD: ER-associated protein degradation
EV: Empty vector
ey: eyeless
F1: First filial generation
FBS: Fetal Bovine Serum
FBX: F-box
FBXL: F-box and leucine rich repeat
FBXO: F-box only
Fbxo42: F-box only protein 42
FBXW: F-box and WD repeat domain containing
Flp: Flippase
FMRP: Fragile X mental retardation protein
FRT: Flippase Recombination Target
G76: Glycine 76

GADD34: Growth arrest and DNA damage inducible 34
GC: Guanine/Cytosine
GET: Guided entry of TA proteins
GFP: Green Fluorescent Protein
Glu: Glutamic acid
Gly: Glycine
GMR: Glass Multimer Reporter
gp78: Glycoprotein 78
GSCs: Glioblastoma stem-like cells
GST: Glutathione S-transferase
HA: Hemagglutinin
HD: Huntington's disease
HDAC2: Histone deacetylase 2
HECT: Homologous to E6AP Carboxyl Terminus
HEK: Human Embryonic Kidney
Hh: Hedgehog
hid: Head involution defective
His: Histidine
HIV-1: Human immunodeficiency virus type 1
HRI: Heme-regulated inhibitor
HRP: Horseradish Peroxidase
Hth: Homothorax
IB: Immunoblot
IBR: In-between-RINGs
iCLIP: Individual-nucleotide resolution UV crosslinking and immunoprecipitation
IDRs: Intrinsically disordered regions
IF: Immunofluorescence
iiCLIP: Improved iCLIP
IMAC: Immobilized-Metal Affinity Chromatography
ING4: Inhibitor of growth protein 4
Insig-2: Insulin-induced gene 2 protein
IP: Immunoprecipitation
IPTG: Isopropyl β-D-1-thiogalactopyranoside
IR: Infrared
irCLIP: Infrared-CLIP
IRE1: Inositol-requiring protein-1
JAMM: JAB1/MPN/Mov34 metalloenzymes
JNK: c-Jun N-terminal kinase
K: Lysine
Kb: kilobase
kDa: Kilodalton

L1: Drosophila first instar larva
LC3: Microtubule-associated protein 1 light chain 3
LC-MS/MS: Liquid Chromatography with tandem Mass Spectrometry
LFQ: Label Free Quantitation
LRRs: Leucine-rich repeats
LSM: like-Sm
LSM-AD: Lsm-associated domain
LUBAC: Linear ubiquitin chain assembly complex
MDa: Megadalton
Mdm2: Murine double minute 2
Me31B: Maternal expression at 31B
MED16: Mediator complex subunit 16
Met1: Methionine 1
MF: Morphogenetic furrow
MHC I: Major histocompatibility complex class I
Min: minutes
MINDY: MIU-containing novel DUB family
MIR1: Modulator of immune recognition 1
miRNA: microRNA
MJDs: Machado-Joseph disease proteases
MN: Macherey-Nagel
MOMP: Mitochondrial outer membrane permeabilization
mRNA: Messenger RNA
mRNP: Messenger ribonucleoprotein
MS: Mass Spectrometry
NEB: New England Biolabs
Nedd4: Neural precursor cell expressed developmentally down-regulated protein 4
NEM: N-ethylmaleimide
NF-κB: Nuclear factor kappa B
Ngn2: Neurogenin-2
Ni: Nickel
N-terminus: Amino-terminus
OD: Optical density
OTUs: Ovarian tumour proteases
PABP: Poly(A)-binding protein
PABPC1: Poly(A) Binding Protein Cytoplasmic 1
PAM2: Poly(A)-binding protein interacting motif 2
PAN: Poly(A) nuclease
PAPD4: Poly(A) RNA Polymerase D4

PAR-CLIP: Photoactivatable-ribonucleoside-crosslinking and immunoprecipitation
P-bodies: Processing-bodies
PBS: Phosphate-buffered saline
PCB: Pyruvate carboxylase
PCR: Polymerase Chain Reaction
PDI: Protein disulphide isomerase
PERK: Protein kinase RNA (PKR)-like ER kinase
PEX5: Peroxin 5
PFA: Paraformaldehyde
PG: Prothoracic gland
polyQ: Polyglutamine
PP1-87B: Serine/threonine-protein phosphatase alpha-2 isoform
PP2A: Serine/threonine-protein phosphatase 2A
PPN: Preproneural
PQC: Protein quality control
PTM: Post-translational modification
PTP: Permeability transition pore
RBM9: RNA-binding motif protein 9
RBP: RNA-binding protein
RBPJ: Recombination signal-binding protein of immunoglobulin kappa J region
RBPMS: RNA-binding protein with multiple splicing
RBR: RING-between-RING
Rbx-1: RING-box protein-1
Rh1: Rhodopsin-1
RIDD: Regulated IRE1-dependent decay
RING: Really Interesting New Gene
RNA: Ribonucleic acid
RNAi: RNA interference
RNC: Ribosome-nascent chain
Roc-1: Regulator of cullins-1
ROS: Reactive oxygen species
RPN: Regulatory particle non-ATPase
RPT: Regulatory particle triple-A
SCA2: Spinocerebellar Ataxia type-2
SCF: Skp–Cullin–F-box
SDS: Sodium Dodecyl Sulfate
SG: Stress granule
Skp-1: S phase kinase-associated protein-1
SkpA: Skp-1-related A
smFISH: Single molecule RNA fluorescence in situ hybridization

SND: SRP-independent targeting pathway
SOD1: Superoxide dismutase-1
SRP: Signal recognition particle
Su: Suppressor
TA membrane protein: Tail-anchored membrane protein
TCP-1: T-complex protein-1
TDP-43: TAR DNA-binding protein 43
TG: Thapsigargin
TGX: Tris-Glycine eXtended
Thr: Threonine
TMD: Transmembrane domain
TNF-R: Tumour necrosis factor receptor
TRAF2: TNF receptor-associated factor 2
TRC: Transmembrane recognition complex
Trp: Tryptophan
TUNEL: Terminal Deoxynucleotidyl transferase dUTP nick-end labeling
TXNIP: Thioredoxin-interacting protein
U2OS: Human Bone Osteosarcoma Epithelial Cells
UAS: Upstream activating sequence
Ub: Ubiquitin
UCHs: Ubiquitin C-terminal hydrolases
UFM1: Ubiquitin-fold modifier 1
UPR: Unfolded Protein Response
USPs: Ubiquitin-specific proteases
UV: Ultraviolet
VNC: Ventral nerve cord
Vps35: Vacuolar protein sorting ortholog 35
Vpu: Viral protein U
w: White gene
WD: Tryptophan-aspartic acid
WT: Wild-type
XBP1: X-box binding protein 1
XBP1s: Xbp1 spliced
XBP1u: Xbp1 unspliced
ZUFSP: Zinc finger with UFM1-specific peptidase domain protein

“The most beautiful thing we can experience
is the mysterious. It is the source
of all true art and science.”

Albert Einstein

CHAPTER I

General Introduction

1.1 The endoplasmic reticulum

The endoplasmic reticulum (ER) is a continuous compartment that extends from nucleus to the cytosol (Bravo *et al.*, 2013). Based on its structure, the ER is subdivided in the ribosome-studded rough endoplasmic reticulum (RER) and the ribosome-free smooth endoplasmic reticulum (SER) (Bravo *et al.*, 2013).

The endoplasmic reticulum is arranged in a dynamic tubular network (Hetz, 2012) and is the first compartment in the secretory pathway of eukaryotic cells (Schröder, 2008). The ER presents multiple physiological functions, including membrane and secretory protein synthesis and protein folding. The majority of secretory and transmembrane proteins fold into their native conformation in the ER (Schröder, 2008; Bravo *et al.*, 2013). These nascent proteins also undergo post-translational modifications (PTMs) in this organelle, specifically the addition of asparagine-linked oligosaccharides and the formation of disulfide bonds (Schröder, 2008). Mechanisms of quality control, ensure that only properly folded proteins exit the ER (Schröder, 2008). The protein-folding machinery in the ER is particularly challenged in specialised secretory cells due to their high demand for protein synthesis, constituting a constant source of stress (Hetz, 2012).

Furthermore, the ER is the major intracellular calcium reservoir in the cell (Schröder, 2008; Hetz, 2012) and is also involved in the biosynthesis of lipids and sterols (Schröder, 2008). Additionally, it contributes to the biogenesis of autophagosomes and peroxisomes (Hetz, 2012). Moreover, the extensive structure of the ER impacts the overall architecture and organization of the eukaryotic cells. For example, the ER tubules extending into the

cytoplasm contact other organelles, such as mitochondria and endosomes, thus impacting their positioning and dynamics (Christianson & Carvalho, 2022).

The ER also accommodates proteins and protein complexes required for different functions including innate immune signalling, stress response and metabolism (Christianson & Carvalho, 2022).

Protein synthesis and folding in the ER

Approximately one-third of the eukaryotic proteome is processed in the endoplasmic reticulum (Chen, 2005).

Secretory proteins and proteins destined for the plasma membrane or for organelles within the secretory or endocytic pathways are inserted into the ER lumen or membrane, either co-translationally or post-translationally (Fregno & Molinari, 2019; Wang & Ye, 2021). The co-translational translocation pathway directs nascent polypeptides into the ER while they are being synthetised by ribosomes. This pathway is utilized by ER client proteins bearing an N-terminal signal sequence or a hydrophobic transmembrane domain (TMD), which is recognized by a signal recognition particle (SRP) in the cytosol (Wang & Ye, 2021). Upon SRP binding, protein translation is temporarily stalled, and the ribosome-nascent chain (RNC) complex is targeted to the ER membrane. At the ER membrane, the SRP interacts with its receptor (Pauwels *et al.*, 2021). The RNC complex is then transferred to the Sec61 translocon. The interaction between the ribosome and the translocon resumes translation. The recognition and subsequent insertion of the polypeptide chain into the Sec61 pore either lead to

lateral insertion into the membrane or to translocation into the ER lumen (Sorout & Helms, 2024).

In the case of post-translational translocation, nascent polypeptides are completely synthesized in the cytosol prior to targeting the ER. This pathway usually applies to nascent chains with low-hydrophobicity signal sequences that are not recognized by SRP. Translocation of the fully synthetised polypeptides is facilitated by cytosolic chaperones, such as Hsp70. In eukaryotic cells, post-translational translocation is mediated by the association of the Sec61 channel with the Sec62/Sec63 protein complex (Wang & Ye, 2021).

Membrane proteins whose targeting sequence is a TMD located within approximately 65 amino acids of the C-terminus are referred to as “tail-anchored (TA) membrane proteins”. These proteins are also targeted post-transcriptionally, and the mechanism of their targeting depends on the hydrophobicity of the TMD. Therefore, TA membrane proteins with high hydrophobicity are targeted via the guided entry of TA proteins (GET) pathway in yeast, or its mammalian equivalent, transmembrane recognition complex (TRC). In contrast, those with low hydrophobicity use cytosolic chaperones and the ER membrane protein complex (EMC) for their biogenesis (Hegde & Keenan, 2022; O’Keefe *et al.*, 2022). Additionally, an alternative pathway known as the SRP-independent targeting (SND) pathway, may also be involved in the biogenesis of transmembrane proteins whose TMD is located in the mid to C-terminal region of the protein. hSnd2, the human orthologue of a yeast SND pathway component, has been shown to exhibit

functional redundancy with the SRP and TRC pathways (O'Keefe *et al.*, 2022).

Upon entry into the ER, the signal sequence is cleaved by a signal peptidase, and nascent polypeptides undergo modifications, such as the addition of N-linked glycans and the formation of disulphide bonds. They are then assembled and folded to acquire their native conformation. The maturation of nascent proteins in the ER is facilitated and monitored by ER-resident chaperones, such as BiP, calnexin (CNX), calreticulin (CRT) and protein disulphide isomerase (PDI), as well as folding enzymes that associate with the newly synthesized proteins, preventing their aggregation and facilitating their correct folding and assembly (Ma & Hendershot, 2004; Dubnikov & Cohen, 2017) (Figure 1.1).

The protein-folding environment in the ER is distinct from that of the cytosol due to its oxidizing nature, which facilitates the formation of disulfide bonds. Additionally, the ER lumen contains a calcium-rich environment that functions as a folding buffer and is essential for chaperone activity (Ma & Hendershot, 2004; Wang & Kaufman, 2016) (Figure 1.1).

Once properly folded and modified, proteins are packaged into vesicles and proceed through the secretory pathway. In contrast, proteins that fail to mature correctly are retained in the ER and eventually retrotranslocated to the cytosol for degradation by the 26S proteasome, through a process known as ER-associated degradation (ERAD) (Ma & Hendershot, 2004) (Figure 1.1).

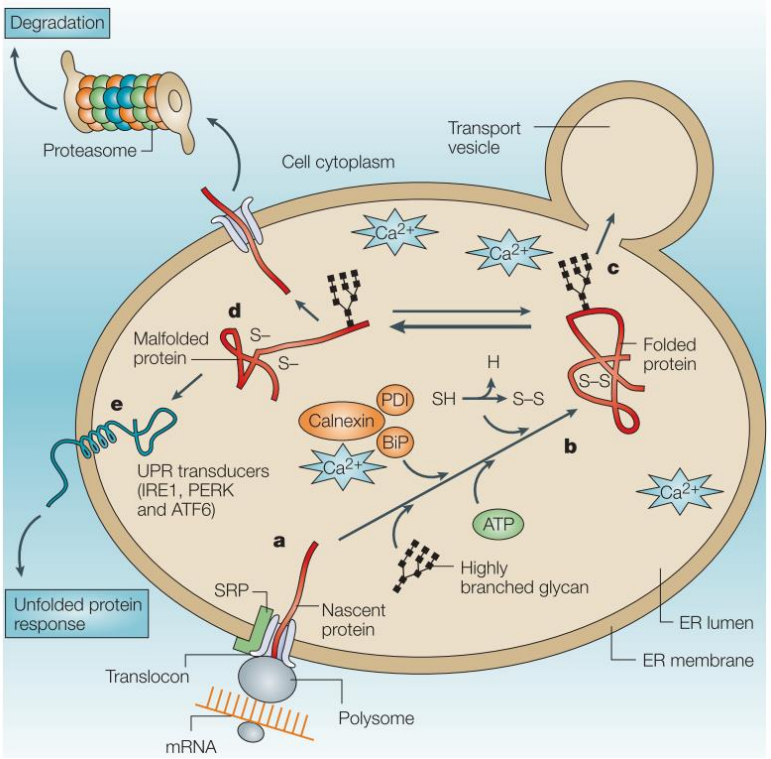

Figure 1.1: Protein folding in the Endoplasmic reticulum (ER). a) Proteins of the secretory pathway are translocated into the ER, through channels in the ER membrane, called translocons. **b)** In the calcium-rich, oxidizing environment of the ER lumen, resident chaperones like BiP, calnexin and protein disulphide isomerase (PDI) facilitate the proper folding of the nascent protein by preventing its aggregation, monitoring the processing of the highly branched glycans and forming disulfide bonds to stabilize the folded proteins. **c)** Once correctly folded and modified, proteins will exit the ER through the formation of transport vesicles and travel through the secretory pathway. **d)** When ER quality-control system deems that proteins are malfolded or unable to fold, they are retrotranslocated to the cytosol and degraded by 26S proteasome. **e)** Changes in the ER environment shift the balance from normal folding for improper folding (thicker arrow), leading to the accumulation of unfolded proteins in the ER. This causes the activation of three ER-stress sensors – IRE1, PERK and ATF6, which trigger the unfolded protein response (UPR). Adapted from (Ma & Hendershot, 2004).

1.2 ER-associated degradation (ERAD)

The best studied ER protein quality control (PQC) mechanism is the ERAD pathway (Figure 1.2). In this pathway, misfolded or misassembled proteins are moved back into the cytoplasm, through a process known as retrotranslocation, which requires a membrane complex and the associated ubiquitylation machinery (Wang & Ye, 2021).

ERAD substrates can be classified into three different categories, according to the compartment in which their lesion/misfolding occurs: ERAD-L (lesions in the ER lumen), ERAD-M (lesions in the ER membrane) and ERAD-C (lesions in the cytoplasm) (Christianson & Carvalho, 2022). At the molecular level, each ERAD class is defined by a specific ER-membrane ubiquitin-ligase complex that recognizes misfolded substrates in the ER lumen or membrane and promotes their transfer into the cytosol for ubiquitylation (Krshnan *et al.*, 2022). In yeast, the best characterized ERAD pathways are mediated by the Hrd1p complex (ERAD-L and ERAD-M) and Doa10p complex (ERAD-C and ERAD-M) (Christianson & Carvalho, 2022; Luo *et al.*, 2023). In mammalian cells, several E3-ubiquitin ligases (further detailed in the corresponding section of this introduction) participate in ERAD, including HRD1, glycoprotein 78 (gp78) and TEB4 (the mammalian homologue of yeast Doa10p) (Christianson & Ye, 2014; Luo *et al.*, 2023).

In yeast, ERAD-L substrates are recognized by the lectin Yos9 and the co-factor Hrd3p, and are subsequently transferred to the ER membrane to interact with the E3 ubiquitin ligase Hrd1p. Once engaged, substrates are polyubiquitylated by Hrd1p. Notably,

Hrp1p is also auto-ubiquitylated, a modification that facilitates the recruitment of the Cdc48p ATPase complex. Finally, ATP hydrolysis by Cdc48p drives the extraction of substrates from the ER membrane into the cytosol, where they are delivered to the proteasome for degradation (Ruggiano *et al.*, 2014; Stein *et al.*, 2014; Luo *et al.*, 2023) (Figure 1.2).

In mammalian cells, substrates are recognized by the lectin-like proteins OS9/XTP3-B in coordination with Sel1L, and are subsequently transferred to the E3 ubiquitin ligase HRD1. FAM8A1, a component of the HRD1 complex, enhances the binding of the adaptor protein HERP to HRD1. HERP, in turn, promotes the recruitment of Derlin-1/2/3 and HRD1 oligomerization. Substrates are then polyubiquitylated and retrotranslocated into the cytosol by the VCP/p97 (ATPase)–UFD1–NPL4 heterotrimeric complex for proteasomal degradation (Krshnan *et al.*, 2022; Luo *et al.*, 2023) (Figure 1.2).

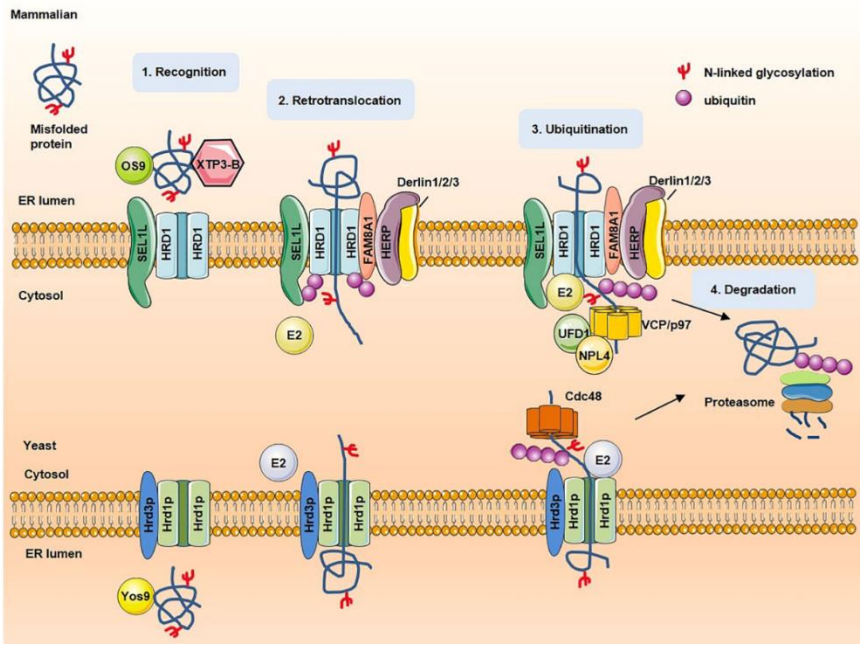

Figure 1.2: Steps and proteins involved in ERAD. In mammalian cells, misfolded proteins are recognized by OS9/XP3-B and transferred to HRD1 complex. Substrates are retrotranslocated through a channel formed by HRD1, then conjugated with polyubiquitin and extracted to cytosol for proteasomal degradation by VCP/p97–UFD1–NPL4 heterotrimer. In yeast, misfolded proteins are recognized by lectin Yos9 and Hrd3p and transferred to Hrd1p. Substrates are then retrotranslocated into the cytosol through the Hrd1p channel. Once exposed to the cytosolic face of the ER membrane, substrates are ubiquitylated. The cytosolic Cdc48 ATPase complex binds the ubiquitylated substrates and extract substrates out of the ER membrane. Substrates are then delivered to the proteasome for degradation (Luo *et al.*, 2023).

1.3 ER stress and UPR

Perturbations in the ER homeostasis, such as increased protein secretion, or disrupted ER protein folding capacity can cause the accumulation of unfolded or misfolded proteins in the lumen of the endoplasmic reticulum – a condition termed as “ER stress” (Hetz *et al.*, 2020). Other causes of ER stress include nutrient deprivation,

hypoxia, point mutations in secreted proteins that stabilize intermediate folding forms or cause aggregation, and loss of calcium homeostasis (Hetz & Papa, 2018). Upon ER stress, cells activate a series of complementary adaptive mechanisms to cope with protein-folding alterations, which are collectively known as the Unfolded Protein Response (UPR) (Hetz, 2012). UPR relieves ER stress and restores homeostasis through distinct strategies, including the attenuation of the translational rate, to reduce ER workload and avoid further accumulation of unfolded proteins, the transcriptional activation of genes encoding ER chaperones and folding enzymes to increase the ER' s folding capacity, and the transcriptional upregulation of genes encoding proteins involved in ER-associated protein degradation (ERAD) to promote the clearance of misfolded proteins (Ryoo *et al.*, 2007; Rasheva & Domingos, 2009; Oslowski & Urano, 2011; Smith *et al.*, 2011; Walter & Ron, 2011; Kadowaki *et al.*, 2015).

The activation of the UPR is mediated by three ER transmembrane protein sensors that detected ER stress: Inositol-requiring protein-1 (IRE1), Protein kinase RNA (PKR)-like ER kinase (PERK) and Activating transcription factor-6 (ATF6) (Ron & Walter, 2007) (Figure 1.3). They consist of three domains: an ER luminal domain, a single pass membrane spanning domain and a cytosolic domain (Adams *et al.*, 2019).

The UPR is activated following cell stress in several human disorders, including neurodegenerative diseases, inflammatory disease, diabetes and metabolic disorders, and cancer (Wang & Kaufman, 2012; Lindholm *et al.*, 2017).

IRE1 signalling

IRE1 is the most evolutionarily conserved ER transmembrane protein sensor and it is found in yeast, plants, *Caenorhabditis elegans*, *Drosophila* and mammals (Rasheva & Domingos, 2009; Acosta-Alvear *et al.*, 2018). IRE1 senses by its luminal domain the presence of misfolded proteins in the ER. Its cytosolic domain contains both kinase and endoribonuclease activities (Walter & Ron, 2011). Upon ER stress, IRE1 oligomerizes and autophosphorylates to elicit its endoribonuclease activity (Hetz *et al.*, 2020). Activated IRE1 cleaves the Xbp1 (X-box binding protein 1) mRNA in two specific positions, excising an intron (Walter & Ron, 2011). The severed exons are then ligated, generating a spliced mRNA, that is translated to the active and stable transcription factor Xbp1 spliced (Xbp1s), which translocates to the nucleus to induce the upregulation of numerous UPR-target genes, including genes encoding proteins involved in protein folding, quality control, ER-associated degradation (ERAD) and ER/Golgi biogenesis (Figure 1.3) (Rasheva & Domingos, 2009; Woehlbier & Hetz, 2011; Hetz, 2012). In a process known as regulated IRE1-dependent decay (RIDD), the endoribonuclease activity of IRE1 also mediates mRNA decay, relieving the burden of protein folding on the ER (Hollien & Weissman, 2006).

Mammals express two isoforms of IRE1: IRE1α and IRE1β. IRE1α is ubiquitously expressed, whereas IRE1β is uniquely expressed in intestinal epithelial cells (Hollien *et al.*, 2009). Both isoforms respond to ER stress; however, IRE1α exhibits higher XBP1 splicing activity compared to IRE1β. Furthermore, IRE1β can

function as a dominant-negative regulator of IRE1α, inhibiting stress-induced XBP1 splicing (Grey *et al.*, 2020; Liu *et al.*, 2024).

PERK signalling

Similar to IRE1, PERK is an ER transmembrane protein that contains both a cytosolic kinase domain and a luminal stress sensing domain (Rasheva & Domingos, 2009; Woehlbier & Hetz, 2011). Activated PERK phosphorylates the eukaryotic translation initiation factor 2 subunit-α (eIF2α), leading to the transient attenuation of protein translation, which reduces the overload synthesis of proteins in the ER (Rasheva & Domingos, 2009; Woehlbier & Hetz, 2011; Hetz *et al.*, 2020). Concomitantly, phosphorylated eIF2α triggers the translation of specific mRNAs, including the transcription factor ATF4 (Activating Transcription Factor 4). This transcription factor activates the expression of genes involved in redox homeostasis, amino acid metabolism, protein synthesis, apoptosis and autophagy (Woehlbier & Hetz, 2011; Hetz *et al.*, 2020). The activation of PERK occurs in a reversible manner. ATF4 participates in a feedback loop to dephosphorylate eIF2α to restore protein synthesis through the upregulation of the protein phosphatase 1 (PP1) regulatory subunit GADD34. During ER stress, GADD34 forms a complex with PP1 to dephosphorylate eIF2α (Figure 1.3) (Hetz *et al.*, 2020).

ATF6 signalling

ATF6 is an ER transmembrane protein with a cytosolic domain containing a basic-leucine zipper motif (bZIP) and a transcription activation domain (TAD), and an ER luminal domain that binds BiP. Upon ER stress, ATF6 translocates from the ER to the Golgi, where it is cleaved by Golgi S1 and S2 proteases, leading to the release of the N-terminal ATF6 cytosolic fragment (ATF6f), which goes to the nucleus and activates the transcription of target genes, including ER chaperones and ERAD-related genes (Figure 1.3) (Rasheva & Domingos, 2009; Woehlbier & Hetz, 2011).

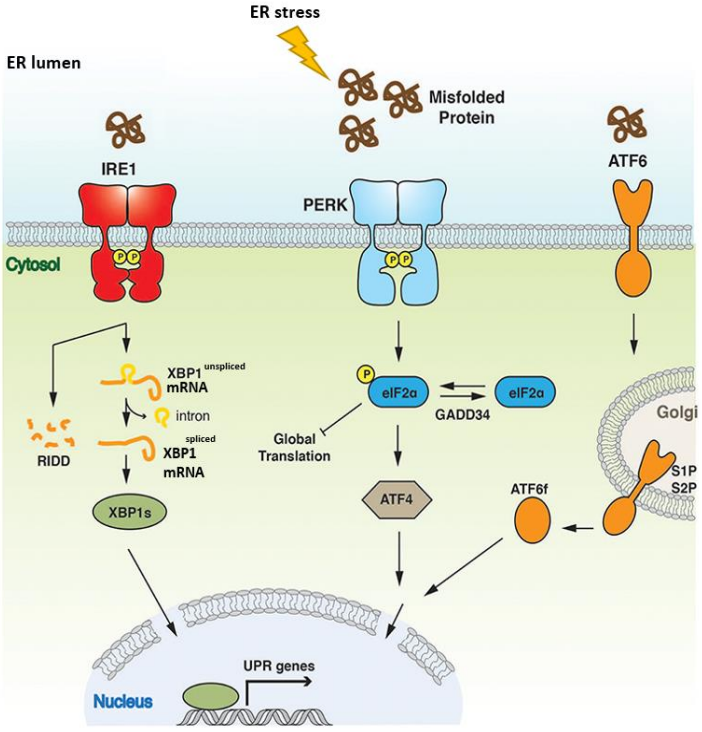

Figure 1.3: Overview of the UPR signalling pathway. The three UPR activator proteins: IRE1, PERK and ATF6 give rise to three separate branches of the response, all of which aim to alleviate the burden of misfolded proteins and to restore homeostasis. Adapted of (Adams *et al.*, 2019).

1.4 Chronic ER stress and Apoptosis

If the adaptive response fails to restore protein-folding homeostasis, or if ER stress is severe and prolonged, the sustained activation of the UPR triggers alternative signalling programs, collectively referred to as the “terminal UPR”, which ultimately lead to apoptosis (Hetz & Papa, 2018; Fu *et al.*, 2021).

Apoptosis is a form of regulated cell death that occurs not only in response to cellular damage or external stress, but also during normal development and morphogenesis. This programmed cell death can be triggered through two pathways: extrinsic and intrinsic (Rehmat & Chaudhry, 2019). The extrinsic pathway is mediated by external stimuli acting through death receptors (DRs) located on the cell surface, such as the Fas receptor, DR4/DR5, and tumour necrosis factor receptors (TNF-R). At cell surface, death receptors interact with their specific ligands, recruit adaptor proteins that, in turn, activate caspase-8, initiating the apoptotic cascade. In contrast, the intrinsic pathway is mitochondria-mediated and is activated by internal stimuli such as DNA damage or oxidative stress. This pathway is regulated by members of the Bcl-2 protein family, which includes both pro-apoptotic (for example Bax) and anti-apoptotic (for example Bcl-2) proteins. These proteins modulate mitochondrial outer membrane permeability, leading to the release of apoptogenic factors and subsequent activation of downstream caspases (Kashyap *et al.*, 2021).

Under prolonged or severe ER stress, the UPR sensors PERK and IRE1 can trigger apoptosis via different pro-apoptotic pathways (Figure 1.4). For example, while the transient phosphorylation of eIF2α by PERK temporarily reduces protein

synthesis and alleviates ER burden, sustained PERK signalling leads to a prolonged translational block, ultimately leading to cell death (Urra *et al.*, 2013; Hetz & Papa, 2018). Furthermore, PERK hyperactivation induces the expression of the pro-apoptotic transcription factor CHOP, which suppresses the anti-apoptotic gene *Bcl-2*, thereby accelerating cell death (Urra *et al.*, 2013; Hetz & Papa, 2018). CHOP also activates the *Gadd34* gene. GADD34 expression can lead to increased production of reactive oxygen species (ROS), likely as a result of renewed protein synthesis, which may contribute to proteotoxic stress (Urra *et al.*, 2013; Hetz & Papa, 2018).

IRE1α signalling can also promote apoptosis. Under chronic ER stress, hyperactivated IRE1α assembles into high-order oligomers, enhancing the activity of its RNase domain and increasing its affinity for RIDD substrates. This leads to a massive endo-nucleolytic cleavage of mRNAs (Hetz & Papa, 2018). In this context, RIDD may contribute to apoptosis by degrading transcripts encoding essential proteins, including ER chaperones such as BiP (Urra *et al.*, 2013). Moreover, IRE1α can interact with TNF receptor-associated factor 2 (TRAF2), activating apoptosis signal-regulating kinase 1 (ASK1) and its downstream target c-Jun N-terminal kinase (JNK), thereby inducing apoptosis. Finally, the RNase activity of IRE1α may also target specific microRNAs that normally repress pro-apoptotic genes, leading to the de-repression of proteins such as thioredoxin-interacting protein (TXNIP), a pro-oxidant factor involved in cell death (Urra *et al.*, 2013; Hetz & Papa, 2018).

Many of the pro-apoptotic signals from the UPR sensors converge on the intrinsic apoptotic pathway. This pathway is

activated when mitochondrial proteins, such as cytochrome *c* and Smac, are released from mitochondria into the cytoplasm, where they contribute to the activation of effector caspases (including caspase 3).

As previously mentioned, the Bcl-2 protein family regulates the intrinsic apoptotic pathway by controlling the integrity of the outer mitochondrial membrane. This pathway is activated when cellular damage triggers the expression or activation of one or more pro-apoptotic members of the Bcl-2 family, known as BH3-only proteins. It has been reported that several BH3-only proteins, including BIM, BID, NOXA and PUMA, are up-regulated during the terminal UPR. Once activated, BH3-only proteins either antagonize mitochondrial-protective proteins, such as Bcl-2, or directly activate the multidomain pro-apoptotic proteins BAX and BAK to permeabilize the outer mitochondrial membrane by a process called MOMP (mitochondrial outer membrane permeabilization) (Hetz & Papa, 2018). This event facilitates the release of apoptogenic factors into the cytosol (Figure 1.4).

Unmitigated ER stress can also promote apoptosis through the activation of death receptor 5 (DR5). ER stressors induce DR5 transcription via CHOP; however, IRE1 transiently catalyses the decay of DR5 mRNA. Under sustained ER stress, DR5 expression increases and triggers apoptosis via activation of caspase-8 (Lu *et al.*, 2014). In addition, a recent study has shown that XBP1s can upregulate the expression of the cell death receptor CD95/Fas. The authors observed that the overexpression of XBP1s increased CD95 expression and sensitized glioblastoma and triple-negative

breast cells to CD95L-induced cell death (Pelizzari-Raymundo *et al.*, 2024).

Under stress conditions, the release of calcium from the ER into the cytoplasm can also lead to apoptosis by influencing the opening of the mitochondrial permeability transition pore (PTP), thereby contributing to mitochondrial dysfunction and cell death (Urra *et al.*, 2013; Hetz & Papa, 2018) (Figure 1.4).

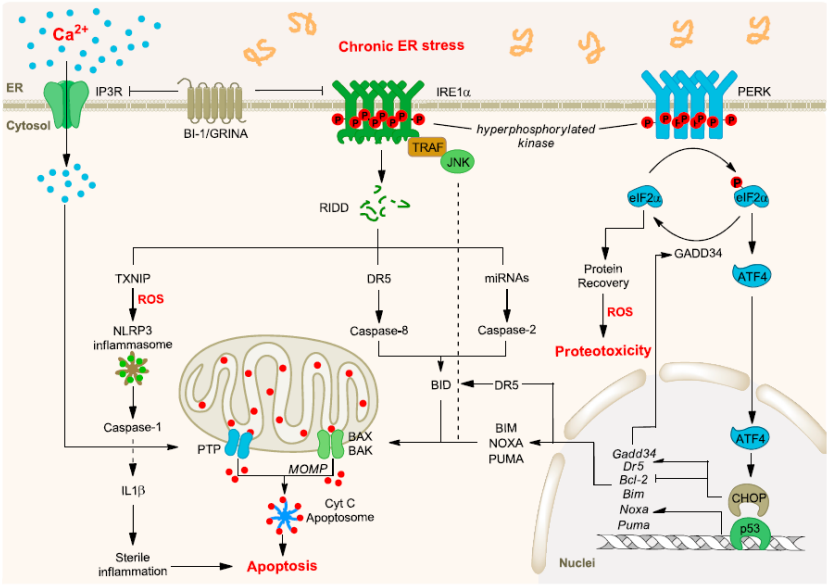

Figure 1.4: ER stress-induced apoptosis pathways. When exposed to chronically high levels of ER stress, IRE1α and PERK activate multiple pathways, that can lead to apoptosis. A key step in the regulation of apoptosis is the crosstalk between the ER and mitochondria, which is mediated by Bcl-2 protein family members. Additionally, calcium release from the ER, exacerbated protein synthesis and ROS production may contribute to the induction of apoptosis (Hetz & Papa, 2018).

1.5 Ubiquitylation

Ubiquitylation, the covalent binding of the small (76 amino acids long, 8.5 kDa), globular and highly conserved protein ubiquitin (Ub) to substrate proteins, is a versatile post-translational modification (PTM) that regulates several fundamental features of the target substrates, including stability, activity and cellular localization (Kelsall, 2022; Sun & Zhang, 2022).

The process of ubiquitylation is achieved by a cascade of sequential biochemical reactions, catalysed by the following three classes of enzymes: ubiquitin-activating enzyme (E1), ubiquitin-conjugating enzyme (E2) and ubiquitin ligase (E3). Firstly, the E1 enzyme catalyses the formation of a high-energy thioester bond between its own active cysteine site and the C-terminus of ubiquitin in an ATP-dependent manner (Ciechanover *et al.*, 1981; Hershko *et al.*, 1981; Hershko, 1988; Ciechanover, 1998; Yang *et al.*, 2021; Kelsall, 2022; Kochańczyk *et al.*, 2024). The “activated” ubiquitin is then transferred from E1 to the active cysteine site of an E2 via a thioester bond (Hershko, 1988; Ciechanover, 1998; Kelsall, 2022). Finally, the E2 enzyme cooperates with an E3 to facilitate the transfer of ubiquitin to the target substrate (Hershko, 1988; Ciechanover, 1998; Kelsall, 2022). The attachment of Ub to the substrate typically occurs via the formation of an isopeptide bond between the α-carboxyl group of the terminal glycine of Ub (G76) and the ε-amino group of a lysine residue of the target substrate, referred to as “canonical” ubiquitylation (Figure 1.5). Less commonly, Ub can be attached to the α-amino group of the N-terminus of the substrate, via the formation of a peptide bond (Ciechanover & Ben-Saadon, 2004). Remarkably, over the past few

decades, different studies have reported that Ub can also bind to substrates via cysteine or serine/threonine residues through the formation of thioester or oxyester bonds, respectively. Ubiquitylation of the N-terminus, cysteine, serine or threonine residues is referred to as “non-canonical” (Wang *et al.*, 2012*b*).

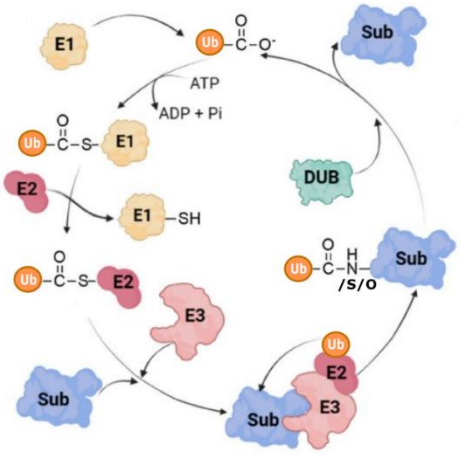

Figure 1.5: Ubiquitylation cascade, catalysed by ubiquitin-activating enzyme (E1), ubiquitin-conjugating enzyme (E2) and ubiquitin ligase (E3). Substrate (Sub) can be ubiquitylated on lysine or N-terminus through the formation of an amide bond. Additionally, substrate can be ubiquitylated on cysteine or serine/threonine residues via the formation of thioester or oxyester bonds, respectively. Ubiquitylation is a reversible process, and removal of ubiquitin molecules is mediated by deubiquitylases (DUBs). Adapted from Pichlak et al. (Pichlak *et al.*, 2023).

Cysteine ubiquitylation has been shown to be relevant in several cellular contexts. The earliest report of cysteine ubiquitylation came from a study on a viral E3 ubiquitin ligase. Modulator of immune recognition 1 (MIR1), an E3 encoded by Kaposi’s sarcoma-associated herpesvirus, was shown to down-regulate the expression of major histocompatibility complex class I (MHC I) heavy chain by ubiquitylating it on a conserved cysteine

residue (Cadwell & Coscoy, 2005). Another study reported that the PEX5 (peroxin 5) protein is also ubiquitylated on cysteine residues. PEX5 recognizes newly synthetised proteins with a peroxisomal targeting signal in the cytosol and promotes their translocation across the peroxisome membrane. After this process, PEX5 is recycled back into the cytosol to start a new round of protein transport. It has been demonstrated that PEX5 is ubiquitylated on a conserved cysteine and that this modification is required for its export from the peroxisome back to the cytosol, allowing it to be recycled (Carvalho *et al.*, 2007; Williams *et al.*, 2007; Kelsall, 2022). In addition, analysis of the proneural transcription factor Ngn2 using *Xenopus* frog egg extract revealed that this protein is ubiquitylated on cysteines as well as lysines and at the N-terminus (Vosper *et al.*, 2009). Interestingly, canonical and non-canonical ubiquitylation can occur simultaneously in the Ngn2 protein, and the relative contribution of each type of ubiquitylation to the rate of protein turnover can vary depending on the cell cycle phase (Vosper *et al.*, 2009; McDowell & Philpott, 2013). The authors also showed that cysteine ubiquitylation may play a greater role in Ngn2 degradation in mitosis (Vosper *et al.*, 2009). Moreover, ubiquitylation of Ngn2 may occur at serine and/or threonine residues in the absence of other available sites (Vosper *et al.*, 2009). Ngn2 was also ubiquitylated on cysteine residues in the *Mus musculus* P19 embryonal carcinoma cell line, suggesting that this type of ubiquitylation is conserved among vertebrate species (McDowell *et al.*, 2010; McDowell & Philpott, 2013).

Some studies on lipids have shown that there is a competition between ubiquitylation and oxidation on cysteines. It is

noteworthy that ACAT2 (acyl-CoA: cholesterol acyltransferase 2), an enzyme that converts cholesterol and fatty acids to cholesteryl esters, is ubiquitylated on a cysteine residue (Cys277) when the cellular lipid levels are low (Wang *et al.*, 2017). On the other hand, high levels of cholesterol and fatty acids induce the generation of reactive oxygen species (ROS) which oxidize Cys277 and inhibit ACAT2 ubiquitylation and degradation (Wang *et al.*, 2017). As a result, stabilized ACAT2 converts excess cholesterol and fatty acids into cholesteryl esters, reducing lipotoxicity (Wang *et al.*, 2017; Kelsall, 2022). Another study revealed that Insig-2, an ER membrane protein that functions as a negative regulator of lipid biosynthesis, is ubiquitylated on a cysteine residue (Cys215) and subsequently degraded (Zhou *et al.*, 2020). In contrast, high levels of ROS oxidize Cys215, blocking ubiquitylation and stabilizing the Insig-2 protein (Zhou *et al.*, 2020). In this way, stabilized Insig-2 down-regulates lipogenesis (lipid synthesis) and prevents excessive accumulation of lipids in muscles (Zhou *et al.*, 2020). Taken together, these results suggest that competitive oxidation and ubiquitylation on cysteine may be a common mechanism for regulating lipid metabolism in response to oxidative stress (Zhou *et al.*, 2020; Kelsall, 2022).

The HIV-1 protein Vpu inhibits the antiviral activity of the innate restriction factor BST-2/tetherin by a mechanism that is partly mediated by its interaction with Fbxw1 or β-TrCP, an F-box protein that is part of an SCF complex, which in turn induces the ubiquitylation of BST-2 (Tokarev *et al.*, 2011). It was found that mutation of all potential ubiquitylation sites in the cytoplasmic domain of BST-2, including lysine, cysteine, serine and threonine

residues was required to abolish Vpu-mediated ubiquitylation, suggesting that canonical and non-canonical ubiquitylation can be mediated by the SCF complex (Tokarev *et al.*, 2011). The E3 ubiquitin ligase HRD1 was found to ubiquitylate the non-secreted NS-1 immunoglobulin light chain, an ERAD substrate, predominantly at serine or threonine residues. Furthermore, mutation of lysine, serine and threonine residues in the NS-1 variable domain of the light chain was required to significantly reduce ubiquitylation and stabilize the protein (Shimizu *et al.*, 2010). In addition, HRD1 E3 ubiquitin ligase activity was necessary to modify all three amino acids (Shimizu *et al.*, 2010). Therefore, it is likely that other ERAD substrates can also be ubiquitylated at non-canonical ubiquitylation sites.

Types of substrate ubiquitylation

Ubiquitylation of the substrate can take different forms, constituting the so-called “ubiquitin code” (Komander & Rape, 2012). Three main types of substrate ubiquitylation have been identified: mono-ubiquitylation, multi-monoubiquitylation and poly-ubiquitylation. Mono-ubiquitylation refers to the attachment of a single Ub molecule to a specific residue of the substrate (Deng *et al.*, 2020; Kelsall, 2022). Mono-ubiquitylation is the most abundant ubiquitylation event and it regulates several cellular processes, including DNA repair, transcription, autophagy, endocytosis, signal transduction and also proteasomal degradation (Braten *et al.*, 2016; Deng *et al.*, 2020; Kliza & Husnjak, 2020). Multi-monoubiquitylation refers to the attachment of multiple single Ub moieties, each modifying a distinct residue of the target substrate. Multi-

monoubiquitylation is important for receptor endocytosis (Haglund *et al.*, 2003; Sadowski *et al.*, 2012) and for the regulation of signalling pathways (Pfleger, 2011; Deng *et al.*, 2020). Polyubiquitylation refers to the attachment of more than two Ub molecules (an Ub chain) to the same residue of the substrate (Deng *et al.*, 2020). Ubiquitin chains can be formed on any of the seven internal lysine (K) residues of an Ub molecule (K6, K11, K27, K29, K33, K48 and K63) or on its N-terminal methionine 1 (Met1) (Komander & Rape, 2012). Thus, there are eight structurally different types of Ub chains and each of them preforms distinct physiological functions (Rajalingam & Dikic, 2016; Deng *et al.*, 2020; Yang *et al.*, 2021). K48-linked chains target proteins for 26S proteasome-mediated degradation (Hershko & Ciechanover, 1998; Husnjak & Dikic, 2012; Rajalingam & Dikic, 2016); K6-linked chains are involved in the process of DNA repair (Husnjak & Dikic, 2012; Rajalingam & Dikic, 2016; Deng *et al.*, 2020); K11-linked chains play a role in cell cycle, in ERAD and mediate proteasomal degradation (Rajalingam & Dikic, 2016); K27-linked chains regulate autophagic clearance of damaged mitochondria (Geisler *et al.*, 2010; Deng *et al.*, 2020); K29-linked chains contribute to the turnover of substrates in the ubiquitin-fusion degradation pathway and play a role in the innate immune response (Metzger & Weissman, 2010; Husnjak & Dikic, 2012; Komander & Rape, 2012; Yu *et al.*, 2016) and K33-linked chains regulate intracellular protein trafficking and are also involved in innate immune response (Yuan *et al.*, 2014; Rajalingam & Dikic, 2016; Liu *et al.*, 2017). K63-linked Ub chains can regulate several biological processes, including autophagy, signal transduction, kinase activation and DNA damage response (Chen &

Sun, 2009; Husnjak & Dikic, 2012; Sadowski *et al.*, 2012; Wang *et al.*, 2012*a*; Rajalingam & Dikic, 2016; Dikic, 2017; Dósa & Csizmadia, 2022). Finally, Met1-linked chains or linear Ub chains are catalysed by linear ubiquitin chain assembly complex (LUBAC). Met1-linked chains can promote the activation of NF-κB signalling and are also capable of inhibiting type I interferon (IFN) signalling (Rahighi *et al.*, 2009; Tokunaga *et al.*, 2009; Belgnaoui *et al.*, 2012; van Huizen & Kikkert, 2020). Ubiquitin chains can be classified as homotypic or heterotypic based on the type of linkages that bind the adjacent Ub monomers within the Ub chain (Rajalingam & Dikic, 2016; French *et al.*, 2021; Gregor *et al.*, 2023). Homotypic chains are uniformly linked through the same acceptor site of Ub (there are only eight homotypic chains: Met1-, K6-, K11-, K27-, K29-, K33-, K48- and K63-linked Ub chains, previously mentioned), whereas heterotypic chains are linked through multiple sites, and can be further classified as mixed or branched. Mixed chains contain more than one type of linkage, but the Ub monomers are modified at a single acceptor site. Branched chains contain at least one Ub subunit modified simultaneously at more than one acceptor site, resulting in a branched or “forked” structure. In this way, there are numerous variations of heterotopic Ub chains (Rajalingam & Dikic, 2016; French *et al.*, 2021; Gregor *et al.*, 2023).

In addition to ubiquitylation, ubiquitin can also be modified by other PTMs, including phosphorylation, acetylation and ADP-ribosylation (Swatek & Komander, 2016; Kliza & Husnjak, 2020; Dikic & Schulman, 2023). Thus, these modifications add further complexity and diversity to the “ubiquitin code” (Swatek & Komander, 2016; Dikic & Schulman, 2023).

Deubiquitylases (DUBs)

Ubiquitylation is a reversible post-translational modification and the cleavage of ubiquitin from substrates or within ubiquitin chains is catalysed by ubiquitin-specific proteases, called deubiquitinases, deubiquitylases or deubiquitylating enzymes (DUBs) (Leznicki & Kulathu, 2017; Kelsall, 2022; Lange *et al.*, 2022). DUBs affect the cellular pool of free ubiquitin by releasing newly generated Ub from the Ub precursors, removing non-essential Ub and recycling Ub from previous ubiquitylation events (Kliza & Husnjak, 2020). According to sequence and structural similarities, DUBs can be classified into two main groups: cysteine proteases and metalloproteases. Among the cysteine proteases, characterized by a catalytic triad consisting of a conserved cysteine, a histidine, and typically an asparagine or aspartate residue, are the following families: Ubiquitin-specific proteases (USPs), Ubiquitin C-terminal hydrolases (UCHs), Ovarian tumour proteases (OTUs), Machado-Joseph disease proteases (MJDs), MINDY proteases (MIU-containing novel DUB family), and the ZUFSP family (Zinc finger with UFM1-specific peptidase domain protein). In contrast, the JAMM family (JAB1/MPN/Mov34 metalloenzymes) comprises zinc-dependent metalloproteases that catalyse isopeptide bond hydrolysis via a catalytic serine and a zinc ion cofactor. Except for the MJDs, the DUB families are highly conserved from yeast to humans (Li & Reverter, 2021; Snyder & Silva, 2021).

The deubiquitylating enzymes regulate fundamental cellular processes, such as the cell cycle, apoptosis, protein turnover, signalling pathways and gene transcription (Leznicki & Kulathu, 2017; Deng *et al.*, 2020; Lange *et al.*, 2022).

Proteasome

The 26S proteasome is a 2.5 MDa, ATP-dependent, multi-subunit protease complex, responsible for protein degradation in both the nucleus and cytoplasm of all eukaryotic cells (Bard *et al.*, 2018; Marshall & Vierstra, 2019) (Figure 1.6).

The 26S proteasome is composed of two functionally distinct sub-complexes: the 20S core particle (CP), which harbours peptidase activity, and one or two 19S regulatory particles (RP) that cap the CP and are responsible for substrate recognition, unfolding and translocation. The 20S CP has a barrel shape formed by four stacked hetero-heptameric rings: two outer α-rings and two inner β-rings, each composed of seven structurally similar α- and β-subunits, respectively. This arrangement results in a C2-symmetric configuration $\alpha_{1-7}/\beta_{1-7}/\beta_{1-7}/\alpha_{1-7}$. Upon assembly, a central chamber is formed at the interface of the β-rings, which houses six catalytic sites responsible for peptide bond cleavage. These sites are provided by β_1, β_2 and β_5 subunits, which confer caspase-like, trypsin-like and chymotrypsin-like cleavage activities, respectively (Murata *et al.*, 2009; Marshall & Vierstra, 2019) (Figure 1.6).

The main regulator of the 20S CP is the 19S RP. The 19S RP consists of at least 18 protein subunits and plays a crucial role in recognizing ubiquitylated substrates, driving their unfolding, opening the α-ring pore, importing substrates into the CP, and releasing the ubiquitin moieties before substrate degradation. The 19S RP can be divided into two subcomplexes: the base and the lid. The base is composed of six AAA-ATPase subunits, regulatory particle triple-A protein 1 (RPT1)–RPT6, and three non-ATPase subunits, regulatory particle non-ATPase 1 (RPN1), RPN2 and

RPN13. The ATPase subunits (RPT) couple ATP hydrolysis to substrate unfolding and the opening of the α-ring channel. The lid is composed of nine non-ATPase subunits: RPN3, RPN5–9, RPN11, RPN12 and RPN15 (also known as SEM1). A key function of the lid is the deubiquitylation of incoming substrates (Murata *et al.*, 2009; Marshall & Vierstra, 2019; Mao, 2021) (Figure 1.6).

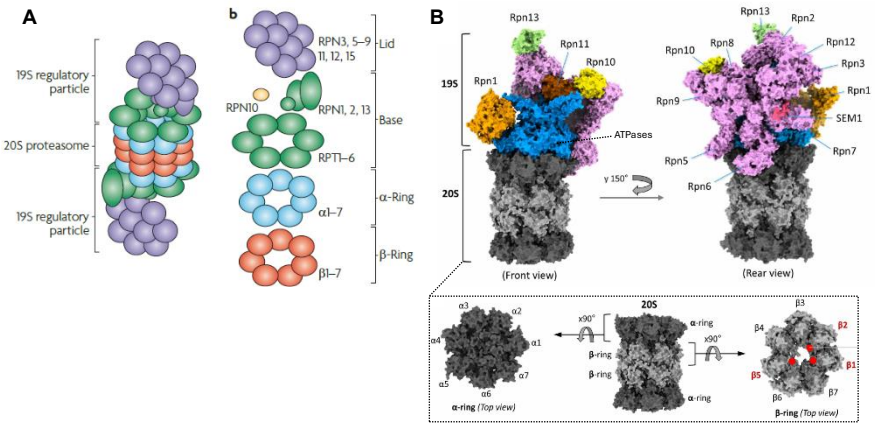

Figure 1.6: 26S Proteasome composition. (A) Diagram of 26S proteasome, consisting of the catalytic 20S proteasome (a barrel of four stacked rings: two outer α-rings and two inner β-rings) and the 19S regulatory particle (RP). The regulatory particle is further divided into the base and the lid, which are composed of regulatory particle triple-A (RPT) and regulatory particle non-ATPase (RPN) subunits. Adapted from (Murata *et al.*, 2009). **(B)** Cryo-electron microscopy structure (front, rear and top views) of the yeast 26S proteasome in resting state (PDB: 6j2x), containing the 20S catalytic core at dark and light grey and 19S regulatory particle coloured. Adapted from (Sahu & Glickman, 2021).

E3 ubiquitin ligases

The E3 ubiquitin ligases are the largest family of enzymes involved in the ubiquitylation cascade (Pickart & Eddins, 2004; Yang *et al.*, 2021; Kelsall, 2022). Based on their structure and function, they can be divided into four subfamilies: RING (Really Interesting New Gene), U-box, HECT (Homologous to E6AP Carboxyl Terminus) and RBR (RING-between-RING) (Figure 1.7).

The RING E3 ligases, characterized by the presence of an N-terminal zinc-binding domain (the RING domain), mediate the direct transfer of ubiquitin from the E2 ubiquitin-conjugating ligase to the target substrate. Among them are the monomeric RING ligases COP1 and Mdm2 and the multi-protein complex SCF (Skp–Cullin–F-box) (Pickart & Eddins, 2004; Deshaies & Joazeiro, 2009; Galimova *et al.*, 2021; Yang *et al.*, 2021).

The U-box E3 ligases contain a conserved C-terminal U-box domain, which is responsible for binding the E2 enzyme and stimulating the transfer of Ub to the substrate (Pickart & Eddins, 2004; Yang *et al.*, 2021; Kelsall, 2022). The E3 ubiquitin ligase CHIP belongs to this subfamily (Pickart & Eddins, 2004; Zhang *et al.*, 2005).

The HECT E3 ligases contain a conserved C-terminal HECT domain and are involved in the ubiquitylation of substrates via a two-step reaction: first, Ub is transferred from the E2 enzyme to the HECT catalytic cysteine (generating a thioester intermediate); second, Ub is transferred from the E3 ligase to the target substrate (Pickart & Eddins, 2004; Yang *et al.*, 2021). Nedd4 and E6-AP are proteins that belong to this subfamily (Galimova *et al.*, 2021; Yang *et al.*, 2021).

The RBR E3 ligases have two predicted RING domains (RING1 and RING2) separated by an IBR (in-between-RINGs) domain. RBR E3 ligases also mediate ubiquitylation of substrates through a two-step reaction: Ub is first transferred from E2 to a RING2 catalytic domain on the E3 enzyme and then Ub is transferred from E3 to the substrate (Yang *et al.*, 2021). This subfamily includes the E3 ubiquitin ligase Parkin (Galimova *et al.*, 2021).

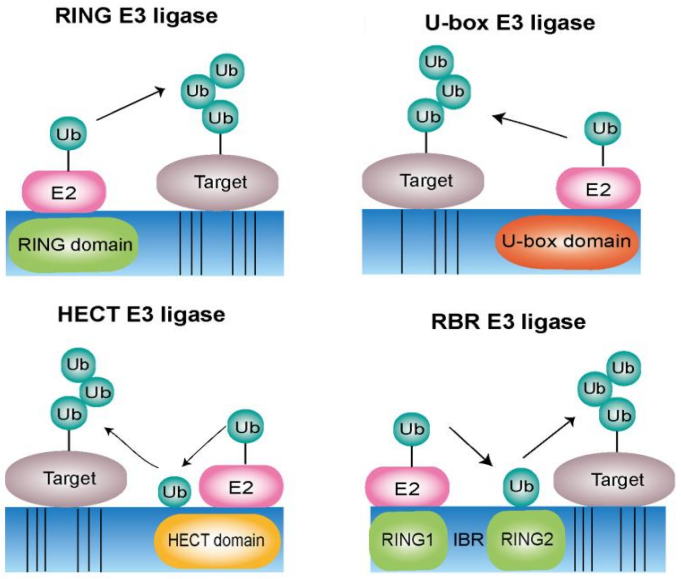

Figure 1.7: The different subfamilies of E3 ubiquitin ligases. The RING (Really Interesting New Gene) and U-box ligases stimulate direct transfer of ubiquitin to the substrate, whereas the HECT (Homologous to E6AP) and RBR (RING-between-RING) ligases mediate ubiquitylation of substrates through a two-step reaction. Adapted from (Yang *et al.*, 2021).

F-box proteins

F-box proteins are evolutionarily conserved among eukaryotes (Ho *et al.*, 2006). In the *Drosophila* genome, 45 genes encoding F-box proteins have been identified (Dui *et al.*, 2012). F-box proteins are E3 ubiquitin ligases and form complexes with Skp-1 (SkpA in *Drosophila*), Cullin-1 (Cul1) and Rbx-1/Roc-1 to mediate the ubiquitylation of specific substrates (Ou *et al.*, 2003; Ho *et al.*, 2006; Dui *et al.*, 2012) (Figure 1.8). These complexes are called SCF (Skp–Cullin–F-box) (Ho *et al.*, 2006; Dui *et al.*, 2012). Within the complex, Cul1 functions as a scaffold protein that interacts with Rbx-1 at its C-terminus to recruit a specific ubiquitin-conjugating enzyme (E2) (Ho *et al.*, 2006). At the N-terminus, Cul1 interacts with Skp-1, which in turn binds to the conserved F-box domain [containing approximately fifty amino acids and named after the presence of this motif in mammalian cyclin F protein (Chang *et al.*, 1996)] of an F-box protein (Ou *et al.*, 2003; Ho *et al.*, 2006). The main role of the F-box proteins is substrate recognition through substrate-binding motifs (Ou *et al.*, 2003). Based on their C-terminus domains, F-box proteins have been classified into three subfamilies: FBXW contains F-box proteins with WD-40 repeat domains [featuring four or more repeat units with a conserved core of approximately forty amino acids, often terminating in a tryptophan-aspartic acid (W-D) dipeptide (Li & Roberts, 2001)], their substrate-binding domain is a β-propeller structure; FBXL harbours F-box proteins with leucine-rich repeats (LRRs), their substrate-binding domain is an arc-shaped α-β-repeat structure and FBXO consists of F-box proteins that do not have WD-40 repeats or LRRs, on the other hand they present different protein-protein interaction

domains at the C-terminus, such as carbohydrate-interacting (CASH), zinc-finger and proline-rich domains (Winston *et al.*, 1999; Kipreos & Pagano, 2000; Cardozo & Pagano, 2004; Jin *et al.*, 2004; Ho *et al.*, 2006; Dui *et al.*, 2012).

In general, a single F-box protein may ubiquitylate multiple substrates, and binding between F-box proteins and their substrates may require substrate phosphorylation (Jackson *et al.*, 2000; Kipreos & Pagano, 2000; Ou *et al.*, 2003). In SCF complexes, F-box proteins are responsible for substrate specificity. Notably, F-box proteins are involved in several cellular processes, such as DNA replication, transcription, cell differentiation and cell death (Ho *et al.*, 2006).

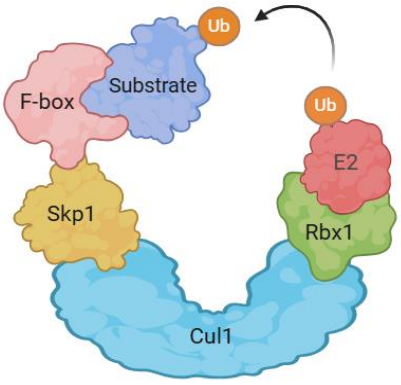

Figure 1.8: SCF (Skp–Cullin–F-box) complex. Created in BioRender.

The Fbxo42 protein

Fbxo42 (F-box only protein 42) belongs to the Fbxo subfamily of the F-box proteins and associates with SkpA, Cullin-1 and Rbx-1/Roc-1 to form an SCF complex, mediating the ubiquitylation of specific substrates. Structurally, Fbxo42 contains an F-box domain at its N-terminus, which binds Skp1 in the SCF

complex and is predicted to also contain Kelch-repeat domains (with a β-propeller architecture) that are involved in protein-protein interactions (Robinson & Cooley, 1997; Adams *et al.*, 2000; Das *et al.*, 2002).

A recent study has shown that Fbxo42 is important for the assembly and maintenance of the synaptonemal complex in *Drosophila* female meiosis by down-regulating the protein levels of the phosphatase PP2A-B56 (Barbosa *et al.*, 2021). However, so far, no other biological functions have been reported for this *Drosophila* F-box protein.

Drosophila Fbxo42 is orthologous to the human *FBXO42* gene. For human FBXO42 protein, several substrates have been identified and different biological roles have been described. Sun and collaborators have shown that FBXO42 (called JFK in their study), through the assembly of an SCF complex, promotes the ubiquitylation and degradation of the tumour suppressor protein p53, thereby regulating p53-mediated transcriptional activation, p53-induced apoptosis, growth suppression and cell cycle checkpoint control (Sun *et al.*, 2009, 2011). Another study reported that FBXO42 (through the association of an SCF complex) also targets the tumour suppressor ING4 for ubiquitylation and degradation (Yan *et al.*, 2015). Destabilization of ING4 induces NF-κB signalling and promotes angiogenesis and metastasis of breast cancer (Yan *et al.*, 2015). Recently, RBPJ was identified as a substrate of FBXO42 (Jiang *et al.*, 2022). FBXO42-mediated Lysine 63-linked polyubiquitylation (not associated with protein degradation) of RBPJ was shown to be involved in Notch signalling activation (Jiang *et al.*, 2022). Furthermore, FBXO42 depletion was

found to attenuate the development of Notch signalling-related leukaemia *in vivo* (Jiang *et al.*, 2022).

Toledo and collaborators performed a genome-wide screen of glioblastoma stem-like cells (GSCs), and found that some GSC isolates were highly dependent on FBXO42 for growth (Toledo *et al.*, 2015). This finding was later supported by a functional genomic lethality screen comparing glioblastoma stem-like cells and control human neural stem cells showing that FBXO42 activity is required for glioblastoma cell viability (Hoellerbauer *et al.*, 2024). Mechanistic studies showed that FBXO42 activity prevented chromosome alignment defects, mitotic cell cycle arrest and cell death (Hoellerbauer *et al.*, 2024). However, the authors did not identify the FBXO42 targets responsible for the observed phenotypes. p53, ING4 and RBPJ, previously reported substrates of FBXO42, were tested, but none of them were associated with the results obtained (Hoellerbauer *et al.*, 2024). These findings were consistent with a previous work from Hundley and collaborators demonstrating that *FBXO42* depletion causes sensitivity to different mitotic inhibitors, delays in cell cycle progression and aberrant mitosis (Hundley *et al.*, 2021).

Recently, Zhou and collaborators identified *FBXO42* as a tumour-promoting factor in neuroblastoma. They showed that FBXO42 promotes neuroblastoma cell proliferation by down-regulating p53 protein levels (Zhou *et al.*, 2024).

1.6 Ataxin-2

Ataxin-2 is an RNA-binding protein (RBP) highly conserved from yeast to mammals (Jiménez-López & Guzmán, 2014; Lee *et al.*, 2018). In *Drosophila*, Ataxin-2 is encoded by a single gene, which is essential for fly survival (Bakthavachalu *et al.*, 2018). In contrast, mammals contain two homologous genes, ATXN2 and ATXN2-L (Ataxin-2-like). ATXN2-L is similar to ATXN2 and provides partially overlapping cellular functions (Jiménez-López & Guzmán, 2014; Bakthavachalu *et al.*, 2018). The presence of ATXN2-L likely explains why ATXN2 knockout mice are viable and display no obvious defects at birth, with only relatively subtle phenotypes in late adult life (Kiehl *et al.*, 2006). Therefore, since the ATXN2-L gene is absent in flies, they are an ideal model organism to investigate the physiological function of Ataxin-2.

Molecular domains of Ataxin-2

All Ataxin-2 proteins, from yeast to mammals, share two conserved domains at the N-terminus – the like-Sm (LSM) domain and the LSM-associated domain (LSM-AD) (Figure 1.9). The LSM domain is involved in RNA binding and in RNA processing events, including RNA modification, pre-mRNA splicing and mRNA decay (Albrecht *et al.*, 2004; Li *et al.*, 2024). The LSM-AD domain harbours an ER exit signal and a clathrin-mediated trans-Golgi signal (Albrecht *et al.*, 2004; Costa *et al.*, 2024). The Ataxin-2 homologs also share a C-terminal poly(A)-binding protein (PABP) interacting motif 2 (PAM2), which enables the physical interaction between Ataxin-2 and PABP (Albrecht *et al.*, 2004; Lee *et al.*, 2018; Costa *et al.*, 2024) (Figure 1.9). The PABP binds to the poly(A) tail of mRNAs

and is essential for translation initiation and mRNA decay (Jiménez-López & Guzmán, 2014). Furthermore, insect Ataxin-2 and mammalian ATXN2 (but not the related ATXN2-L) also contain endogenous polyglutamine (polyQ) repeats (Bakthavachalu *et al.*, 2018). Human ATXN2 contains an uninterrupted polyQ tract of 22-23 repeats, located in the N-terminal region (Figure 1.9). Among insects, all species from the order Diptera (which includes the family Drosophilidae) contain more than one polyQ tract, with variable sizes of polyQ residues, located between the LSM-AD and PAM2 domains (Jiménez-López & Guzmán, 2014; Lee *et al.*, 2018). In humans, mutations resulting in the expansion of the polyQ tract in the ATXN2, give rise to neurodegenerative diseases. Intermediate-length polyQ expansions (from 27 to 33 repeats) increase Amyotrophic Lateral Sclerosis (ALS) risk (Elden *et al.*, 2010), whereas longer expansions (>34 repeats) cause Spinocerebellar Ataxia type-2 (SCA2) (Riess *et al.*, 1997; Elden *et al.*, 2010). Moreover, intermediate-length expansions of the ATXN2 polyQ tract were also associated with Parkinson's disease (Gwinn-Hardy *et al.*, 2000; Satterfield & Pallanck, 2006).

Additionally, Ataxin-2 proteins contain intrinsically disordered regions (IDRs). In *Drosophila*, two IDRs were identified: the intermediate IDR (mIDR), comprising polyQ and prion-like motifs, and the C-terminal IDR (cIDR) (Bakthavachalu *et al.*, 2018). It was demonstrated that these IDRs function to support the assembly of messenger ribonucleoproteins (mRNPs) into granules in *Drosophila* neurons (Bakthavachalu *et al.*, 2018) (Figure 1.9).

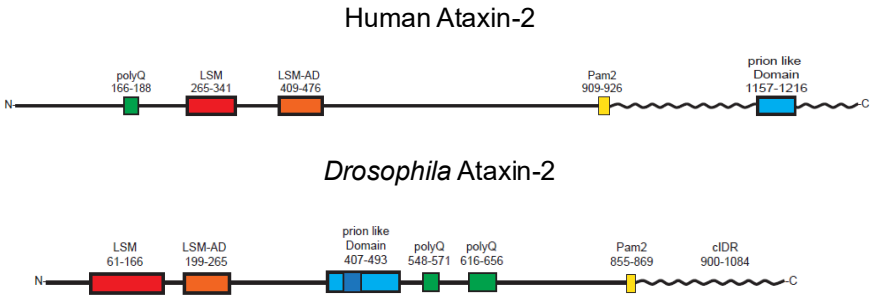

Figure 1.9: Schematic representation of human and *Drosophila* Ataxin-2 proteins. At the N-terminus are the conserved LSM (red box) and LSM-AD (orange box) domains. At the C-terminal is the conserved PAM2 motif (yellow box). PolyQ domains (green boxes) differ in number and location between human and *Drosophila*. In addition, prion-like domains (blue box) vary in size and location between human and fly. Adapted from (Bakthavachalu *et al.*, 2018).

Molecular functions of Ataxin-2

mRNA metabolism and translation

Ataxin-2 is involved in several steps of mRNA metabolism, including mRNA stabilization, splicing and decay. Studies employing PAR-CLIP and high-throughput sequencing techniques have demonstrated that human ATXN2 can enhance the stability of its target mRNAs and increase their corresponding protein abundance, by binding to AU-rich regions, within the 3' UTRs of these mRNAs (Yokoshi *et al.*, 2014). This interaction is mediated by the ATXN2 LSM domain, in a PABP-independent manner (Yokoshi *et al.*, 2014). Furthermore, another study showed that *Drosophila* Atx-2 stabilizes the majority of its target mRNAs, by binding to AU-rich elements in the 3' UTRs of these targets (Singh *et al.*, 2021) (Figure 1.10).

ATXN2 interacts with proteins associated with RNA alternative splicing, including Ataxin-2 binding protein 1 (A2BP1), RNA-binding motif protein 9 (RBM9) and the RNA-binding protein with multiple splicing (RBPMS), and in this manner ATXN2 might modulate RNA splicing. However, further studies are required to clarify the mechanisms behind this regulation (Shibata *et al.*, 2000; Magaña *et al.*, 2013; Costa *et al.*, 2024) (Figure 1.10).

ATXN2 may stabilize its associated mRNAs by inhibiting mRNA decay induced by deadenylation (Li *et al.*, 2024). In yeast, it has been shown that Ataxin-2 participates in the regulation of mRNA poly(A) tail length by inhibiting the activity of the poly(A) nuclease (PAN) deadenylation complex (Mangus *et al.*, 1998, 2004). Moreover, it has been shown that human ATXN2 enhances translation through post-transcriptional polyadenylation of the target mRNAs, including cyclin D1 and TDP-43 (Inagaki *et al.*, 2020). In this context, ATXN2 physically interacts with PABPC1 and PAPD4, inducing the lengthening of the poly(A) tail, which leads to the activation of translation (Inagaki *et al.*, 2020).

On the other hand, Ataxin-2 can repress the translation of target mRNAs. In *Drosophila*, depletion of Atx-2 in projecting neurons of antenna lobes impairs long-term olfactory habituation (McCann *et al.*, 2011). In this context, strong genetic interactions of Atx-2 with the microRNA pathway proteins Me31B and argonaute 1 (ago1, a key player in microRNA-mediated gene silencing) have been demonstrated, indicating that Atx-2 is necessary for long-term olfactory habituation, through microRNA-mediated translation repression (McCann *et al.*, 2011; Lee *et al.*, 2018) (Figure 1.10).

Furthermore, it was shown that Atx-2 also interacts with Fragile X mental retardation protein (FMRP) and that translation of the mRNA encoding Ca^{2+}/calmodulin-dependent protein kinase II (CaMKII) undergoes translational repression via this Atx-2-FMRP complex (Sudhakaran *et al.*, 2014). As CaMKII is necessary for long-term olfactory habituation, these data indicate that FMRP and Atx-2 act via at least one common mRNA target for long-term synaptic plasticity (Sudhakaran *et al.*, 2014). These studies identified Ataxin-2 as a component of the microRNA pathway.

Biochemical studies showed that Ataxin-2 plays a crucial role in the regulation of translation (Figure 1.10). In 2006, Satterfield and Pallack demonstrated that both human ATXN2 and *Drosophila* Atx-2 interact directly with translational machinery by assembling with polyribosomes (Satterfield & Pallanck, 2006). The assembly of *Drosophila* Atx-2 with polyribosomes was further shown to be mediated independently by the LSM/LSM-AD domains and the PAM2 motif of Atx-2 (Satterfield & Pallanck, 2006). Through the PAM2 motif, the authors proposed that Atx-2 is also able to bind to mRNA poly(A)-bound PABP, promoting or preventing the interaction between PABP and the translation initiation complex. PABP promotes translation by physically interacting with eIF4G, a component of the 5' cap-binding translation initiation complex. It has been suggested that, Atx-2 may influence the activity of PABP in a way to promote or inhibit translation of particular mRNA targets (Satterfield & Pallanck, 2006; Nóbrega *et al.*, 2015).

Furthermore, Satterfield and Pallanck showed that although both human and *Drosophila* Ataxin-2 assemble with polyribosomes, they are not structural components of ribosomes. Instead, it was

suggested that Ataxin-2 assembles into mRNP complexes (Satterfield & Pallanck, 2006).

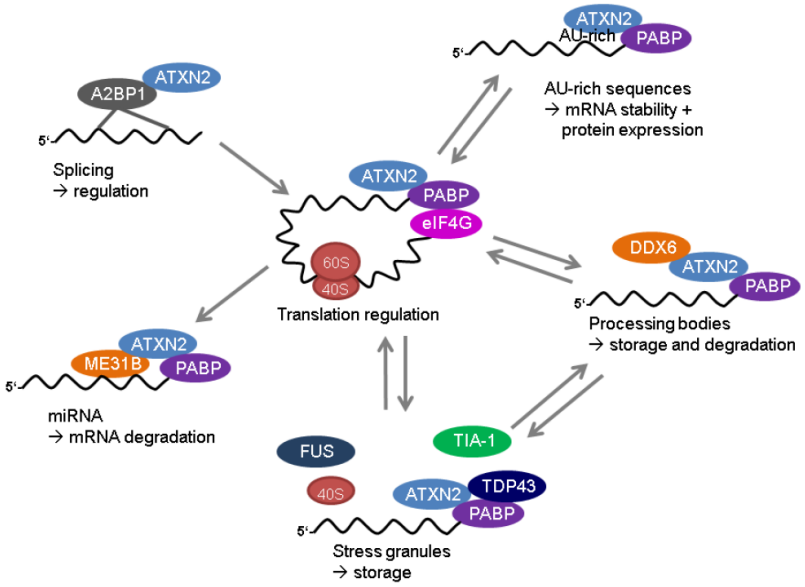

Figure 1.10: Molecular functions of Ataxin-2 protein. Ataxin-2 functions in translation regulation by binding to PABP, regulating PABP-dependent processes. Moreover, Ataxin-2 is involved in several biological processes, including mRNA stabilization, translation regulation, splicing modulation and miRNA-mediated mRNA degradation. Under stress conditions, Ataxin-2 has been found in stress granules and processing (p)-bodies. Adapted from (Halbach, 2015).

Ataxin-2 as a component of cytoplasmic granules

When cells are exposed to environmental stress, such as heat, oxidative conditions, viral infections, UV irradiation and hypoxia, one of their responses is the formation of membrane-less organelles called stress granules (SGs) (Anderson & Kedersha, 2006; Protter & Parker, 2016; Buddika *et al.*, 2020; Marcelo *et al.*, 2021). These are messenger ribonucleoprotein (mRNP) granules,

harbouring non-translating mRNAs. Their formation is associated with a global reduction in protein translation (Buddika *et al.*, 2020; Marcelo *et al.*, 2021). The assembly of SGs is essential for cell survival, as SGs are involved in regulating translation, mRNA storage and stabilization, and cell signalling during cellular stress (Marcelo *et al.*, 2021). A defining characteristic of SGs is their dynamism, as these foci rapidly assemble upon stress induction and quickly disperse when stress conditions subside (Marcelo *et al.*, 2021).

Based on biochemical experiments, SGs contain a solid core surrounded by a liquid-like shell that enhances the rapid exchange of molecules with the cytoplasm (Buddika *et al.*, 2020). The formation of SGs when translation initiation is inhibited suggests that these granules contain mRNAs stalled in the translation initiation process, which is consistent with their composition. SGs are mainly composed of poly(A)$^+$ mRNAs, translation initiation factors, 40S ribosomal subunits and several RBPs (Figure 1.11) (Buchan & Parker, 2009; Buddika *et al.*, 2020; Marcelo *et al.*, 2021). While the components and requirements for SG formation can differ depending on stress treatment, a few of these RBPs are considered integral to SG assembly. Among the integral components are Ataxin-2, PABP, G3BP1/2, TIA1 and TIA1-related family proteins (Buddika *et al.*, 2020; Marcelo *et al.*, 2021). Overexpression of these integral RBPs can induce SG-like structures in the absence of stress, while their knockdown or elimination interferes with SG formation (Buddika *et al.*, 2020). SGs can be distinguished from other types of granules by the presence of marker protein TIA-1 (Li *et al.*, 2024).

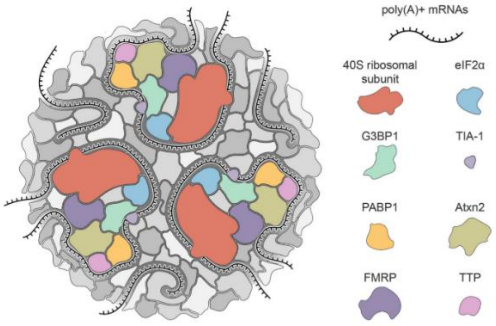

Figure 1.11: Stress granule components. Stress granules are multimolecular foci that assemble as part of the cellular response to stress. They are mainly composed of poly(A)+ mRNA molecules, translation initiation factors (including eIF2α), 40S ribosomal subunits and RBPs, such as, G3BP1, TIA-1, PABP1, Ataxin-2, FMRP and TTP. The unspecified shapes, coloured in greyscale, represent the remaining proteins that have been associated with SG (Marcelo *et al.*, 2021).

The assembly of SGs is advantageous in the context of cellular stress for several reasons, including: i) important cellular molecules are protected from degradation upon SG assembly during stress, and ii) SG disassembly after stress relief allows cells to have proteins and mRNA ready for use (Marcelo *et al.*, 2021).

In addition to be a core component of SGs, several studies demonstrated that Ataxin-2 influences SG formation and regulation. It is noteworthy that siRNA-mediated knockdown of human ATXN2 in HEK293T cells decreases the number and size of stress granules (Nonhoff *et al.*, 2007; Ostrowski *et al.*, 2017). Moreover, genomic deletion of the yeast orthologue of *ATXN2* leads to a strong reduction in stress granule formation under glucose deprivation (Buchan *et al.*, 2008). Becker and collaborators observed that *Ataxin-2* knockdown in U2OS cells delayed the maturation of SGs –

at each time point, the SGs were smaller and in this case more numerous than in the control condition (Becker *et al.*, 2017). Furthermore, the expression level of human ATXN2L protein is positively correlated with SG formation (Kaehler *et al.*, 2012).

It was showed that a distinct class of cytoplasmic RNA granules, called Processing (P)-bodies, can co-localize with stress granules under specific stress conditions (Kedersha *et al.*, 2005). P-bodies contain components of the 5'-3' mRNA decay machinery, the nonsense-mediated decay pathway and the RNA-induced silencing complex (Anderson & Kedersha, 2006). These RNA granules have been implicated in mRNA decapping, nonsense-mediated decay, mRNA storage, general translation repression, microRNA-mediated repression and viral life-cycles (Buchan *et al.*, 2008). Yeast two-hybrid experiments revealed that human ATXN2 interacts with the key P-body component the RNA helicase DDX6 (Nonhoff *et al.*, 2007; Ostrowski *et al.*, 2017). Moreover, immunofluorescence assays indicated that ATXN2 and DDX6 co-localize under stress conditions (Nonhoff *et al.*, 2007; Ostrowski *et al.*, 2017). Additionally, overexpression of ATXN2 disrupts DDX6-marked P-bodies, causing them to appear more diffuse in the cytoplasm, and leading to a decrease in the number of P-bodies. This result suggests that high ATXN2 levels interfere with P-body structures (Nonhoff *et al.*, 2007; Ostrowski *et al.*, 2017).

Other cellular functions of Ataxin-2 include regulation of actin filament formation in the female germline (Satterfield *et al.*, 2002), microtubule organization in mitosis (Gnazzo *et al.*, 2016) and calcium mediated signalling (Costa *et al.*, 2024).

Several studies demonstrated that Ataxin-2 is involved in a wide variety of physiological processes such as, regulation of circadian rhythm (Lim & Allada, 2013; Zhang *et al.*, 2013), long-term memory (Bakthavachalu *et al.*, 2018) and metabolism regulation (Carmo-Silva *et al.*, 2017).

Expression of the Ataxin-2 protein

Human ATXN2 is a ubiquitous protein, being expressed in every organs, with highest expression levels in the nervous system, specifically in cerebellar Purkinje cells, where its expression increases with age (Ostrowski *et al.*, 2017; Costa *et al.*, 2024). ATXN2 localizes to cytoplasmic puncta (Lee *et al.*, 2018). At the subcellular level, ATXN2 is present in the endoplasmic reticulum, Golgi apparatus and RNA granules (Costa *et al.*, 2024).

Drosophila Atx-2 is also ubiquitously expressed, presenting high expression levels in the central nervous system (Satterfield *et al.*, 2002) and ovaries (Satterfield *et al.*, 2002; Vianna *et al.*, 2016). Consistent with the subcellular localization of human ATXN2, *Drosophila* Atx-2 localizes mostly to the cytoplasm (Satterfield *et al.*, 2002).

1.7 The Drosophila eye

The *Drosophila* eye is composed of approximately 800 hexagonal units, called ommatidia. Each ommatidial unit contains 8 photoreceptor cells, 4 cone cells and 2 primary pigment cells and is surrounded by a hexagonal lattice of 12 interommatidial cells,

including bristle, secondary and tertiary pigment cells (Mollereau & Domingos, 2005) (Figure 1.12).

Photoreceptor (PR) cells can be divided into two main classes, according to their morphology and functional properties: the outer (R1–R6) and the inner PRs (R7 and R8). The outer PRs (R1–R6) extend the full depth of the retina and assemble together forming a trapezoidal pattern surrounding the two inner photoreceptors (R7 and R8). R7 and R8 occupy the distal and proximal regions of the ommatidia, respectively (Wang & Montell, 2007), span approximately half of the retina, and R7 is located on top of R8 (Mollereau & Domingos, 2005) (Figure 1.12B). Furthermore, outer PRs express only one type of rhodopsin (Rh1), and are involved in image formation, motion detection and vision in dim light (Cook & Desplan, 2001; Mollereau & Domingos, 2005). In contrast, inner PRs are involved in colour vision and express several rhodopsins, specifically, R7 cells express UV-sensitive Rh3 or Rh4, while R8 cells express either blue-sensitive Rh5 or green-sensitive Rh6 (Mollereau & Domingos, 2005; Sharkey *et al.*, 2020).

In *Drosophila*, the photoreceptive membrane is organized into tightly packed, tubular microvilli, together forming a rhabdomere (Hardie & Raghu, 2001). Approximately 50 000 microvilli are present in the R1–R6 and about 17 000 microvilli are present in the R7/R8 cells (Wang & Montell, 2007; Montell, 2012).

The main cells that surround the photoreceptor cells are secondary pigment cells. The vertices of the ommatidia alternate between tertiary pigment cells and mechanosensory bristle cells (Figure 1.12C) (Wang & Montell, 2007).

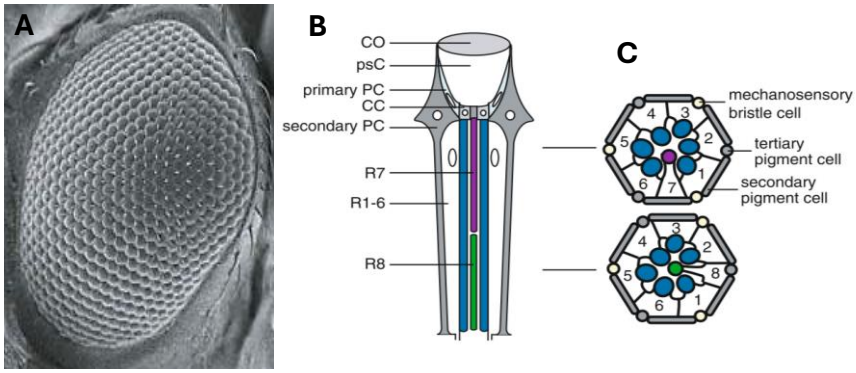

Figure 1.12: Structure of the *Drosophila* compound eye. (A) Scanning electron micrograph of a *Drosophila* eye. **(B)** Single ommatidium at an angle of 90° from the surface of the compound eye: CO, cornea; psC, pseudocone; primary PC, primary pigment cell; CC, clone cell; secondary PC, secondary pigment cell. R1–6, photoreceptor cells 1–6; R7, photoreceptor cell 7; R8, photoreceptor cell 8. **(C)** Cross-sections through the distal and proximal regions of the ommatidia. Seven photoreceptor cells are present in any given plane of section. The ovals represent the rhabdomeres. The R cell bodies are numbered. A secondary pigment cell, a tertiary pigment cell and a mechanosensory bristle cell are indicated. Adapted from (Wang & Montell, 2007).

The *Drosophila* adult eye develops from a larval primordium known as the eye-antennal imaginal disc. In addition to the adult eye, the eye-antennal imaginal disc also gives rise to antenna, ocelli and other head structures. The eye disc is an epithelial bilayer: one layer, called the disc proper, is composed of columnar cells and gives rise to the retina; while the other layer, the peripodial membrane, plays a role in modulating the fates of columnar cells. Disc proper cells divide, grow and then differentiate into photoreceptors and accessory cells (Billes *et al.*, 2018). During the first two larval instar stages, cells of the eye imaginal disc remain undifferentiated. In the third larval instar, photoreceptor differentiation begins at the posterior margin of the eye disc and

progresses anteriorly in a wave of differentiation, following a dorsal-ventral groove known as the morphogenetic furrow (MF) (Moses, 2002) (Figure 1.13A). The photoreceptor differentiation occurs progressively over a two-day period. The MF is formed through apical constriction and apical-basal contraction of the epithelial cells (Roignant & Treisman, 2009). Anterior to the MF, cells are undifferentiated and actively undergo cell division. Immediately anterior to and within the MF, cells become arrested in G1 phase of the cell cycle (Ou *et al.*, 2003; Estella & Baonza, 2015). As cells emerge from the furrow, most exit the cell cycle and begin differentiating (Kumar, 2018). Neuronal differentiation is initiated with the selection of R8 photoreceptor precursors from preclusters, followed by sequential recruitment of the R2/R5 and R3/R4 photoreceptor pairs (Ou *et al.*, 2003; Kumar, 2018). A subset of the remaining undifferentiated cells undergoes a final round of division (the second mitotic wave), which gives rise to R1/R6 and R7 photoreceptors, as well as lens secreting cone cells and pigment cells (Kumar, 2018).

Several signalling pathways are involved in the formation and progression of the MF. A key signal driving the initiation and advancement of the MF is the Hedgehog (Hh) protein. Hh is initially expressed at the posterior margin of the eye disc prior to MF initiation and induces the differentiation of adjacent anterior cells. As these anterior cells begin differentiating into photoreceptors, they in turn start expressing Hh, thereby propagating the furrow anteriorly. Hh signalling activates decapentaplegic (Dpp), a member of the Bone Morphogenic Protein (BMP) family, which also contributes to MF progression. Another crucial Hh target is the transcription factor

Atonal (Ato), which is required for the specification of R8 cells. Ato is initially expressed in a broad stripe anterior to the MF, and its expression is progressively refined to single R8 cells within the MF, this process requires lateral inhibition mediated by Notch receptor (Roignant & Treisman, 2009) (Figure 1.13B). Once specified, R8 photoreceptors coordinate subsequent ommatidial development by recruiting surrounding uncommitted cells to differentiate into other photoreceptors, cone and pigment cells. The secretion of the epidermal growth factor receptor (EGFR) ligand Spitz from R8 and subsequently recruited cells promotes the sequential differentiation of photoreceptors R2/R5, R3/R4, R1/R6 and R7, followed by cone cells, primary pigment cells, as well as the survival of secondary and tertiary pigment cells (Roignant & Treisman, 2009).

On the other hand, several signalling mechanisms act to constrain the pace and ensure the precise positioning of the MF. Hedgehog not only promotes MF progression but also plays a critical role in controlling its precise spatial position. One of the Hedgehog downstream targets, Dpp, represses the expression of Homothorax (Hth), a transcription factor that prevents retinal differentiation at the anterior margin of the eye disc. This repression allows cells to enter a preproneural (PPN) state. Dpp also induces the expression of Hairy (H) within the preproneural domain. Hairy functions as a repressor of Ato, thereby preventing premature differentiation of photoreceptors. Interestingly, Hth has also been shown to repress Hairy. The down-regulation of Hairy, which is necessary to relieve the repression on Ato and allow R8 specification, requires a signal provided by Delta (Dl), a transmembrane ligand for the Notch receptor expressed in MF

under the control of Hedgehog and Dpp (Roignant & Treisman, 2009) (Figure 1.13B).

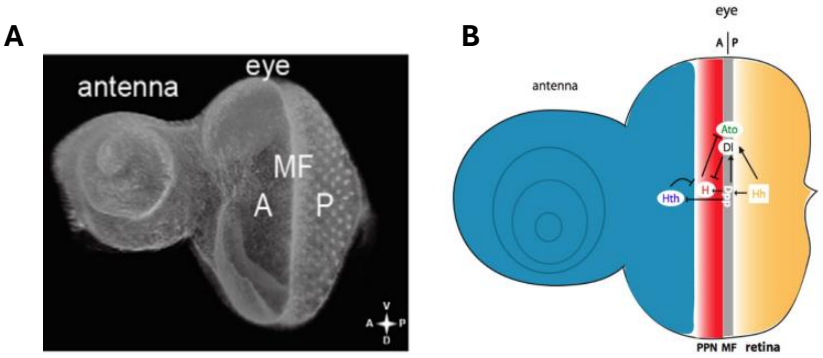

Figure 1.13: The eye-antennal imaginal disc and its components. (A) 3D reconstruction of the eye-antennal imaginal disc. The prospective antenna and eye are labelled. MF, morphogenetic furrow; A, anterior area; P, posterior area. Axes are marked as V (ventral), D (dorsal), A (anterior) and P (posterior) (Vollmer *et al.*, 2016). **(B)** Schematic representation of the eye imaginal disc with the signalling mechanisms that control the precise position of the MF. Hedgehog (Hh) induces the expression of Decapentaplegic (Dpp), which diffuses over a long range to turn off Homothorax (Hth) and turn on Hairy (H), establishing a preproneural domain (PPN). Hh and Dpp also induce the expression of Delta (Dl), a transmembrane ligand that acts on adjacent cells to turn off Hairy and allow Atonal (Ato) expression, initiating photoreceptor differentiation (Roignant & Treisman, 2009).

1.8 The GAL4/UAS system

The GAL4/UAS expression system allows ectopic expression of a gene of interest in a specific tissue or cell type (Brand & Perrimon, 1993) (Figure 1.14). This bipartite system is based on the properties of the yeast *Saccharomyces cerevisiae* GAL4 transcription factor, which activates the transcription of its target genes by binding to specific cis-regulatory sites, termed as

UAS (Upstream activating sequence). In *Drosophila*, the two components of the system are carried in two separate parental lines: the GAL4 driver line and the effector line. The GAL4 driver line harbours the GAL4 transcription factor under the control of an endogenous promoter or enhancer (allowing GAL4 expression in a specific tissue or cell type). The effector line carries the gene of interest under the control of a UAS, the GAL4 binding motif. The UAS-transgene is inactive in the absence of GAL4. Upon crossing the driver and effector lines, the progeny inherits both components, and the target gene will be expressed in the GAL4 specific tissue or cell type (Brand & Perrimon, 1993; Odenthal & Brinkkoetter, 2019) (Figure 1.14).

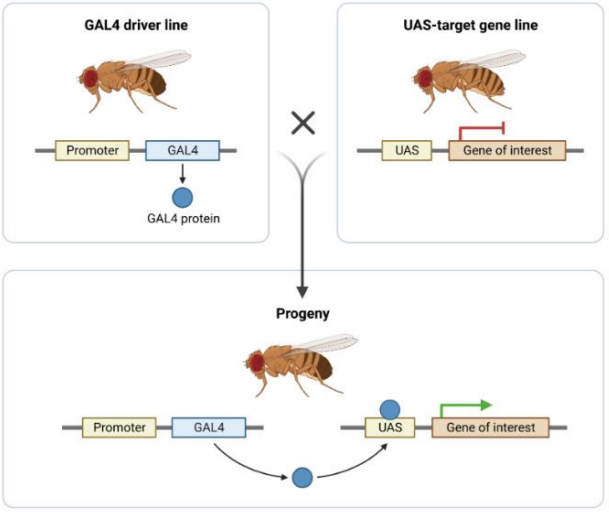

Figure 1.14: *Drosophila* GAL4/UAS system. After crossing the GAL4 driver line and the effector line (bearing the gene of interest under the control of an Upstream activating sequence, UAS), the progeny will express the gene of interest in the GAL4 specific tissue or cell type. Template from BioRender.

1.9 The Flippase/FRT system

The Flippase (Flp) /FRT system utilizes Flippase (a yeast site-specific recombinase) to mediate DNA recombination between homologous chromosomes at defined Flippase Recombination Target (FRT) sites. When recombination occurs in mitotically dividing heterozygous cells (+/–), chromosome segregation can result in the formation of two daughter cells that are homozygous for the respective alleles (+/+ and –/–) in the recombined region (Zhou *et al.*, 2017).

In *Drosophila*, the Flp/FRT system is widely used to induce the formation of mutant clones. Flp recombinase drives site-specific recombination between FRT sites located on homologous chromosomes. If somatic recombination occurs in a heterozygous cell carrying a mutation of interest, subsequent cell divisions can generate two distinct populations of daughter cells: one homozygous for the mutant allele (mutant clone) and the other homozygous for the wild-type allele (twin-spot clone) (Tabata, 2001) (Figure 1.15). To facilitate clone identification, a cellular marker, such as GFP, can be placed in trans to the mutant allele in the parental genotype. After recombination, the homozygous mutant clone will lack the marker, while the twin-spot clone will exhibit two copies of the marker (Tabata, 2001) (Figure 1.15).

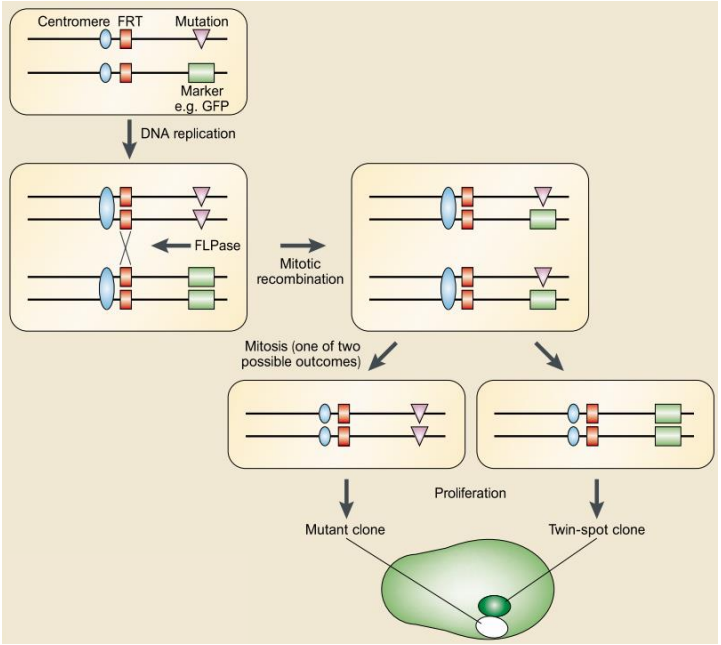

Figure 1.15: Flippase/FRT system. Mitotic recombination can be induced between FRT sites of homologous chromosomes by a site-specific recombinase (Flipasse, FLPase). When somatic recombination occurs in a cell that is heterozygous for a mutant gene of interest, the resulting cell divisions can give rise to two populations of daughter cells, one homozygous for the mutant gene of interest (mutant clone) and another mutant for its wild-type gene (twin-spot clone). Adapted from (Tabata, 2001).

1.10 Scope of this thesis

A previous work performed in our laboratory showed that the overexpression of Xbp1s, an important UPR mediator, leads to cell death and retinal degeneration. In attempt to rescue this phenotype, a genetic screen was performed. Through this screen, we found several loss-of-function mutations in the *Fbxo42* gene. Therefore, with this work, our major aim is to understand the mechanism behind the rescue of the Xbp1s-induced cell death by *Fbxo42* mutants.

Additionally, this thesis aims to address the following objectives:

1- Analyse the cellular and tissue localization of the F-box protein Fbxo42, through the production of an antibody against Fbxo42.

2- Identify the specific substrates of Fbxo42 by proteomics.

3- Confirm the proteomic results by immunofluorescence and biochemical experiments.

4- Analyse the interaction between Fbxo42 and Ataxin-2, through co-immunoprecipitation and immunofluorescence assays.

5- Investigate the role of Ataxin-2 on Xbp1 mRNA stability and translation.

1.11 References

Acosta-Alvear D, Karagöz GE, Fröhlich F, Li H, Walther TC & Walter P (2018). The unfolded protein response and endoplasmic reticulum protein targeting machineries converge on the stress sensor IRE1. *Elife*; DOI: 10.7554/eLife.43036.

Adams CJ, Kopp MC, Larburu N, Nowak PR & Ali MMU (2019). Structure and molecular mechanism of ER stress signaling by the unfolded protein response signal activator IRE1. *Front Mol Biosci* **6,** 1–12.

Adams J, Kelso R & Cooley L (2000). The kelch repeat superfamily of proteins: propellers of cell function. *Trends Cell Biol* **10,** 17–24.

Albrecht M, Golatta M, Wüllner U & Lengauer T (2004). Structural and functional analysis of ataxin-2 and ataxin-3. *Eur J Biochem* **271,** 3155–3170.

Anderson P & Kedersha N (2006). RNA granules. *J Cell Biol* **172,** 803–808.

Bakthavachalu B, Huelsmeier J, Sudhakaran IP, Hillebrand J, Singh A, Petrauskas A, Thiagarajan D, Sankaranarayanan M, Mizoue L, Anderson EN, Pandey UB, Ross E, VijayRaghavan K, Parker R & Ramaswami M (2018). RNP-Granule Assembly via Ataxin-2 Disordered Domains Is Required for Long-Term Memory and Neurodegeneration. *Neuron* **98,** 754-766.e4.

Barbosa P, Zhaunova L, Debilio S, Steccanella V, Kelly V, Ly T & Ohkura H (2021). SCF-Fbxo42 promotes synaptonemal complex assembly by downregulating PP2A-B56. *J Cell Biol*; DOI: 10.1083/JCB.202009167.

Bard JAM, Goodall EA, Greene ER, Jonsson E, Dong KC & Martin A (2018). Structure and Function of the 26S Proteasome. *Annu Rev Biochem* **87,** 697–724.

Becker LA, Huang B, Bieri G, Ma R, Knowles DA, Jafar-Nejad P, Messing J, Kim HJ, Soriano A, Auburger G, Pulst SM, Taylor JP, Rigo F & Gitler AD (2017). Therapeutic reduction of ataxin-2 extends lifespan and reduces pathology in TDP-43 mice. *Nature* **544,** 367–371.

Belgnaoui SM, Paz S, Samuel S, Goulet ML, Sun Q, Kikkert M, Iwai K, Dikic I, Hiscott J & Lin R (2012). Linear ubiquitination of NEMO negatively regulates the interferon antiviral response through disruption of the MAVS-TRAF3 complex. *Cell Host Microbe* **12,** 211–222.

Billes V, Kovács T, Manzéger A, Lőrincz P, Szincsák S, Regős Á, Kulcsár

PI, Korcsmáros T, Lukácsovich T, Hoffmann G, Erdélyi M, Mihály J, Takács-Vellai K, Sass M & Vellai T (2018). Developmentally regulated autophagy is required for eye formation in Drosophila. *Autophagy* **14,** 1499–1519.

Brand AH & Perrimon N (1993). Targeted gene expression as a means of altering cell fates and generating dominant phenotypes. *Development* **118,** 401–415.

Braten O, Livneh I, Ziv T, Admon A, Kehat I, Caspi LH, Gonen H, Bercovich B, Godzik A, Jahandideh S, Jaroszewski L, Sommer T, Kwon YT, Guharoy M, Tompa P & Ciechanover A (2016). Numerous proteins with unique characteristics are degraded by the 26S proteasome following monoubiquitination. *Proc Natl Acad Sci U S A* **113,** E4639–E4647.

Bravo R, Parra V, Gatica D, Rodriguez AE, Torrealba N, Paredes F, Wang Z V., Zorzano A, Hill JA, Jaimovich E, Quest AFG & Lavandero S (2013). *Endoplasmic Reticulum and the Unfolded Protein Response. Dynamics and Metabolic Integration.*

Buchan JR, Muhlrad D & Parker R (2008). P bodies promote stress granule assembly in Saccharomyces cerevisiae. *J Cell Biol* **183,** 441–455.

Buchan JR & Parker R (2009). Eukaryotic Stress Granules: The Ins and Outs of Translation. *Mol Cell* **36,** 932–941.

Buddika K, Ariyapala IS, Hazuga MA, Riffert D & Sokol NS (2020). Canonical nucleators are dispensable for stress granule assembly in Drosophila intestinal progenitors. *J Cell Sci*; DOI: 10.1242/jcs.243451.

Cadwell K & Coscoy L (2005). Ubiquitination on Nonlysine Residues by a Viral E3 Ubiquitin Ligase. *Science (80-)* **309,** 127–130.

Cardozo T & Pagano M (2004). The SCF ubiquitin ligase: Insights into a molecular machine. *Nat Rev Mol Cell Biol* **5,** 739–751.

Carmo-Silva S, Nobrega C, Pereira de Almeida L & Cavadas C (2017). Unraveling the Role of Ataxin-2 in Metabolism. *Trends Endocrinol Metab* **28,** 309–318.

Carvalho AF, Pinto MP, Grou CP, Alencastre IS, Fransen M, Sá-Miranda C & Azevedo JE (2007). Ubiquitination of mammalian Pex5p, the peroxisomal import receptor. *J Biol Chem* **282,** 31267–31272.

Chang B, Partha S, Hofmann K, Lei M, Goebl M, Harper JW & Elledge SJ (1996). SKP1 connects cell cycle regulators to the ubiquitin proteolysis machinery through a novel motif, the F-box. *Cell* **86,** 263–274.

Chen ZJ & Sun LJ (2009). Nonproteolytic Functions of Ubiquitin in Cell Signaling. *Mol Cell* **33,** 275–286.

Christianson JC & Carvalho P (2022). Order through destruction: how ER-associated protein degradation contributes to organelle homeostasis. *EMBO J* **41,** 1–15.

Christianson JC & Ye Y (2014). Cleaning up in the endoplasmic reticulum: Ubiquitin in charge. *Nat Struct Mol Biol* **21,** 325–335.

Ciechanover A (1998). The ubiquitin-proteasome pathway: On protein death and cell life. *EMBO J* **17,** 7151–7160.

Ciechanover A & Ben-Saadon R (2004). N-terminal ubiquitination: More protein substrates join in. *Trends Cell Biol* **14,** 103–106.

Ciechanover A, Heller H, Katz-Etzion R & Hershko A (1981). Activation of the heat-stable polypeptide of the ATP-dependent proteolytic system. *Proc Natl Acad Sci U S A* **78,** 761–765.

Cook T & Desplan C (2001). Photoreceptor subtype specification: From flies to humans. *Semin Cell Dev Biol* **12,** 509–518.

Costa RG, Conceição A, Matos CA & Nóbrega C (2024). The polyglutamine protein ATXN2: from its molecular functions to its involvement in disease. *Cell Death Dis*; DOI: 10.1038/s41419-024-06812-5.

Das T, Purkayastha-Mukherjee C, D'Angelo J & Weir M (2002). A conserved F-box gene with unusual transcript localization. *Dev Genes Evol* **212,** 134–140.

Deng L, Meng T, Chen L, Wei W & Wang P (2020). The role of ubiquitination in tumorigenesis and targeted drug discovery. *Signal Transduct Target Ther*; DOI: 10.1038/s41392-020-0107-0.

Deshaies RJ & Joazeiro CAP (2009). RING domain E3 ubiquitin ligases. *Annu Rev Biochem* **78,** 399–434.

Dikic I (2017). Proteasomal and autophagic degradation systems. *Annu Rev Biochem* **86,** 193–224.

Dikic I & Schulman BA (2023). An expanded lexicon for the ubiquitin code. *Nat Rev Mol Cell Biol* **24,** 273–287.

Dósa A & Csizmadia T (2022). The role of K63-linked polyubiquitin in several types of autophagy. *Biol Futur* **73,** 137–148.

Dubnikov T & Cohen E (2017). The emerging roles of early protein folding events in the secretory pathway in the development of neurodegenerative maladies. *Front Neurosci* **11,** 1–8.

Dui W, Lu W, Ma J & Jiao R (2012). A Systematic Phenotypic Screen of F-box Genes Through a Tissue-specific RNAi-based Approach in Drosophila. *J Genet Genomics* **39,** 397–413.

Elden AC et al. (2010). Ataxin-2 intermediate-length polyglutamine expansions are associated with increased risk for ALS. *Nature* **466,** 1069–1075.

Estella C & Baonza A (2015). Cell proliferation control by Notch signalling during imaginal discs development in Drosophila. *AIMS Genet* **02,** 070–096.

Fregno I & Molinari M (2019). Proteasomal and lysosomal clearance of faulty secretory proteins: ER-associated degradation (ERAD) and ER-to-lysosome-associated degradation (ERLAD) pathways. *Crit Rev Biochem Mol Biol* **54,** 153–163.

French ME, Koehler CF & Hunter T (2021). Emerging functions of branched ubiquitin chains. *Cell Discov*; DOI: 10.1038/s41421-020-00237-y.

Fu X, Cui J, Meng X, Jiang P, Zheng Q, Zhao W & Chen X (2021). Endoplasmic reticulum stress, cell death and tumor: Association between endoplasmic reticulum stress and the apoptosis pathway in tumors (Review). *Oncol Rep* **45,** 801–808.

Galimova IA, Dorogova N V. & Fedorova SA (2021). Functions of E3 Ubiquitin Ligase Hyd in Drosophila Tissues. *Mol Biol* **55,** 305–310.

Geisler S, Holmström KM, Skujat D, Fiesel FC, Rothfuss OC, Kahle PJ & Springer W (2010). PINK1/Parkin-mediated mitophagy is dependent on VDAC1 and p62/SQSTM1. *Nat Cell Biol* **12,** 119–131.

Gnazzo MM, Uhlemann EME, Villarreal AR, Shirayama M, Dominguez EG & Skop AR (2016). The RNA-binding protein ATX-2 regulates cytokinesis through PAR-5 and ZEN-4. *Mol Biol Cell* **27,** 3052–3064.

Gregor JB, Xu D & French ME (2023). Assembly and disassembly of branched ubiquitin chains. *Front Mol Biosci* **10,** 1–7.

Grey MJ, Cloots E, Simpson MS, LeDuc N, Serebrenik Y V., de Luca H, de Sutter D, Luong P, Thiagarajah JR, Paton AW, Paton JC, Seeliger MA, Eyckerman S, Janssens S & Lencer WI (2020). IRE1β negatively regulates IRE1α signaling in response to endoplasmic reticulum stress. *J Cell Biol* **219,** 1–17.

Gwinn-Hardy K, Chen JY, Liu HC, Liu TY, Boss M, Seltzer W, Adam A, Singleton A, Koroshetz W, Waters C, Hardy J & Farrer M (2000). Spinocerebellar ataxia type 2 with parkinsonism in ethnic Chinese. *Neurology* **55,** 800–805.

Haglund K, Sigismund S, Polo S, Szymkiewicz I, Di Fiore PP & Dikic I (2003). Multiple monoubiquitination of RTKs is sufficient for their endocytosis and degradation. *Nat Cell Biol* **5,** 461–466.

Halbach M (2015). *Characterization of Ataxin-2 and its interaction partners* (thesis).

Hardie RC & Raghu P (2001). Visual transduction in Drosophila. *Nature* **413,** 186–193.

Hegde RS & Keenan RJ (2022). The mechanisms of integral membrane protein biogenesis. *Nat Rev Mol Cell Biol* **23,** 107–124.

Hershko A (1988). Ubiquitin-mediated protein degradation. *J Biol Chem* **263,** 15237–15240.

Hershko A & Ciechanover A (1998). The ubiquitin system. *Annu Rev Biochem* **67,** 425–479.

Hershko A, Ciechanover A & Rose IA (1981). Identification of the active amino acid residue of the polypeptide of ATP-dependent protein breakdown. *J Biol Chem* **256,** 1525–1528.

Hetz C (2012). The unfolded protein response: Controlling cell fate decisions under ER stress and beyond. *Nat Rev Mol Cell Biol* **13,** 89–102.

Hetz C & Papa FR (2018). The Unfolded Protein Response and Cell Fate Control. *Mol Cell* **69,** 169–181.

Hetz C, Zhang K & Kaufman RJ (2020). Mechanisms, regulation and functions of the unfolded protein response. *Nat Rev Mol Cell Biol* **21,** 421–438.

Ho MS, Tsai PI & Chien CT (2006). F-box proteins: The key to protein degradation. *J Biomed Sci* **13,** 181–191.

Hoellerbauer P, Kufeld M, Arora S, Mitchell K, Girard EJ, Herman JA, Olson JM & Paddison PJ (2024). FBXO42 activity is required to prevent mitotic arrest, spindle assembly checkpoint activation and lethality in glioblastoma and other cancers. *NAR Cancer*; DOI: 10.1093/narcan/zcae021.

Hollien J, Lin JH, Li H, Stevens N, Walter P & Weissman JS (2009). Regulated Ire1-dependent decay of messenger RNAs in mammalian cells. *J Cell Biol* **186,** 323–331.

Hollien J & Weissman JS (2006). Decay of Endoplasmic Reticulum-Localized mRNAs During the Unfolded Protein Response. *Science (80-)* **313,** 104–107.

van Huizen M & Kikkert M (2020). The Role of Atypical Ubiquitin Chains in the Regulation of the Antiviral Innate Immune Response. *Front Cell Dev Biol* **7,** 1–8.

Hundley F V., Sanvisens Delgado N, Marin HC, Carr KL, Tian R & Toczyski DP (2021). A comprehensive phenotypic CRISPR-Cas9 screen of the ubiquitin pathway uncovers roles of ubiquitin ligases in mitosis. *Mol Cell* **81,** 1319-1336.e9.

Husnjak K & Dikic I (2012). Ubiquitin-binding proteins: Decoders of ubiquitin-mediated cellular functions. *Annu Rev Biochem* **81,** 291–322.

Inagaki H, Hosoda N, Tsuiji H & Hoshino SI (2020). Direct evidence that ataxin-2 is a translational activator mediating cytoplasmic polyadenylation. *J Biol Chem* **295,** 15810–18525.

Jackson PK, Eldridge AG, Freed E, Furstenthal L, Hsu JY, Kaiser BK & Reimann JDR (2000). The lore of the RINGs: Substrate recognition and catalysis by ubiquitin ligases. *Trends Cell Biol* **10,** 429–439.

Jiang H, Bian W, Sui Y, Li H, Zhao H, Wang W & Li X (2022). FBXO42 facilitates Notch signaling activation and global chromatin relaxation by promoting K63-linked polyubiquitination of RBPJ. *Sci Adv* **8,** 1–18.

Jiménez-López D & Guzmán P (2014). Insights into the evolution and domain structure of ataxin-2 proteins across eukaryotes. *BMC Res Notes* **7,** 1–12.

Jin J, Cardozo T, Lovering RC, Elledge SJ, Pagano M & Harper JW (2004). Systematic analysis and nomenclature of mammalian F-box proteins. *Genes Dev* **18,** 2573–2580.

Kadowaki H, Nagai A, Maruyama T, Takami Y, Satrimafitrah P, Kato H, Honda A, Hatta T, Natsume T, Sato T, Kai H, Ichijo H & Nishitoh H (2015). Pre-emptive Quality Control Protects the ER from Protein Overload via the Proximity of ERAD Components and SRP. *Cell Rep* **13,** 944–956.

Kaehler C, Isensee J, Nonhoff U, Terrey M, Hucho T, Lehrach H & Krobitsch S (2012). Ataxin-2-Like Is a Regulator of Stress Granules and Processing Bodies. *PLoS One* **7,** 1–12.

Kashyap D, Garg VK & Goel N (2021). *Intrinsic and extrinsic pathways of apoptosis: Role in cancer development and prognosis*, 1st edn. Elsevier Inc. Available at: http://dx.doi.org/10.1016/bs.apcsb.2021.01.003.

Kedersha N, Stoecklin G, Ayodele M, Yacono P, Lykke-Andersen J, Fitzler MJ, Scheuner D, Kaufman RJ, Golan DE & Anderson P (2005).

Stress granules and processing bodies are dynamically linked sites of mRNP remodeling. *J Cell Biol* **169,** 871–884.

Kelsall IR (2022). Non-lysine ubiquitylation: Doing things differently. *Front Mol Biosci* **9,** 1–28.

Kiehl TR, Nechiporuk A, Figueroa KP, Keating MT, Huynh DP & Pulst SM (2006). Generation and characterization of Sca2 (ataxin-2) knockout mice. *Biochem Biophys Res Commun* **339,** 17–24.

Kipreos ET & Pagano M (2000). The F-box protein family. *Genome Biol* **1,** 1–7.

Kliza K & Husnjak K (2020). Resolving the Complexity of Ubiquitin Networks. *Front Mol Biosci*; DOI: 10.3389/fmolb.2020.00021.

Kochańczyk T, Hann ZS, Lux MC, Delos Reyes AM V., Ji C, Tan DS & Lima CD (2024). Structural basis for transthiolation intermediates in the ubiquitin pathway. *Nature* **633,** 216–223.

Komander D & Rape M (2012). The ubiquitin code. *Annu Rev Biochem* **81,** 203–229.

Krshnan L, van de Weijer ML & Carvalho P (2022). Endoplasmic Reticulum–Associated Protein Degradation. *Cold Spring Harb Perspect Biol* **14,** 1–22.

Kumar JP (2018). The fly eye: Through the looking glass. *Dev Dyn* **247,** 111–123.

Lange SM, Armstrong LA & Kulathu Y (2022). Deubiquitinases: From mechanisms to their inhibition by small molecules. *Mol Cell* **82,** 15–29.

Lee J, Kim M, Itoh TQ & Lim C (2018). Ataxin-2: A versatile posttranscriptional regulator and its implication in neural function. *Wiley Interdiscip Rev RNA* **9,** 1–13.

Leznicki P & Kulathu Y (2017). Mechanisms of regulation and diversification of deubiquitylating enzyme function. *J Cell Sci* **130,** 1997–2006.

Li D & Roberts R (2001). WD-repeat proteins: Structure characteristics, biological function, and their involvement in human diseases. *Cell Mol Life Sci* **58,** 2085–2097.

Li L, Wang M, Huang L, Zheng X, Wang L & Miao H (2024). Ataxin-2: a powerful RNA-binding protein. *Discov Oncol*; DOI: 10.1007/s12672-024-01158-y.

Li Y & Reverter D (2021). Molecular mechanisms of dubs regulation in

signaling and disease. *Int J Mol Sci* **22,** 1–26.

Lim C & Allada R (2013). ATAXIN-2 Activates PERIOD Translation to Sustain Circadian Rhythms in Drosophila. *Science (80-)* **340,** 875–880.

Lindholm D, Korhonen L, Eriksson O & Kõks S (2017). Recent insights into the role of unfolded protein response in ER stress in health and disease. *Front Cell Dev Biol* **5,** 1–16.

Liu S, Jiang M, Wang W, Liu W, Song X, Ma Z, Zhang S, Liu L, Liu Y & Cao X (2017). Nuclear RNF2 inhibits interferon function by promoting K33-linked STAT1 disassociation from DNA article. *Nat Immunol* **19,** 41–52.

Liu Y, Xu C, Gu R, Han R, Li Z & Xu X (2024). Endoplasmic reticulum stress in diseases. *MedComm* **5,** 1–31.

Lu M, Lawrence DA, Marsters S, Acosta-Alvear D, Kimmig P, Mendez AS, Paton AW, Paton JC, Walter P & Ashkenazi A (2014). Opposing unfolded-protein-response signals converge on death receptor 5 to control apoptosis. *Science (80-)* **345,** 98–101.

Luo H, Jiao Q, Shen C, Shao C, Xie J, Chen Y, Feng X & Zhang X (2023). Unraveling the roles of endoplasmic reticulum-associated degradation in metabolic disorders. *Front Endocrinol (Lausanne)* **14,** 1–10.

Ma Y & Hendershot LM (2004). The role of the unfolded protein response in tumour development: Friend or foe? *Nat Rev Cancer* **4,** 966–977.

Magaña JJ, Velázquez-Pérez L & Cisneros B (2013). Spinocerebellar ataxia type 2: Clinical presentation, molecular mechanisms, and therapeutic perspectives. *Mol Neurobiol* **47,** 90–104.

Mangus DA, Amrani N & Jacobson A (1998). Pbp1p, a Factor Interacting with Saccharomyces cerevisiae Poly(A)-Binding Protein, Regulates Polyadenylation . *Mol Cell Biol* **18,** 7383–7396.

Mangus DA, Smith MM, McSweeney JM & Jacobson A (2004). Identification of Factors Regulating Poly(A) Tail Synthesis and Maturation. *Mol Cell Biol* **24,** 4196–4206.

Mao Y (2021). *Structure, Dynamics and Function of the 26S Proteasome*. Springer International Publishing. Available at: http://dx.doi.org/10.1007/978-3-030-58971-4_1.

Marcelo A, Koppenol R, de Almeida LP, Matos CA & Nóbrega C (2021). Stress granules, RNA-binding proteins and polyglutamine diseases: too much aggregation? *Cell Death Dis*; DOI: 10.1038/s41419-021-

03873-8.

Marshall RS & Vierstra RD (2019). Dynamic regulation of the 26S proteasome: From synthesis to degradation. *Front Mol Biosci*; DOI: 10.3389/fmolb.2019.00040.

McCann C, Holohan EE, Das S, Dervan A, Larkin A, Lee JA, Rodrigues V, Parker R & Ramaswami M (2011). The ataxin-2 protein is required for microRNA function and synapse-specific long-term olfactory habituation. *Proc Natl Acad Sci U S A*; DOI: 10.1073/pnas.1107198108.

McDowell GS, Kucerova R & Philpott A (2010). Non-canonical ubiquitylation of the proneural protein Ngn2 occurs in both Xenopus embryos and mammalian cells. *Biochem Biophys Res Commun* **400,** 655–660.

McDowell GS & Philpott A (2013). Non-canonical ubiquitylation: Mechanisms and consequences. *Int J Biochem Cell Biol* **45,** 1833–1842.

Metzger MB & Weissman AM (2010). Working on a chain: E3s ganging up for ubiquitylation. *Nat Cell Biol* **12,** 1124–1126.

Mollereau B & Domingos PM (2005). Photoreceptor differentiation in Drosophila: From immature neurons to functional photoreceptors. *Dev Dyn* **232,** 585–592.

Montell C (2012). Drosophila visual transduction. *Trends Neurosci* **35,** 356–363.

Moses K (2002). *Introduction. Drosophila eye development.*

Murata S, Yashiroda H & Tanaka K (2009). Molecular mechanisms of proteasome assembly. *Nat Rev Mol Cell Biol* **10,** 104–115.

Nóbrega C, Carmo-Silva S, Albuquerque D, Vasconcelos-Ferreira A, Vijayakumar UG, Mendonça L, Hirai H & Pereira De Almeida L (2015). Re-establishing ataxin-2 downregulates translation of mutant ataxin-3 and alleviates Machado-Joseph disease. *Brain* **138,** 3537–3554.

Nonhoff U, Ralser M, Welzel F, Piccini I, Balzereit D, Yaspo M-L, Lehrach H & Krobitsch S (2007). Ataxin-2 Interacts with the DEAD/H-Box RNA Helicase DDX6 and Interferes with P-Bodies and Stress Granules. *Mol Biol Cell* **18,** 1385–1396.

O'Keefe S, Pool MR & High S (2022). Membrane protein biogenesis at the ER: the highways and byways. *FEBS J* **289,** 6835–6862.

Odenthal J & Brinkkoetter PT (2019). *Drosophila melanogaster and its nephrocytes: A versatile model for glomerular research*, 1st edn. Elsevier Inc. Available at: http://dx.doi.org/10.1016/bs.mcb.2019.03.011.

Oslowski CM & Urano F (2011). *Measuring ER stress and the unfolded protein response using mammalian tissue culture system*, 1st edn. Elsevier Inc. Available at: http://dx.doi.org/10.1016/B978-0-12-385114-7.00004-0.

Ostrowski LA, Hall AC & Mekhail K (2017). Ataxin-2: From RNA control to human health and disease. *Genes (Basel)* **8,** 2–21.

Ou CY, Pi H & Chien CT (2003). Control of protein degradation by E3 ubiquitin ligases in Drosophila eye development. *Trends Genet* **19,** 382–389.

Pauwels E, Schülein R & Vermeire K (2021). Inhibitors of the Sec61 complex and novel high throughput screening strategies to target the protein translocation pathway. *Int J Mol Sci*; DOI: 10.3390/ijms222112007.

Pelizzari-Raymundo D, Maltret V, Nivet M, Pineau R, Papaioannou A, Zhou X, Caradec F, Martin S, Le Gallo M, Avril T, Chevet E & Lafont E (2024). IRE1 RNase controls CD95-mediated cell death. *EMBO Rep* **25,** 1792–1813.

Pfleger CM (2011). Ubiquitin on Ras: Warden or partner in crime? *Sci Signal*; DOI: 10.1126/scisignal.2001874.

Pichlak M, Sobierajski T, Błażewska KM & Gendaszewska-Darmach E (2023). Targeting reversible post-translational modifications with PROTACs: a focus on enzymes modifying protein lysine and arginine residues. *J Enzyme Inhib Med Chem* **38,** 1–37.

Pickart CM & Eddins MJ (2004). Ubiquitin: Structures, functions, mechanisms. *Biochim Biophys Acta - Mol Cell Res* **1695,** 55–72.

Protter DSW & Parker R (2016). Principles and Properties of Stress Granules. *Trends Cell Biol* **26,** 668–679.

Rahighi S, Ikeda F, Kawasaki M, Akutsu M, Suzuki N, Kato R, Kensche T, Uejima T, Bloor S, Komander D, Randow F, Wakatsuki S & Dikic I (2009). Specific Recognition of Linear Ubiquitin Chains by NEMO Is Important for NF-κB Activation. *Cell* **136,** 1098–1109.

Rajalingam K & Dikic I (2016). SnapShot: Expanding the Ubiquitin Code. *Cell* **164,** 1074-1074.e1.

Rasheva VI & Domingos PM (2009). Cellular responses to endoplasmic

reticulum stress and apoptosis. *Apoptosis* **14,** 996–1007.

Rehmat J & Chaudhry G-S (2019). Understanding Apoptosis and Apoptotic Pathways Targeted Cancer Therapeutics. *Adv Parmaceutical Bull* **9,** 205–218.

Riess O et al. (1997). SCA2 trinucleotide expansion in German SCA patients. *Neurogenetics* **1,** 59–64.

Robinson DN & Cooley L (1997). Drosophila kelch is an oligomeric ring canal actin organizer. *J Cell Biol* **138,** 799–810.

Roignant JY & Treisman JE (2009). Pattern formation in the Drosophila eye disc. *Int J Dev Biol* **53,** 795–804.

Ron D & Walter P (2007). Signal integration in the endoplasmic reticulum unfolded protein response. *Nat Rev Mol Cell Biol* **8,** 519–529.

Ruggiano A, Foresti O & Carvalho P (2014). ER-associated degradation: Protein quality control and beyond. *J Cell Biol* **204,** 869–879.

Ryoo HD, Domingos PM, Kang MJ & Steller H (2007). Unfolded protein response in a Drosophila model for retinal degeneration. *EMBO J* **26,** 242–252.

Sadowski M, Suryadinata R, Tan AR, Roesley SNA & Sarcevic B (2012). Protein monoubiquitination and polyubiquitination generate structural diversity to control distinct biological processes. *IUBMB Life* **64,** 136–142.

Sahu I & Glickman MH (2021). Proteasome in action: Substrate degradation by the 26S proteasome. *Biochem Soc Trans* **49,** 629–644.

Satterfield TF, Jackson SM & Pallanck LJ (2002). A drosophila homolog of the polyglutamine disease gene SCA2 is a dosage-sensitive regulator of actin filament formation. *Genetics* **162,** 1687–1702.

Satterfield TF & Pallanck LJ (2006). Ataxin-2 and its Drosophila homolog, ATX2, physically assemble with polyribosomes. *Hum Mol Genet* **15,** 2523–2532.

Schröder M (2008). Endoplasmic reticulum stress responses. *Cell Mol Life Sci* **65,** 862–894.

Sharkey CR, Blanco J, Leibowitz MM, Pinto-Benito D & Wardill TJ (2020). The spectral sensitivity of Drosophila photoreceptors. *Sci Rep* **10,** 1–13.

Shibata H, Huynh DP & Pulst SM (2000). A novel protein with RNA-binding motifs interacts with ataxin-2. *Hum Mol Genet* **9,** 1303–1313.

Shimizu Y, Okuda-Shimizu Y & Hendershot LM (2010). Ubiquitylation of an ERAD Substrate Occurs on Multiple Types of Amino Acids. *Mol Cell* **40,** 917–926.

Singh A, Hulsmeier J, Kandi AR, Pothapragada SS, Hillebrand J, Petrauskas A, Agrawal K, Krishnan RT, Thiagarajan D, Jayaprakashappa D, Vijayraghavan K, Ramaswami M & Bakthavachalu B (2021). Antagonistic roles for ataxin-2 structured and disordered domains in rnp condensation. *Elife* **10,** 1–25.

Smith MH, Ploegh HL & Weissman JS (2011). Road to ruin: Targeting proteins for degradation in the endoplasmic reticulum. *Science (80-)* **334,** 1086–1090.

Snyder NA & Silva GM (2021). Deubiquitinating enzymes (DUBs): Regulation, homeostasis, and oxidative stress response. *J Biol Chem* **297,** 101077.

Sorout N & Helms V (2024). Toward Understanding the Mechanism of Client-Selective Small Molecule Inhibitors of the Sec61 Translocon. *J Mol Recognit*1–18.

Stein A, Ruggiano A, Carvalho P & Rapoport TA (2014). Key steps in ERAD of luminal ER proteins reconstituted with purified components. *Cell* **158,** 1375–1388.

Sudhakaran IP, Hillebrand J, Dervan A, Das S, Holohan EE, Hülsmeier J, Sarov M, Parker R, VijayRaghavan K & Ramaswami M (2014). FMRP and Ataxin-2 function together in long-term olfactory habituation and neuronal translational control. *Proc Natl Acad Sci U S A*; DOI: 10.1073/pnas.1309543111.

Sun L, Shi L, Li W, Yu W, Liang J, Zhang H, Yang X, Wang Y, Li R, Yao X, Yi X & Shang Y (2009). JFK, a Kelch domain-containing F-box protein, links the SCF complex to p53 regulation. *Proc Natl Acad Sci U S A* **106,** 10195–10200.

Sun L, Shi L, Wang F, Huangyang P, Si W, Yang J, Yao Z & Shang Y (2011). Substrate phosphorylation and feedback regulation in JFK-promoted p53 destabilization. *J Biol Chem* **286,** 4226–4235.

Sun M & Zhang X (2022). Current methodologies in protein ubiquitination characterization: from ubiquitinated protein to ubiquitin chain architecture. *Cell Biosci* **12,** 1–17.

Swatek KN & Komander D (2016). Ubiquitin modifications. *Cell Res* **26,** 399–422.

Tabata T (2001). Genetics of morphogen gradients. *Nat Rev Genet* **2,** 620–630.

Tokarev AA, Munguia J & Guatelli JC (2011). Serine-Threonine Ubiquitination Mediates Downregulation of BST-2/Tetherin and Relief of Restricted Virion Release by HIV-1 Vpu. *J Virol* **85,** 51–63.

Tokunaga F, Sakata SI, Saeki Y, Satomi Y, Kirisako T, Kamei K, Nakagawa T, Kato M, Murata S, Yamaoka S, Yamamoto M, Akira S, Takao T, Tanaka K & Iwai K (2009). Involvement of linear polyubiquitylation of NEMO in NF-κB activation. *Nat Cell Biol* **11,** 123–132.

Toledo CM et al. (2015). Genome-wide CRISPR-Cas9 Screens Reveal Loss of Redundancy between PKMYT1 and WEE1 in Glioblastoma Stem-like Cells. *Cell Rep* **13,** 2425–2439.

Urra H, Dufey E, Lisbona F, Rojas-Rivera D & Hetz C (2013). When ER stress reaches a dead end. *Biochim Biophys Acta - Mol Cell Res* **1833,** 3507–3517.

Vianna MCB, Poleto DC, Gomes PF, Valente V & Paçó-Larson ML (2016). Drosophila ataxin-2 gene encodes two differentially expressed isoforms and its function in larval fat body is crucial for development of peripheral tissues. *FEBS Open Bio* **6,** 1040–1053.

Vollmer J, Fried P, Sánchez-Aragón M, Lopes CS, Casares F & Iber D (2016). A quantitative analysis of growth control in the Drosophila eye disc. *Dev* **143,** 1482–1490.

Vosper JMD, McDowell GS, Hindley CJ, Fiore-Heriche CS, Kucerova R, Horan I & Philpott A (2009). Ubiquitylation on canonical and non-canonical sites targets the transciption factor neurogenin for ubiquitin-mediated proteolysis. *J Biol Chem* **284,** 15458–15468.

Walter P & Ron D (2011). The Unfolded Protein Response: From Stress Pathway to Homeostatic Regulation. *Science (80-)* **334,** 1081–1086.

Wang G, Gao Y, Li L, Jin G, Cai Z, Chao JI & Lin HK (2012*a*). K63-linked ubiquitination in kinase activation and cancer. *Front Oncol* **2,** 1–13.

Wang L & Ye Y (2021). Clearing Traffic Jams During Protein Translocation Across Membranes. *Front Cell Dev Biol* **8,** 1–10.

Wang M & Kaufman RJ (2016). Protein misfolding in the endoplasmic reticulum as a conduit to human disease. *Nature* **529,** 326–335.

Wang S & Kaufman RJ (2012). The impact of the unfolded protein response on human disease. *J Cell Biol* **197,** 857–867.

Wang T & Montell C (2007). Phototransduction and retinal degeneration in Drosophila. *Pflugers Arch Eur J Physiol* **454,** 821–847.

Wang X, Herr RA & Hansen TH (2012*b*). Ubiquitination of substrates by esterification. *Traffic* **13,** 19–24.

Wang YJ, Bian Y, Luo J, Lu M, Xiong Y, Guo SY, Yin HY, Lin X, Li Q, Chang CCY, Chang TY, Li BL & Song BL (2017). Cholesterol and fatty acids regulate cysteine ubiquitylation of ACAT2 through competitive oxidation. *Nat Cell Biol* **19,** 808–819.

Williams C, Van Den Berg M, Sprenger RR & Distel B (2007). A conserved cysteine is essential for Pex4p-dependent ubiquitination of the peroxisomal import receptor Pex5p. *J Biol Chem* **282,** 22534–22543.

Winston JT, Koepp DM, Cihui Z, Elledge SJ & Harper JW (1999). A family of mammalian F-box proteins. *Curr Biol* **9,** 1180–1182.

Woehlbier U & Hetz C (2011). Modulating stress responses by the UPRosome: A matter of life and death. *Trends Biochem Sci* **36,** 329–337.

Yan R, He L, Li Z, Han X, Liang J, Si W, Chen Z, Li L, Xie G, Li W, Wang P, Lei L, Zhang H, Pei F, Cao D, Sun L & Shang Y (2015). SCFJFK is a bona fide e3 ligase for ING4 and a potent promoter of the angiogenesis and metastasis of breast cancer. *Genes Dev* **29,** 672–685.

Yang Q, Zhao J, Chen D & Wang Y (2021). E3 ubiquitin ligases: styles, structures and functions. *Mol Biomed*; DOI: 10.1186/s43556-021-00043-2.

Yokoshi M, Li Q, Yamamoto M, Okada H, Suzuki Y & Kawahara Y (2014). Direct binding of Ataxin-2 to distinct elements in 3' UTRs promotes mRNA stability and protein expression. 186–198.

Yu Z, Chen T, Li X, Yang M, Tang S, Zhu X, Gu Y, Su X, Xia M, Li W, Zhang X, Wang Q, Cao X & Wang J (2016). Lys29-linkage of ASK1 by Skp1-Cullin 1-Fbxo21 ubiquitin ligase complex is required for antiviral innate response. *Elife* **5,** 1–23.

Yuan WC, Lee YR, Lin SY, Chang LY, Tan YP, Hung CC, Kuo JC, Liu CH, Lin MY, Xu M, Chen ZJ & Chen RH (2014). K33-Linked Polyubiquitination of Coronin 7 by Cul3-KLHL20 Ubiquitin E3 Ligase Regulates Protein Trafficking. *Mol Cell* **54,** 586–600.

Zhang M, Windheim M, Roe SM, Peggie M, Cohen P, Prodromou C & Pearl LH (2005). Chaperoned ubiquitylation - Crystal structures of the CHIP U box E3 ubiquitin ligase and a CHIP-Ubc13-Uev1a complex. *Mol Cell* **20,** 525–538.

Zhang Y, Ling J, Yuan C, Dubruille R & Emery P (2013). A role for Drosophila ATX2 in activation of PER translation and circadian

behavior. *Science (80-)* **340,** 879–882.

Zhou J, Li Q, Deng X, Peng L, Sun J, Zhang Y & Du Y (2024). Comprehensive analysis identifies ubiquitin ligase FBXO42 as a tumor-promoting factor in neuroblastoma. *Sci Rep* **14,** 1–15.

Zhou Q, Neal SJ & Pignoni F (2017). Mutant Analysis by Rescue Gene Excision: a technique for mosaic studies in Drosophila. *Genesis* **54,** 589–592.

Zhou Z Sen, Li MX, Liu J, Jiao H, Xia JM, Shi XJ, Zhao H, Chu L, Liu J, Qi W, Luo J & Song BL (2020). Competitive oxidation and ubiquitylation on the evolutionarily conserved cysteine confer tissue-specific stabilization of Insig-2. *Nat Commun*; DOI: 10.1038/s41467-019-14231-w.

CHAPTER II

Fbxo42 mediates the ubiquitylation of the RNA-binding protein Ataxin-2 in adult fly eyes and in *Drosophila* S2 cells

---

Authors: Santos CC, Schweizer N, Cairrão F, Ramirez J, Osinalde N, Gaspar CJ, Rasheva V, Adrain C, Mayor U and Domingos PM.

2.1 Abstract

The Unfolded Protein Response (UPR) is composed by homeostatic signalling pathways that are activated by the accumulation of misfolded/unfolded proteins in the Endoplasmic Reticulum (ER), a condition known as ER stress. Prolonged ER stress and UPR activation can lead to cell death through mechanisms that remain poorly understood.

Previous work performed in our laboratory showed that overexpression of $Xbp1^{spliced}$ (Xbp1s), an important mediator of the UPR, causes cell death and retinal degeneration, leading to the "glossy" eye phenotype. From a genetic screen using the mutagenic agent EMS (ethyl methanesulfonate), we identified several loss-of-function mutations in *Fbxo42* that suppress the Xbp1s-induced "glossy" eye phenotype. *Fbxo42* encodes one of the 45 F-box proteins identified in the *Drosophila* genome, and its biological function remains to be fully elucidated. F-box proteins form complexes with Skp-A, Cullin-1 and RBX (SCF complexes) to promote the ubiquitylation of specific substrates. To find the substrates of Fbxo42, we performed two different proteomic approaches: the first one using human cell lysates and the second using fly extracts. The proteomic analysis with fly head extracts, based on the ^{bio}Ub strategy, allowed us to identify the RNA-binding protein Ataxin-2 as a substrate of Fbxo42. Biochemically, we showed that Fbxo42 mediates the ubiquitylation of Ataxin-2 in adult fly heads and in *Drosophila* S2 cells.

Additionally, we developed an anti-Fbxo42 antibody to study the cellular and tissue localization of the Fbxo42 protein. This antibody enabled us to detect Fbxo42 expression in several larval

tissues, as well as in the brain, ovaries and testis of adult flies. Furthermore, we observed that Ataxin-2 RNAi abolished the suppression of the Xbp1s-induced “glossy” eye phenotype, by Fbxo42 mutants.

In conclusion, our results suggest that Fbxo42 regulates Ataxin-2 protein levels, which impacts retinal degeneration induced by Xbp1s overexpression.

2.2 Introduction

The Endoplasmic Reticulum (ER) is the cellular organelle where membrane and secretory proteins are synthesized, folded and acquire post-translational modifications (PTMs) (Schröder, 2008; Bravo *et al.*, 2013). ER is also implicated in the biosynthesis of lipids and sterols, and it is the place of storage of calcium ions (Schröder, 2008; Bravo *et al.*, 2013; Hetz *et al.*, 2020).

Perturbations in ER homeostasis may lead to an accumulation of misfolded/unfolded proteins in the ER, a cellular condition termed as “ER stress” (Patil & Walter, 2001; Ryoo *et al.*, 2007; Walter & Ron, 2011). Upon ER stress, cells activate several signalling mechanisms to cope with protein-folding alterations, which are collectively known as the Unfolded Protein Response (UPR) (Patil & Walter, 2001; Harding *et al.*, 2002; Ryoo *et al.*, 2007; Rasheva & Domingos, 2009).

The activation of the UPR is mediated by three ER protein sensors that detected ER stress: IRE1, PERK and ATF6 (Ron & Walter, 2007; Walter & Ron, 2011). IRE1 contains an ER luminal domain, that senses ER stress, and a cytosolic domain possessing

both kinase and endoribonuclease activities (Rasheva & Domingos, 2009; Walter & Ron, 2011). Under ER stress conditions, IRE1 oligomerizes and autophosphorylates to activate its endoribonuclease activity (Walter & Ron, 2011; Hetz *et al.*, 2020). Activated IRE1, through its endoribonuclease domain, cleaves Xbp1 mRNA in two sites, catalysing an unconventional splicing of an intron from XBP1 (X-box binding protein 1) mRNA (Walter & Ron, 2011). Xbp1 spliced (Xbp1s) is a basic leucine zipper (bZIP) transcription factor and it translocates to the nucleus to induce the transcription of genes encoding proteins involved in protein folding, ERAD and protein quality control (Rasheva & Domingos, 2009; Hetz, 2012; Hetz *et al.*, 2020).

When ER stress is prolonged or severe, leading to “chronic” UPR activation, cells can trigger apoptosis. The mechanisms that activate the pro-apoptotic events are still not clear (Rasheva & Domingos, 2009; Tabas & Ron, 2011; Woehlbier & Hetz, 2011).

Ryoo and colleagues (Ryoo *et al.*, 2007) showed that, in the *Drosophila* eye, Xbp1 plays a protective role against the retinal degeneration caused by mutations in *ninaE* (the gene encoding the Rhodopsin-1 protein). Another study demonstrated that, in a fly model of Alzheimer’s disease (AD), Xbp1s suppresses the neurotoxicity caused by the expression of human amyloid-β 1-42 (Aβ) in the *Drosophila* eye (Casas-Tinto *et al.*, 2011). In addition to these beneficial effects observed in flies, a different study reported that, the virus-mediated administration of Xbp1s into the hippocampus of a mouse model of Alzheimer’s disease improves synaptic plasticity and memory function (Cissé *et al.*, 2017).

On the other hand, in a mouse model of amyotrophic lateral sclerosis (ALS) (containing mutant superoxide dismutase-1, SOD1), conditional genetic deletion of *Xbp1* in the nervous system made the mice more resistant to developing ALS, this was associated with increased autophagy in motor neurons which increased the clearance of mutant SOD1 (Hetz *et al.*, 2009; Hetz & Saxena, 2017). In addition, *Xbp1* deficiency in the nervous system also increased the lifespan of the mice, correlating with a decrease in apoptosis in the ventral horn of spinal cord (Hetz *et al.*, 2009; Hetz & Saxena, 2017). Accordingly, a mouse model of Huntington's disease (HD), carrying the human *Huntingtin* gene with 128 glutamine repeats, with *Xbp1* deletion in the nervous system showed reduced neuronal apoptosis levels, enhanced huntingtin degradation by autophagy and improved motor performance (Vidal *et al.*, 2012). Consistent with these findings, in a fly model of HD, down-regulation of IRE1 expression rescued the rough-eye phenotype induced by mutant huntingtin overexpression (Lee *et al.*, 2012).

In this chapter, our specific aims are the following:

- Analyse the cellular and tissue localization of the F-box protein Fbxo42, through the development of an antibody against Fbxo42.
- Identify the specific substrates of Fbxo42, through Mass Spectrometry (MS).
- Confirm the MS results through immunofluorescence assays and biochemical experiments.

2.3 Methods

Plasmids

The cDNA clone GH02866 [*Drosophila* Genomics Resource Center (DGRC), DGRC Stock 6307; https://dgrc.bio.indiana.edu//stock/6307; RRID: DGRC_6307] was used to clone *Fbxo42* into the Gateway® destination vectors pTFHW (to generate a N-terminally 3xFLAG-3xHA-tagged fusion protein) and pTWG (to create a C-terminally GFP-tagged fusion protein) following Invitrogen Gateway® protocol (Invitrogen). Primers used to generate pTFHW-Fbxo42 and pTWG-Fbxo42 are listed in supplementary table S1.

The pTFHW-ΔFbxo42 vector contains the deletion of the first 201 base pairs of *Fbxo42* gene. This region encodes the first 67 amino acids of Fbxo42, and it includes the F-box domain. Δ*Fbxo42* sequence was cloned into the Gateway® destination vector pTFHW (primers in supplementary table S1).

The pUAST-Ataxin-2-GFP construct was generated by Gibson Assembly® (New England Biolabs, NEB). Briefly, the *Ataxin-2* gene was amplified by PCR from flies expressing Ataxin-2 isoform A C-terminally fused with HA-tag (FlyORF F001031) and subcloned into the pJET1.2/blunt vector (CloneJET™ PCR Cloning Kit, Fermentas/Thermo Fisher Scientific), generating the pJET1.2-Ataxin-2-HA construct.

Afterwards, *Ataxin-2* sequence was PCR amplified from pJET1.2-Ataxin-2-HA and *gfp* was amplified from pUAST-Xbp1-EGFP (primers in table S1). Finally, the Ataxin-2 and GFP DNA fragments were cloned into the pUAST vector at XhoI

(Fermentas/Thermo Fisher Scientific)/BglII (Thermo Fisher Scientific) restriction sites by Gibson reaction.

To generate the pUAST-Ataxin-2-HA construct, the DNA sequence encoding Ataxin-2 C-terminally fused with HA-tag was PCR amplified (primers in table S1) from pJET1.2-Ataxin-2-HA vector and cloned into pUAST plasmid at XhoI/BglII restriction sites by Gibson Assembly®.

The *Ataxin-2* mutations were generated by site-directed mutagenesis using the NZYMutagenesis kit (NZYtech) according to the manufacturer's instructions. All constructs were confirmed by sequencing (Stabvida). The pUAST-His-Myc-Ubiquitin plasmid (Domingues & Ryoo, 2012) was kindly provided by HD Ryoo. The pMT-SkpA-HA and UAS-FLAG-Fblx7 (Bosch *et al.*, 2014) plasmids were a gift from Iswar Hariharan.

Drosophila stocks

Fly stocks and crosses were raised with standard cornmeal fly food, at 25°C under 12 h light/12 h dark cycles. New transgenic fly lines were generated either at Bestgene or the Champalimaud Foundation transgenics facility. The fly stocks UAS-Xbp1u (Huang *et al.*, 2017), UAS-Xbp1s (Ryoo *et al.*, 2007), UAS-P35 (Grether *et al.*, 1995), UAS-DIAP1 (Ryoo *et al.*, 2002) and UAS-Rh1 (Kang & Ryoo, 2009) were gifts from HD Ryoo. The stock GMR-hid, eyFlp (Xu *et al.*, 2005) was a gift from Andreas Bergmann. The stock UAS-FLAG-Fblx7 (Bosch *et al.*, 2014) was a gift from Iswar Hariharan.

To identify the Fbxo42 substrates by mass spectrometry, flies bearing on the second chromosome a polyubiquitin chain

conjugated with biotin and fused with *E.coli* BirA (biotin ligase), UAS-(^{bio}Ub)$_6$-BirA (Franco *et al.*, 2011; Ramirez *et al.*, 2015) were crossed with flies carrying on the third chromosome the full-length Fbxo42 N-terminally tagged by 3xFLAG-3xHA-tag or the F-box control constructs: UAS-3xFLAG-3xHA-ΔFbxo42 (containing the deletion of the F-box domain) or UAS-FLAG-FbxI7 (carrying a different fly F-box protein). Flies containing UAS-3xFLAG-3xHA-Fbxo42 without UAS-(^{bio}Ub)$_6$-BirA were used as an additional control. The constructs were expressed in the *Drosophila* eye using the Glass Multimer Reporter-GAL4 driver (GMR-GAL4).

To confirm the mass spectrometry results, virgin female flies from the GMR-GAL4, UAS-(^{bio}Ub)$_6$-BirA; UAS-FLAG-HA-Fbxo42 stock were crossed with male flies overexpressing Ataxin-2 isoform A C-terminally fused with 3xHA-tag (UAS-Ataxin-2-HA), obtained from FlyORF – Zurich ORFeome Project (fly line ID: F001031).

Mutant clones in eye imaginal discs were generated by FLP (flipase recombinase)/FRT (FLP recombination target) recombination system (Golic, 1991), where flipase expression is under the control of the *eyeless* (*ey*) promoter (Newsome *et al.*, 2000).

To express Ataxin-2 RNAi in Xbp1s-induced “glossy eye” with Fbxo42 mutant suppressor clones, female flies carrying one of the Fbxo42 suppressors, FRT42D, Su218 (Fbxo42^{N423*}) were crossed with male flies bearing UAS-Ataxin-2 RNAi (BL 36114). Males from the progeny containing FRT42D, Su218 and UAS-Ataxin-2 RNAi were crossed with female flies with the genotype eyFlp, GMR-GAL4, UAS-Xbp1^{spliced}; FRT42D, ubiGFP. Flies bearing

eyFlp, GMR-GAL4, UAS-Xbp1^{spliced}; FRT42D, Su218/ FRT42D, ubiGFP without UAS-Ataxin-2 RNAi were used as control.

Mosaic genetic screen and mapping

The FRT42D stock was isogenized and males were collected for ethyl methanesulfonate (EMS) treatment. The males were starved for 8 hours in empty plastic vials and fed with a 25 mM EMS solution overnight for 16-18 hours (paper tissue soaked with EMS solution on the bottom of the vials). After EMS treatment, around 60 males were given one hour for recovery on tissue paper and were then crossed in mass to around 150 virgins of the genotype eyFlp, GMR-GAL4, UAS-Xbp1^{spliced}; FRT42D, ubiGFP. The crosses were settled in new bottles every day, for four days in total and the F1 generation was screened for mosaic clones with suppression of the “glossy” eye phenotype. Suppressors of the “glossy” eye phenotype were balanced over CyO and retested for a reproducible phenotype. Only suppressor stocks that were homozygous lethal were kept, which was necessary for mapping of the mutations. For complementation analysis, each suppressor stock obtained from the screen was crossed to each other to bring the mutations in trans in the progeny to analyse whether unbalanced flies or flies only with the balancer CyO existed. When only CyO balanced progeny existed, the two suppressor mutations are lethal in trans and likely have a lethal hit in the same gene. For mapping of the suppressor mutations, we used the 2R deficiency kit (from the Bloomington *Drosophila* Stock Center). Virgins of the suppressor mutations balanced over CyO were crossed to males of each of the stocks bearing the balanced deficiencies and the F1 generation was

screened for trans-heterozygosity. The existence of only balanced flies in F1 generation, indicated that the mutation is located within the region of the deficiency. The process was repeated with other smaller deficiencies until it could be defined the smallest region harbouring the suppressor mutation. When available, we then tested lethal mutations in candidate genes in the region for trans-lethality with our mutations. The molecular identification of the mutations was done by genomic DNA sequencing of candidate genes from larvae homozygous for the suppressor mutations, collected from stocks balanced over CyO-GFP and also from the parental FRT42D stock before EMS mutagenesis. Genomic DNA preparation was done with the High Pure PCR Template Preparation kit from Roche and sequencing was performed by Stabvida.

Anti-Fbxo42 antibody generation:

A) Cloning of Fbxo42 into pETM-30 plasmid

To generate the anti-Fbxo42 rabbit polyclonal antibody, the DNA sequence coding for amino acids 384 to 667 of Fbxo42 was cloned into pETM-30 at XhoI/NcoI (NEB) restriction sites, to generate a N-terminal GST tagged protein. In addition to GST, Fbxo42 was tagged with two Histidine (His)-tags placed on N- and C- terminals (pETM-30-His-GST-Fbxo42-His). Protein expression was performed in Rosetta bacterial cells.

B) Expression and purification of Fbxo42 antigen

Rosetta bacterial cells were transformed with the pETM-30-His-GST-Fbxo42-His plasmid. A single colony per condition was then picked and placed in 50 ml of liquid LB medium (pre-inoculum) together with antibiotics. Cultures were grown overnight at 37ºC with shaking at 200 rpm. Three cultures containing the pETM-30-His-GST-Fbxo42-His plasmid were prepared. One of these was used as a control for IPTG induction.

The next day, the absorbance of the cultures was measured and the volume of culture to be inoculated in 400 ml of LB medium was calculated to give an optical density (OD) of 0.2. Cultures were incubated for 1 hour and 30 minutes, at 37ºC, with shaking at 200 rpm. The OD was measured again (it should be less than 1). After this time, 1 mM IPTG was added to induce the expression of the Fbxo42 peptide, except for the control (no IPTG induction). Cultures were further incubated at 37ºC with shaking at 220 rpm for 3 hours. The OD was checked at the end of this incubation time. Cultures were then centrifuged at 3500*g*, for 10 minutes, at 4ºC. Supernatants were discarded and pellets were stored at -20ºC until further use. Cell pellets were resuspended in 8 ml of native extraction buffer (50 mM Tris-HCl pH 8.0; 500 mM NaCl; 0.1% Triton X-100). 10 mg/ml of lysozyme was added to the cell suspensions, and these were incubated for 30 minutes at room temperature and 30 minutes at 4ºC. Afterwards, samples were sonicated once for 15 minutes (with 30 second on/off pulses) on ice. These samples were centrifuged for 15 minutes at 3739*g*, 20ºC and supernatants were collected (supernatants will contain the soluble protein). 8 ml of denaturing extraction buffer (50 mM Tris-HCl pH 8.0; 500 mM NaCl;

10 mM imidazole; 8 M urea) was added to the cell pellets and samples were sonicated once again for 15 minutes (with 30 second on/off pulses). Samples were incubated on ice for 30 minutes and centrifuged for 15 minutes at 3739*g*, at 20ºC. Supernatants were collected and stored at -20ºC. Finally, supernatant and pellet extracts were run in 8% SDS-PAGE gels.

His-tagged Fbxo42 was purified using a nickel-containing resin [Profinity™ IMAC (Immobilized-Metal Affinity Chromatography) Ni-Charged Resin (cat. no. 156-0131, Bio-Rad)], as follows: 1.5 ml of resin was used per condition; the resin was washed thrice with distilled water and once with denaturing extraction buffer, with centrifugation at 1000*g* for 3 minutes between washes. Supernatants (7 ml each) were incubated with nickel-containing resin for 2 hours at 4ºC in a shaker. The resins were loaded onto PD-10 columns, and these were washed with denaturing washing buffer (50 mM Tris-HCl pH 8.0; 500 mM NaCl; 50 mM imidazole and 8 M urea). Finally, the Fbxo42 peptide was eluted with 2.5 ml of denaturing elution buffer (50 mM Tris-HCl pH 8.0; 500 mM NaCl; 300 mM imidazole; 8 M urea).

The purified Fbxo42 antigen in solution (1.5 mg) was sent to Eurogentec for antibody production (rabbits were injected with the Fbxo42 antigen), with subsequent in-gel affinity purification of the antibody being performed in the laboratory.

Affinity purification of anti-Fbxo42 antibody

To perform the affinity purification of anti-Fbxo42 antibody, the GST-Fbxo42 peptide (antigen) was loaded onto an 8% SDS-PAGE gel. To load the maximum volume of antigen onto the gel, a

wide comb was used. This comb contained one well of regular size for protein ladder and one large well for antigen. Following electrophoresis, gel was transferred onto a nitrocellulose membrane of 0.2 µm (Bio-Rad) and, after its staining with Ponceau S solution, a strip containing the antigen was cut out. This membrane strip was then rinsed in water until the background was clean. Afterwards, the membrane strip was pre-eluted with 100 mM glycine (pH 2.5) for 10 minutes and washed thrice with TBS-T (10 mM Tris, 300 mM NaCl, 0.1% Tween-20), 5 minutes each. Next, the membrane strip was blocked with 5% of non-fat milk in TBS-T for 1 hour at room temperature. Following three washes with TBS-T, membrane was incubated with 1 ml of rabbit (#0451) antiserum (containing the anti-Fbxo42 antibody) overnight at 4°C.

The day after, membrane was washed thrice with TBS-T, and anti-Fbxo42 antibody was eluted by incubating the membrane with 100 mM glycine (pH 2.5) for 8 minutes. Subsequently, to neutralize the acidic glycine, the eluted anti-Fbxo42 was mixed with 2 M Tris-HCl (pH 8.5). The elution steps were repeated three times and the eluted anti-Fbxo42 was stored at -20°C.

Preabsorption of anti-Fbxo42 antibody

To minimize the background staining observed by immunofluorescence and the presence of nonspecific bands detected by immunoblot, affinity purified anti-Fbxo42 antibody was preabsorbed before use. Briefly, L1 larvae homozygous for Su226 ($Fbxo42^{H436*}$) (collected from Su226, FRT42D/ CyO-GFP stock) were incubated overnight at 4°C with affinity purified anti-Fbxo42 antibody diluted in BBT-250 (1:3 dilution). The following day,

supernatant was collected and centrifuged at 8000 rpm for 2 minutes to remove larval debris. The clarified supernatant (containing the preabsorbed anti-Fbxo42 antibody) was then stored at 4°C and tested by immunofluorescence and immunoblot.

Fbxo42 protein expression in fly tissues

In order to detect the Fbxo42 protein expression in adult and larval tissues of *Drosophila*, larvae and adult flies were dissected in 1× PBS. From adult flies were collected brains, testis and ovaries [organs in which Fbxo42 protein is predicted to have a moderate expression according to FlyAtlas Anatomical Expression Data (https://flybase.org/reports/FBgn0034704.htm)]. From larvae were harvested eye imaginal discs, salivary glands, brains, lymph/ring glands, carcasses, fat bodies and midguts. The different tissues were then lysed in denaturing lysis buffer [8 M Urea, 50 mM N-ethylmaleimide (NEM, Sigma-Aldrich) and 1% SDS] supplemented with protease inhibitors (cOmplete™, Mini, EDTA-free Protease Inhibitor Cocktail, Roche), and protein concentration was determined by *DC*™ Protein Assay Kit from Bio-Rad. Equal amounts of protein lysates were loaded onto 8% SDS-PAGE gels. Immunoblots were performed with rabbit anti-Fbxo42 (1:1000) and mouse anti-alpha-Tubulin (1:500, AA4.3, Developmental Studies Hybridoma Bank, DSHB) antibodies.

To test the specificity of Fbxo42 antibody, L1 larvae homozygous and heterozygous for Su226 ($Fbxo42^{H436*}$) were collected from Su226, FRT42D/ CyO-GFP stock and processed as above-mentioned. The larval extracts were then analysed by

immunoblot with rabbit anti-Fbxo42 (1:1000) and mouse anti-alpha-Tubulin (1:500, AA4.3, DSHB) antibodies.

Immunofluorescence and imaging

Drosophila adult or larval tissues were dissected in 1× PBS, fixed with 4% PFA (paraformaldehyde) in 1× PBS at room temperature for at least 45 minutes and washed three times with PBT (1× PBS + 0.3% Triton X-100), 10 minutes each. Afterwards, fly's tissues were incubated with primary antibodies diluted in BBT-250 (0.1% BSA, 0.1% Triton X-100, 250 mM NaCl in 1× PBS) overnight, at 4°C under gentle agitation. The primary antibodies used were as follow: rat anti-ELAV (1:200, 7E8A10, DSHB), mouse anti-HA (1:200, Covance, MMS101P) and rabbit anti-Fbxo42 (1:100). Incubation with anti-Fbxo42 antibody was preceded by an extra step of blocking and permeabilization; tissues were incubated in block-permeabilization solution (1% BSA, 0.3% Triton X-100 in 1× PBS) for 1 hour at room temperature. After overnight incubation with primary antibodies, fly's tissues were washed three times with PBT for 10 minutes each and incubated with fluorescent conjugated secondary antibodies (Jackson ImmunoResearch Laboratories) for 2 hours at room temperature. Following three washes in PBT, the tissues were mounted in VECTASHIELD® Antifade Mounting Medium with DAPI (Vector Laboratories, H-1200-10) and image acquisition was performed on a confocal microscope (Leica SP5 Live or Zeiss LSM 880). For imaging of adult fly eyes, 2-5 days old flies were anesthetized with CO_2 and transferred to a microscope slide where fly bodies were immobilized with transparent nail polish. *Drosophila* eye' s pictures were acquired using a Leica Z16 APO

macroscope equipped with a Leica DFC 420C camera with Leica's extended depth of focus (Montage) software.

^{bio}Ub pulldowns

For the biotin pulldowns were used the aforementioned fly stocks carrying GMR-GAL4, UAS-(^{bio}Ub)$_6$-BirA together with one of the following F-box constructs: UAS-FLAG-HA-Fbxo42; UAS-FLAG-HA-ΔFbxo42 or UAS-FLAG-Fbxl7, the latter two used as controls. Flies bearing only UAS-FLAG-HA-Fbxo42 without ^{bio}Ub or BirA were used as an additional control. Adult flies with 2-5 days old were collected and fragmented by several rounds of flash freezing in liquid nitrogen and vortexing. Afterwards, fly heads were separated from the remaining body parts using a set of sieves with a nominal cut-off of 850, 710 and 425 µm on dry ice. Biotin pull-downs from *Drosophila* heads were performed as previously described (Ramirez *et al.*, 2015). Briefly, 500 mg of fly heads from each genotype was homogenized in 2.9 ml of lysis buffer (8 M urea, 1% SDS, 1× PBS, 50 mM N-ethylmaleimide from Sigma, and a protease inhibitor cocktail from Roche). After the centrifugation of lysates at 16,000*g* at 4 ºC for 5 min, the supernatant was applied to a PD10 desalting column (GE Healthcare) previously equilibrated with binding buffer (3 M urea, 1 M NaCl, 0.25% SDS, 1× PBS and 50 mM N-ethylmaleimide). Eluates, except 50 µl kept as input fraction, were incubated with 250 µl of NeutrAvidin agarose beads (Thermo Scientific) for 40 min at room temperature and further 2 h and 20 min at 4 ºC with gentle rolling. The material bound to the beads was washed with the following washing buffers (WB) (buffer

composition can be found below): twice with WB1, thrice with WB2, once with WB3, thrice with WB4, once again with WB1, once with WB5, and thrice with WB6. The ubiquitylated material, still bound to the beads, was then eluted by heating the beads at 95 ºC for 5 min in 125 µl of elution buffer (250 mM Tris-HCl, pH 7.5, 40% glycerol, 4% SDS, 0.2% bromophenol blue, and 100 mM DTT). Finally, samples were centrifuged at 16,000*g* at room temperature for 2 min in a Vivaclear Mini 0.8 µm PES-micro-centrifuge filter unit (Sartorious) to discard the NeutrAvidin resin. The composition of the washing buffers used for the biotin pulldown assays were: WB1, 8 M urea, 0.25 SDS, 1× PBS; WB2, 6 M guanidine-HCl, 1× PBS; WB3, 6.4 M urea, 1 M NaCl, 0.2% SDS, 1× PBS; WB4, 4 M urea, 1 M NaCl, 10% isopropanol, 10% ethanol, 0.2% SDS, 1× PBS; WB5, 8 M urea, 1% SDS, 1× PBS; WB6, 2% SDS, 1× PBS.

Before proceeding with mass spectrometry, inputs and eluted fractions were analysed by immunoblotting with mouse anti-FLAG (1:1000, M2 clone, cat. no. F1804, Sigma-Aldrich), goat anti-Biotin-HRP (1:1000, cat. no. 7075, Cell Signalling Technology, CST) and mouse anti-alpha-Tubulin (1:500, cat. no. AA4.3, DSHB) antibodies.

In-gel trypsin digestion and peptide extraction

Ubiquitylated material eluted from biotin pulldown assays was concentrated in a Vivaspin 500 centrifugal filter units (Sartorius) and resolved by SDS-PAGE in 4–12% Bolt Bis-Tris precast gels (Invitrogen). Proteins were visualized with GelCode blue stain reagent (Invitrogen) and gel lanes were cut into 4 slices to remove known endogenously biotinylated proteins and avidin monomers, as

previously described (Ramírez *et al.*, 2021). Selected slices were subjected to in-gel trypsin digestion according to Shevchenko et al. (1996) with minor modifications (Shevchenko *et al.*, 1996). Proteins were reduced with DTT (10 mM in 50 mM NH_4HCO_3, 56 ºC, 45 min), alkylated with chloroacetamide (25 mM in 50 mM NH4HCO3, room temperature, 30 min, dark) and incubated with trypsin (12.5 ng/ml in 50mM NH4HCO3, 37 ºC, overnight). The supernatant was recovered, and peptides were extracted twice from the gel: first, with 25mM NH4HCO3 and acetonitrile and then with 0.1% trifluoracetic acid and acetonitrile. The recovered supernatants and the extracted peptides were pooled, dried in a SpeedVac (Thermo Fisher Scientific) and subsequently desalted with homemade C18 tips (3M Empore C18).

Liquid Chromatography with tandem Mass Spectrometry (LC-MS/MS)

An EASY-nLC 1200 liquid chromatography system interfaced with a Q Exactive HF-X mass spectrometer (Thermo Scientific) via a nanospray flex ion source was employed for the mass spectrometric analyses. Peptides were loaded onto an Acclaim Pep-Map100 pre-column (75 µm × 2 cm, Thermo Scientific) connected to an Acclaim PepMap RSLC C18 (75 µm × 25 cm, Thermo Scientific) analytical column. Peptides were eluted from the column using the following gradient: 18 min from 2.4 to 24%, 2 min from 24 to 32% and 12 min at 80% of acetonitrile in 0.1% formic acid at a flow rate of 300 nl min^{-1}. The mass spectrometer was operated in positive ion mode. Full MS scans were acquired from m/z 375 to 1800 with a resolution of 120,000 at m/z 200. The 10 most intense

ions were fragmented by higher energy C-trap dissociation with normalized collision energy of 28. MS/MS spectra were recorded with a resolution of 15,000 at m/z 200. The maximum ion injection times were 100 ms and 120 ms, whereas AGC target values were 3 × 106 and 5 × 105 for survey and MS/MS scans, respectively. In order to avoid repeat sequencing of peptides, dynamic exclusion was applied for 12 s. Singly charged ions or ions with unassigned charge state were also excluded from MS/MS. Data were acquired using Xcalibur software (Thermo Scientific).

MS data processing and bioinformatics

Acquired raw data files were processed with the MaxQuant (Cox & Mann, 2008) software (version 1.6.0.16) using the internal search engine Andromeda (Cox *et al.*, 2011) and tested against the UniProt database filtered for *Drosophila melanogaster* entries (release 2017_11; 43,868 entries). Mass tolerance was set to 8 and 20 ppm at the MS and MS/MS level, respectively. Enzyme specificity was set to trypsin, allowing for a maximum of three missed cleavages. Match between runs option was enabled with 1.5 min match time window and 20 min alignment window to match identification across samples. The minimum peptide length was set to seven amino acids. The false discovery rate for peptides and proteins was set to 1%. Normalized spectral protein LFQ (Label Free Quantitation) intensities were calculated using the MaxLFQ algorithm (Cox *et al.*, 2014).

MaxQuant output data were analyzed with the Perseus module (version 1.5.6.0) (Tyanova *et al.*, 2016) in order to determine the proteins significantly enriched in each of the genotypes. During

the procedure, contaminants, reverse hits, as well as proteins with no intensity were removed, as well as those proteins only identified by site and/or with no unique peptides. Protein abundance was determined by LFQ intensity. Missing intensity values were replaced with values from a normal distribution (width 0.3 and down shift 1.8), meant to simulate expression below the detection limit (Tyanova *et al.*, 2016). Statistically significant changes in protein abundance were assessed by two-tailed Student's t-test.

Immunoblots from ^{bio}Ub pulldowns

In order to confirm the results obtained by mass spectrometry, ^{bio}Ub pulldowns were carried out using flies bearing GMR-Gal4, UAS-(^{bio}Ub)$_6$-BirA; UAS-FLAG-HA-Fbxo42/UAS-Ataxin-2-HA. All Biotin pulldown steps were identical to those described above, with the modification of the elution step. The elution of biotinylated Ataxin-2-HA from the beads was performed with 4× Laemmli buffer (250 mM Tris-HCl pH 6.8, 40% glycerol, 8% SDS, 0.02% bromophenol blue) without reducing agents. Afterwards, the eluted volume was divided into two: half of the volume was incubated with 100 mM of DTT and heated at 65°C for 20 minutes. Input and eluted samples (in the presence/absence of DTT) were loaded onto 7.5% Mini-Protean® TGX™ (Tris-Glycine eXtended) Precast Protein Gels (Bio-Rad) and immunoblots were performed with rat anti-HA (1:1000, 7C9, Chromotek) antibody.

Cell culture, transfections and RNAi treatments

Drosophila S2 cells (Schneider, 1972) were cultured at 24°C without CO_2 in Schneider's *Drosophila* medium (Biowest) supplemented with 10% heat inactivated Fetal Bovine Serum (FBS, Biowest), 100 U/ml of penicillin plus 100 µg/ml of streptomycin (Thermo Fisher Scientific). The complete medium was filtered with 0,2 µm PES filter (VWR). S2 cells were transfected with the indicated plasmids using Effectene transfection reagent (QIAGEN) according to the manufacturer's instructions.

RNA-mediated interference (RNAi) was performed as described in (Clemens *et al.*, 2000). Primer pairs bearing a 5' end T7 RNA polymerase binding site were used to PCR amplify specific sequences of the genes to be inhibited. PCR products (with approximately 500-600 bp in length) were then purified with NucleoSpin® Gel and PCR Clean-up kit (Macherey-Nagel, MN) or with NZYGelpure kit (NZYtech) and used as templates for dsRNA synthesis with T7 RiboMAX™ Express Large Scale RNA Production System (Promega). After the DNase treatment, dsRNAs were purified and concentrated with RNA Clean & Concentrator™-5 kit (Zymo Research).

Ubiquitylation assays in S2 cells

For the ubiquitylation assay, 5.0 x 10^5 S2 cells/ well were seeded in 6-well plates and treated with 25-30 µg of Fbxo42 dsRNA for 8 days. S2 cells endogenously expressing Fbxo42, and cells treated with Fbxo42 dsRNA were transfected with 200 ng of each one of the following plasmids: pActin-Gal4, pUAST-Ataxin-2-GFP and pUAST-His-Myc-Ubiquitin. Empty pUAST was used instead of

pUAST-His-Myc-Ubiquitin as ubiquitylation control. 3 days after transfection, cells were incubated with 50 µM of MG132 (Z-Leu-Leu-Leu-al, C2211, Merck) for 4 hours, to inhibit proteasome activity, and resuspended in lysis buffer (50 mM Tris-HCl pH 7.5, 150 mM NaCl, 1 mM EDTA, 0.5% Triton X-100) supplemented with protease inhibitors (cOmplete™, Mini, EDTA-free Protease Inhibitor Cocktail, Roche) and 0.7% of NEM. Cell extracts were harvested and incubated on ice for at least 30 minutes. To perform the pulldown of proteins conjugated with His-myc-Ubiquitin, each cell lysate was incubated with 15 µl of a nickel-charged resin suspension (Profinity™ IMAC Ni-Charged Resin, cat. no. 156-0131, Bio-Rad) for 2 hours and 20 minutes at 4°C. Afterwards, resin was washed thrice in 1× PBS + 20mM imidazole. The elution of the ubiquitylated molecules from the resin was performed with elution buffer containing 1× PBS + 250 mM imidazole at room temperature. The eluted volume was divided into two: half of the volume was incubated with 100 mM of DTT and heated at 65°C for 20 minutes. Then, 4× Laemmli buffer (240 mM Tris-HCl pH 6.8, 8% SDS, 40% glycerol, 250 mM DTT, 0.04% bromophenol blue) was added to the samples (with/without DTT), and these were boiled for 5 minutes at 95 °C. Finally, samples were loaded onto 4-15% Mini-Protean TGX™ Precast Protein Gels (Bio-Rad) and immunoblots were performed with rat anti-GFP (1:1000, 3H9, Chromotek) and rat anti-Myc (1:2000, 9E1, Chromotek) antibodies.

Co-Immunoprecipitation

For co-immunoprecipitation of Fbxo42 and SkpA, S2 cells were transfected with pMT-SkpA-HA, pActinGal4, UAS-FLAG-HA-

Fbxo42 or UAS-FLAG-HA-ΔFbxo42. Three days after, to induce the expression of SkpA-HA, 500 mM $CuSO_4$ was added to the culture media 24 h before harvesting the cells in lysis buffer (20 mM HEPES 7.5 pH, 5 mM KCl, 1 mM $MgCl_2$, 0.1% NP-40) supplemented with protease inhibitors (cOmplete™, Mini, EDTA-free Protease Inhibitor Cocktail, Roche). The immunoprecipitation was done using Anti-FLAG M2 Affinity gel (A2220, Sigma). Samples (inputs and eluates) were further analysed by immunoblotting with mouse anti-HA antibody (1:1000, cat. no. MMS-101P, Covance).

Immunoblots

Fly extracts or cell lysates were prepared in the above-mentioned lysis buffers supplemented with protease inhibitors (cOmplete™, Mini, EDTA-free Protease Inhibitor Cocktail, Roche). Protein concentration was determined by *DC*™ Protein Assay Kit from Bio-Rad. Afterwards, samples were mixed with 4× SDS Laemmli buffer (240 mM Tris-HCl pH 6.8, 8% SDS, 40% glycerol, 250 mM DTT, 0.04% bromophenol blue) and boiled at 95°C for 5 minutes. Proteins were size separated by SDS-PAGE and transferred onto nitrocellulose membranes of 0.2 µm (Bio-Rad). Immunoblots were blocked with 5% non-fat milk in TBS-T containing 0.1% Tween-20 or in PBS-T containing 0.05-0.1% Tween-20 for 1 hour. After blocking, membranes were incubated overnight at 4°C with the following primary antibodies (table S2): mouse anti-alpha-Tubulin (1:500, AA4.3, DSHB), rabbit anti-Fbxo42 (1:1000), rat anti-GFP (1:1000, 3H9, Chromotek), rat anti-HA (1:1000, 7C9, Chromotek), mouse anti-HA (1:1000, 16B12 clone, BioLegend; previously cat. no. MMS-101P, Covance), rat anti-Myc (1:2000, 9E1,

Chromotek), goat anti-Biotin-HRP conjugated (1:1000, cat. no. 7075, CST) and mouse anti-FLAG (1:1000, M2 clone, cat. no. F1804, Sigma-Aldrich).

The following day, membranes were washed 4x for 10 minutes in TBS-T or PBS-T and incubated with HRP-conjugated secondary antibodies respective to the primary antibodies' species, specifically, sheep anti-mouse HRP (1:10000, cat. no. NXA931, Cytiva), goat anti-rat HRP (1:2000, cat. no. R-05075-500, Advansta) and goat anti-rabbit HRP (1:5000, product no. AS10 668, Agrisera) for 2 hours at room temperature. Membranes were washed 4x for 10 minutes in TBS-T/PBS-T, and the signal was developed using ECL™ Prime Western Blotting Detection Reagent (RPN2232, Cytiva) and detected using a Chemidoc XRS+ (Bio-Rad) or an iBright™ FL 1500 Imaging System (Thermo Fisher Scientific). iBright™ Analysis Software was used for densitometry.

2.4 Results

Overexpression of the Xbp1s in the *Drosophila* adult eye induces the "glossy" eye phenotype

Previous work performed in our laboratory by Nadine Schweizer, who conducted the experiments from Figure 2.1 to 2.11, showed that the overexpression of Xbp1s in the *Drosophila* eye via the Glass Multimer Reporter-GAL4 driver (GMR-GAL4) leads to the "glossy" eye phenotype (Schweizer, 2015). Remarkably, compared to the wild-type eye (Figure 2.1A), the "glossy" eye is smaller, and its external structure becomes a thin layer of yellow cuticle (Figure 2.1B). This "glossy" eye phenotype is caused by the death of

photoreceptors, cone and pigment cells (Liao *et al.*, 2006). To attempt to rescue the "glossy" eye phenotype, we co-expressed Xbp1 unspliced (Xbp1u) together with Xbp1s, in the *Drosophila* eye, and observed a partial recovery of the red pigment and the restoration of the ommatidial structure of the eye (Figure 2.1C). This result is consistent with the finding that mammalian Xbp1u acts as a negative regulator of Xbp1s in the ER stress response (Yoshida *et al.*, 2006).

In order to test whether the cell death detected in the "glossy" eye was due to apoptosis, a genetically programmed form of cell death, we co-expressed Xbp1s together with the anti-apoptotic proteins, baculovirus P35 or DIAP-1 (*Drosophila* inhibitor of apoptosis 1), in the *Drosophila* eye, and in both cases we observed partial rescue of the red pigment and the recovery of the external lens structure of the eye (Figure 2.1D, E). Therefore, these results suggest that apoptotic cell death plays a role in the induction of the "glossy" eye phenotype by Xbp1s.

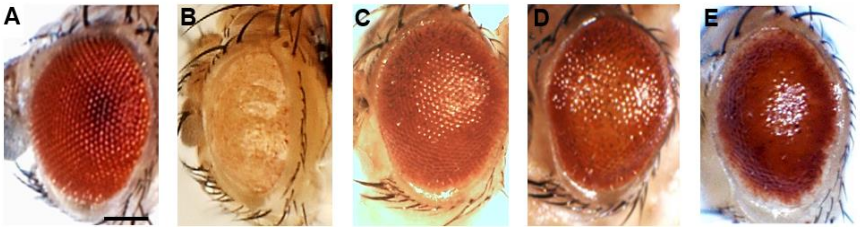

Figure 2.1: Overexpression of Xbp1s in the *Drosophila* eye by the GMR-GAL4 driver leads to cell death. (A) wild-type adult *Drosophila* eye (Canton S); **(B)** "glossy" eye phenotype caused by Xbp1s-overexpression (genotype: GMR-GAL4, UAS-Xbp1s, UAS-DsRed); **(C)** partial suppression of the "glossy" eye phenotype by co-expression of Xbp1u (genotype: GMR-GAL4, UAS-Xbp1s, UAS-Xbp1u); **(D)** partial suppression of the "glossy" eye phenotype by co-expression of caspase inhibitor P35 (genotype: GMR-GAL4, UAS-Xbp1s, UAS-P35); **(E)** partial suppression of the

(Figure 2.1 continued):... "glossy" eye phenotype by co-expression of DIAP-1 (genotype: GMR-GAL4, UAS-Xbp1s, UAS-DIAP-1). Scale bar = 200 μm.

In adult flies, mosaic expression of the UAS-DsRed control, by the Flipase/FRT system (Golic, 1991), results in an eye where approximately two-thirds of the cells express DsRed (Figure 2.2A). On the other hand, mosaic expression of UAS-DsRed together with UAS-Xbp1s results in a much-reduced number of DsRed-positive cells (presenting the "glossy" eye phenotype) (Figure 2.2B). These results indicate that Xbp1s induces the "glossy" eye phenotype in a cell-autonomous manner and that most of the cells overexpressing Xbp1s die during the eye development, being replaced by "wild-type" cells.

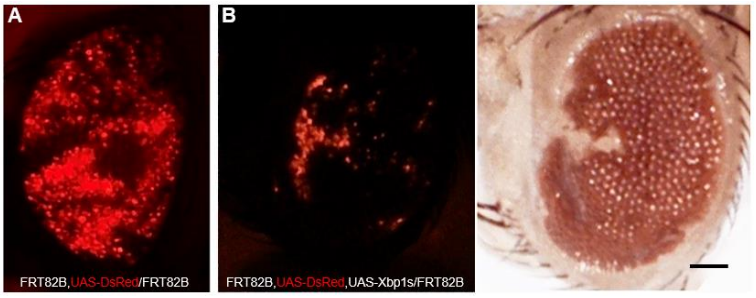

Figure 2.2: Most of the Xbp1s-overexpressing cells die during the eye development. (A) Mosaic adult eye presenting UAS-DsRed clones (around 66% of the eye), genotype: eyFlp, GMR-GAL4; Sco/CyO; FRT82B, UAS-DsRed/FRT82B; **(B)** Mosaic adult eye containing Xbp1s-overexpressing clones, labelled by DsRed, showing the "glossy" eye phenotype (genotype: eyFlp, GMR-GAL4; Sco/CyO; FRT82B, UAS-DsRed, UAS-Xbp1s/FRT82B). Scale bar = 100 μm.

Moreover, TUNEL staining (a method for detecting apoptotic cells) of third instar larval eye imaginal discs containing clones of cells expressing UAS-Xbp1s labelled by DsRed, revealed the

presence of higher apoptosis levels in Xbp1s-overexpressing cells (Figure 2.3).

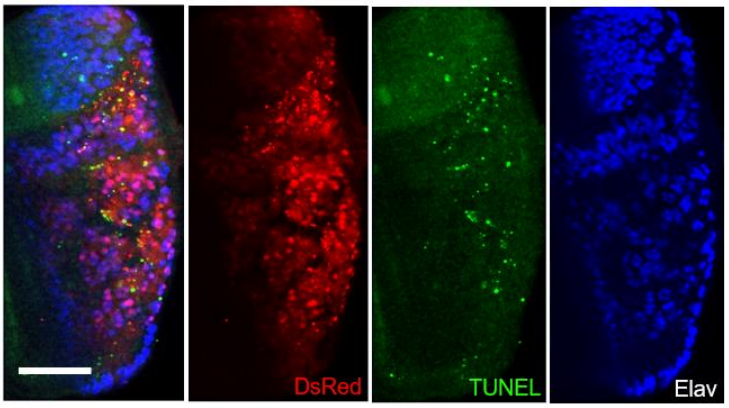

Figure 2.3: Overexpression of Xbp1s activates apoptosis in the eye imaginal discs of third instar larvae.
Immunofluorescence of eye discs containing Xbp1s-overexpressing clones, labelled by DsRed, showing increased levels of TUNEL labelling (green). ELAV (in blue) is a marker of the photoreceptors. Scale bar = 60 µm.

In addition to apoptosis, the presence of autophagy was also analysed in the Xbp1s-overexpressing cell clones. Autophagy usually plays a protective role in cells, however, disruption of autophagy mechanisms or excessive autophagic flux can lead to cell death (Liu *et al.*, 2023). To investigate whether autophagy is involved in the induction of the "glossy" eye phenotype, we performed the immunostaining of eye imaginal discs from third instar larvae containing DsRed-labelled Xbp1s clones and detected high levels of the autophagy marker LC3-GFP in Xbp1s-overexpressing cells (Figure 2.4). This is consistent with the findings from a previous report showing that *Drosophila* fat body cells

overexpressing Xbp1s also have increased levels of GFP-Atg8a/LC3 (Arsham & Neufeld, 2009).

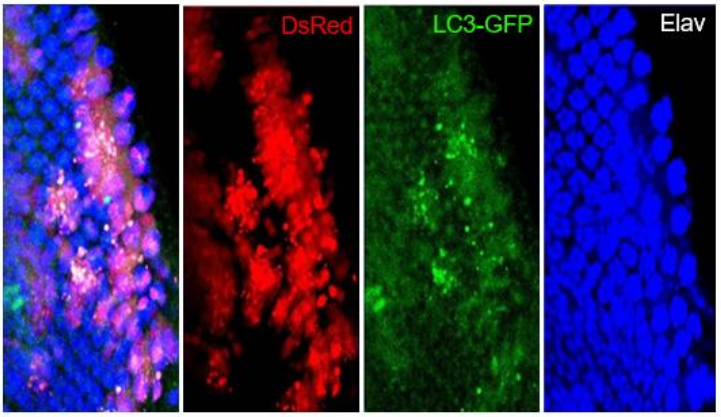

Figure 2.4: Overexpression of Xbp1s activates autophagy in the eye imaginal discs of third instar larvae.
Immunofluorescence of eye discs containing Xbp1s-overexpressing clones, labelled by DsRed, showing high levels of the autophagy marker LC3-GFP (in green). ELAV (in blue) is a marker of the photoreceptors.

Loss-of-function mutations in *Fbxo42* suppress the "glossy" eye phenotype induced by Xbp1s

In order to search for mutations that suppress the "glossy" eye phenotype induced by GMR-GAL4 driven overexpression of Xbp1s, a genetic screen with the mutagenic alkylating agent EMS (Ethyl methanesulfonate) was performed. EMS induces new mutations, mostly GC to AT transitions by guanine alkylation, at random sites of the genome (Lin *et al.*, 2014). Most of the EMS-induced mutagenesis result in point mutations (Lin *et al.*, 2014).

In our mutagenesis screen, male flies (carrying the FRT42D) were starved for 8 hours and fed with a sugar-EMS solution overnight. Afterwards, they were crossed with female virgins

bearing eyFlp, GMR-GAL4, UAS-Xbp1s and the corresponding FRT42D together with the UbiGFP construct (Figure 2.5). The progeny of this cross exhibits mosaic eyes, induced by the Flp/FRT system (Golic, 1991).

The F1 generation (Figure 2.5) was analysed to look for mutations that would suppress the “glossy” eye phenotype induced by Xbp1s, which could be identified by more pigmentation (and more structured ommatidial patterning) in homozygous mutant cell clones.

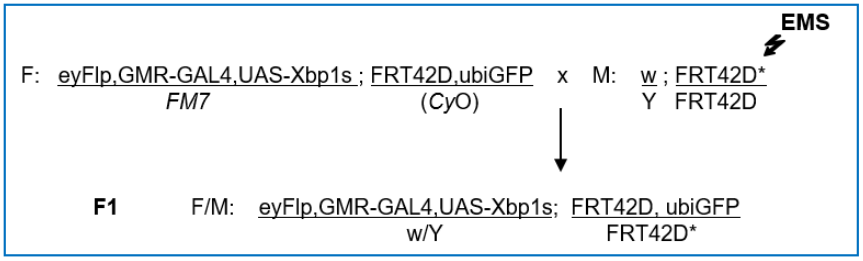

Figure 2.5: Crossing scheme of the EMS screen. For this cross, male flies (M) mutagenized with EMS, carrying the FRT42D, were crossed with virgin females (F), overexpressing Xbp1s, containing flipase and the corresponding FRT42D. Flies from the F1 generation were analysed to look for suppressors of the “glossy” eye phenotype induced by Xbp1s.

By screening around 80 000 EMS mutagenized flies, we were able to identify 32 mutations on the right arm of the second chromosome (2R), that suppressed the “glossy” eye phenotype induced by Xbp1s.

The mutations identified in our genetic screen were mapped by lethality. To be sure that the suppression of the “glossy” eye phenotype (Figure 2.6A) and the lethality were due to a mutation in the same gene, and since EMS (at the concentration used in our screen, 25 mM) induces on average one mutation per 400 kb

(Cooper *et al.*, 2008; Blumenstiel *et al.*, 2009), we attempted to identify complementation groups among the mutants. Thus, if two suppressors were lethal in trans, we could be sure that the lethality and suppression were due to mutations in the same gene.

The 32 suppressors obtained from the EMS screen were crossed to each other, allowing us to identify four different complementation groups. The biggest complementation group contained the following 14 suppressor (Su) mutations (the number indicates the bottle in which they were identified): Su209b (Figure 2.6B), Su212b, Su217c, Su218b (Figure 2.6C), Su226a, Su273-1, Su274-1, Su311, Su323, Su336, Su357-3, Su359, Su397 and Su442. These suppressors show clones of cells with suppression of the "glossy" eye phenotype, with partial recovery of the red pigmentation and partial restoration of the external lens structure of the eye. This complementation group was mapped by crossing the mutant alleles with a set of deficiencies (a collection of stocks containing different deletions in the genome), from the Bloomington *Drosophila* Stock Center, covering the right arm of the second chromosome.

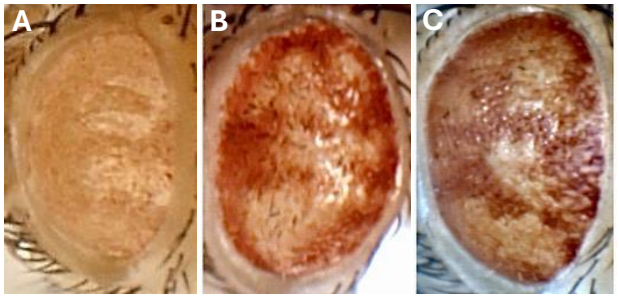

Figure 2.6: Suppressors of the "glossy" eye phenotype induced by Xbp1s. (A) "Glossy" eye phenotype (genotype: GMR-GAL4, UAS-Xbp1s, UAS-DsRed); **(B)** Su209, containing clones of cells that suppress the

(Figure 2.6 continued):…"glossy" eye phenotype (genotype: eyFlp, GMR-Gal4, UAS-Xbp1s; FRT42D, Su209/FRT42D, UbiGFP); **(C)** Su218, containing clones of cells that suppress the "glossy" eye phenotype (genotype: eyFlp, GMR-Gal4, UAS-Xbp1s; FRT42D, Su218/FRT42D, UbiGFP).

In order to identify the gene mutated in the above-mentioned complementation group, several crosses were performed. From the crosses of the mutant alleles with the deficiency Df(2R)BSC597 (58A2-58F1), we did not obtain non-balanced viable progeny, only a few adult escapers with the out-held wing phenotype. However, by testing different deficiencies covering the region 58A2-58F1, we were able to get viable non-balanced progeny with deficiencies Df(2R)Exel7170 and Df(2R)01D01W-L133, mapping this complementation group to an interval of twelve genes between 58C1 and 58D1 (Figure 2.7).

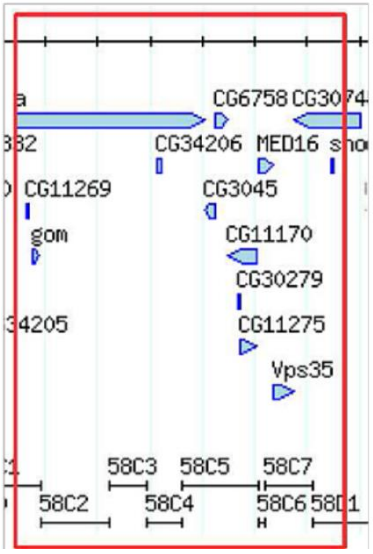

Figure 2.7: Schematic representation of the genomic region 58C1-58D1, mapped by the 2R deficiency kit (Bloomington *Drosophila* Stock Center), harbouring several candidate genes, including *CG6758* (*Fbxo42*).

Regarding the region 58C1-58D1, viable non-balanced progeny was obtained with the deficiency Df(2R)a[7] (this harbours the *arc* gene and two intergenic genes, *CG11269* and *gom*), but not with Df(2R)a^{EX1}.Since the distal end of the deficiency Df(2R)a^{EX1} was not molecularly defined (Liu & Lengyel, 2000), we tested how far distantly this deficiency reaches, by crossing Df(2R)a^{EX1} with P-element insertions in *Vps35* (P(EV)Vps35^{EY16641} and P(EP)Vp35^{EY14200}) and in *CG3074* (P(GawB) CG3074^{NP7371}) genes. From these crosses we obtained viable non-balanced progeny, and in this manner, we can conclude that Df(2R)a^{EX1} does not reach *Vps35*. Also, our suppressors were not lethal over the P-element insertions in *Vps35*. With this, we rendered our region of interest to six genes: *CG6758* (*Fbxo42*), *MED16*, *CG3045*, *CG11170*, *CG30279* and *CG11275* (Figure 2.7). Since there were no lethal alleles for these candidate genes, we sequenced the genomic DNA extracted from homozygous larvae for Su218, Su359, and the FRT42D line (exposed to EMS mutagenesis) as a control. *MED16* was sequenced first, but no mutation was found in this gene. The second gene to be sequenced was *Fbxo42*, in which we found several mutations. We sequenced six (Su209, Su212, Su217, Su218, Su226 and Su359) of the fourteen mutant alleles and all of them contained mutations in *Fbxo42*. This gene encodes a 667 amino acid (aa) protein. Most of the mutations identified in Fbxo42 were premature Stop codons. Specifically, Su209 had a point mutation (G>A), resulting in a premature Stop codon at position 131. For Su212, Su217 and Su218 the same 11 bp deletion was identified, corresponding to the deletion of amino acids 344-347, leading to a frameshift and a premature Stop codon at position 423.

Two mutations were identified in Su226: a point mutation (C>T), leading to the substitution of threonine 218 by methionine, and an early Stop codon at position 436. For Su359, one point mutation (C>T) was found, resulting in the substitution of glycine 639 by glutamic acid (Figure 2.8).

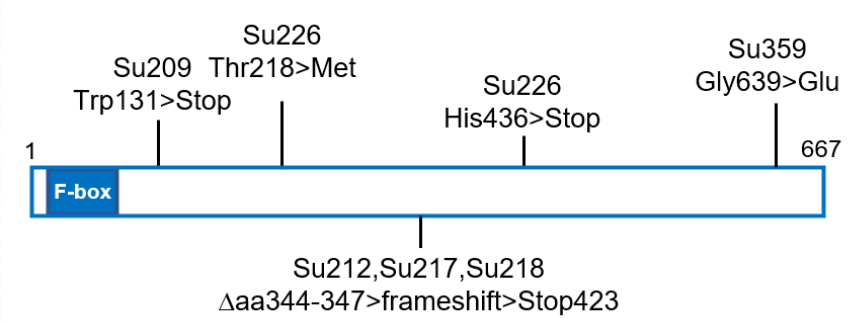

Figure 2.8: Schematic representation of the Fbxo42 protein (1 to 667 amino acids), showing the mutations obtained in the EMS screen. At the N-terminus is the F-box domain (blue box, 21 to 70 aa). The mutations identified in six of the suppressor alleles (Su209, Su212, Su217, Su218, Su226 and Su359) are highlighted in the protein scheme. Su209 has an early Stop codon at position 131 [Tryptophan (Trp) 131>Stop]. Su212, Su217 and Su218 have a small deletion (344-347 aa), leading to a frameshift and a premature Stop codon at position 423. Su226 contains the substitution of Threonine (Thr) 218 for Methionine (Met) and a premature Stop codon at position 436 [Histidine (His) 436>Stop]. Su359 contains the substitution of Glycine (Gly) 639 for Glutamic acid (Glu).

Rescue of the mosaic suppression of the Xbp1s-induced "glossy" eye phenotype by Fbxo42 constructs

To show that the mosaic suppression of the Xbp1s-induced "glossy" eye phenotype was indeed due to mutations in *Fbxo42*, we overexpressed tagged versions of Fbxo42 [Fbxo42-GFP (Figure 2.9B) and FLAG-HA-Fbxo42 (Figure 2.9D)] in the background of

Fbxo42 mutant suppressor clones in the *Drosophila* eye (Figure 2.9A, C, respectively). Using these constructs, we were able to revert the mosaic suppression of the "glossy" eye phenotype by mutations in *Fbxo42*. The same result was obtained when we overexpressed a Pacman genomic rescue construct (CH322-12H15) containing *Fbxo42* (Figure 2.9F), in the background of *Fbxo42* mutant suppressor clones in the fly eye (Figure 2.9E). Taken together these results demonstrate that mutations in *Fbxo42*, and not any other mutation that may be present in the genome, are indeed responsible for the suppression of the Xbp1s-induced "glossy" eye phenotype.

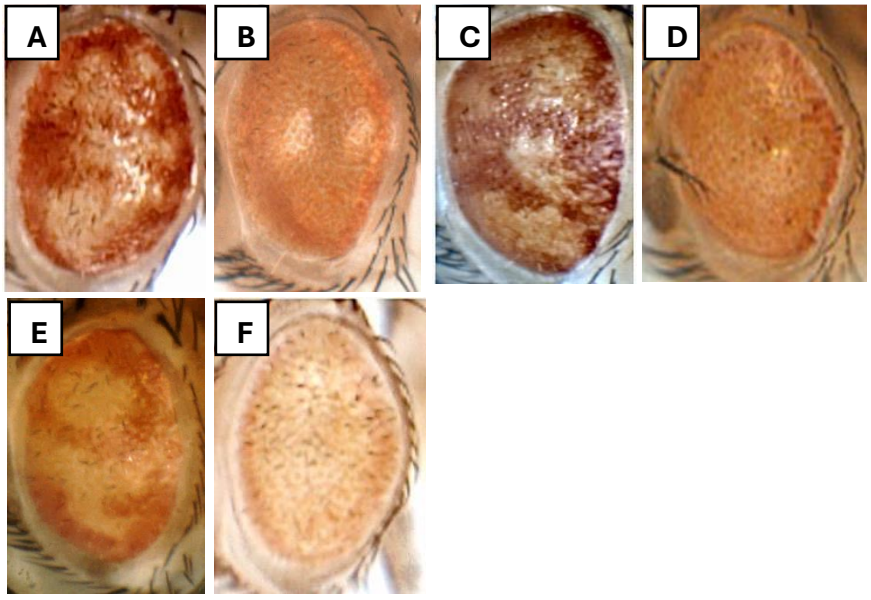

Figure 2.9: Rescue of the mosaic suppression of the Xbp1s-induced "glossy" eye phenotype by Fbxo42 constructs. (A) Su209, containing suppression clones of the Xbp1s-induced "glossy" eye phenotype (genotype: eyFlp, GMR-Gal4, UAS-Xbp1s; FRT42D, Su209/FRT42D, UbiGFP); **(B)** rescue of the suppression observed in (A) with the Fbxo42-GFP construct (genotype: eyFlp, GMR-GAL4, UAS-Xbp1s; FRT42D, Su209/FRT42D, UbiGFP; UAS-Fbxo42-GFP); **(C)** Su218, containing

(Figure 2.9 continued):…suppression clones of the Xbp1s-induced "glossy" eye phenotype (genotype: eyFlp, GMR-GAL4, UAS-Xbp1s; FRT42D, Su218/FRT42D, UbiGFP); **(D)** rescue of the suppression observed in (C) with the FLAG-HA-Fbxo42 construct (genotype: eyFlp, GMR-GAL4, UAS-Xbp1s; FRT42D, Su218/FRT42D, UbiGFP; UAS-FLAG-HA-Fbxo42); **(E)** Su359, containing suppression clones of the Xbp1s-induced "glossy" eye phenotype (genotype: eyFlp, GMR-GAL4, UAS-Xbp1s; FRT42D, Su359/FRT42D, UbiGFP); **(F)** rescue of the suppression observed in (E) with a Pacman genomic rescue construct (CH322-12H15), containing Fbxo42 (genotype: eyFlp, GMR-GAL4, UAS-Xbp1s; FRT42D, Su359/FRT42D, UbiGFP; CH322-12H15).

To ensure that Fbxo42 was not required for transcriptional activation by the GAL4/UAS system (method used in the EMS screen), we generated Fbxo42 (Su218 – Fbxo42^{N423*}) clones in eye imaginal discs of third instar *Drosophila* larvae and observed the expression levels of the control transgene UAS-DsRed. Using this technique, we showed that the expression levels of UAS-DsRed were similar in homozygous Fbxo42 mutant cells (in black in Figure 2.10) and wild-type cells (in green in Figure 2.10). Therefore, Fbxo42 is not necessary for the activation of the UAS-transgene.

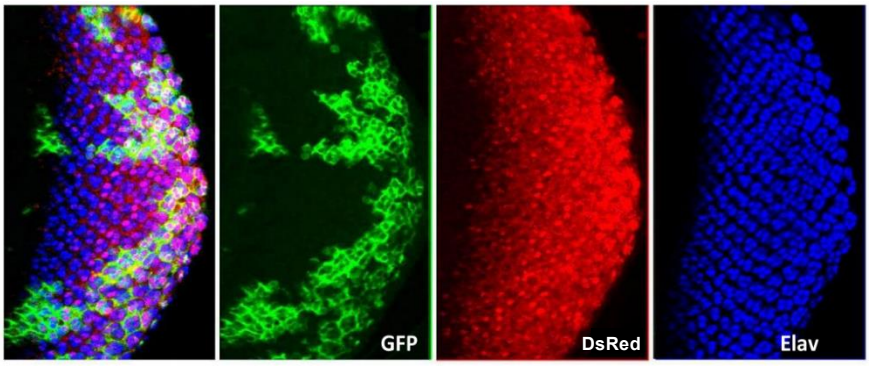

Figure 2.10: Immunofluorescence of third instar larval eye imaginal discs, containing Su218 (Fbxo42^{N423*})/ubiGFP clones. Wild-type cells are labelled by ubiGFP (in green) and Fbxo42 mutant cells are identified by the absence of ubiGFP. GMR-GAL4 driven expression of UAS-DsRed

(Figure 2.10 continued):…is similar in Su218 and ubiGFP clones. Elav (in blue) is a marker of the photoreceptors. Genotype of the larvae: eyFlp, GMR-GAL4, UAS-DsRed; FRT42D, Su218/ FRT42D, ubiGFP). Scale bar = 30 μm.

Overexpression of wild-type rhodopsin-1 (Rh1) under the control of GMR-GAL4 in the adult *Drosophila* eye leads to a strong rough eye phenotype (Figure 2.11A). It has been shown that accumulation of misfolded Rh1 in the ER induced ER stress, UPR activation and IRE1-mediated splicing of Xbp1 (Kang & Hyung, 2009; Kang *et al.*, 2012). Thus, we tested whether mutations in *Fbxo42* could rescue the Rh1-induced rough eye phenotype. By generating eyes composed exclusively of homozygous mutant clones of one of the Fbxo42 suppressors (Su218), we were able to suppress the rough eye phenotype caused by Rh1 overexpression (Figure 2.11B). We also tested whether Su218 could rescue the small eye phenotype induced by overexpression of the pro-apoptotic gene *hid* (Figure 2.11C), in order to see if Fbxo42 might be involved in the apoptosis pathway. Using mosaic adult eyes containing clones of Su218, we found that Su218 did not suppress the atrophic eye phenotype caused by *hid* overexpression (Figure 2.11D). Taken together, these results indicate that Fbxo42 acts downstream of the UPR activation but upstream of the apoptotic pathway.

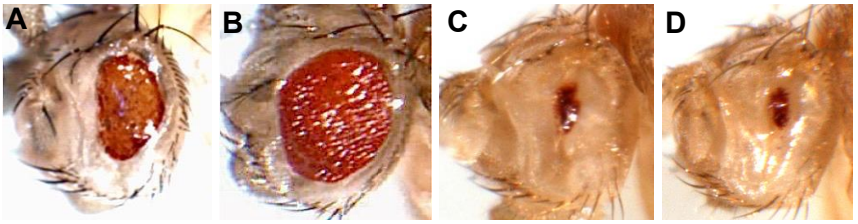

Figure 2.11: The effect of Su218 on fly eye phenotypes caused by Rhodopsin-1 or hid overexpression. (A) "Glossy" eye phenotype caused by Rhodopsin-1 (Rh1) overexpression. Genotype: eyFlp, GMR-GAL4; FRT42D/FRT42D, GMR-hid, CL; UAS-Rh1. **(B)** Whole eye mutant clones of Su218 suppress "glossy" phenotype caused by Rh1 overexpression. Genotype: eyFlp, GMR-GAL4; FRT42D, Su218/FRT42D, GMR-hid, CL; UAS-Rh1. **(C)** Small eye phenotype caused by overexpression of hid. Genotype: eyFlp, GMR-hid; FRT42D/FRT42D, ubiGFP. **(D)** Clones of Su218 do not suppress the small eye phenotype caused by hid overexpression. Genotype: eyFlp, GMR-hid; FRT42D, Su218/FRT42D, ubiGFP.

Production of a polyclonal antibody against Fbxo42

One of the aims of our project was to study the cellular and tissue localization of the Fbxo42 protein. Since no antibody is available for this F-box protein, we decided to generate a polyclonal antibody against Fbxo42. Several attempts were made to obtain the anti-Fbxo42 antibody, but the only successful approach was to use part of the *Fbxo42* coding sequence, after the Kelch-repeat domains, in order to increase the chances of having a specific antibody for Fbxo42, that does not recognize other proteins that also contain F-box or Kelch domains. We therefore generated a construct bearing the DNA sequence encoding amino acids 384 to 667 of Fbxo42, cloned into pETM-30. The Fbxo42 protein was tagged with GST at the N-terminus and with two histidine tags placed at the N- and C-terminus (His-GST-Fbxo42-His). The

expression of the Fbxo42 peptide (58.6 kDa) was induced with 1 mM IPTG for 3 hours in Rosetta bacterial cells, and its purification was carried out using a nickel-containing resin (IMAC Ni-charged) via the histidine tags. To confirm the expression and purification of the Fbxo42 peptide, an 8% polyacrylamide gel was run, including a control condition (without IPTG induction) (Figure 2.12).

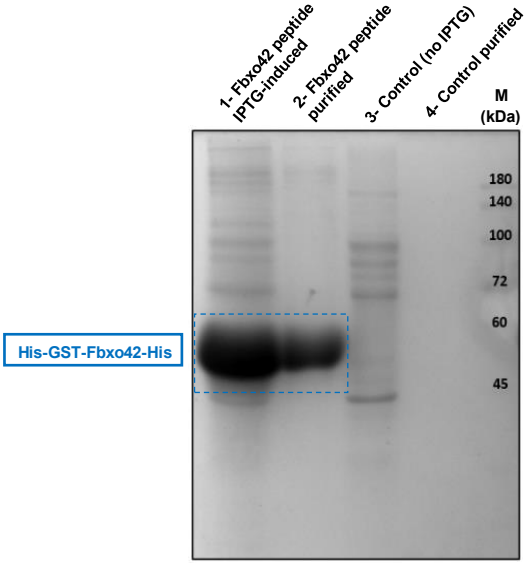

Figure 2.12: Coomassie staining of an 8% polyacrylamide gel, containing non-purified/purified Fbxo42 peptide (IPTG-induced) and non-purified/purified control samples (without IPTG induction). Lane 1 contains the Fbxo42 peptide whose expression was induced by 1 mM IPTG for 3 hours; lane 2 contains the Fbxo42 peptide purified with a nickel-containing resin; lane 3 contains the control without IPTG induction; lane 4 contains the control sample purified with a nickel-containing resin. M indicates a lane with molecular weight markers (in kDa).

The polyacrylamide gel (Figure 2.12) shows that the expression of the Fbxo42 with 1 mM IPTG was successful, as we can see a prominent band of 58.6 kDa corresponding to the expression of the His-GST-Fbxo42-His peptide. Some non-specific

bands are also present, but most of them disappear after purifying the Fbxo42 peptide using a nickel-containing resin. As a control, we used a culture containing the pETM30-His-GST-Fbxo42-His but, in this case, the expression of the Fbxo42 peptide was not induced by IPTG. After purifying the control with a nickel-containing resin, all the bands present in the control sample completely vanished.

The purified Fbxo42 peptide (antigen) in solution, specifically 1.5 mg, was sent to Eurogentec, for anti-Fbxo42 antibody production. This company injected the Fbxo42 antigen into rabbits, and approximately two months later, they provided us with the pre-bleed and the bleed containing the antibody produced against the Fbxo42 protein. We then performed the in-gel affinity purification of the antibody. To minimize the background staining in immunofluorescence and immunoblot experiments, the affinity purified anti-Fbxo42 antibody was preabsorbed with L1 larvae homozygous for Su226 ($Fbxo42^{H436*}$), one of the suppressors identified in our EMS screen. The following step was to confirm that the affinity purified, and pre-absorbed antibody was functional for immunofluorescence and immunoblotting. In order to do this, we extracted protein from flies overexpressing Fbxo42 or Fbxl7 (a different fly F-box protein) in the eyes, under the control of the GMR-GAL4 driver (Figure 2.13). We also used lysates from HEK (Human Embryonic Kidney)-293 cells transfected with *Drosophila* FLAG-HA-Fbxo42 or an empty control vector (EV). By immunoblotting with anti-Fbxo42, we examined whether, in addition to the overexpressed *Drosophila* Fbxo42, we could detect a band in the non-transfected lane, that could correspond to human FBXO42 (Figure 2.13).

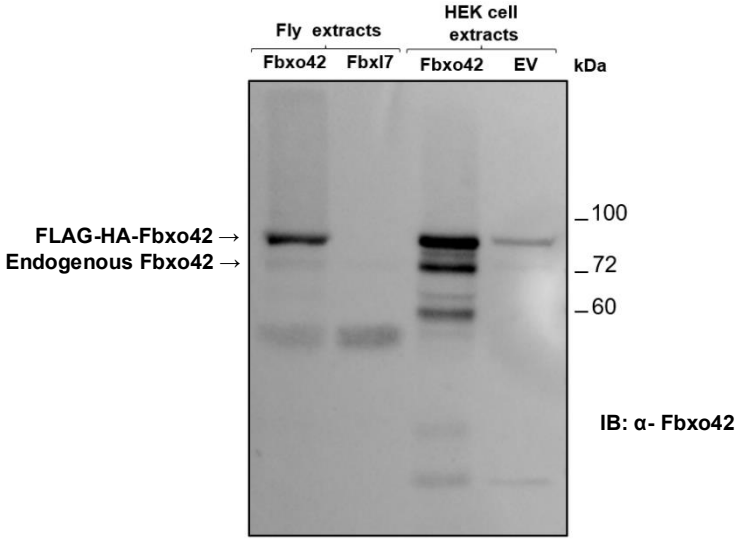

Figure 2.13: Immunoblot to test the rabbit polyclonal anti-Fbxo42 antibody. For this immunoblot, protein was extracted from fly's heads bearing the following genotypes: W; GMR-GAL4, UAS-(^{bio}Ub)$_6$-BirA; UAS-FLAG-HA-Fbxo42 or control W; GMR-GAL4, UAS-(^{bio}Ub)$_6$-BirA; UAS-FLAG-Fbxl7. Protein was also extracted from HEK-293 cells transfected with FLAG-HA-Fbxo42 or an empty control vector (EV). This immunoblot was probed with the homemade rabbit anti-Fbxo42. The arrows indicate the endogenous (74.4 kDa) and the overexpressed (80.7 kDa) *Drosophila* Fbxo42. Human FBXO42 has a molecular weight of 77.8 kDa.

In the immunoblot containing protein extracts from flies (expressing Fbxo42 or control Fbxl7) and HEK cells (transfected with Fbxo42 or EV), probed with the anti-Fbxo42 polyclonal antibody (Figure 2.13), a band just above the 72 kDa marker is visible in both the Fbxo42 and Fbxl7 fly extracts. The expected size for endogenous Fbxo42 is 74.4 kDa. Therefore, this band is likely to correspond to the Fbxo42 protein. Additionally, a strong band of approximately 80.7 kDa is present in samples from flies and HEK cells overexpressing Fbxo42, which is consistent with the molecular weight of the tagged version of this F-box protein. In the lysates from HEK cells transfected with the empty control vector, we observe a

band that may correspond to the expression of human FBXO42, as its molecular weight is close to the expected size of 77.8 kDa.

To ensure that the band observed at 74.4 kDa (Figure 2.13) did indeed correspond to the endogenous *Drosophila* Fbxo42 protein, we checked whether this band is not present in a homozygous mutant for Fbxo42. To do this, we extracted protein from L1 larvae homozygous for Su226 ($Fbxo42^{H436*}$), and used protein extracted from L1 larvae heterozygous for Su226 as a control. The latter contains one copy of the Su226 allele and one copy of the CyOGFP allele, expressing wild-type Fbxo42 (Figure 2.14).

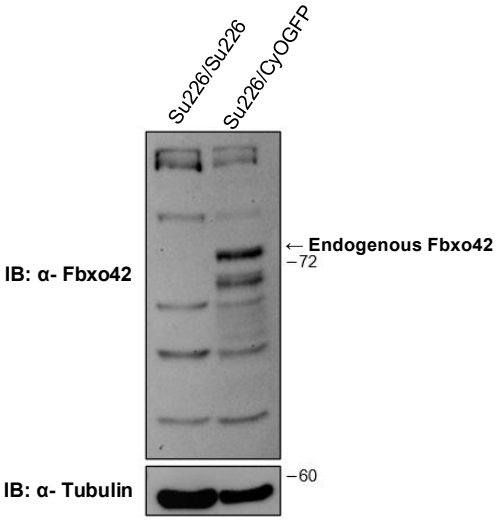

Figure 2.14: Immunoblot from L1 larvae homozygous or heterozygous for Su226 probed with rabbit anti-Fbxo42 and mouse anti-tubulin antibodies. The arrow points to the band corresponding to the endogenous Fbxo42.

In the immunoblot probed with the rabbit anti-Fbxo42 antibody containing protein extracts from L1 larvae heterozygous for

Su226 (Su226/CyoGFP), a strong band is observed just above the 72 kDa marker (Figure 2.14). This band is absent in protein extracts from L1 larvae homozygous for Su226 (Su226/Su226), confirming that the 74.4 kDa band corresponds to the Fbxo42 protein, and that this antibody is suitable for the immunoblot detection of this F-box protein.

To test whether the anti-Fbxo42 antibody also worked for immunofluorescence, we performed immunostaining of eye imaginal discs from third instar larvae with the anti-Fbxo42 antibody. For this, we generated Su218 (Fbxo42^{N423*})/ubiGFP clones in the eye imaginal discs, using the Flipase/FRT technique, where flippase expression is under the control of the *eyeless* (*ey*) promoter (Newsome *et al.*, 2000). This approach enables to distinguish wild-type cells for Fbxo42, labelled by ubiGFP, from homozygous mutant cells for this F-box protein, which are identified by the absence of ubiGFP, within the same eye imaginal disc.

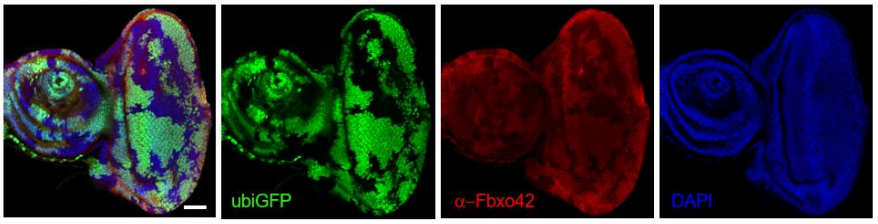

Figure 2.15: Immunofluorescence of third instar larval eye imaginal discs containing Su218(Fbxo42^{N423*})/ubiGFP clones, with the homemade anti-Fbxo42 antibody (in red). Wild-type Fbxo42 cells are labelled by ubiGFP (in green), and homozygous mutant cells for Fbxo42 are identified by the absence of ubiGFP. DAPI (in blue) labels the nucleus. Genotype of the larvae: eyFlp, GMR-GAL4; FRT42D, Su218/ FRT42D, ubiGFP. Scale bar = 60 µm.

Immunofluorescence of eye imaginal discs containing Su218 (Fbxo42^{N423*})/ubiGFP clones, using the rabbit anti-Fbxo42

antibody, shows that cells homozygous for Su218, labelled by the absence of ubiGFP, exhibit reduced immunoreactivity for anti-Fbxo42 compared to neighbouring wild-type cells (labelled by ubiGFP) (Figure 2.15). This result demonstrates that our anti-Fbxo42 antibody is indeed effective for immunofluorescence.

Fbxo42 expression levels in different fly tissues

Since the biological function of the *Drosophila* Fbxo42 protein is not yet fully understood, we decided to investigate the expression of this F-box protein in different tissues from larvae and adult flies. Therefore, we extracted protein from the following larval tissues: eye imaginal discs, salivary glands, brain, lymph/ring glands, carcass, fat body and midgut. From adult flies, protein was extracted from testis, ovaries and brain. The protein extracts were then analysed by immunoblotting using the homemade anti-Fbxo42 antibody (Figure 2.16).

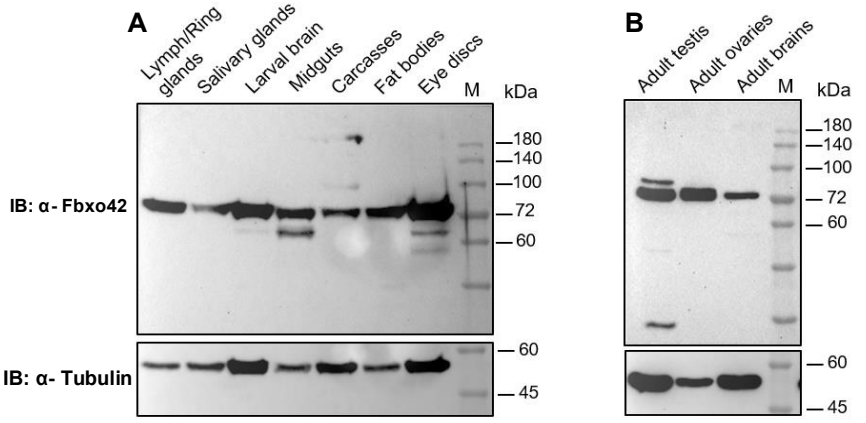

Figure 2.16: Analysis of the Fbxo42 expression levels in different fly tissues. A) Immunoblot showing Fbxo42 expression in different tissues of

(Figure 2.16 continued):…third instar larvae; **B)** Immunoblot showing Fbxo42 expression in adult testis, ovaries and brain. Both immunoblots were probed with rabbit anti-Fbxo42 and mouse anti-Tubulin, the latter used as loading control.

Regarding the immunoblots showing Fbxo42 expression levels in different fly tissues, we observe that the Fbxo42-specific band (74.4 kDa) is present in all analysed tissues (Figure 2.16). Since Fbxo42 is expressed in various tissues and at different developmental stages in the fly, this F-box protein may be essential for a variety of biological functions. This is further supported by the fact that the Fbxo42 loss-of-function mutations identified in our EMS screen are homozygous lethal during development.

Fbxo42 protein co-immunoprecipitates with SkpA

F-box proteins form complexes with SkpA, Cullin-1 and Rbx-1, known as SCF complexes, to mediate the ubiquitylation of specific substrates. In these complexes, F-box proteins bind to SkpA through the conserved F-box domain, which is located at the N-terminus of the F-box protein. To confirm that Fbxo42 interacts with SkpA, we performed an immunoprecipitation (IP) using *Drosophila* S2 cells. We transfected S2 cells with SkpA-HA and either full-length Fbxo42 (FLAG-HA-Fbxo42) or ΔFbxo42 (FLAG-HA-ΔFbxo42), the latter containing a deletion of the F-box domain. After protein extraction from the S2 cells, an IP was performed using anti-FLAG resin to capture the overexpressed Fbxo42 proteins, followed by immunoblotting with anti-HA antibody to detect SkpA-HA and the tagged F-box proteins (Figure 2.17).

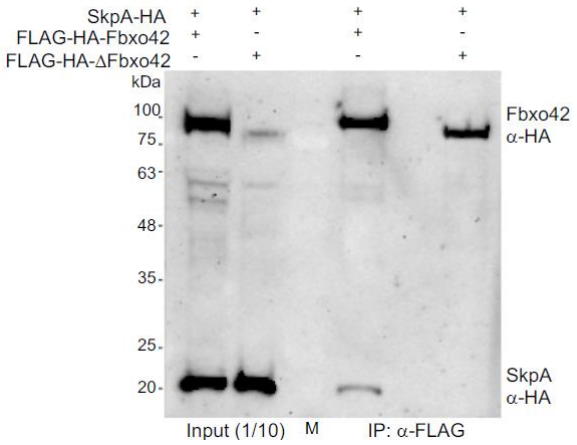

Figure 2.17: Full-length Fbxo42 co-immunoprecipitates with SkpA. Immunoblot of S2 cell protein extracts expressing SkpA-HA and either FLAG-HA-Fbxo42 or FLAG-HA-ΔFbxo42 before and after immunoprecipitation (IP) with anti-FLAG resin. This immunoblot was probed with anti-HA antibody.

By immunoblotting (Figure 2.17), we are able to see that SkpA co-immunoprecipitates with FLAG-HA-Fbxo42 but not with the Fbxo42 mutant containing a deletion of the F-box domain (FLAG-HA-ΔFbxo42). This result is consistent with previous findings showing binding of Fbxo42 with SkpA in the *Drosophila* ovary (Barbosa *et al.*, 2021).

Identification of the Fbxo42 protein binders by using Mass Spectrometry in HEK cell extracts

In order to identify the specific substrates of the Fbxo42 protein, we employed two different proteomic approaches. For the first experiment, we used mass spectrometry from pulldowns of HEK-293 cells expressing *Drosophila* Fbxo42. These cells were stably transfected with different versions of the *Drosophila* Fbxo42

protein using the viral vector pLex. Specifically, HEK cells were transfected with full-length FLAG-HA-Fbxo42, as well as control constructs FLAG-HA-ΔFbxo42 and FLAG-HA-Su359 (a Fbxo42 mutant obtained from the genetic screen that contains the point mutation Gly639>Glu). Cells transfected with empty pLex were used as an additional control. The expression of the F-box constructs was confirmed by immunoblotting with anti-HA antibody (Figure 2.18). The cell lysates were then used for immunoprecipitation with anti-HA resin. This resin binds to the HA-tagged F-box proteins from the cell lysates, allowing us to detect the binders of Fbxo42 that may co-immunoprecipitate with Fbxo42. The eluted fractions were sent to the Mass Spectrometry facility for analysis and identification of the Fbxo42 candidate substrates.

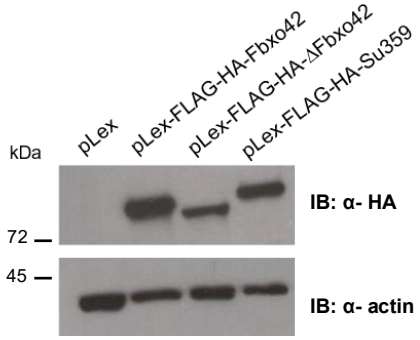

Figure 2.18: Stable transfection of HEK cells with pLex-Fbxo42 constructs or empty pLex.
Immunoblot with HEK cell extracts to confirm their stable transfection with full-length Fbxo42 (pLex-FLAG-HA-Fbxo42), control constructs ΔFbxo42 (pLex-FLAG-HA-ΔFbxo42), Su359 (pLex-FLAG-HA-Su359) or empty pLex, probed with anti-HA and with the loading control anti-actin.

The mass spectrometry facility provided us with the MS results, which were then analysed and sorted in the laboratory. The

sorted data are shown in Table 1. This table contains the number of unique peptides detected for each protein in each sample.

Table 1: Mass Spectrometry results obtained using HEK-293 cells, which were transfected with full-length *Drosophila* Fbxo42, ΔFbxo42, Su359 and the control empty vector.

Uniprot number	Protein identification	Full-length Fbxo42	ΔFbxo42	Su359	Empty vector
Q03701	CCAAT/enhancer-binding protein zeta OS=Homo sapiens GN=CEBPZ PE=1 SV=3 - [CEBPZ_HUMAN]	8	0	0	0
O00311	Cell division cycle 7-related protein kinase OS=Homo sapiens GN=CDC7 PE=1 SV=1 - [CDC7_HUMAN]	0	1	1	0
P04637	Cellular tumor antigen p53 OS=Homo sapiens GN=TP53 PE=1 SV=4 - [P53_HUMAN]	3	0	0	0
Q9BT78	COP9 signalosome complex subunit 4 OS=Homo sapiens GN=COPS4 PE=1 SV=1 - [CSN4_HUMAN]	5	0	1	0
Q7L5N1	COP9 signalosome complex subunit 6 OS=Homo sapiens GN=COPS6 PE=1 SV=1 - [CSN6_HUMAN]	3	0	2	0
Q9UBW8	COP9 signalosome complex subunit 7a OS=Homo sapiens GN=COPS7A PE=1 SV=1 - [CSN7A_HUMAN]	2	0	0	0
Q99627	COP9 signalosome complex subunit 8 OS=Homo sapiens GN=COPS8 PE=1 SV=1 - [CSN8_HUMAN]	2	0	0	0
Q13616	Cullin-1 OS=Homo sapiens GN=CUL1 PE=1 SV=2 - [CUL1_HUMAN]	27	0	13	0
P24928	DNA-directed RNA polymerase II subunit RPB1 OS=Homo sapiens GN=POLR2A PE=1 SV=2 - [RPB1_HUMAN]	9	0	0	0
O60216	Double-strand-break repair protein rad21 homolog OS=Homo sapiens GN=RAD21 PE=1 SV=2 - [RAD21_HUMAN]	3	0	0	0
P62877	E3 ubiquitin-protein ligase RBX1 OS=Homo sapiens GN=RBX1 PE=1 SV=1 - [RBX1_HUMAN]	2	0	0	0
Q08945	FACT complex subunit SSRP1 OS=Homo sapiens GN=SSRP1 PE=1 SV=1 - [SSRP1_HUMAN]	9	0	0	0
Q9NXS2	Glutaminyl-peptide cyclotransferase-like protein OS=Homo sapiens GN=QPCTL PE=1 SV=2 - [QPCTL_HUMAN]	0	2	1	0
Q92769	Histone deacetylase 2 OS=Homo sapiens GN=HDAC2 PE=1 SV=2 - [HDAC2_HUMAN]	3	1	1	0
P39880	Homeobox protein cut-like 1 OS=Homo sapiens GN=CUX1 PE=1 SV=3 - [CUX1_HUMAN]	2	0	0	0
Q9NZI8	Insulin-like growth factor 2 mRNA-binding protein 1 OS=Homo sapiens GN=IGF2BP1 PE=1 SV=2 - [IF2B1_HUMAN]	4	3	3	1
Q9Y6M1	Insulin-like growth factor 2 mRNA-binding protein 2 OS=Homo sapiens GN=IGF2BP2 PE=1 SV=2 - [IF2B2_HUMAN]	2	2	1	0
Q07666	KH domain-containing, RNA-binding, signal transduction-associated protein 1 OS=Homo sapiens GN=KHDRBS1 PE=1 SV=1 - [KHDR1_HUMAN]	4	0	0	0
P20700	Lamin-B1 OS=Homo sapiens GN=LMNB1 PE=1 SV=2 - [LMNB1_HUMAN]	13	0	0	0
O03252	Lamin-B2 OS=Homo sapiens GN=LMNB2 PE=1 SV=3 - [LMNB2_HUMAN]	6	0	0	0
P07196	Neurofilament light polypeptide OS=Homo sapiens GN=NEFL PE=1 SV=3 - [NFL_HUMAN]	16	4	4	0
Q8N4Q1	Mitochondrial intermembrane space import and assembly protein 40 OS=Homo sapiens GN=CHCHD4 PE=1 SV=1 - [MIA40_HUMAN]	1	1	1	0
Q12769	Nuclear pore complex protein Nup160 OS=Homo sapiens GN=NUP160 PE=1 SV=3 - [NU160_HUMAN]	2	0	0	0
O75530	Polycomb protein EED OS=Homo sapiens GN=EED PE=1 SV=2 - [EED_HUMAN]	3	0	0	0
O60925	Prefoldin subunit 1 OS=Homo sapiens GN=PFDN1 PE=1 SV=2 - [PFD1_HUMAN]	0	3	3	0
Q8ND56	Protein LSM14 homolog A OS=Homo sapiens GN=LSM14A PE=1 SV=3 - [LS14A_HUMAN]	8	8	9	6
Q13283	Ras GTPase-activating protein-binding protein 1 OS=Homo sapiens GN=G3BP1 PE=1 SV=1 - [G3BP1_HUMAN]	1	2	2	0
P27694	Replication protein A 70 kDa DNA-binding subunit OS=Homo sapiens GN=RPA1 PE=1 SV=2 - [RFA1_HUMAN]	14	16	12	13
Q01844	RNA-binding protein EWS OS=Homo sapiens GN=EWSR1 PE=1 SV=1 - [EWS_HUMAN]	4	5	5	4
Q9Y230	RuvB-like 2 OS=Homo sapiens GN=RUVBL2 PE=1 SV=3 - [RUVB2_HUMAN]	12	2	2	0
P30153	Serine/threonine-protein phosphatase 2A 65 kDa regulatory subunit A alpha isoform OS=Homo sapiens GN=PPP2R1A PE=1 SV=4 - [2AAA_HUMAN]	7	11	12	0
P30154	Serine/threonine-protein phosphatase 2A 65 kDa regulatory subunit A beta isoform OS=Homo sapiens GN=PPP2R1B PE=1 SV=3 - [2AAB_HUMAN]	0	2	2	0
O00743	Serine/threonine-protein phosphatase 6 catalytic subunit OS=Homo sapiens GN=PPP6C PE=1 SV=1 - [PPP6_HUMAN]	2	2	1	0
P05023	Sodium/potassium-transporting ATPase subunit alpha-1 OS=Homo sapiens GN=ATP1A1 PE=1 SV=1 - [AT1A1_HUMAN]	6	8	8	0
P63208	S-phase kinase-associated protein 1 OS=Homo sapiens GN=SKP1 PE=1 SV=2 - [SKP1_HUMAN]	6	2	6	0
P23246	Splicing factor, proline- and glutamine-rich OS=Homo sapiens GN=SFPQ PE=1 SV=2 - [SFPQ_HUMAN]	9	3	3	2
P78371	T-complex protein 1 subunit beta OS=Homo sapiens GN=CCT2 PE=1 SV=4 - [TCPB_HUMAN]	7	15	10	1
P55072	Transitional endoplasmic reticulum ATPase OS=Homo sapiens GN=VCP PE=1 SV=4 - [TERA_HUMAN]	16	18	17	19
Q9UIG0	Tyrosine-protein kinase BAZ1B OS=Homo sapiens GN=BAZ1B PE=1 SV=2 - [BAZ1B_HUMAN]	13	0	0	0
P62979	Ubiquitin-40S ribosomal protein S27a OS=Homo sapiens GN=RPS27A PE=1 SV=2 - [RS27A_HUMAN]	2	2	2	2

Table1: the numbers displayed in the table indicate the number of unique peptides detected for each protein in each sample. Components of the SCF complex are highlighted in green; members of the COP9 signalosome are highlighted in orange; proteins detected with more unique peptides in full-length Fbxo42 sample than in controls are highlighted in yellow; Lamin-B1 and Lamin-B2 are highlighted in purple. Highlighted in blue are the proteins whose fly homologues were included in the analysis by immunofluorescence.

Regarding Table 1, which shows the MS data, we observe that the members of the SCF complex, specifically, Cullin-1, Skp-1 and Rbx-1 (highlighted in green in Table 1), were detected by mass spectrometry with a higher number of unique peptides in the full-length Fbxo42 sample compared to the controls. This result suggests that *Drosophila* Fbxo42 can bind to human Skp-1, allowing

the formation of the SCF-complex and enabling Fbxo42-mediated ubiquitylation of specific substrates in HEK cells. This result can be explained by the high conservation of the F-box domain between humans and flies. Since Fbxo42 binds to Skp-1 via the F-box domain, the formation of the SCF-complex remains possible, even though Fbxo42 is from *Drosophila* and the remaining components are from human cells. In addition to the full-length Fbxo42 sample, Cullin-1 and Skp-1 were also detected in Su359 sample.

Some members of the COP9 signalosome complex (highlighted in orange in Table 1) were also detected by MS with a higher number of unique peptides in the full-length Fbxo42 sample compared to the controls. COP9 is involved in the deneddylation of the Cullin subunits in SCF-type E3 complexes. Additionally, COP9 is an interactor of human FBXO42 (Jiang *et al.*, 2022). Other proteins, including P53 (a substrate of the human FBXO42), Lamin-B, RAD21 and SSRP1, were also identified in the full-length Fbxo42 sample but not in the controls.

To confirm that the Fbxo42 interactors identified by MS are substrates of this F-box protein, we tested each one of them by immunofluorescence in eye imaginal discs of third instar *Drosophila* larvae, containing Fbxo42 mutant clones (in this case, Su218 clones). Protein levels of a given Fbxo42 substrate are expected to accumulate in mutant clones of this F-box protein.

To investigate the Fbxo42 candidate substrates, the first step was to cross the flies to obtain larvae containing Su218/ubiGFP clones in eye discs, along with the expression of each Fbxo42 interactor identified by MS. For these crosses, we ordered FlyORF

lines (when available) corresponding to each Fbxo42 interactor. FlyORF flies carry the proteins of interest fused at the C-terminus with a 3xHA-tag, allowing their detection by immunofluorescence with an anti-HA antibody. Alternatively, when available, specific antibodies were used to detect the candidate substrates.

Approximately fifty Fbxo42 interactors were analysed using immunofluorescence assays. The results of three of these interactors, p53 (Figure 2.19), Rpd3 (Figure 2.20) and Ssrp (Figure 2.20) are shown.

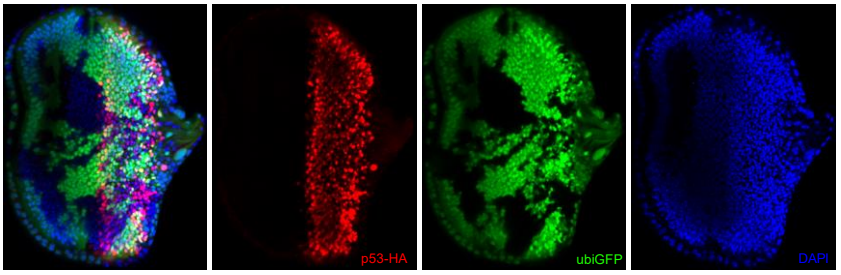

Figure 2.19: Immunofluorescence of third instar larval eye imaginal discs, containing Su218/ubiGFP clones with HA antibody to label p53. Wild-type Fbxo42 cells are labelled by ubiGFP (in green), and homozygous mutant cells for Fbxo42 are identified by the absence of ubiGFP. p53 (in red), containing a 3xHA tag at the C-terminus, is detected with anti-HA antibody. DAPI (in blue) labels the nucleus.

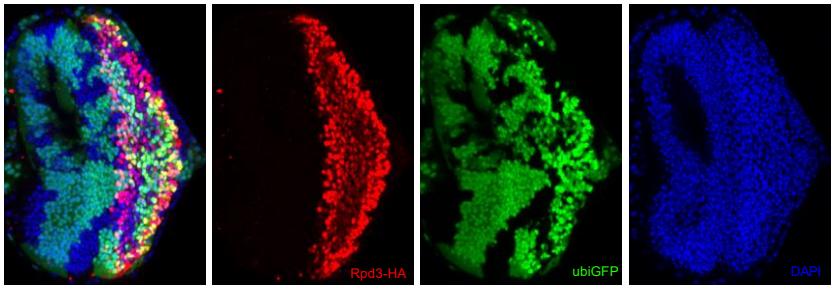

Figure 2.20: Immunofluorescence of third instar larval eye imaginal discs, containing Su218/ubiGFP clones with HA antibody to label Rpd3 (homologous to histone deacetylase 2, HDAC2). Wild-type Fbxo42 cells are labelled by ubiGFP (in green), and homozygous mutant

(Figure 2.20 continued):…cells for Fbxo42 are identified by the absence of ubiGFP. Rpd3 (in red), containing a 3xHA tag at the C-terminus, is detected with anti-HA antibody. DAPI (in blue) labels the nucleus.

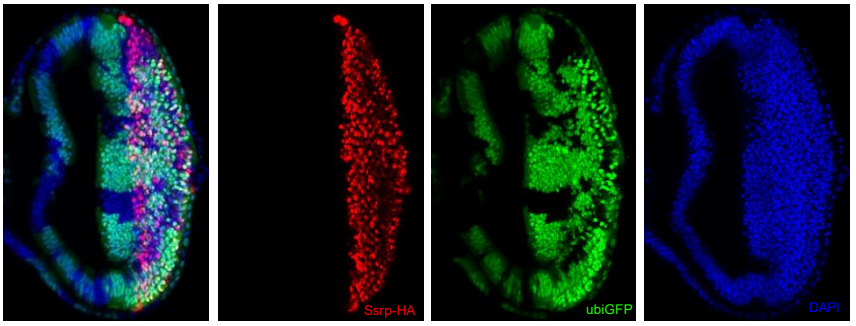

Figure 2.21: Immunofluorescence of third instar larval eye imaginal discs, containing Su218/ubiGFP clones with HA antibody to label Ssrp (homologous to human SSRP1). Wild-type Fbxo42 cells are labelled by ubiGFP (in green), and homozygous mutant cells for Fbxo42 are identified by the absence of ubiGFP. Ssrp (in red), containing a 3xHA tag at the C-terminus, is detected with anti-HA antibody. DAPI (in blue) labels the nucleus.

Most of the Fbxo42 candidate substrates tested by immunofluorescence, including p53 (Figure 2.19), Rpd3 (Figure 2.20) and Ssrp (Figure 2.21), did not accumulate in mutant clones of Fbxo42, suggesting that Fbxo42 is not mediating their ubiquitylation/degradation by the proteosome. The only positive result we obtained was for Lamin-B, when its detection by immunofluorescence was performed with the ADL84 antibody. In this case, we are able to observe the accumulation of Lamin-B in Fbxo42 mutant cells of the peripodial membrane (Figure 2.22). This antibody recognizes Lamin-B when it is dephosphorylated at Serine 25 (Stuurman *et al.*, 1995). In contrast, when we performed the immunostaining with the ADL67 antibody, which recognizes both dephosphorylated and phosphorylated isoforms of Lamin-B, we

observed no difference between wild-type and Fbxo42 mutant cells of the peripodial membrane (Figure 2.23). Taken together, these results suggest that Lamin-B is an indirect target of Fbxo42, and that a phosphatase could be the substrate of this F-box protein. In Fbxo42 mutant cells, this phosphatase is not degraded, allowing it to dephosphorylate Lamin-B, which is then recognized by immunofluorescence using the ADL84 antibody.

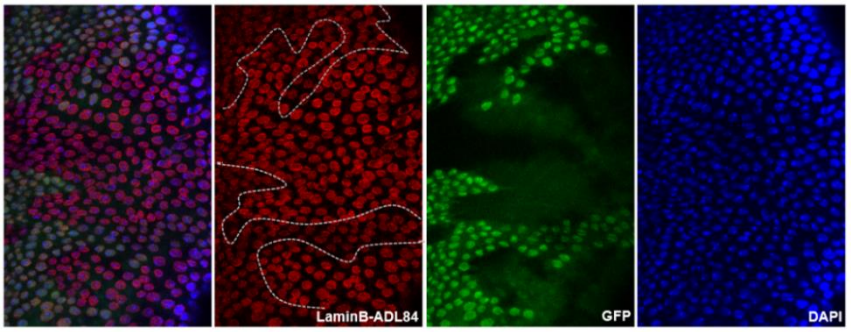

Figure 2.22: Immunofluorescence of third instar larval eye imaginal discs, containing Su218/ubiGFP clones with ADL84 antibody. Wild-type Fbxo42 cells are labelled by ubiGFP (in green), and homozygous mutant cells for Fbxo42 are identified by the absence of ubiGFP. LaminB (in red) is detected with ADL84 antibody. DAPI (in blue) labels the nucleus. Genotype of the larvae: eyFlp, GMR-GAL4; FRT42D, Su218/ FRT42D, ubiGFP.

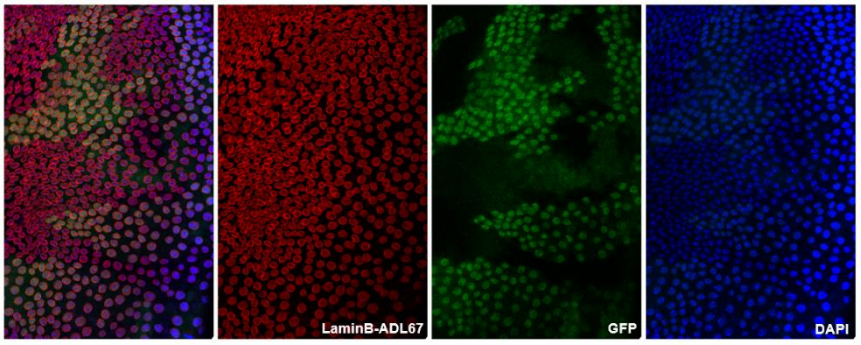

Figure 2.23: Immunofluorescence of third instar larval eye imaginal discs, containing Su218/ubiGFP clones with ADL67 antibody. Wild-type Fbxo42 cells are labelled by ubiGFP (in green), and homozygous mutant cells for Fbxo42 are identified by the absence of ubiGFP. LaminB

(Figure 2.23 continued):… (in red) is detected with ADL67 antibody. DAPI (in blue) labels the nucleus. Genotype of the larvae: eyFlp, GMR-GAL4; FRT42D, Su218/ FRT42D, ubiGFP.

In an attempt to identify the phosphatase responsible for the dephosphorylation of Lamin-B, we tested whether one of the phosphatase RNAi lines available in the laboratory would modify the staining with ADL84. To do this, we generated larvae with Su218/ubiGFP clones in the eye imaginal discs together with the expression of PP1-87B (serine/threonine-protein phosphatase alpha-2 isoform) RNAi. By performing immunofluorescence on these eye discs with ADL84, it is possible to observe that Lamin-B staining is uniform in wild-type and Fbxo42 mutant cells of the peripodial membrane (Figure 2.24). This result suggests that PP1-87B phosphatase may be involved in the dephosphorylation of Lamin-B and may also be a substrate of Fbxo42.

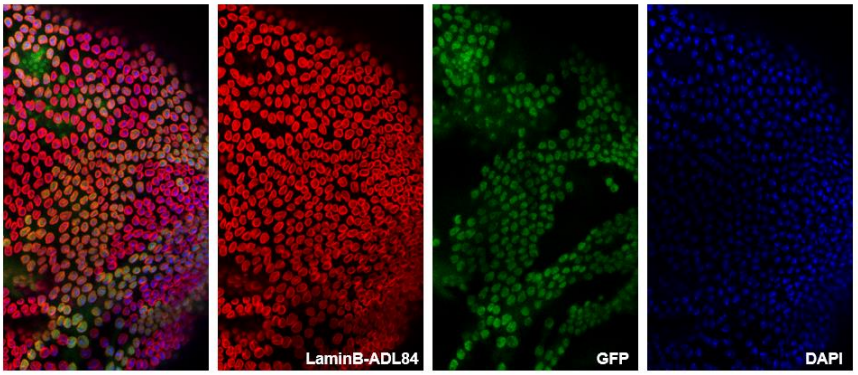

Figure 2.24: Immunofluorescence of third instar larval eye imaginal discs, containing Su218/ubiGFP clones and expressing PP1-87B RNAi with ADL84 antibody. Wild-type Fbxo42 cells are labelled by ubiGFP (in green), and homozygous mutant cells for Fbxo42 are identified by the absence of ubiGFP. LaminB (in red) is detected with ADL84 antibody. DAPI (in blue) labels the nucleus. Genotype of the larvae: eyFlp, GMR-GAL4; FRT42D, Su218/ FRT42D, ubiGFP; UAS(RNAiPP1-87B).

Identification of the Fbxo42 substrates using the ^{bio}Ub approach

Since the first mass spectrometry experiment to identify *Drosophila* Fbxo42 candidate substrates was carried out using human cells, we decided to perform a second mass spectrometry experiment using flies and an alternative approach, based on the ^{bio}Ub strategy, developed by Ugo Mayor's laboratory (Franco *et al.*, 2011; Ramirez *et al.*, 2015). To use this approach, transgenic flies expressing full-length FLAG-HA-Fbxo42, or controls FLAG-HA-ΔFbxo42 and FLAG-Fbxl7 (a different fly F-box protein), were independently crossed with flies carrying a polyubiquitin chain conjugated with biotin and fused with *E. coli* BirA (biotin ligase), UAS-(^{bio}Ub)$_6$-BirA. As an additional control, FLAG-HA-Fbxo42 flies without BirA or ^{bio}Ub were used. These constructs were expressed in the *Drosophila* eye under the control of the GMR-GAL4 driver. We performed total protein extraction from the adult fly heads of the aforementioned genotypes and subsequently confirmed the expression of the F-box constructs and the biotinylation of target proteins by immunoblotting with anti-FLAG and anti-Biotin antibodies, respectively (Figure 2.25).

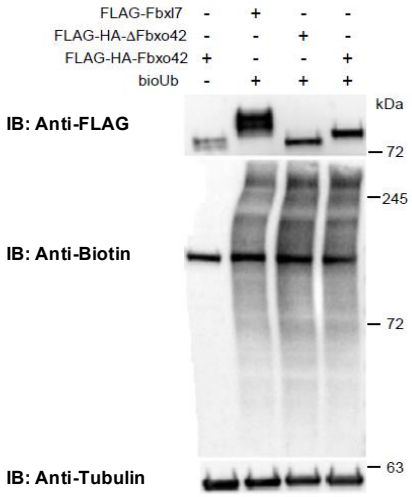

Figure 2.25: Immunoblots to confirm the expression of the F-box constructs and the biotinylation of target proteins in fly head protein extracts. The expression of the F-box constructs UAS-FLAG-HA-Fbxo42; UAS-FLAG-Fbxl7 and UAS-FLAG-ΔFbxo42 driven by GMR-GAL4 was confirmed by immunoblot with anti-FLAG antibody. These flies also carried UAS-(^{bio}Ub)$_6$-BirA, except the control UAS-FLAG-HA-Fbxo42 (without expression of bioUb or BirA). Biotinylation of target proteins was verified by immunoblot with anti-Biotin-HRP conjugated antibody. Tubulin was used as loading control.

Based on the molecular weights of the different F-box constructs observed in the immunoblot probed with anti-FLAG, we can confirm that the flies are expressing the correct F-box constructs (Figure 2.25). Regarding the immunoblot probed with anti-Biotin, we observe a smear, typical of protein biotinylation, which in this case corresponds to the biotinylated ubiquitin conjugates. At 130 kDa, we detect a band in all samples, corresponding to an endogenously biotinylated protein (Figure 2.25).

In order to purify the ubiquitylated proteins conjugated to biotin, we performed pulldowns using high-capacity streptavidin resin, from triplicate samples. Due to the strong binding between streptavidin and biotin, this strategy enables the enrichment of biotinylated, ubiquitylated proteins in the eluted fractions. To remove non-ubiquitylated proteins, the streptavidin resin was subjected to stringent washes. After the biotin pulldowns, we confirmed the enrichment of biotinylated, ubiquitylated proteins in the elution fractions by immunoblotting with anti-Biotin antibody (Figure 2.26). The eluted samples were then processed for MS identification of the Fbxo42 candidate substrates. This MS was carried out by Ugo Mayor's laboratory.

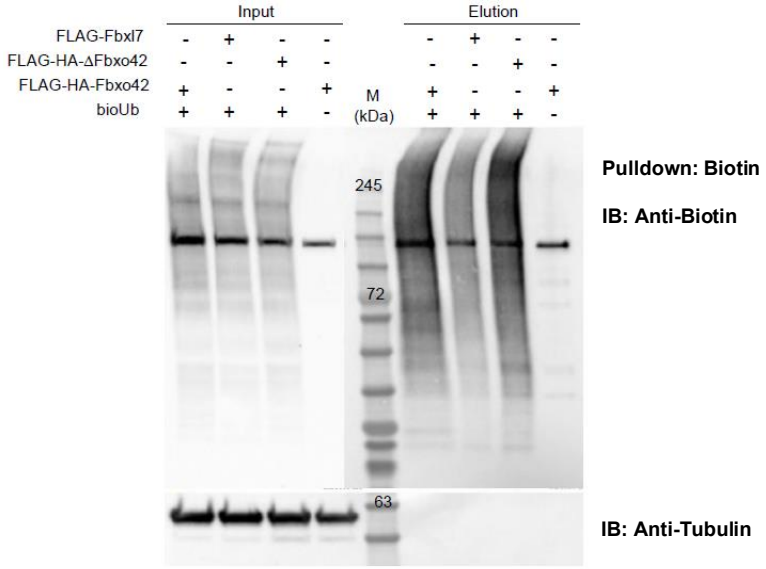

Figure 2.26: Immunoblots of fly head protein extracts before (input) and after (elution) streptavidin/biotin pulldowns. Protein extraction was performed from flies expressing UAS-(^{bio}Ub)$_6$-BirA together with UAS-FLAG-HA-Fbxo42; UAS-FLAG-Fbxl7; UAS-FLAG-ΔFbxo42 or the negative control UAS-FLAG-HA-Fbxo42 (without expression of bioUb or BirA) under the control of GMR-GAL4 driver. Immunoblots were probed with anti-Biotin-HRP conjugated and anti-Tubulin (used as loading control).

After processing the samples and analysing the data, our collaborators provided the MS results, which are represented as volcano plots. In the first plot are shown the proteins identified in full-length Fbxo42 samples compared with those detected in control Fbxl7 samples (Figure 2.27). Above the grey horizontal line (this line indicates the statistical significance, *p*-value < 0.05) are the proteins identified with a high confidence level. In the middle of the plot, between two vertical dashed lines, are proteins equally ubiquitylated in both samples. In this region, we observe ubiquitin as well as the endogenously biotinylated proteins acetyl-coenzyme A (ACC) and pyruvate carboxylase (PCB). This observation, along with the detection of the overexpressed F-box proteins Fbxo42 and Fbxl7 confirms that proportional amounts of biological material were isolated in these F-box samples. The vertical dashed lines represent a two-fold increase ($\log_2$ LFQ Fbxo42/control = 1) or a two-fold decrease ($\log_2$ LFQ Fbxo42/control = -1) of the ubiquitylation levels in Fbxo42-overexpressing samples, compared to the control (Fbxl7-overexpressing) samples. Thus, on the right side of the plot, we are able to see proteins in which ubiquitylation increases two-fold in full-length Fbxo42 samples compared to Fbxl7 samples. On this side of the plot, we can see that Ataxin-2 is detected, being identified with 2 unique peptides and with a high confidence level, making it a candidate substrate of Fbxo42. In addition to Ataxin-2, CCT3 (chaperonin containing T-complex protein-1, TCP-1, subunit 3) was also detected on this side of the plot, being identified with 2 unique peptides (Figure 2.27).

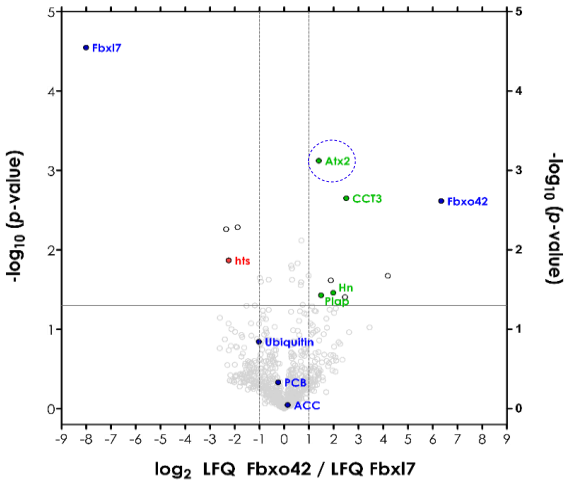

Figure 2.27: Volcano plot showing the proteins identified by MS in Fbxo42-overexpressing samples, compared with those detected in control (Fbxl7-overexpressing) samples. Results are presented as $\log_2$ LFQ (Label Free Quantitation) intensity ratios. As blue dots are ACC and PCB, endogenously biotinylated carboxylases, which should have a $\log_2$ ratio of around 0, if similar amount of biological material have been isolated during the biotin pulldown. Also, as blue dots are ubiquitin, Fbxl7 and Fbxo42. As green and red dots are proteins identified by at least two unique peptides, which are either enriched or depleted, respectively. Ataxin-2 (Atx2) is highlighted by a blue dashed circle. Statistical analysis was performed by two-sided Student's t-test.

In the second volcano plot are shown the proteins identified in full-length Fbxo42 samples compared with those detected in control ΔFbxo42 samples (Figure 2.28). In the middle of the plot are the proteins equally ubiquitylated in both samples, including ubiquitin and the endogenously biotinylated proteins ACC and PCB. On the right side of the plot, we can see proteins in which ubiquitylation increases two-fold in full-length Fbxo42 samples compared to ΔFbxo42 samples. Regarding this side of the plot, we observed that another subunit of the chaperonin containing TCP-1 (CCT) complex is detected, specifically CCT4 (Chaperonin

containing TCP-1, subunit 4), being identified with 2 unique peptides.

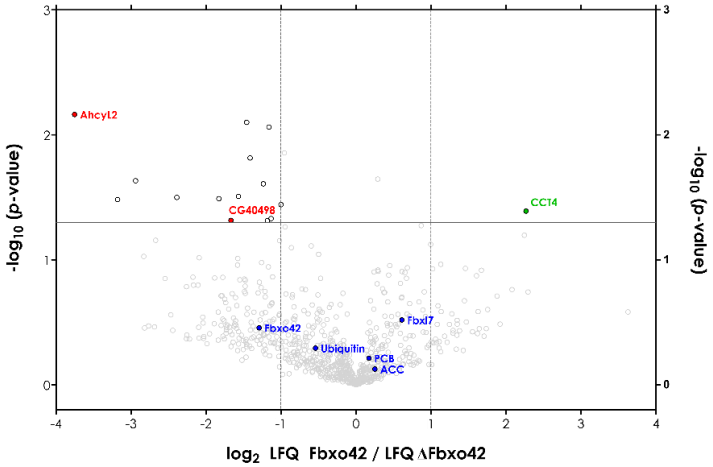

Figure 2.28: Volcano plot showing the proteins identified by MS in Fbxo42-overexpressing samples, compared with those detected in control ΔFbxo42-overexpressing samples. As blue dots are ubiquitin, Fbxl7, Fbxo42 and the endogenously biotinylated carboxylases ACC and PCB. As green and red dots are proteins identified by at least two unique peptides, which are either enriched or depleted, respectively.

We have begun the study of the *Drosophila* Fbxo42 candidate substrates by Ataxin-2, which is an RNA-binding protein. In order to confirm biochemically that Ataxin-2 is indeed a substrate of Fbxo42, we made use of the flies overexpressing full-length Fbxo42 along with ^{bio}Ub and BirA in the eye (GMR-GAL4) and crossed them with flies bearing UAS-Ataxin-2-HA. We then extracted protein from the adult fly heads of the progeny and performed a pulldown with streptavidin resin to attach the biotinylated, ubiquitylated Ataxin-2-HA. After incubating the protein extracts with the streptavidin resin, several stringent washes were performed, and the elution of Ataxin-2-HA from the resin was carried

out either in the presence or absence of DTT. The input and eluted fractions were analysed by immunoblotting with anti-HA (Figure 2.29).

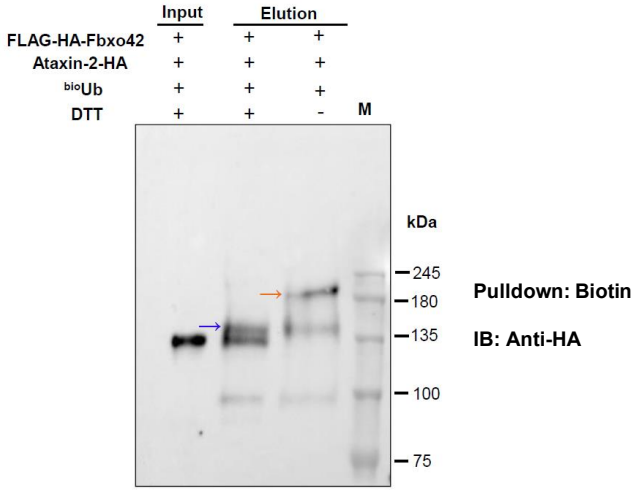

Figure 2.29: Fbxo42 promotes Ataxin-2/ubiquitin conjugates in *Drosophila* eyes. Immunoblot from adult fly heads expressing ^{bio}Ub, Fbxo42 and Ataxin-2-HA, under the control of the GMR-GAL4 driver. Fly head protein extracts were subjected to a biotin pulldown and immunoblot with anti-HA. DTT-sensitive Ataxin-2-HA ^{bio}Ub conjugates are detected by an upwards shift of the bands on the gel. The orange arrow indicates the DTT-sensitive band while the blue arrow indicates the DTT-insensitive band.

By immunoblotting, we observed that Ataxin-2-HA presents a band at 135-140 kDa (Figure 2.29). When a ubiquitin molecule (8.6 kDa) is added to the protein, its size increases by approximately 9 kDa. Regarding the eluted fractions (Figure 2.29), we observed that ubiquitylated Ataxin-2-HA shows two bands of slower mobility on the membrane, with the top band (orange arrow) being sensitive to the presence of the reducing agent DTT in the elution buffer, while the lower band (blue arrow) is not. This result suggests that Fbxo42

could be promoting the ubiquitylation of Ataxin-2 on one or more cysteine residues.

To further confirm the results obtained in flies regarding Fbxo42-mediated ubiquitylation of Ataxin-2 on cysteine residues, we performed an ubiquitylation assay using *Drosophila* S2 cells. For this assay, we transfected S2 cells with UAS-Ataxin-2-GFP and UAS-His-myc-ubiquitin, either in the presence or absence of Fbxo42 RNAi. To purify the ubiquitylated proteins from cell lysates, we performed a histidine pulldown using a nickel-containing resin (IMAC Ni-charged). Elution was performed in the presence or absence of DTT. The histidine pulldown was followed by immunoblotting with anti-myc, to detect protein ubiquitylation and anti-GFP, to detect the Ataxin-2-GFP protein (Figure 2.30).

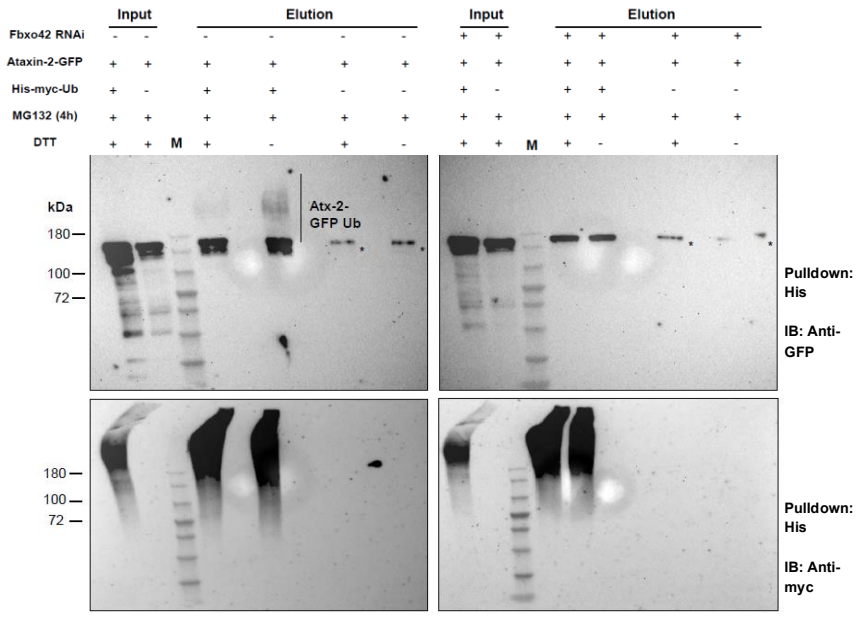

Figure 2.30: Fbxo42 promotes Ataxin-2/ubiquitin conjugates in *Drosophila* S2 cells. Immunoblot of protein extracts from *Drosophila* S2 cells expressing Ataxin-2-GFP, His-myc-ubiquitin and in the presence or absence of Fbxo42 RNAi. Cell lysates were subjected to histidine (His) pulldown and immunoblots with anti-GFP (top panels) and anti-myc (bottom panels). DTT-sensitive Ataxin-2-GFP/His-myc-ubiquitin conjugates are detected by an upwards shift of the bands on the gel. *indicates residual His-myc-Ub-independent pulldown of Ataxin-2-GFP, presumably by direct interaction with the nickel resin.

By immunoblotting with anti-GFP after histidine pulldown (Figure 2.30), we were able to detect Ataxin-2-GFP/His-myc-ubiquitin conjugates in the eluted fraction of protein extracts from S2 cells expressing Ataxin-2-GFP, His-myc-Ub, and endogenous Fbxo42. In the presence of DTT, these ubiquitin conjugates drastically decreased, confirming that Ataxin-2 ubiquitylation occurs on cysteine residues. Furthermore, RNAi depletion of Fbxo42 completely abolished the formation of Ataxin-2-GFP/ubiquitin

conjugates, thereby demonstrating that Ataxin-2 ubiquitylation on cysteine residues is mediated by Fbxo42.

Ataxin-2 RNAi abrogates the suppression of the "glossy" eye phenotype (Xbp1s-induced) caused by *Fbxo42* mutations

To assess the effect of Ataxin-2 in the context of the assay used in the original genetic screen, we crossed Xbp1s-overexpressing flies (eyFlp, GMR-GAL4, UAS-Xbp1^{spliced}; FRT42D, ubiGFP) with flies carrying Ataxin-2 RNAi, together with FRT42D and Su218 (Fbxo42^{N423*}). We analysed the progeny and found that RNAi depletion of Ataxin-2 abolished the suppression of the Xbp1s-induced "glossy" eye phenotype by Su218 (Figure 2.31). This result indicates that Ataxin-2 is a relevant substrate of Fbxo42, being involved in the suppression of the Xbp1s-induced "glossy" eye phenotype by *Fbxo42* loss-of-function mutations.

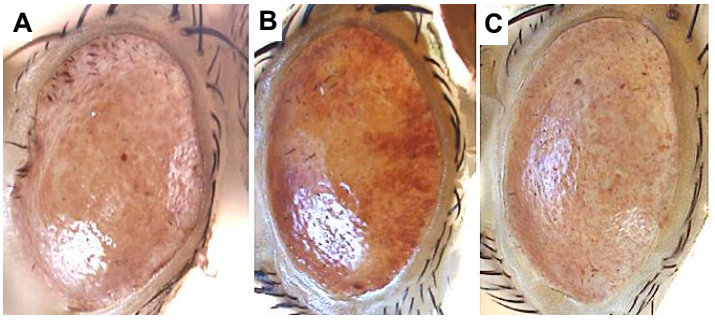

Figure 2.31: Ataxin-2 RNAi abrogates the suppression of the "glossy" eye phenotype by clones of Su218 (Fbxo42^{N423*}). (A) "Glossy" eye phenotype caused by overexpression of Xbp1s under the control of GMR-GAL4 (genotype: eyFlp, GMR-GAL4, UAS-Xbp1s/FM7; FRT42D, ubiGFP); **(B)** "Glossy" eye phenotype is reduced in clones of suppressor 218 (genotype: eyFlp, GMR-GAL4, UAS-Xbp1s; FRT42D, Su218/ FRT42D, ubiGFP); **(C)** RNAi for Ataxin-2 suppresses the reduction of the "glossy" eye phenotype by clones of suppressor 218 (genotype: eyFlp, GMR-GAL4, UAS-Xbp1s; FRT42D, Su218/ FRT42D, ubiGFP; UAS-Ataxin-2 RNAi).

2.5 Discussion

A previous work performed in our laboratory showed that the overexpression of the Xbp1^{spliced}, a mediator of UPR, leads to the "glossy" eye phenotype (Schweizer, 2015). This phenotype is caused by the death of photoreceptors, cone and pigment cells.

In order to identify mutations that could rescue the Xbp1s-induced "glossy" eye phenotype, we performed an EMS screen. Through this genetic screen, we found that different loss-of-function mutations in *Fbxo42* suppressed the "glossy" eye phenotype. Thus, one of our main aims was to understand how mutations in *Fbxo42* could rescue the retinal degeneration induced by Xbp1s-overexpression.

Fbxo42 encodes an F-box protein, whose function is not yet fully understood. To investigate this protein, we began by generating an antibody against it. We produced a rabbit polyclonal anti-Fbxo42 antibody raised against amino acids 384-667 of Fbxo42. This antibody enabled us to study the cellular and tissue localization of this F-box protein. We verified that Fbxo42 was expressed in all analysed tissues of *Drosophila* larvae, including the brain, eye imaginal discs and ring gland. In adult flies, we observed expression of this F-box protein in the brain, ovary and testis. We also tested this antibody for immunofluorescence and found that homozygous mutant cells for Fbxo42 presented reduced immunoreactivity for anti-Fbxo42, compared to wild-type control cells.

Interestingly, when we tested the anti-Fbxo42 antibody (raised against *Drosophila* Fbxo42) in HEK cell lysates, we observed a band that presumably corresponded to human FBXO42. This result highlights the conservation between fly and human

Fbxo42 proteins. However, further studies will be needed to confirm that the anti-DrosoFbxo42 antibody can reliably recognize human FBXO42.

The next step was to identify the specific substrates of the Fbxo42 protein. For that, we employed two different mass spectrometry strategies. Since the function of Fbxo42 is conserved from fly to human, we used HEK-293 cells to perform the first MS experiment. These cells were stably transfected with full-length *Drosophila* Fbxo42, ΔFbxo42, Su359 or empty vector. With this first mass spectrometry analysis, we identified several Fbxo42 interactors, including the SCF components Cullin-1, Skp-1 and Rbx-1, as well as members of COP9 signalosome complex. However, when we tested the Fbxo42 candidate substrates by immunofluorescence, to check whether they accumulate in Fbxo42 homozygous mutant cell clones, we found that most of them failed to accumulate in these clones. In fact, the only positive result we obtained was Lamin-B, when its immunostaining was carried out with the ADL84 antibody, but not with ADL67. We further investigated why we observed this difference and found in the literature that ADL84 specifically recognizes Lamin-B when it is dephosphorylated on Serine 25 (Stuurman ***et al.***, 1995). Therefore, a phosphatase could be the direct substrate of Fbxo42. To test this hypothesis, we used an RNAi line for one of the fly phosphatases, PP1-87B. We crossed flies to generate larvae with eye imaginal discs containing Su218/ubiGFP clones, along with PP1-87B RNAi expression, to determine whether this RNAi modify the ADL84 staining. We verified that RNAi for PP1-87B phosphatase resulted

in uniform ADL84 staining in both wild-type and Fbxo42 mutant cells, suggesting that this phosphatase could be a substrate of Fbxo42. A recent study of Barbosa and collaborators showed that *Drosophila* Fbxo42 downregulates the protein levels of the phosphatase PP2A-B56 (Barbosa *et al.*, 2021). Also, a MS analysis in HEK-293 cells searching for substrates of FBXO42 detected the interaction between the human FBXO42 and different phosphatases (Jiang *et al.*, 2022). Despite the results obtained with the PP1-87B RNAi fly line regarding LaminB-ADL84 staining, further studies will be needed to prove the interaction between Fbxo42 and PP1-87B.

Since the first mass spectrometry was performed with human cells, we decided to perform a second mass spectrometry, this time using fly extracts. This second proteomic approach was based on the ^{bio}Ub strategy (Franco *et al.*, 2011; Ramirez *et al.*, 2015), developed by Ugo Mayor laboratory. To use this approach, we generated flies expressing full-length Fbxo42, ΔFbxo42 and Fbxl7 (a different fly F-box protein) along with a polyubiquitin tag containing a short biotinylatable motif and BirA. Through this MS, we were able to identify the RNA-binding protein Ataxin-2 as a candidate substrate of Fbxo42. Ataxin-2 was the Fbxo42 interactor detected with the highest confidence level. Additionally, some subunits of the chaperonin containing TCP-1 (CCT) complex were also detected, specifically CCT3 and CCT4. Some subunits of CCT were also identified as interactors of human FBXO42 (Jiang *et al.*, 2022). However, preliminary results with RNAi for one of the CCT complex subunits (CCT2) did not show that CCT was relevant in the context of the assay used in the original genetic screen. We

observed that CCT2 RNAi did not abolish the suppression of the Xbp1s-induced “glossy” eye phenotype by Su218.

Regarding Ataxin-2, we have biochemically confirmed that Fbxo42 mediates the ubiquitylation of Ataxin-2 in fly eyes and in *Drosophila* S2 cells. We overexpressed Fbxo42 and Ataxin-2-HA together with ^{bio}Ub in fly eyes under the control of the GMR-GAL4 driver. We performed the pulldown of the biotinylated, ubiquitylated Ataxin-2 using streptavidin resin, and elution was performed either in the absence or presence of DTT. By immunoblotting, we were able to detect a band corresponding to Ataxin-2-HA/ubiquitin conjugates, which was sensitive to the presence of DTT in the elution buffer, indicating that the ubiquitylation of Ataxin-2 mediated by Fbxo42 could occur on cysteine residues. This was further demonstrated by an ubiquitylation assay using *Drosophila* S2 cells, transfected with UAS-Ataxin-2-GFP and UAS-His-myc-ubiquitin, in the presence or absence of Fbxo42 RNAi. We performed a histidine pulldown to capture the ubiquitylated Ataxin-2-GFP. By immunoblotting, we observed the presence of Ataxin-2-GFP/ubiquitin conjugates in the absence of DTT. In contrast, when elution was performed in the presence of DTT, we observed a drastic decrease in Ataxin-2-GFP/ubiquitin conjugates. Additionally, RNAi depletion of Fbxo42 led to the disappearance of ubiquitin conjugates associated with Ataxin-2-GFP.

Finally, we demonstrated that Ataxin-2 is a relevant Fbxo42 substrate in the context of the suppression of Xbp1s-induced retinal degeneration by Fbxo42 mutations, showing that RNAi depletion of Ataxin-2 abolished the suppression of the Xbp1s-induced “glossy”

eye phenotype by Su218. Further analysis will be required to investigate the interaction between Ataxin-2 and Xbp1s.

2.6 Acknowledgments

I would like to thank Nadine Schweizer, who performed the EMS screen and identified the Fbxo42 mutants. I express my gratitude to Vanya Rasheva, who also worked on the EMS screen. Furthermore, I acknowledge Fátima Cairrão, who taught me to work with *Drosophila* S2 cells and performed the Fbxo42/SkpA co-immunoprecipitation experiment in S2 cells. I would like to thank Catarina Gaspar, who designed the pLex constructs and performed the MS in HEK cells, and Colin Adrain for supervising this part of the work. I express my gratitude to Juanma Ramirez and Nerea Osinalde for performing the mass spectrometry using fly head extracts. Furthermore, I thank Ugo Mayor for his collaboration on this project over the years, for the ^{bio}Ub reagents and for analysing the MS data. I acknowledge Hyung Don Ryoo for proving several fly reagents and the pUAST-His-myc-Ub plasmid. Finally, I would like to thank Pedro Domingos for performing the EMS screen, analysing the data, helping with the construction of fly reagents and supervising the work.

2.7 References

Arsham AM & Neufeld TP (2009). A genetic screen in Drosophila reveals novel cytoprotective functions of the autophagy-lysosome pathway. *PLoS One*; DOI: 10.1371/journal.pone.0006068.

Barbosa P, Zhaunova L, Debilio S, Steccanella V, Kelly V, Ly T & Ohkura H (2021). SCF-Fbxo42 promotes synaptonemal complex assembly by downregulating PP2A-B56. *J Cell Biol*; DOI:

10.1083/JCB.202009167.

Blumenstiel JP, Noll AC, Griffiths JA, Perera AG, Walton KN, Gilliland WD, Hawley RS & Staehling-Hampton K (2009). Identification of EMS-induced mutations in Drosophila melanogaster by whole-genome sequencing. *Genetics* **182,** 25–32.

Bosch JA, Sumabat TM, Hafezi Y, Pellock BJ, Gandhi KD & Hariharan IK (2014). The Drosophila F-box protein Fbxl7 binds to the protocadherin Fat and regulates Dachs localization and Hippo signaling. *Elife* **3,** 1–25.

Bravo R, Parra V, Gatica D, Rodriguez AE, Torrealba N, Paredes F, Wang Z V., Zorzano A, Hill JA, Jaimovich E, Quest AFG & Lavandero S (2013). *Endoplasmic Reticulum and the Unfolded Protein Response. Dynamics and Metabolic Integration.*

Casas-Tinto S, Zhang Y, Sanchez-Garcia J, Gomez-Velazquez M, Rincon-Limas DE & Fernandez-Funez P (2011). The ER stress factor XBP1s prevents amyloid-β neurotoxicity. *Hum Mol Genet* **20,** 2144–2160.

Cissé M, Duplan E, Lorivel T, Dunys J, Bauer C, Meckler X, Gerakis Y, Lauritzen I & Checler F (2017). The transcription factor XBP1s restores hippocampal synaptic plasticity and memory by control of the Kalirin-7 pathway in Alzheimer model. *Mol Psychiatry* **22,** 1562–1575.

Clemens JC, Worby CA, Simonson-Leff N, Muda M, Maehama T, Hemmings BA & Dixon JE (2000). Use of double-stranded RNA interference in Drosophila cell lines to dissect signal transduction pathways. *Proc Natl Acad Sci U S A* **97,** 6499–6503.

Cooper JL, Greene EA, Till BJ, Codomo CA, Wakimoto BT & Henikoff S (2008). Retention of induced mutations in a Drosophila reverse-genetic resource. *Genetics* **180,** 661–667.

Cox J, Hein MY, Luber CA, Paron I, Nagaraj N & Mann M (2014). Accurate proteome-wide label-free quantification by delayed normalization and maximal peptide ratio extraction, termed MaxLFQ. *Mol Cell Proteomics* **13,** 2513–2526.

Cox J & Mann M (2008). MaxQuant enables high peptide identification rates, individualized p.p.b.-range mass accuracies and proteome-wide protein quantification. *Nat Biotechnol* **26,** 1367–1372.

Cox J, Neuhauser N, Michalski A, Scheltema RA, Olsen J V. & Mann M (2011). Andromeda: A peptide search engine integrated into the MaxQuant environment. *J Proteome Res* **10,** 1794–1805.

Domingues C & Ryoo HD (2012). Drosophila BRUCE inhibits apoptosis

through non-lysine ubiquitination of the IAP-antagonist REAPER. *Cell Death Differ* **19,** 470–477.

Franco M, Seyfried NT, Brand AH, Peng J & Mayor U (2011). A novel strategy to isolate ubiquitin conjugates reveals wide role for ubiquitination during neural development. *Mol Cell Proteomics* **10,** 1–15.

Golic KG (1991). Site-specific recombination between homologous chromosomes in Drosophila. *Science (80-)* **252,** 958–961.

Grether ME, Abrams JM, Agapite J, White K & Steller H (1995). The head involution defective gene of Drosophila melanogaster functions in programmed cell death. *Genes Dev* **9,** 1694–1708.

Harding HP, Calfon M, Urano F, Novoa I & Ron D (2002). Transcriptional and translational control in the mammalian unfolded protein response. *Annu Rev Cell Dev Biol* **18,** 575–599.

Hetz C (2012). The unfolded protein response: Controlling cell fate decisions under ER stress and beyond. *Nat Rev Mol Cell Biol* **13,** 89–102.

Hetz C & Saxena S (2017). ER stress and the unfolded protein response in neurodegeneration. *Nat Rev Neurol* **13,** 477–491.

Hetz C, Thielen P, Matus S, Nassif M, Court F, Kiffin R, Martinez G, Cuervo AM, Brown RH & Glimcher LH (2009). XBP-1 deficiency in the nervous system protects against amyotrophic lateral sclerosis by increasing autophagy. *Genes Dev* **23,** 2294–2306.

Hetz C, Zhang K & Kaufman RJ (2020). Mechanisms, regulation and functions of the unfolded protein response. *Nat Rev Mol Cell Biol* **21,** 421–438.

Huang HW, Zeng X, Rhim T, Ron D & Ryoo HD (2017). The requirement of IRE1 and XBP1 in resolving physiological stress during Drosophila development. *J Cell Sci* **130,** 3040–3049.

Jiang H, Bian W, Sui Y, Li H, Zhao H, Wang W & Li X (2022). FBXO42 facilitates Notch signaling activation and global chromatin relaxation by promoting K63-linked polyubiquitination of RBPJ. *Sci Adv* **8,** 1–18.

Kang MJ, Chung J & Ryoo HD (2012). CDK5 and MEKK1 mediate pro-apoptotic signalling following endoplasmic reticulum stress in an autosomal dominant retinitis pigmentosa model. *Nat Cell Biol* **14,** 409–415.

Kang MJ & Hyung DR (2009). Suppression of retinal degeneration in Drosophila by stimulation of ER-associated degradation. *Proc Natl*

Acad Sci U S A **106,** 17043–17048.

Kang MJ & Ryoo HD (2009). Suppression of retinal degeneration in Drosophila by stimulation of ER-associated degradation. *Proc Natl Acad Sci U S A* **106,** 17043–17048.

Lee H, Noh JY, Oh Y, Kim Y, Chang JW, Chung CW, Lee ST, Kim M, Ryu H & Jung YK (2012). IRE1 plays an essential role in ER stress-mediated aggregation of mutant huntingtin via the inhibition of autophagy flux. *Hum Mol Genet* **21,** 101–114.

Liao TSV, Call GB, Guptan P, Cespedes A, Marshall J, Yackle K, Owusu-Ansah E, Mandal S, Fang QA, Goodstein GL, Kim W & Banerjee U (2006). An efficient genetic screen in Drosophila to identify nuclear-encoded genes with mitochondrial function. *Genetics* **174,** 525–533.

Lin SC, Chang YY & Chan CC (2014). Strategies for gene disruption in Drosophila. *Cell Biosci* **4,** 1–9.

Liu SZ, Yao SJ, Yang H, Liu SJ & Wang YJ (2023). Autophagy: Regulator of cell death. *Cell Death Dis*; DOI: 10.1038/s41419-023-06154-8.

Liu X & Lengyel JA (2000). Drosophila arc encodes a novel adherens junction-associated PDZ domain protein required for wing and eye development. *Dev Biol* **221,** 419–434.

Newsome TP, Åsling B & Dickson BJ (2000). Analysis of Drosophila photoreceptor axon guidance in eye-specific mosaics. *Development* **127,** 851–860.

Patil C & Walter P (2001). Intracellular signaling from the endoplasmic reticulum to the nucleus: The unfolded protein response in yeast and mammals. *Curr Opin Cell Biol* **13,** 349–355.

Ramirez J, Martinez A, Lectez B, Lee SY, Franco M, Barrio R, Dittmar G & Mayor U (2015). Proteomic analysis of the ubiquitin landscape in the Drosophila embryonic nervous system and the adult photoreceptor cells. *PLoS One* **10,** 1–24.

Ramírez J, Morales M, Osinalde N, Martínez-Padrón I, Mayor U & Ferrús A (2021). The ubiquitin ligase Ariadne-1 regulates neurotransmitter release via ubiquitination of NSF. *J Biol Chem* **296,** 100408.

Rasheva VI & Domingos PM (2009). Cellular responses to endoplasmic reticulum stress and apoptosis. *Apoptosis* **14,** 996–1007.

Ron D & Walter P (2007). Signal integration in the endoplasmic reticulum unfolded protein response. *Nat Rev Mol Cell Biol* **8,** 519–529.

Ryoo HD, Bergmann A, Gonen H, Ciechanover A & Steller H (2002).

Regulation of Drosophila IAP1 degradation and apoptosis by reaper and ubcD1. *Nat Cell Biol* **4,** 432–438.

Ryoo HD, Domingos PM, Kang MJ & Steller H (2007). Unfolded protein response in a Drosophila model for retinal degeneration. *EMBO J* **26,** 242–252.

Schröder M (2008). Endoplasmic reticulum stress responses. *Cell Mol Life Sci* **65,** 862–894.

Schweizer NS (2015). The Role of the Fbox Protein CG6758 in Xbp1s Induced Retinal Degeneration in Drosophila.

Shevchenko A, Wilm M, Vorm O & Mann M (1996). Mass spectrometric sequencing of proteins from silver-stained polyacrylamide gels. *Anal Chem* **68,** 850–858.

Stuurman N, Maus N & Fisher PA (1995). Interphase phosphorylation of the Drosophila nuclear lamin: Site-mapping using a monoclonal antibody. *J Cell Sci* **108,** 3137–3144.

Tabas I & Ron D (2011). Integrating the mechanisms of apoptosis induced by endoplasmic reticulum stress. *Nat Cell Biol* **13,** 184–190.

Tyanova S, Temu T, Sinitcyn P, Carlson A, Hein MY, Geiger T, Mann M & Cox J (2016). The Perseus computational platform for comprehensive analysis of (prote)omics data. *Nat Methods* **13,** 731–740.

Vidal RL, Figueroa A, Court FA, Thielen P, Molina C, Wirth C, Caballero B, Kiffin R, Segura-Aguilar J, Cuervo AM, Glimcher LH & Hetz C (2012). Targeting the UPR transcription factor XBP1 protects against Huntington's disease through the regulation of FoxO1 and autophagy. *Hum Mol Genet* **21,** 2245–2262.

Walter P & Ron D (2011). The Unfolded Protein Response: From Stress Pathway to Homeostatic Regulation. *Science (80-)* **334,** 1081–1086.

Woehlbier U & Hetz C (2011). Modulating stress responses by the UPRosome: A matter of life and death. *Trends Biochem Sci* **36,** 329–337.

Xu D, Li Y, Arcaro M, Lackey M & Bergmann A (2005). The CARD-carrying caspase Dronc is essential for most, but not all, developmental cell death in Drosophila. *Development* **132,** 2125–2134.

Yoshida H, Oku M, Suzuki M & Mori K (2006). pXBP1(U) encoded in XBP1 pre-mRNA negatively regulates unfolded protein response activator pXBP1(S) in mammalian ER stress response. *J Cell Biol* **172,** 565–575.

CHAPTER III

Fbxo42 promotes the proteasomal degradation of Ataxin-2

Authors: Santos CC, Cordeiro TN and Domingos PM.

3.1 Abstract

We have identified the RNA-binding protein Ataxin-2 as a substrate of Fbxo42 through a proteomic approach (Chapter II). To further confirm the interaction between Fbxo42 and Ataxin-2, we performed co-immunoprecipitation (co-IP) experiments using *Drosophila* S2 cells and fly extracts. These experiments revealed that both endogenous and overexpressed Fbxo42 co-immunoprecipitate with Ataxin-2. Furthermore, immunofluorescence experiments on ring gland cells of *Drosophila* larvae and follicle cells of the adult ovary showed that, upon ER stress induction, Ataxin-2 and Fbxo42 localize in close proximity.

To investigate whether Fbxo42 regulates the activity of Ataxin-2 or promotes its proteasomal degradation, we performed cycloheximide (CHX) chase assays in S2 cells. These assays demonstrated that overexpression of Fbxo42 leads to faster degradation of Ataxin-2, while Fbxo42 RNAi depletion protects Ataxin-2 from degradation. In the previous chapter, we showed that Fbxo42 promotes the formation of Ataxin-2/ubiquitin conjugates, which are DTT-sensitive, suggesting that cysteine residue(s) might be the ubiquitylation sites for Fbxo42. To test this hypothesis, we mutagenized the cysteine residues of Ataxin-2. Among the mutants, we observed that Ataxin-2^{C244A}-GFP showed increased stability in CHX-chase experiments and did not present DTT-sensitive Ataxin-2-GFP/ubiquitin conjugates in ubiquitylation assays.

Finally, an AlphaFold-3 structural prediction for the SCF complex containing Fbxo42 and Ataxin-2, shows that Ataxin-2 binds to Fbxo42 and that cysteine 244 of Ataxin-2 is in close proximity to the reactive C-terminus of ubiquitin.

3.2 Introduction

In the previous chapter, we described the identification of Ataxin-2 as a substrate of Fbxo42, through mass spectrometry and biochemical analysis. In this Chapter, we present additional experiments that further support the interaction between Fbxo42 and Ataxin-2 and address the question of whether Fbxo42 promotes the proteasomal degradation of Ataxin-2. Some of the experiments were done using the ring gland of *Drosophila* larvae and the follicle cells of the adult ovary, so we will briefly introduce these systems.

Drosophila ring gland

The ring gland is an endocrine organ of *Drosophila* larva, being responsible for the production and release of developmental hormones (Harvie *et al.*, 1998). The ring gland is located anterior to the brain, in between the two brain lobes. This organ is composed of three distinct glands: the corpus allatum (CA), the prothoracic gland (PG) and the corpora cardiaca (CC) (Figure 3.1) (De Velasco *et al.*, 2004). The large prothoracic cells (grouped as lateral lobes in the ring gland) synthetize the steroid hormone ecdysone, while the corpus allatum (a group of small medial cells in the ring gland) secretes the juvenile hormone (Harvie *et al.*, 1998; Dubrovsky, 2005). Ecdysone and juvenile hormone control insect growth and development (Dubrovsky, 2005).

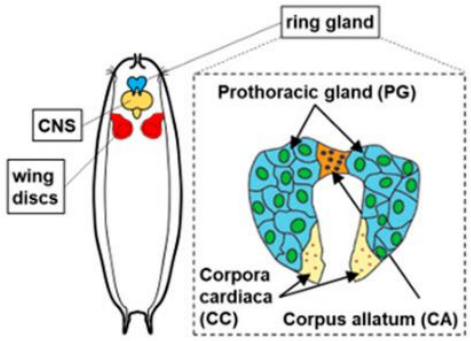

Figure 3.1: Structure of ring gland of *Drosophila* larva. Ring gland is composed by prothoracic gland (PG), corpora cardiaca (CC) and corpus allatum (CA) (Setiawan *et al.*, 2018).

Drosophila ovary

The female fly harbours a pair of ovaries, each consisting of 15-20 ovarioles (Hinnant *et al.*, 2020). Each ovariole contain the germarium, located at the anterior tip, followed by sequentially maturing egg chambers (Hinnant *et al.*, 2020; Xu *et al.*, 2024). Each egg chamber encompasses one oocyte and fifteen nurse cells that support oocyte growth, surrounded by a monolayer of somatic epithelial cells, called follicle cells (Hinnant *et al.*, 2020; Xu *et al.*, 2024). The egg chamber development is subdivided into 14 stages (Figure3.2) (Hinnant *et al.*, 2020).

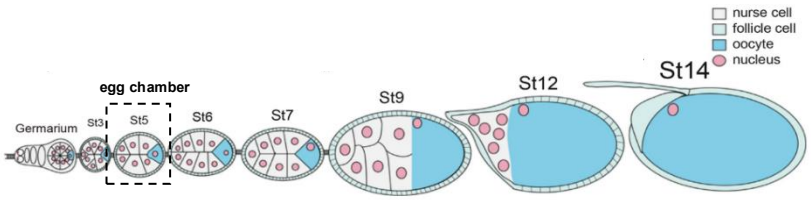

Figure 3.2: Diagram of *Drosophila* oogenesis. Each ovariole contain a germarium at the anterior tip, followed by sequentially maturing egg chambers. Adapted from (Xu *et al.*, 2024).

In this Chapter, our specific aims are as follows:

- Study the interaction between Fbxo42 and Ataxin-2 through co-immunoprecipitation experiments, using S2 *Drosophila* cells and fly extracts.
- Investigate the interaction between Fbxo42 and Ataxin-2 via immunofluorescence assays in different tissues, including the ring gland and ovary, under both physiological and ER stress conditions.
- Analyse the stability of Ataxin-2, through cycloheximide chase assays.
- Test whether the accumulation of Ataxin-2 is observed in Fbxo42 mutant clones.
- Identify the cysteine residue(s) of Ataxin-2 that are ubiquitylated by Fbxo42.
- Predict the structure of the Ataxin-2/Fbxo42/Cullin-1/Skp-1/Rbx1/E2/Ub complex using AlphaFold-3.

3.3 Methods

Immunofluorescence and imaging

Drosophila adult or larval tissues were dissected in 1× PBS, fixed with 4% PFA in 1× PBS at room temperature for at least 45 minutes and washed three times with PBT (1× PBS + 0.3% Triton X-100), 10 minutes each. Afterwards, fly's tissues were incubated with primary antibodies diluted in BBT-250 (0.1% BSA, 0.1% Triton X-100, 250 mM NaCl in 1× PBS) overnight, at 4°C under gentle agitation. The following primary antibodies were used: guinea-pig anti-Ataxin-2 [1:200, (Zhang *et al.*, 2013), a kind gift from Patrick

Emery] and rabbit anti-Fbxo42 (1:100). Incubation with anti-Fbxo42 antibody was preceded by an extra step of blocking and permeabilization; tissues were incubated in block-permeabilization solution (1% BSA, 0.3% Triton X-100 in 1× PBS) for 1 hour at room temperature. After overnight incubation with primary antibodies, fly's tissues were washed 3x with PBT for 10 minutes each and incubated with fluorescent conjugated secondary antibodies (Jackson ImmunoResearch Laboratories) for 2 hours at room temperature. Following three washes in PBT, the tissues were mounted in VECTASHIELD® Antifade Mounting Medium with DAPI (Vector Laboratories, H-1200-10) and image acquisition was performed on a confocal microscope (Leica SP5 Live or Zeiss LSM 880).

Treatments of the fly's tissues

To promote UPR activation and the formation of Ataxin-2 granules, larval tissues were exposed to 5 mM DTT for 4 hours in PBS. As an alternative method to induce the formation of Ataxin-2 granules, larval tissues were treated with 0.5 mM arsenite for 2 hours. Untreated larval tissues were used as control.

Adult ovaries were dissected in 1× PBS and then transferred to Schneider's *Drosophila* medium (Biowest). Ataxin-2 granules were induced by incubating ovaries with 0.5 mM arsenite in Schneider's medium for 2 hours at 25°C (Gareau *et al.*, 2013). Untreated ovaries were kept in Schneider's medium and used as control.

Cell culture, transfections and RNAi treatments

Drosophila S2 cells (Schneider, 1972) were cultured at 24°C without CO_2 in Schneider's *Drosophila* medium (Biowest) supplemented with 10% heat inactivated FBS (Biowest), 100 U/ml of penicillin plus 100 µg/ml of streptomycin (Thermo Fisher Scientific). The complete medium was filtered with 0,2 µm PES filter (VWR). S2 cells were transfected with the indicated plasmids using Effectene transfection reagent (QIAGEN) according to the manufacturer's instructions.

RNA-mediated interference (RNAi) was performed as described in (Clemens *et al.*, 2000). Primer pairs bearing a 5' end T7 RNA polymerase binding site were used to PCR amplify specific sequences of the genes to be inhibited. PCR products (with approximately 500-600 bp in length) were then purified with NucleoSpin® Gel and PCR Clean-up kit (MN) or with NZYGelpure kit (NZYtech) and used as templates for dsRNA synthesis with T7 RiboMAX™ Express Large Scale RNA Production System (Promega). After the DNase treatment, dsRNAs were purified and concentrated with RNA Clean & Concentrator™-5 kit (Zymo Research).

Co-Immunoprecipitation

For co-immunoprecipitation (Co-IP) of Fbxo42 and Ataxin-2, S2 cells endogenously expressing Fbxo42 protein or treated with Fbxo42 RNAi were transfected with pActinGal4 and pUAST-Ataxin-2-GFP plasmids. Three days after, cells were resuspended in lysis buffer (50 mM Tris-HCl pH 7.5, 150 mM NaCl, 1 mM EDTA, 0.5%

Triton X-100) supplemented with protease inhibitors (cOmplete™, Mini, EDTA-free Protease Inhibitor Cocktail, Roche).

To produce fly head extracts for Co-IP of Fbxo42 and Ataxin-2, flies expressing: GMR-GAL4, UAS-(^{bio}Ub)$_6$-BirA/UAS-Ataxin-2-GFP; UAS-FLAG-HA-Fbxo42 or GMR-GAL4, UAS-(^{bio}Ub)$_6$-BirA/UAS-Ataxin-2-GFP; UAS-FLAG-Fbxl7 were used. Fly heads were collected and homogenized in lysis buffer (50 mM Tris-HCl pH 7.4, 150 mM NaCl, 1mM EDTA, 1% Triton X-100) supplemented with protease inhibitors (cOmplete™, Mini, EDTA-free Protease Inhibitor Cocktail, Roche) using glass beads (0.5 mm Glass Beads, Scientific Industries) in a bead beater homogenizer.

Equal amounts of protein lysates were incubated with GFP-Trap agarose beads (ChromoTek GFP-Trap® Agarose) with rotation end-over-end for 2 hours and 30 minutes at 4°C. After that, tubes were centrifuged at 2700*g* for 2 minutes at 4°C. Then, GFP-Trap beads were washed three times in ice cold dilution buffer (10 mM Tris-HCl pH 7.5, 150 mM NaCl, 0.5 mM EDTA) supplemented with protease inhibitors (cOmplete™, Mini, EDTA-free Protease Inhibitor Cocktail, Roche). After the last wash, supernatants were removed and beads were resuspended in SDS-sample buffer (250 mM Tris-HCl pH 7.5, 40% glycerol, 4% SDS and 0.2% bromophenol blue). Finally, beads were boiled for 10 minutes at 95°C to dissociate immunocomplexes from the GFP-Trap beads and eluted fractions were recovered after centrifugation for 2 minutes at room temperature. In the case of the fly samples, the elution volume was divided into two: to half of the volume was added 100 mM DTT and this was then heated at 65°C for 15 minutes. Regarding the cell eluates, it was added 100 mM DTT to the entire eluted volume.

Samples (inputs and eluates) were further analysed by immunoblotting with rat anti-GFP (1:1000, 3H9, Chromotek) and rabbit anti-Fbxo42 (1:1000) antibodies.

Cycloheximide (CHX) chase experiments

Drosophila S2 cells were transfected with pActinGal4, wild-type (WT) or mutant versions of pUAST-Ataxin-2-GFP in the presence/absence of FLAG-HA-Fbxo42. Three days after transfection, cells were treated with 100 µg/ml cycloheximide (cat. no. J66901.03, Alfa Aesar) for 0, 6 and 12 hours, to inhibit the protein translation. S2 cells treated with Fbxo42 RNAi or with control RNAi and transfected with pActinGal4 and pUAST-Ataxin-2-GFP were also incubated with cycloheximide as aforementioned. At the indicated timepoints, cells were resuspended in lysis buffer (50 mM Tris-HCl pH 7.5, 150 mM NaCl, 1 mM EDTA, 0.5% Triton X-100) supplemented with protease inhibitors (cOmplete™, Mini, EDTA-free Protease Inhibitor Cocktail, Roche). Total cell extracts were analysed by immunoblotting with rat anti-GFP (1:1000, 3H9, Chromotek) and rabbit anti-Fbxo42 (1:1000) antibodies. Tubulin, detected with mouse anti-alpha-Tubulin antibody (1:500, AA4.3, DSHB) was used as loading control. Where indicated, 50 µM MG132 (Z-Leu-Leu-Leu-al, C2211, Merck) was added to the S2 cells to inhibit the proteosome.

Ubiquitylation assays in S2 cells

For the ubiquitylation assay, 5.0 x 10^5 S2 cells/ well were seeded in 6-well plates. On the next day, S2 cells were transfected with 200 ng of each one of the following plasmids: pActin-Gal4,

pUAST-His-myc-Ubiquitin and either wild-type pUAST-Ataxin-2-GFP or mutant pUAST-Ataxin-2^{C244A}-GFP. Three days after transfection, cells were incubated with 50 μM of MG132 (Z-Leu-Leu-Leu-al, C2211, Merck) for 4 hours, to inhibit proteasome activity, and resuspended in lysis buffer (50 mM Tris-HCl pH 7.5, 150 mM NaCl, 1 mM EDTA, 0.5% Triton X-100) supplemented with protease inhibitors (cOmplete™, Mini, EDTA-free Protease Inhibitor Cocktail, Roche) and 0.7% of NEM. Cell extracts were harvested and incubated on ice for at least 30 minutes. To perform the pulldown of proteins conjugated with His-myc-Ubiquitin, each cell lysate was incubated with 15 μl of a nickel-charged resin suspension (Profinity™ IMAC Ni-Charged Resin, cat. no. 156-0131, Bio-Rad) for 2 hours and 20 minutes at 4°C. Afterwards, resin was washed thrice in 1× PBS + 20mM imidazole. The elution of the ubiquitylated molecules from the resin was performed with elution buffer containing 1× PBS + 250 mM imidazole at room temperature. The eluted volume was divided into two: half of the volume was incubated with 100 mM of DTT and heated at 65°C for 20 minutes. Then, 4× Laemmli buffer (240 mM Tris-HCl pH 6.8, 8% SDS, 40% glycerol, 250 mM DTT, 0.04% bromophenol blue) was added to the samples (with/without DTT), and these were boiled for 5 minutes at 95 °C. Finally, samples were loaded onto 4-15% Mini-Protean TGX™ Precast Protein Gels (Bio-Rad) and immunoblots were probed with rat anti-GFP (1:1000, 3H9, Chromotek) and rat anti-Myc (1:2000, 9E1, Chromotek) antibodies.

Immunoblots

Fly extracts or cell lysates were prepared in the above-mentioned lysis buffers supplemented with protease inhibitors (cOmplete™, Mini, EDTA-free Protease Inhibitor Cocktail, Roche). Protein concentration was determined by *DC*™ Protein Assay Kit from Bio-Rad. Afterwards, samples were mixed with 4× SDS Laemmli buffer (240 mM Tris-HCl pH 6.8, 8% SDS, 40% glycerol, 250 mM DTT, 0.04% bromophenol blue) and boiled at 95°C for 5 minutes. Proteins were size separated by SDS-PAGE and transferred onto nitrocellulose membranes of 0.2 µm (Bio-Rad). Immunoblots were blocked with 5% non-fat milk in TBS-T containing 0.1% Tween-20 or in PBS-T containing 0.05-0.1% Tween-20 for 1 hour. After blocking, membranes were incubated overnight at 4°C with the following primary antibodies (table S2): mouse anti-alpha-Tubulin (1:500, AA4.3, DSHB), rabbit anti-Fbxo42 (1:1000) and rat anti-GFP (1:1000, 3H9, Chromotek).

The following day, membranes were washed 4x for 10 minutes in TBS-T or PBS-T and incubated with HRP-conjugated secondary antibodies respective to the primary antibodies' species, specifically, sheep anti-mouse HRP (1:10000, cat. no. NXA931, Cytiva), goat anti-rabbit HRP (1:5000, product no. AS10 668, Agrisera) and goat anti-rat HRP (1:2000, cat. no. R-05075-500, Advansta) for 2 hours at room temperature. Membranes were washed 4x for 10 minutes in TBS-T/PBS-T, and the signal was developed using ECL™ Prime Western Blotting Detection Reagent (RPN2232, Cytiva) and detected using a Chemidoc XRS+ (Bio-Rad) or an iBright™ FL 1500 Imaging System (Thermo Fisher Scientific). iBright™ Analysis Software was used for densitometry.

AlphaFold-3 structural predictions

We utilized AlphaFold-3 (https://alphafoldserver.com/) to predict the structure of the Ataxin-2/Fbxo42/Cullin-1/Skp-1/Rbx1/E2/Ub complex based on the protein sequences. Since AlphaFold struggles to accurately predict disordered or dynamic regions, we pre-processed the sequences by trimming large intrinsically disordered regions (IDRs), typically located in the N- and C-terminal tails. To identify these disordered regions, we employed the Metapredict V2 (Emenecker *et al.*, 2021, 2022) tool (https://metapredict.net/), which allowed us to remove these regions prior to structure prediction. This resulted in more stable poses with improved structural metrics. For the final AlphaFold-3 prediction, the sequences were: Ataxin-2 (aa 57 to 270), Fbxo42 (aa 21 to 347 and 586 to 667), Cullin-1 (aa 11 to 774), Skp-1 (full-length protein), Rbx1 (aa 47 to 122), E2 (effete, full-length protein) and Ub (full-length protein). The resulting model was visualized using ChimeraX (Meng *et al.*, 2023).

Quantification and statistical analysis

The confocal images were analysed using the Fiji software and the ZEN Imaging Software (Zeiss). The number of granules and their components were quantified manually. Statistical analysis was carried out using GraphPad Prism 8 software. Two-way ANOVAs were performed as mentioned in the figure legends. p values refer to: ****$p < 0.0001$, ***$p < 0.001$, **$p < 0.01$ and *$p < 0.05$.

3.4 Results

Fbxo42 co-immunoprecipitates with Ataxin-2-GFP in S2 *Drosophila* cells

To investigate further the interaction between Fbxo42 and Ataxin-2, we performed an immunoprecipitation assay. For this experiment, we used S2 *Drosophila* cells transfected with the Ataxin-2-GFP plasmid, in the presence or absence of Fbxo42 RNAi. The pulldown of Ataxin-2-GFP was carried out using anti-GFP beads. Afterwards, to confirm that Fbxo42 co-immunoprecipitated with Ataxin-2-GFP, an immunoblot containing the input and eluted fractions, probed with anti-Fbxo42 antibody, was performed. Additionally, this immunoblot was also probed with anti-GFP antibody (Figure 3.3).

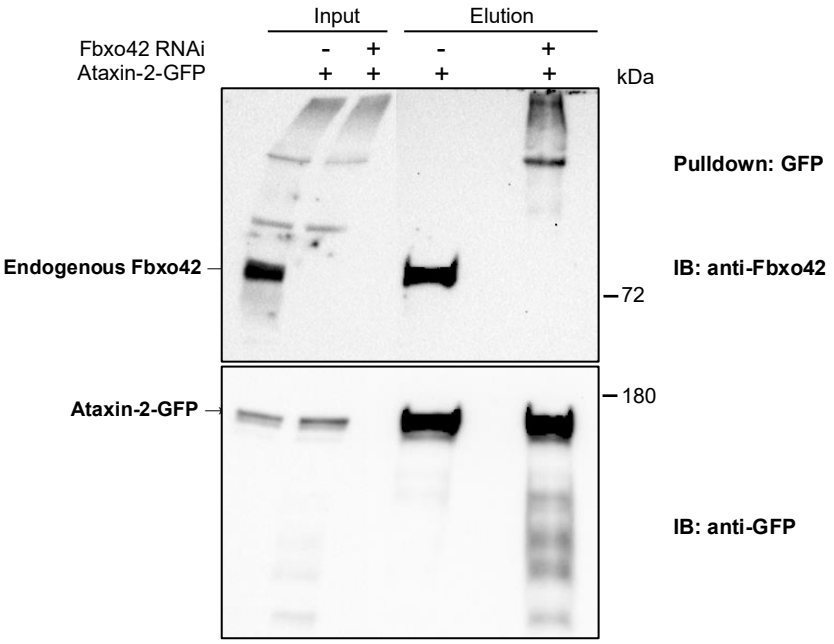

Figure 3.3: Fbxo42 co-immunoprecipitates with Ataxin-2-GFP in S2 *Drosophila* cells. Immunoblots probed with anti-Fbxo42 and anti-GFP antibodies, containing the protein lysates of S2 cells transfected with Ataxin-2-GFP plasmid (in the presence or absence of Fbxo42 RNAi), before/after GFP pulldown with anti-GFP beads. The arrows indicate the bands corresponding to the endogenous Fbxo42 (74.4 kDa) and the overexpressed Ataxin-2-GFP (approximately 170 kDa).

By immunoblotting (Figure 3.3), we observe that, in the absence of Fbxo42 RNAi, the endogenous Fbxo42 protein (74.4 kDa) is co-eluted with the overexpressed Ataxin-2-GFP protein (approximately 170 kDa). In samples with Fbxo42 RNAi depletion, the band corresponding to the endogenous Fbxo42 protein disappears. This result further confirms that Fbxo42 interacts with Ataxin-2.

Fbxo42 co-immunoprecipitates with Ataxin-2-GFP in *Drosophila* eyes

Furthermore, to observe the interaction between Fbxo42 and Ataxin-2 in the fly, we performed an immunoprecipitation assay using fly head extracts overexpressing FLAG-HA-Fbxo42 or the control FLAG-FbxI7, together with Ataxin-2-GFP, in the eye, under the control of the GMR-GAL4 driver. The pulldown of Ataxin-2-GFP was performed using anti-GFP beads. This was followed by immunoblotting with anti-Fbxo42 and anti-GFP antibodies (Figure 3.4).

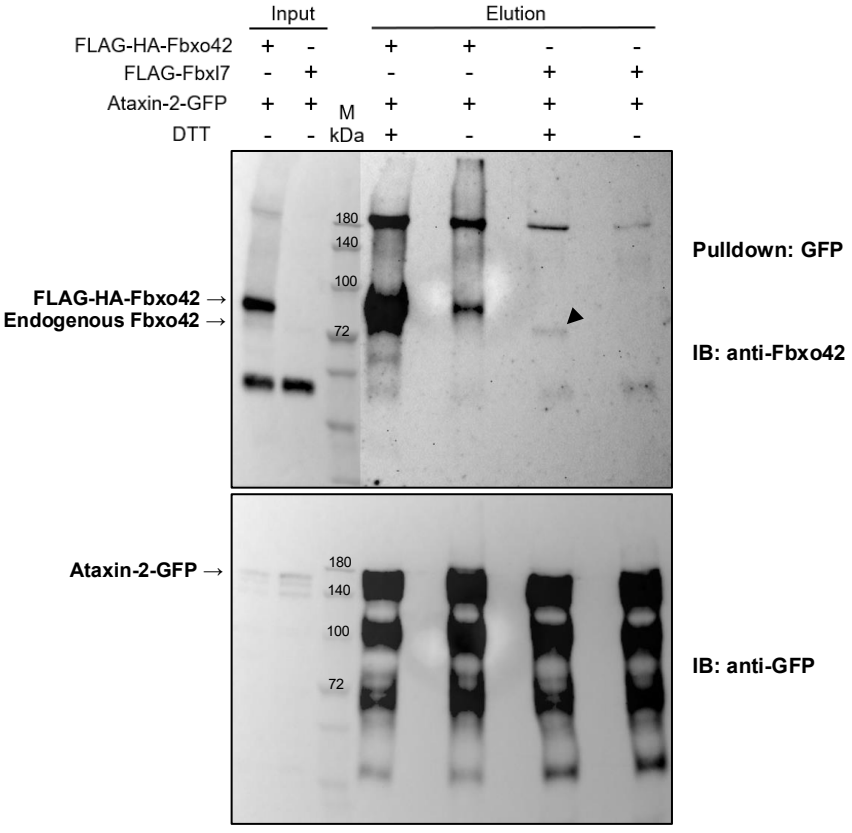

Figure 3.4: Fbxo42 co-immunoprecipitates with Ataxin-2-GFP in *Drosophila* eyes. Immunoblots probed with anti-Fbxo42 and anti-GFP

(Figure 3.4 continued):…antibodies, containing protein extracts of fly adult heads expressing FLAG-HA-Fbxo42 or FLAG-Fbxl7 together with Ataxin-2-GFP (under the control of the GMR-GAL4 driver and all in the presence of ^{bio}Ub), before/after GFP pulldown with anti-GFP beads. Elution was performed in the presence or absence of DTT. The arrows indicate the bands corresponding to the endogenous Fbxo42 (74.4 kDa), overexpressed FLAG-HA-Fbxo42 (80.7 kDa) and Ataxin-2-GFP (approximately 170 kDa). The black arrowhead indicates the band with size corresponding to the endogenous Fbxo42, detected in the elution (with DTT) of the Fbxl7 sample.

The immunoblots probed with anti-GFP and anti-Fbxo42 antibodies from protein extracts of fly heads overexpressing FLAG-HA-Fbxo42 or FLAG-Fbxl7 (control) together with Ataxin-2-GFP, before and after GFP pulldown (Figure 3.4), show that both endogenous (at 74.4 kDa) and overexpressed Fbxo42 (at 80.7 kDa) can co-immunoprecipitate with Ataxin-2-GFP (at approximately 170 kDa). These co-immunoprecipitation results are therefore consistent with those obtained using *Drosophila* S2 cells.

Fbxo42 localizes in close proximity to Ataxin-2 in the ring gland cells of *Drosophila* larvae, under ER stress conditions

To analyse whether Fbxo42 and Ataxin-2 co-localize, we carried out immunofluorescence assays. For these assays, we decided to use ring gland cells of *Drosophila* larvae. In the ring gland, the prothoracic cells are large, contain polytene chromosomes and exhibit endogenous activation of Ire1 signalling, which we confirmed by the expression of Xbp1s-GFP from a reporter of Ire1 activation, UAS-Xbp1-HA-GFP (Cairrão *et al.*, 2022) (Figure 3.5). As previously mentioned, the ring gland is responsible

for the production of ecdysone (in the prothoracic gland) and Juvenile hormone (in the corpus allatum) (Dubrovsky, 2005; Mirth *et al.*, 2005). These hormones control molting and growth throughout the development (Dubrovsky, 2005; Mirth *et al.*, 2005).

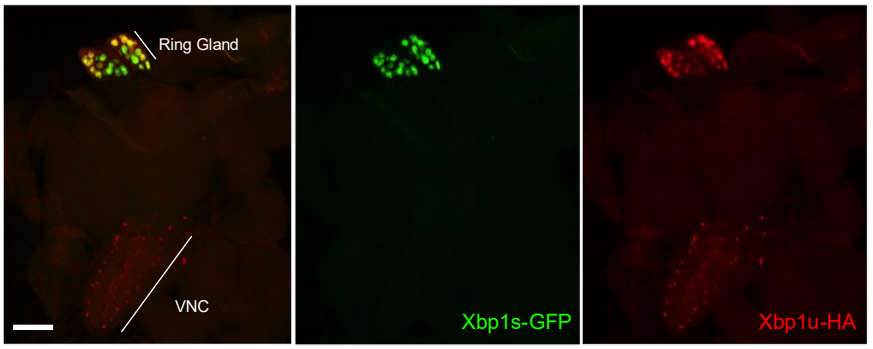

Figure 3.5: Immunofluorescence of ring gland (third instar larva), containing the attached brain/ventral nerve cord (VNC), expressing the XBP1-HA-GFP reporter under the control of phm-GAL4, a prothoracic gland driver. The expression of XBP1s-GFP (in green) is observed in the prothoracic gland cells, while the expression of XBP1u-HA (in red), detected with anti-HA, is observed in the prothoracic cells and some cells of the VNC. Scale bar = 100 µm.

Furthermore, the ring gland cells endogenously express Ataxin-2 and Fbxo42, and can be easily exposed to DTT, to induce high levels of ER stress and UPR activation. To investigate the co-localization between Ataxin-2 and Fbxo42 under ER stress conditions, we performed the immunostaining of the ring gland cells with anti-Ataxin-2 and anti-Fbxo42 antibodies, upon 5 mM DTT treatment for 4 hours. Untreated tissues were used as a control.

Through immunofluorescence of untreated ring gland cells, we were able to observe that Ataxin-2 and Fbxo42 exhibit mostly uniform expression, with little co-localization (Figure 3.6A, B). Notably, Fbxo42 presents higher expression levels in the corpus allatum compared to the rest of the ring gland tissue (Figure 3.6A). After 4 hours of DTT treatment, Ataxin-2 forms cytoplasmic granules, and Fbxo42 foci localize in close proximity, decorating the Ataxin-2 granules (Figure 3.6C, D). The number of granules containing Ataxin-2 only or Fbxo42-decorated Ataxin-2 granules was quantified and presented as percentages in a bar chart (Figure 3.6E). We observed that, in untreated ring glands, the granules predominantly contain Ataxin-2 (95.4% on average across two replicates) with a small percentage (4.6%) also containing Fbxo42 in their proximity. In contrast, for ring gland cells treated with 5 mM DTT for 4 hours, the opposite is observed. The percentage of Ataxin-2 granules decorated with Fbxo42 is significantly higher (96.3% on average across two replicates), while those containing only Ataxin-2 are much lower (3.7% on average across two replicates). These results indicate that Fbxo42 is recruited to Ataxin-2 granules upon induction of ER stress.

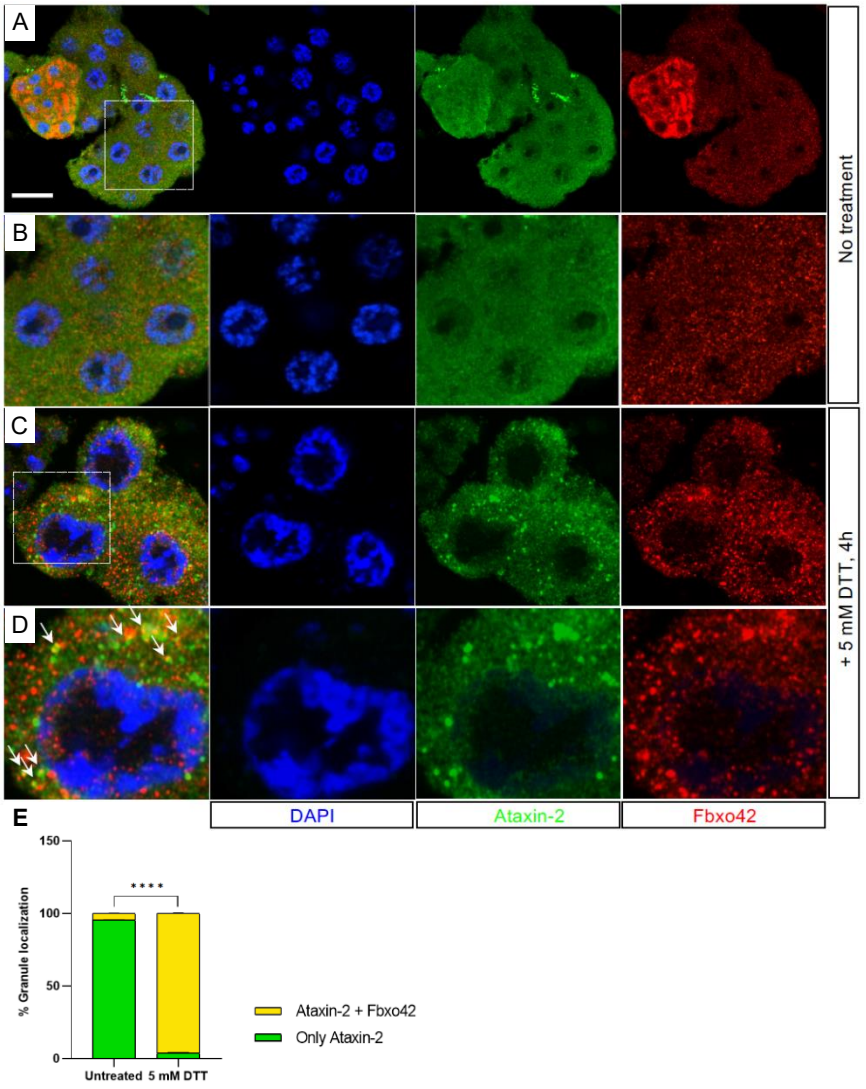

Figure 3.6: Immunofluorescences of ring gland cells (third instar larva) with anti-Ataxin-2 and anti-Fbxo42 antibodies. (A) Immunofluorescence of untreated ring gland cells, showing uniform staining of Ataxin-2 (in green) and Fbxo42 (in red). DAPI (in blue) labels the nucleus. Scale bar = 30 µm. **(B)** Inset of (A). **(C)** Immunofluorescence of ring gland cells after 5 mM DTT treatment for 4h, showing Ataxin-2 (in green) aggregates decorated with Fbxo42 (in red). **(D)** Inset of (C); white arrows indicate examples of Ataxin-2 granules decorated with Fbxo42. **(E)** Quantification of the number of granules containing Ataxin-2 only (green bar) or Fbxo42-decorated Ataxin-2 granules (yellow bar), present in

(Figure 3.6 continued):…untreated ring gland cells and in ring gland cells treated with 5 mM DTT for 4h. The quantification was performed in 2 biological replicates per condition, and is presented in percentage (%) as mean + SD. Two-way ANOVA coupled with Sidak' s multiple-comparison test, ****$p < 0.0001$ was performed. The number of granules scored in untreated ring glands was n=277 (replicate 1) and n=269 (replicate 2). The number of granules scored in ring gland cells treated with DTT was n=523 (replicate 1) and n=552 (replicate 2).

As an alternative method to induce the formation of Ataxin-2 granules in *Drosophila* cells, we used arsenite treatments, as previously described (Gareau *et al.*, 2013; Buddika *et al.*, 2020). Arsenite induces oxidative stress, leading to the activation of the kinase heme-regulated inhibitor (HRI), phosphorylation of eIF2α, inhibition of translation initiation and the formation of stress granules (Szczerba *et al.*, 2023). For this experiment, we treated ring gland cells of *Drosophila* larvae and ovaries of adult flies with 0.5 mM arsenite for 2 hours. Untreated tissues were used as control.

By immunofluorescence of the ring gland cells and adult ovaries with anti-Ataxin-2 and anti-Fbxo42 antibodies (Figure 3.7), we observed that, upon arsenite treatment, both ring gland cells and follicle cells of the ovary exhibit Fbxo42 foci decorating Ataxin-2 granules (Figure 3.7A, C). In contrast, untreated follicle cells (Figure 3.7B) show uniform expression of Ataxin-2 and some Fbxo42 foci. These results are consistent with those obtained with DTT treatment (shown previously in Figure 3.6), indicating that arsenite treatment can also induce the recruitment of Fbxo42 to Ataxin-2 granules.

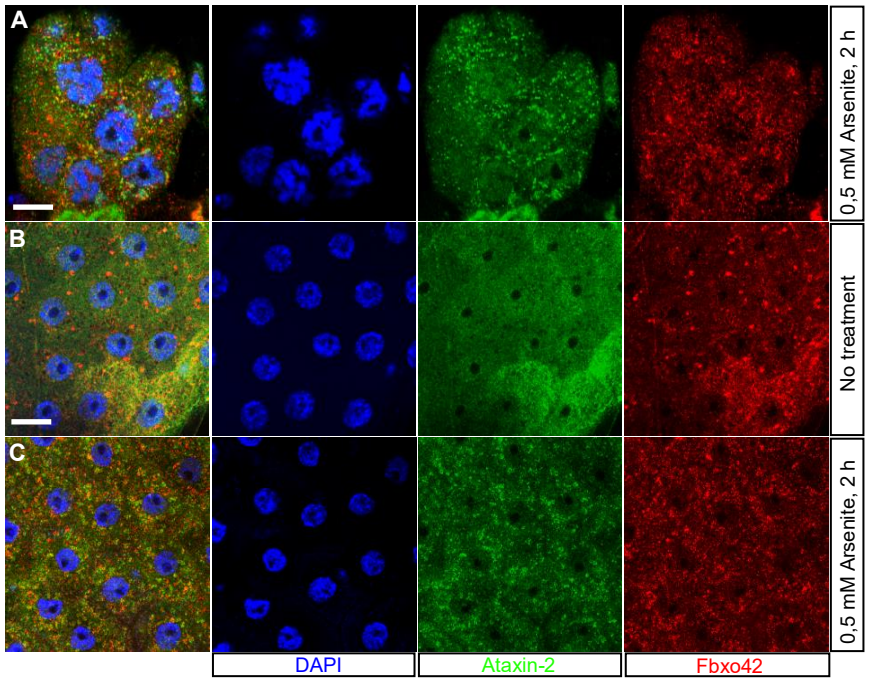

Figure 3.7: Immunofluorescence of ring gland cells (third instar larva) (A) and follicle cells (adult ovary) (B, C) using anti-Ataxin-2 and anti-Fbxo42 antibodies. (A) Immunofluorescence of ring gland cells after 0.5 mM arsenite treatment for 2 hours shows Ataxin-2 (green) granules decorated with Fbxo42 (red). Scale bar = 10µm. **(B)** Immunofluorescence of untreated follicle cells of the adult ovary showing uniform expression of Ataxin-2 (green) and foci with increased Fbxo42 (red). Scale bar = 10µm. **(C)** Immunofluorescence of follicle cells of the adult ovary after 0.5 mM arsenite treatment for 2 hours, presenting Ataxin-2 (green) granules decorated with Fbxo42 (red). DAPI is a marker for nuclei in A, B and C.

Analysis of Ataxin-2-GFP protein stability using cycloheximide (CHX) chase assays

As previously mentioned, F-box proteins mediate the ubiquitylation of target substrates, thereby regulating their activity or promoting their degradation. To investigate whether Fbxo42 promotes the degradation of Ataxin-2, we performed cycloheximide-chase assays using *Drosophila* S2 cells. Cycloheximide inhibits protein translation, allowing us to monitor protein degradation over time via immunoblotting. For the CHX-chase assays with S2 cells, we first determined the optimal concentration of CHX to use and the time required for Ataxin-2-GFP degradation. Our initial CHX-chase assays revealed that Ataxin-2 is a highly stable protein, with a turnover time of over 12 hours.

MG132, a proteosome inhibitor, increases the stability of Ataxin-2-GFP

We investigated the stability of Ataxin-2-GFP protein by immunoblotting after transfection of S2 cells with the Ataxin-2-GFP plasmid and treatment with 100 µg/ml CHX for 0, 6, and 12 hours. Additionally, to determine whether Ataxin-2-GFP was degraded by the proteasome, we treated the S2 cells with both CHX and MG132, a proteasome inhibitor. The immunoblot probed with anti-GFP (Figure 3.8A and quantification in Figure 3.8B) shows that proteasome inhibition led to a significant increase in the stability of the Ataxin-2-GFP protein compared to the control condition. This result suggests that Ataxin-2-GFP is degraded by the proteasome.

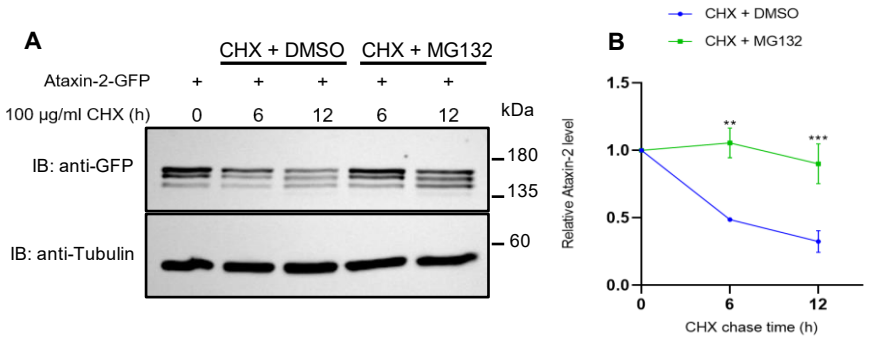

Figure 3.8: Analysis of Ataxin-2-GFP protein stability, in the presence or absence of the proteasome inhibitor MG132. (A) Immunoblot probed with anti-GFP antibody from protein extracts of S2 cells expressing Ataxin-2-GFP. S2 cells were treated with CHX to inhibit protein translation and protein extracts were "chased" at the indicated time points, in the presence or in the absence of the proteosome inhibitor MG132. Tubulin was used as loading control. **(B)** Quantification of the Ataxin-2-GFP (WT) protein levels from 3 independent experiments. Quantification for Ataxin-2-GFP is presented as mean + SEM. Two-way ANOVA coupled with Sidak's multiple-comparation test, $^{**}p < 0.01$ and $^{***}p < 0.001$.

Fbxo42 overexpression/depletion affects the stability of Ataxin-2-GFP

We then asked whether the expression levels of Fbxo42 affect the degradation of Ataxin-2-GFP by performing CHX-chase assays. For this, we transfected S2 cells with Ataxin-2-GFP and either overexpressed FLAG-HA-Fbxo42 or depleted Fbxo42 (using RNAi). S2 cells transfected with an empty vector or treated with LacZ RNAi were used as controls. After treatment with CHX for 0, 6 and 12 hours, cells were harvested for protein extraction. The stability of Ataxin-2-GFP was investigated by immunoblotting with anti-GFP. To analyse Fbxo42 protein levels, the immunoblots were also probed with anti-Fbxo42 antibody.

The immunoblots probed with anti-GFP show that overexpression of Fbxo42 promotes Ataxin-2-GFP degradation (Figure 3.9A and quantification in Figure 3.9B), while Fbxo42 RNAi depletion protects Ataxin-2-GFP from degradation (Figure 3.9C and quantification in Figure 3.9D).

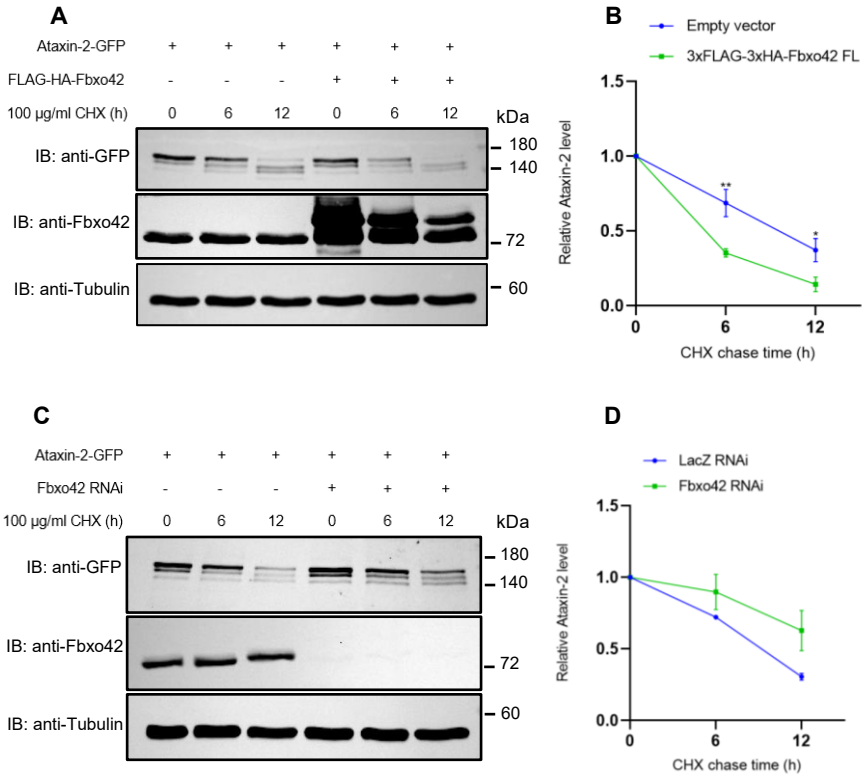

Figure 3.9: Analysis of Ataxin-2-GFP protein stability, upon Fbxo42 overexpression (A, B) or Fbxo42 RNAi depletion (C, D). (A) Immunoblots probed with anti-GFP, anti-Fbxo42 and anti-Tubulin antibodies from protein extracts of *Drosophila* S2 cells expressing Ataxin-2-GFP and FLAG-HA-Fbxo42 or Ataxin-2-GFP and empty vector negative control. S2 cells were treated with cycloheximide for 0, 6 and 12 hours, and protein extracts were "chased" at the indicated timepoints. Tubulin was used as loading control. **(B)** Quantification of Ataxin-2-GFP protein levels from (A) and two other independent experiments is presented as mean + SEM. Two-way ANOVA coupled with Sidak's multiple-comparation test, $*p < 0.05$ and $**p < 0.01$. **(C)** Immunoblots probed with anti-GFP, anti-Fbxo42

(Figure 3.9 continued):…and anti-Tubulin antibodies from protein extracts of *Drosophila* S2 cells expressing Ataxin-2-GFP and Fbxo42 RNAi or Ataxin-2-GFP and LacZ RNAi, used as negative control. S2 cells were treated with cycloheximide for 0,6 and 12 hours, and protein extracts were "chased" at the indicated timepoints. Tubulin was used as loading control. **(D)** Quantification of Ataxin-2-GFP protein levels from (C) and another independent experiment is presented as mean + SEM.

To confirm the results from the CHX-chase assays, we performed an immunofluorescence experiment using anti-Ataxin-2 antibody to investigate whether Ataxin-2 protein accumulates in Fbxo42 homozygous mutant cells. For this experiment, we used *Drosophila* third instar larval eye imaginal discs containing Su218/ubiGFP clones. In these mosaic eye discs, cells homozygous for Su218 – Fbxo42^{N423*} are labelled by the absence of green fluorescence, while Fbxo42 wild-type cells within the same tissue are labelled with GFP. These wild-type cells were used as control.

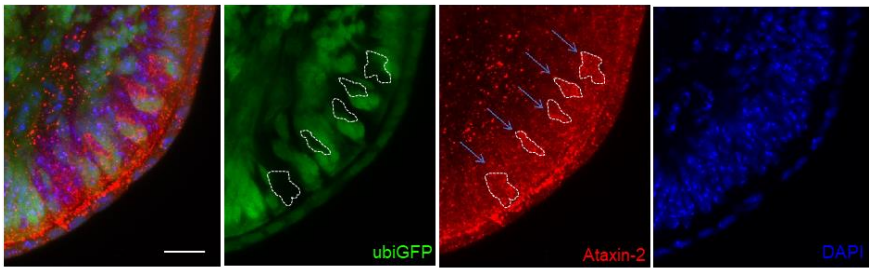

Figure 3.10: Immunofluorescence of *Drosophila* third instar larval eye imaginal discs containing Su218 (Fbxo42^{N423*})/ubiGFP clones. Fbxo42 mutant clones are labelled by the absence of ubiGFP (green). Endogenous Ataxin-2 is labelled by anti-Ataxin-2 antibody (red). DAPI (blue) is a marker for nuclei. Whole brain/eye disc tissues were exposed to 5 mM DTT for 4 hours, before fixation with paraformaldehyde. Genotype: eyFlp; FRT42D, Su218/ FRT42D, ubiGFP. Scale bar = 10 μm.

The immunofluorescence of eye imaginal discs containing Su218/ubiGFP clones with anti-Ataxin-2 (Figure 3.10), revealed

increased immunoreactivity for Ataxin-2 in Fbxo42 homozygous mutant cells (blue arrows in Figure 3.10). Interestingly, this result was observed only when the eye imaginal discs were treated with 5 mM DTT for 4 hours, to induce ER stress, and only in the cells located at the edge of the eye discs, presumably those exposed to higher amounts of DTT.

Fbxo42 ubiquitylates Ataxin-2-GFP on cysteine 244

So far, our results have shown that Fbxo42 ubiquitylates Ataxin-2, promoting its proteasomal degradation. Furthermore, the Ataxin-2/ubiquitin conjugates detected in ubiquitylation assays are DTT-sensitive (Chapter II of this thesis), suggesting that cysteine residues may be the sites of Fbxo42-mediated ubiquitylation. Therefore, to identify the cysteine residue(s) in Ataxin-2 that are ubiquitylated by Fbxo42, we mutagenized C103, C154 and C244 to alanine (A) in Ataxin-2-GFP and performed CHX-chase experiments with these mutants, using S2 cells. We then compared the stability of each mutant with that of wild-type Ataxin-2-GFP by immunoblotting.

The immunoblots probed with anti-GFP from protein extracts of S2 cells transfected with wild-type Ataxin-2-GFP or mutants Ataxin-2^{C103A}-GFP, Ataxin-2^{C154A}-GFP, and Ataxin-2^{C244A}-GFP, treated with CHX for 0, 6 and 12 hours (Figure 3.11A), show that the Ataxin-2^{C244A}-GFP mutant presents a significant increase in protein stability compared to wild-type Ataxin-2-GFP (Figure 3.11A, B). In contrast, Ataxin-2^{C103A}-GFP and Ataxin-2^{C154A}-GFP present protein degradation profiles similar to the wild-type protein (Figure 3.11A, B).

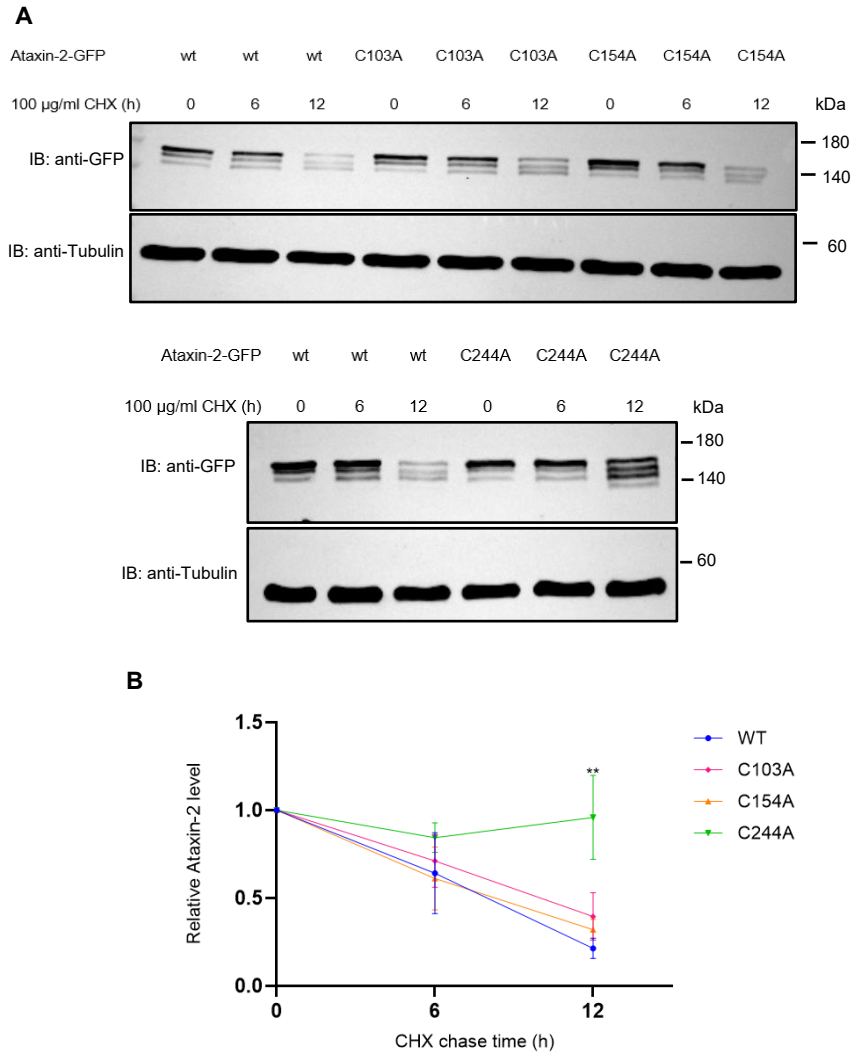

Figure 3.11: Analysis of the protein stability of wild-type Ataxin-2-GFP and its cysteine mutants. (A) Immunoblots probed with anti-GFP and anti-Tubulin from protein extracts of *Drosophila* S2 cells expressing Ataxin-2-GFP (wt, blue), Ataxin-2^{C103A}-GFP (pink), Ataxin-2^{C154A}-GFP (orange) or Ataxin-2^{C244A}-GFP (green). S2 cells were treated with CHX to inhibit protein translation, and protein extracts were "chased" at the indicated timepoints. Tubulin was used as loading control. **(B)** Quantification of Ataxin-2-GFP (wt) and cysteine mutants from (A) and two other independent experiments is presented as mean + SEM. Two-way ANOVA coupled with Sidak's multiple-comparation test, $^{**}p < 0.01$.

Ataxin-2^{C244A}-GFP does not present DTT-sensitive Ataxin-2-GFP/ubiquitin conjugates

To further confirm that cysteine 244 of Ataxin-2 is the ubiquitylation site for the Fbxo42 protein, we performed an ubiquitylation assay. For this experiment, we transfected S2 cells with wild-type Ataxin-2-GFP or mutant Ataxin-2^{C244A}-GFP, along with a plasmid containing His-myc-ubiquitin. We then performed a histidine pulldown to capture the ubiquitylated Ataxin-2. Elution was carried out in the presence or absence of DTT. By immunoblotting with anti-GFP and anti-myc antibodies (Figure 3.12), we observe that, in contrast to wild-type Ataxin-2-GFP, Ataxin-2^{C244A}-GFP does not present DTT-sensitive Ataxin-2-GFP/Ubiquitin conjugates in the elution fraction. Therefore, these results, together with the CHX-chase data demonstrate that Fbxo42 ubiquitylates Ataxin-2 at cysteine 244.

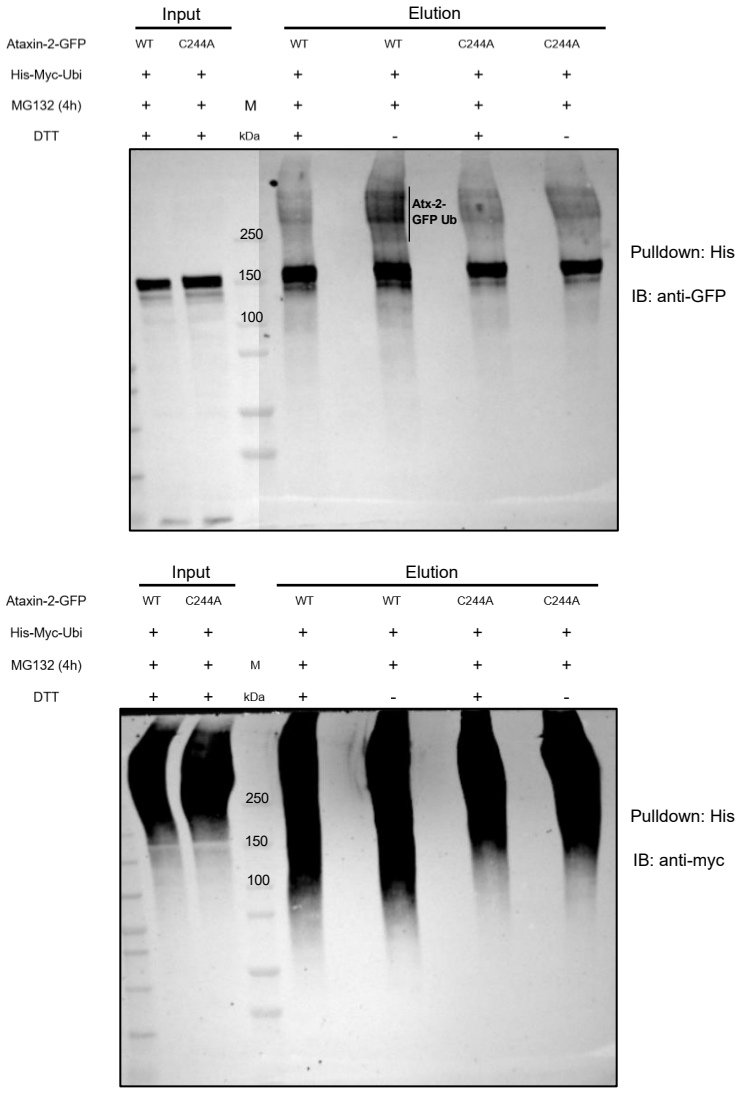

Figure 3.12: Ataxin-2^{C244A}-GFP does not present Ataxin-2-GFP/ubiquitin conjugates. Immunoblot of protein extracts from S2 cells expressing wild-type Ataxin-2-GFP or mutant Ataxin-2^{C244A}-GFP, together with His-myc-ubiquitin. S2 cells were subjected to histidine pulldown and immunoblots with anti-GFP (top panel) or anti-myc (bottom panel). DTT sensitive His-myc-Ub conjugates (black vertical line) are detected for wild-type Ataxin-2-GFP, but not for Ataxin-2^{C244A}-GFP.

AlphaFold prediction of the Ataxin-2/Fbxo42/Cullin-1/Skp-1/Rbx1/E2/Ub complex

To obtain a structure for the Fbxo42/Cul1/Skp1/E2/Ub complex together with Ataxin-2, and to determine the spatial location of the Cys244 of Ataxin-2 as well as its proximity to the E2-ubiquitin conjugating enzyme and ubiquitin, we used AlphaFold-3. This AlphaFold structural prediction was made by Tiago Cordeiro.

In the AlphaFold-3 (Abramson *et al.*, 2024) prediction showing the LSM and LSM-AD domains (aa 62 to 269) of Ataxin-2 together with the Fbxo42/Cullin-1/Skp-1/Rbx/E2/Ub complex (Figure 3.13), we can observe that Cys244 of Ataxin-2 is located in the vicinity of the reactive C-terminus of ubiquitin (Gly76) and the catalytic Cys85 of the E2-ubiquitin conjugating enzyme, Effete.

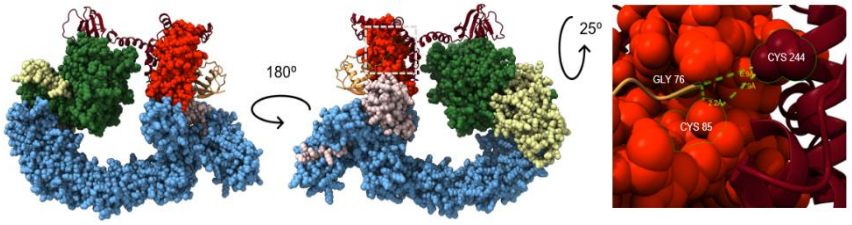

Figure 3.13: AlphaFold-3 prediction of the Ataxin-2/Fbxo42/Cullin-1/Skp-1/Rbx1/E2/Ub complex. This complex contains the LSM and LSM-AD domains (N57 to Q270) of Ataxin-2 (oxblood) together with Fbxo42 (green), Skp-1 (yellow), Cullin-1 (light blue), Rbx1 (light pink), E2 (Effete, red) and ubiquitin (orange). All proteins are represented as spheres except for Ataxin-2 and ubiquitin that are in ribbon view. The right panel is a zoom in the region highlighted by the dashed grey rectangle, with a green highlight in Cys 244 of Ataxin-2, the catalytic Cys 85 of the E2 (Effete) and the reactive C-terminus of Ub (Gly 76).

Additionally, the ribbon view of the Ataxin-2/Fbxo42/Cullin-1/Skp-1/Rbx1/E2/Ub complex (Figure 3.14A) and its confidence values are shown (Figure 3.14B).

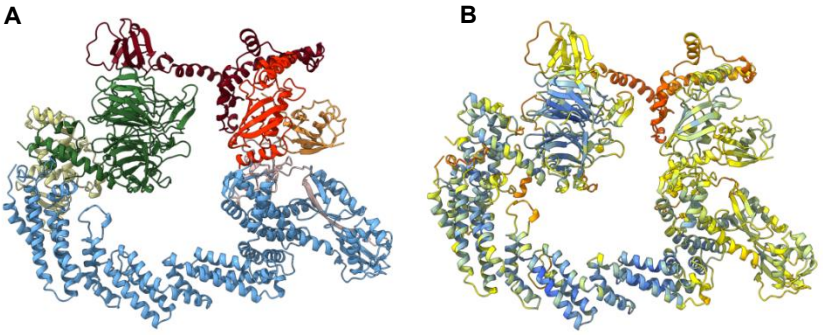

Figure 3.14: AlphaFold-3 prediction of the Ataxin-2/Fbxo42/Cullin-1/Skp-1/Rbx1/E2/Ub complex with the corresponding confidence values. (A) Ribbon view of the AlphaFold-3 prediction for Ataxin-2/Fbxo42/Cul1/Skp-1/Rbx1/E2/Ub complex, containing the LSM and LSM-AD domains (N57 to Q270) of Ataxin-2 (oxblood) together with Fbxo42 (green), Skp-1 (yellow), Cullin-1 (light blue), Rbx1 (light pink), E2 (Effete, red) and ubiquitin (orange), as in Figure 3.15. **(B)** Confidence values (pLDDT – Local Distance Difference Test) corresponding to the complex displayed in (A). pLDDT values are colour-coded on a scale from 0 to 100. Dark blue, pLDDT>90; light blue, 90>pLDDT>70; yellow, 70>pLDDT>50 and orange, pLDDT<50.

Thus, the AlphaFold-3 prediction of the Ataxin-2/Fbxo42/Cullin-1/Skp-1/Rbx1/E2/Ub complex supports the CHX-chase and ubiquitylation results for the Ataxin-2^{C244A}-GFP mutant, indicating that Fbxo42 promotes the proteasomal degradation of Ataxin-2 by mediating the ubiquitylation of cysteine 244.

3.5 Discussion

By mass spectrometry, we identified the RNA-binding protein Ataxin-2 as a substrate of Fbxo42. To confirm the interaction between Fbxo42 and Ataxin-2, we performed co-immunoprecipitation assays, using S2 cells and fly head extracts. Through these experiments, we observed that endogenous Fbxo42 co-immunoprecipitates with Ataxin-2-GFP in S2 cells. Additionally, using fly head extracts, we observed co-immunoprecipitation of both endogenous and overexpressed Fbxo42 with Ataxin-2-GFP, further confirming that Fbxo42 interacts with Ataxin-2. To investigate the intracellular localization and interaction between these two proteins, we performed several immunofluorescence experiments with anti-Ataxin-2 and anti-Fbxo42 antibodies, using ring gland cells of larvae and follicle cells of the adult ovary. In untreated ring gland cells, we observed that Ataxin-2 and Fbxo42 exhibited mostly uniform expression, with little co-localization. In contrast, upon DTT treatment of the ring gland cells, to induce ER stress and UPR activation, we observed the formation of cytoplasmic Ataxin-2 granules. These granules were located in close proximity to Fbxo42 foci, suggesting that these two proteins interact. Our results suggest that Fbxo42 is not part of the Ataxin-2 granules, but instead is recruited to these granules during UPR activation.

Furthermore, Ataxin-2 granules decorated by Fbxo42, were also detected upon arsenite treatment (to induce oxidative stress) of ring gland cells and adult ovaries. This indicates that, the recruitment of Fbxo42 to Ataxin-2 granules is not an exclusive of the induction of ER stress by DTT treatment. Previous reports have demonstrated that both DTT and arsenite treatments induce the

formation of stress granules (Zhang *et al.*, 2018; Child *et al.*, 2021). In addition, Ataxin-2 is a core component of stress granules, as previously mentioned. However, in this report, we refer to the granules containing Ataxin-2 as “Ataxin-2 granules”, since we did not explore the presence of other stress granule-associated proteins. Moreover, to the best of our knowledge, this is the first report of Ataxin-2-containing granules detected in the ring gland cells.

Regarding the ubiquitylation of Ataxin-2 mediated by Fbxo42, we previously demonstrated (Chapter II), through ubiquitylation assays, that Fbxo42 induces the formation of Ataxin-2/ubiquitin conjugates. However, this result was only evident after removing DTT from the elution buffer, indicating that Fbxo42-mediated ubiquitylation of Ataxin-2 is linked to cysteine residues. Ubiquitin molecules attached to cysteine residues of substrates via thioester bonds are sensitive to reducing agents like DTT. This type of ubiquitylation, known as “non-canonical”, contrasts with the canonical ubiquitylation form, where ubiquitin is attached to lysine residues on substrate through the formation of amide bonds. Thioester bonds, although more labile and thermodynamically less stable than amide bonds, are formed more rapidly (Kelsall, 2022). This makes them ideal for processes requiring quick transient modifications, such as the ubiquitin transfer, observed in the ubiquitylation cascade from E1 to E3 enzymes. Interestingly, evidence suggests that protein structure can stabilize thioesters, with the half-life of a thioester-linked model calculated to be several hours (Song *et al.*, 2009; Kelsall, 2022). Thus, thioester bonds may not be as labile as previously though, and this type of ubiquitylation

can provide a quicker response for rapid signalling events. Previous reports have highlighted the importance of cysteine ubiquitylation in different cellular contexts, including peroxisomal protein translocation (Carvalho *et al.*, 2007; Williams *et al.*, 2007), lipid metabolism (Wang *et al.*, 2017; Zhou *et al.*, 2020) and transcriptional regulation of the cell fate (Vosper *et al.*, 2009; McDowell & Philpott, 2013). Moreover, mono-ubiquitylation of cysteine residues on substrates has been associated with proteasomal degradation. For instance, Insign-2, an ER membrane protein that functions as a negative regulator of lipid synthesis is ubiquitylated on a cysteine residue and subsequently degraded (Zhou *et al.*, 2020).

Our next goal was to determine whether Fbxo42-mediated ubiquitylation of Ataxin-2 resulted in its regulation or degradation. To investigate this, we performed cycloheximide-chase assays, using S2 cells. These experiments showed that Ataxin-2 is a highly stable protein with a turnover time of more than 12 hours. By immunoblotting, we observed that the overexpression of Fbxo42 leads to faster degradation of Ataxin-2, while Fbxo42 RNAi depletion protects Ataxin-2 from degradation. Immunofluorescence assays further confirmed these results, revealing an accumulation of Ataxin-2 in Fbxo42 homozygous mutant cells of eye imaginal discs. Additionally, treating S2 cells with both cycloheximide and the proteosome inhibitor MG132 stabilized Ataxin-2. Taken together, these results demonstrate that Fbxo42 promotes the proteasomal degradation of the Ataxin-2 protein.

We also aimed to identify the cysteine residue(s) in Ataxin-2 that are ubiquitylated by Fbxo42. In order to do this, we

mutagenized C103, C154 and C244 to alanine, and performed CHX-chase experiments. Using this approach, we found that the C244A mutation increased the stability of the Ataxin-2 protein. To assess the effect of C244A on the Ataxin-2 ubiquitylation profile, we performed an ubiquitylation assay. This revealed that Ataxin-2^{C244A}-GFP did not present DTT-sensitive Ataxin-2-GFP/ubiquitin conjugates, indicating that Fbxo42 mediates the ubiquitylation of Ataxin-2 at cysteine 244. This residue is located within the conserved LSM-AD domain of Ataxin-2, suggesting that it may influence Ataxin-2's interaction with target RNAs.

To obtain a structural prediction for the Ataxin-2/Fbxo42/Cullin-1/Skp-1/Rbx1/E2/Ub complex, we used AlfaFold-3. Through this prediction, we were able to see that cysteine 244 of Ataxin-2 is located in the vicinity of the C-terminus of Gly76 of ubiquitin and in close proximity to the catalytic cysteine of the E2 enzyme. This structural prediction further supported our CHX-chase and ubiquitylation results.

In conclusion, we found that Fbxo42 mediates the proteasomal degradation of Ataxin-2 via cysteine ubiquitylation. Furthermore, our results show that during UPR activation, Fbxo42 is recruited to Ataxin-2 granules, to mediate the ubiquitylation and degradation of Ataxin-2, ultimately leading to the degradation of these granules.

In the future, it will be worthwhile to investigate whether Fbxo42 can promote the ubiquitylation and degradation of pathogenic forms of Ataxin-2 (containing polyQ expansions, involved in SCA2, ALS or Parkinson's disease). Additionally, it would

be valuable to study whether human ATXN2 is a substrate of human FBXO42.

3.6 Acknowledgments

I would like to thank Tiago Cordeiro for performing the AlphaFold structural prediction of the Ataxin-2/Fbxo42/Cullin-1/Skp-1/Rbx1/E2/Ub complex. Figures 3.15 and 3.16 were created by Tiago Cordeiro. I am grateful to Pedro Domingos for performing experiments and acquiring Figure 3.8, and for supervising this work. I also express my gratitude to Hyung Don Ryoo for providing fly reagents and the pUAST-His-myc-Ub plasmid. Finally, I would like to thank Patrick Emery for providing the anti-Ataxin-2 antibody used in this study.

3.7 References

Abramson J et al. (2024). Accurate structure prediction of biomolecular interactions with AlphaFold 3. *Nature* **630,** 493–500.

Buddika K, Ariyapala IS, Hazuga MA, Riffert D & Sokol NS (2020). Canonical nucleators are dispensable for stress granule assembly in Drosophila intestinal progenitors. *J Cell Sci*; DOI: 10.1242/jcs.243451.

Cairrão F, Santos CC, Le Thomas A, Marsters S, Ashkenazi A & Domingos PM (2022). Pumilio protects Xbp1 mRNA from regulated Ire1-dependent decay. *Nat Commun* **13,** 1–13.

Carvalho AF, Pinto MP, Grou CP, Alencastre IS, Fransen M, Sá-Miranda C & Azevedo JE (2007). Ubiquitination of mammalian Pex5p, the peroxisomal import receptor. *J Biol Chem* **282,** 31267–31272.

Child JR, Chen Q, Reid DW, Jagannathan S & Nicchitta C V. (2021). Recruitment of endoplasmic reticulum-targeted and cytosolic mRNAs into membrane-associated stress granules. *Rna* **27,** 1241–1256.

Clemens JC, Worby CA, Simonson-Leff N, Muda M, Maehama T, Hemmings BA & Dixon JE (2000). Use of double-stranded RNA interference in Drosophila cell lines to dissect signal transduction pathways. *Proc Natl Acad Sci U S A* **97,** 6499–6503.

Dubrovsky EB (2005). Hormonal cross talk in insect development. *Trends Endocrinol Metab* **16,** 6–11.

Emenecker RJ, Griffith D & Holehouse AS (2021). Metapredict: a fast, accurate, and easy-to-use predictor of consensus disorder and structure. *Biophys J* **120,** 4312–4319.

Emenecker RJ, Griffith D & Holehouse AS (2022). Metapredict V2: An update to metapredict, a fast, accurate, and easy-to-use predictor of consensus disorder and structure. *bioRxiv*; DOI: https://doi.org/10.1101/2022.06.06.494887.

Gareau C, Houssin E, Martel D, Coudert L, Mellaoui S, Huot ME, Laprise P & Mazroui R (2013). Characterization of Fragile X Mental Retardation Protein Recruitment and Dynamics in Drosophila Stress Granules. *PLoS One*; DOI: 10.1371/journal.pone.0055342.

Harvie PD, Filippova M & Bryant PJ (1998). Genes expressed in the ring gland, the major endocrine organ of Drosophila melanogaster. *Genetics* **149,** 217–231.

Hinnant TD, Merkle JA & Ables ET (2020). Coordinating Proliferation, Polarity, and Cell Fate in the Drosophila Female Germline. *Front Cell Dev Biol* **8,** 1–22.

Kelsall IR (2022). Non-lysine ubiquitylation: Doing things differently. *Front Mol Biosci* **9,** 1–28.

McDowell GS & Philpott A (2013). Non-canonical ubiquitylation: Mechanisms and consequences. *Int J Biochem Cell Biol* **45,** 1833–1842.

Meng EC, Goddard TD, Pettersen EF, Couch GS, Pearson ZJ, Morris JH & Ferrin TE (2023). UCSF ChimeraX: Tools for structure building and analysis. *Protein Sci* **32,** 1–13.

Mirth C, Truman JW & Riddiford LM (2005). The role of the prothoracic gland in determining critical weight for metamorphosis in Drosophila melanogaster. *Curr Biol* **15,** 1796–1807.

Setiawan L, Pan X, Woods AL, O'Connor MB & Hariharan IK (2018). The BMP2/4 ortholog dpp can function as an inter-organ signal that regulates developmental timing. *Life Sci Alliance* **1,** 1–17.

Song J, Wang J, Jozwiak AA, Hu W, Swiderski PM & Chen Y (2009).

Stability of thioester intermediates in ubiquitin-like modifications. *Protein Sci* **18,** 2492–2499.

Szczerba M, Johnson B, Acciai F, Gogerty C, McCaughan M, Williams J, Kibler K V. & Jacobs BL (2023). Canonical cellular stress granules are required for arsenite-induced necroptosis mediated by Z-DNA-binding protein 1. *Sci Signal*; DOI: 10.1126/scisignal.abq0837.

De Velasco B, Shen J, Go S & Hartenstein V (2004). Embryonic development of the Drosophila corpus cardiacum, a neuroendocrine gland with similarity to the vertebrate pituitary, is controlled by sine oculis and glass. *Dev Biol* **274,** 280–294.

Vosper JMD, McDowell GS, Hindley CJ, Fiore-Heriche CS, Kucerova R, Horan I & Philpott A (2009). Ubiquitylation on canonical and non-canonical sites targets the transciption factor neurogenin for ubiquitin-mediated proteolysis. *J Biol Chem* **284,** 15458–15468.

Wang YJ, Bian Y, Luo J, Lu M, Xiong Y, Guo SY, Yin HY, Lin X, Li Q, Chang CCY, Chang TY, Li BL & Song BL (2017). Cholesterol and fatty acids regulate cysteine ubiquitylation of ACAT2 through competitive oxidation. *Nat Cell Biol* **19,** 808–819.

Williams C, Van Den Berg M, Sprenger RR & Distel B (2007). A conserved cysteine is essential for Pex4p-dependent ubiquitination of the peroxisomal import receptor Pex5p. *J Biol Chem* **282,** 22534–22543.

Xu F, Suyama R, Inada T, Kawaguchi S & Kai T (2024). HemK2 functions for sufficient protein synthesis and RNA stability through eRF1 methylation during Drosophila oogenesis. *Dev*; DOI: 10.1242/dev.202795.

Zhang K, Daigle JG, Cunningham KM, Coyne AN, Ruan K, Grima JC, Bowen KE, Wadhwa H, Yang P, Rigo F, Taylor JP, Gitler AD, Rothstein JD & Lloyd TE (2018). Stress Granule Assembly Disrupts Nucleocytoplasmic Transport. *Cell* **173,** 958-971.e17.

Zhang Y, Ling J, Yuan C, Dubruille R & Emery P (2013). A role for Drosophila ATX2 in activation of PER translation and circadian behavior. *Science (80-)* **340,** 879–882.

Zhou Z Sen, Li MX, Liu J, Jiao H, Xia JM, Shi XJ, Zhao H, Chu L, Liu J, Qi W, Luo J & Song BL (2020). Competitive oxidation and ubiquitylation on the evolutionarily conserved cysteine confer tissue-specific stabilization of Insig-2. *Nat Commun*; DOI: 10.1038/s41467-019-14231-w.

CHAPTER IV

Ataxin-2 stabilizes Xbp1 mRNA and protects it from degradation under ER stress conditions

---

Authors: Santos CC, Cairrão F, Yang M, Hensel Z, Voigt F, Gameiro PA and Domingos PM.

4.1 Abstract

In this Chapter, we investigate the regulatory link between Ataxin-2 and Xbp1 mRNA. To determine whether Ataxin-2 interacts with Xbp1 mRNA, we employed a combination of immunofluorescence and smFISH in ring gland cells of *Drosophila* third instar larvae. Using this method, we observed that, upon ER stress induction, Xbp1 mRNA co-localizes with cytoplasmic Ataxin-2 granules, suggesting that Ataxin-2 binds to Xbp1 mRNA. Furthermore, this result was also observed in human HeLa cells, where human Xbp1 mRNA accumulates in Ataxin-2 granules.

In order to confirm the binding between *Drosophila* Ataxin-2 and Xbp1 mRNA and to identify the Ataxin-2 binding sites on Xbp1 mRNA, we performed iCLIP experiments. The iCLIP results showed that Ataxin-2 binds to Xbp1 mRNA, in particular to its 3' UTR.

Additionally, we assessed the effect of Ataxin-2 protein on Xbp1 mRNA stability and translation during UPR activation, demonstrating that Ataxin-2 depletion reduces the stability of a Xbp1 reporter mRNA and decreases Xbp1s protein expression.

Finally, we examined the impact of Fbxo42 protein on Xbp1 mRNA translation, during UPR activation, showing that knockdown of Fbxo42 leads to a reduction in Xbp1s protein levels.

Overall, our results suggest that during UPR activation, Ataxin-2 binds to Xbp1 mRNA within cytoplasmic Ataxin-2 granules, promoting its stabilization and preventing its degradation. Importantly, the Fbxo42 protein is required for Xbp1 mRNA translation.

4.2 Introduction

We have shown that Ataxin-2 plays an important role in the context of the "glossy" eye phenotype, as RNAi depletion of Ataxin-2 abolished the rescue by Fbxo42 loss-of-function mutations. The last part of this work focused on determining the role of Ataxin-2 protein in the regulation of Xbp1 mRNA stability and translation.

As previously mentioned, Ataxin-2 is an RNA-binding protein (RBP), that plays different roles in mRNA metabolism, including mRNA stability, splicing and decay. Moreover, Ataxin-2 is also involved in translation.

Often RNA-binding proteins bind to the 3' UTR of target mRNAs to enhance mRNA stability and protein abundance, while micro-RNAs bind to this region to repress translation or promote degradation (Barreau *et al.*, 2005; Yokoshi *et al.*, 2014). Yokoshi and collaborators have shown that human Ataxin-2 (ATXN2) stabilizes target mRNAs that contain U-rich elements, including AU-rich elements (AREs) present in 3'UTR of target mRNAs, increasing the abundance of the corresponding proteins. These authors showed that depletion of ATXN2 in HEK293T reduced the stability of target mRNAs, whereas its overexpression increased the levels of target mRNAs. Depending on the mRNA stability, the protein expression was decreased or increased, respectively (Yokoshi *et al.*, 2014). Consistent with these results, a study from Singh and collaborators, using S2 cells and fly brains, demonstrated that *Drosophila* Ataxin-2 (Atx-2) preferentially associates with the 3'UTR of target mRNAs, particularly to AU-rich sequences. Knockdown of Atx-2 in *Drosophila* brain and S2 cells resulted in a reduction of a large fraction of Atx-2 target mRNAs. Their results suggested that Atx-2 directly or

indirectly associates with AREs to protect mRNAs from degradation (Singh *et al.*, 2021).

ER stress and UPR activation

As previously mentioned, the accumulation of misfolded or unfolded proteins in the ER causes ER stress and activates UPR to restore homeostasis in the ER (Walter & Ron, 2011). Upon ER stress, the transmembrane ER stress sensor IRE1 is activated, and its endoribonuclease domain cleaves the Xbp1 mRNA in two sites, an unconventional splicing event that causes a frameshift during translation, introducing a longer carboxyl domain in the protein encoded by Xbp1s mRNA (Walter & Ron, 2011). Xbp1s in an effective transcription factor, and it translocates to the nucleus where induces the transcription of UPR-target genes encoding proteins involved in protein folding, quality control and ERAD (Walter & Ron, 2011; Woehlbier & Hetz, 2011).

UPR activation alleviates the burden of unfolded proteins through pro-survival mechanisms, facilitating the cellular adaptation and recovery from stress. This adaptive response consists of two phases: early and late UPR. The first phase is an immediate response aimed at reducing the load of unfolded proteins in the ER (early UPR). During this phase PERK is activated and inhibits overall protein synthesis by phosphorylating eIF2α. In addition, IRE1 controls the degradation of mRNAs encoding ER-localized proteins in a process termed as RIDD (Regulated IRE1-dependent decay) (Hollien & Weissman, 2006). Furthermore, ER stress can induce autophagy during this phase (Woehlbier & Hetz, 2011; Liu *et al.*, 2024).

A second phase of the adaptive UPR mechanism (late UPR) involves the expression of transcription factors and subsequent de novo mRNA and protein synthesis, which increases the folding and control capacity of the ER. In this phase each UPR sensor activates a transcription factor (XBP1s, ATF6f and ATF4) and upregulates specific UPR-target genes (Woehlbier & Hetz, 2011; Liu *et al.*, 2024).

Regarding Xbp1, a report by Mithu Majumder and collaborators suggested that Xbp1s mRNA is stabilized during the early UPR, when translation is inhibited, allowing it to be translated once the inhibition is relieved, as part of the late ER stress response (Majumder *et al.*, 2012).

Activation of the UPR by ER stress conditions aims to re-establish homeostasis and normal ER function. However, if stress is too severe or prolonged, leading to “chronic” activation of the UPR, cells may trigger apoptosis (Rasheva & Domingos, 2009; Tabas & Ron, 2011). The mechanisms underlying the transition from adaptive to pro-apoptotic events are still poorly understood (Woehlbier & Hetz, 2011).

In this Chapter, our specific goals are as follows:

- Investigate the interaction between Ataxin-2 protein and Xbp1 mRNA using immunofluorescence and smFISH experiments.
- Identify the Ataxin-2 binding sites on XBP1 mRNA, through iCLIP experiments.
- Assess the effect of Ataxin-2 depletion on Xbp1 mRNA stability, using actinomycin D assays.

- Evaluate the effect of Ataxin-2 depletion on Xbp1 mRNA translation.

4.3 Methods

Sequential Immunofluorescence and single molecule RNA fluorescence in situ hybridization (smFISH)

Single molecule RNA fluorescence in situ hybridization was performed with custom Stellaris RNA FISH probes labelled with Quasar 670 dye (LGC Biosearch Technologies) targeting the Xbp1 mRNA.

Sequential IF and smFISH was performed according to LGC Biosearch Technologies' recommendations. Briefly, larvae were dissected in 1× PBS and fixed in 4% PFA in 1× PBS for 1 hour at room temperature. Tissues were then rinsed twice, 10 minutes each in 1× PBS followed by two washes in 0.1% Triton X-100. Subsequently, larval tissues were washed with 1× PBS and incubated with primary antibodies diluted in 1× PBS, overnight at 4°C with gentle agitation. Primary antibodies used were the following: mouse anti-ELAV (1:200) (cat. no. 9F8A9, DSHB) and guinea-pig anti-Ataxin-2 (1:200, a kind gift from Patrick Emery).

After overnight incubation with primary antibodies, tissues were washed three times with 1× PBS and incubated with appropriate secondary antibodies (Jackson ImmunoResearch Laboratories) diluted in 1× PBS for 2 hours at room temperature. Then, tissues were washed three times with 1× PBS, 10 minutes

each, and incubated with freshly prepared Wash Buffer A, containing 1× Stellaris RNA FISH Wash Buffer A (cat. no. SMF-WA1-60, LGC Biosearch Technologies) and 10% (v/v) formamide (F9037, Sigma-Aldrich) in RNase free water, for 10 minutes at room temperature. Afterwards, samples were transferred to a 96-well plate and Wash Buffer A was discarded and replaced by freshly prepared Hybridization buffer [Stellaris RNA FISH Hybridization Buffer (cat. no. SMF-HB1-10, LGC Biosearch Technologies) + 10% (v/v) formamide] containing the Xbp1 probe set. Xbp1 probe stock (12.5 μM) was diluted 1:100 in Hybridization buffer to create a working probe solution of 125 nM. Larval tissues were incubated with Xbp1 probe solution in the dark at 37°C, overnight.

The following day, Xbp1 probe solution was discarded, and unbound probes were removed by incubation with Wash Buffer A in the dark at 37°C for 30 minutes. Tissues were mounted in VECTASHIELD® Antifade Mounting Medium with DAPI (Vector Laboratories, H-1200-10) and image acquisition was performed on a Zeiss LSM 880 confocal microscope.

Where indicated, the larval anterior parts' (containing the ring glands and eye imaginal discs) were exposed to 5 mM DTT for 4 hours. Untreated tissues were used as control.

The confocal images were analysed using the Fiji software and the ZEN Imaging Software (Zeiss). The number of granules and their components were quantified manually.

Single-molecule fluorescence in situ hybridization and immunofluorescence (smFISH-IF) in HeLa cells

The combined smFISH-IF experiments in HeLa cells were conducted as previously described (Gómez-Puerta *et al.*, 2022). Briefly, HeLa 11ht cells in 1 mL culture medium [89% DMEM (Gibco), 10% (v/v) FBS (Gibco) and 1% penicillin-streptomycin (Gibco)] were cultured in a 12-well plate (Greiner) at 37°C with 5% CO_2. At 90% confluency, cells were either incubated with 1μM thapsigargin-treated (TG, Alomone) or untreated culture medium for 3 h. Cells were then washed twice with PBS and fixed with 4% PFA (Electron Microscopy Sciences) for 10 min at room temperature (RT), followed by permeabilization with 0.2% Triton-X for another 10 min. Afterwards, a wash buffer [2 × SSC (Invitrogen) and 30% v/v deionized formamide (Ambion)] containing 3% (w/v) BSA (Sigma) was used to pre-block cells for 30 min at RT. FISH probes targeting human XBP1 mRNA (table S3) were designed using the anglerFISH probe designer and were made by enzymatic oligonucleotide labelling using Atto565-NHS as described before (Piskadlo et al 2022). Cells were first hybridized with hybridization buffer [150 nM smFISH probes, 2 × SSC, 30% v/v formamide, 10% w/v dextran sulphate (Sigma)] for 4 h at 37 °C. Following three washes with wash buffer for 30 min, cells were incubated with primary antibody against human Ataxin-2 (Proteintech, 1776-1-AP, 1: 300) at RT for 4 h. After two washes with PBS containing 0.1% (v/v) Tween (Promega) for 30 min, the anti-rabbit IgG secondary antibody conjugated with ATTO 488 (Rockland, 611-152-122, 1: 5000) was added for incubation of another 30 min. Coverslips were washed

twice with PBS before mounting them onto microscopy slides using ProLong Gold antifade reagent incl. DAPI (Molecular Probes).

smFISH-IF images were acquired on a Nikon spinning disk microscope equipped with a Yokogawa CSU W1 scan head, a Plan-APOCHROMAT 100 × 1.4 NA oil objective and iXon-888Life Back-illuminated EMCCD. Z-stacks were acquired with a step size of 0.2 µm. The maximum laser intensities were employed for all the channels, with exposure times of 1000 ms for Atto565 (200 gain), 1000 ms for ATTO 488 (200 gain) and 200 ms for DAPI (400 gain), respectively.

smFISH-IF data analysis

Detection of single XBP1 mRNA spots in data from smFISH-IF experiments was performed in KNIME (Berthold *et al.*, 2009) analogous to what was previously described (Voigt *et al.*, 2019). Briefly, individual Z-slices were projected as maximum intensity projections. Following background-substraction, XBP1 mRNA spots were detected using threshold-based spot detection. Nuclear segmentation was performed on the DAPI signal using the Huang thresholding method while cytoplasmic segmentation was done using the background signal in the immunofluorescence (Ataxin-2) channel and a manual intensity threshold. Final masks were generated via substraction of nuclear from cytoplasmic segmentations and the number of XBP1 mRNAs per cell was quantified as the number of spots in each of these masks. To quantify XBP1-Ataxin-2 colocalization, mean Ataxin-2 IF intensities in all pixel positions obtained from XBP1 spot detection were quantified and normalized to the average Ataxin-2 background

intensity of each cell. Results were exported for subsequent statistical analysis in Excel and GraphPad Prism 10.

Cell culture, transfections and RNAi treatments

Drosophila S2 cells (Schneider, 1972) were cultured at 24°C without CO_2 in Schneider's *Drosophila* medium (Biowest) supplemented with 10% heat inactivated FBS (Biowest), 100 U/ml of penicillin plus 100 µg/ml of streptomycin (Thermo Fisher Scientific). The complete medium was filtered with 0,2 µm PES filter (VWR). S2 cells were transfected with the indicated plasmids using Effectene transfection reagent (QIAGEN) according to the manufacturer's instructions.

RNAi-mediated gene silencing was performed as described in (Clemens *et al.*, 2000). Primer pairs bearing a 5' end T7 RNA polymerase binding site were used to PCR amplify specific sequences of the genes to be inhibited. PCR products (with approximately 500-600 bp in length) were then purified with NucleoSpin® Gel and PCR Clean-up kit (MN) or with NZYGelpure kit (NZYtech) and used as templates for dsRNA synthesis with T7 RiboMAX™ Express Large Scale RNA Production System (Promega). After the DNase treatment, dsRNAs were purified and concentrated with RNA Clean & Concentrator™-5 kit (Zymo Research).

Individual-nucleotide resolution UV crosslinking and immunoprecipitation (iCLIP)

The iCLIP method was carried out as described by Ule and collaborators (König *et al.*, 2010; Huppertz *et al.*, 2014) with some modifications according to the improved iCLIP (iiCLIP) method (Lee *et al.*, 2021), namely i) the introduction of an infrared adaptor as described in infrared-CLIP (irCLIP) (Zarnegar *et al.*, 2016), ii) using reverse transcriptase (RT) Superscript IV and RT primers that contain carbon spacers as in irCLIP, and iii) ampure beads-based purification of cDNAs. Briefly, S2 cells transfected with Ataxin-2-HA or Ataxin-2^{C244A}-HA were grown in 10 cm dishes. Three dishes were used per condition, including: a dish in which S2 cells were UV irradiated (+UV), a negative control in which no UV crosslinking was carried out (no UV) and an additional control in which UV irradiation was performed, although no antibody was used during the IP.

Three days after transfection, S2 cells of each condition were incubated with 5 mM DTT for 4 h (to induce UPR activation). After DTT incubation, the culture medium was removed, replaced by ice-cold PBS, and cells (from +UV and IgG dishes) were UV crosslinked twice with 0.15 J/cm^2 in a Stratalinker 2400 (Analytic Jena) at 254 nm. Next, cells were harvested by scraping and the cell suspensions were centrifuged at 500*g* at 4°C for 5 min. Cell pellets were stored at - 80 °C until use.

Cell pellets were lysed in iCLIP lysis buffer (50 mM Tris-HCl pH 7.4, 100 mM NaCl, 1% Igepal, 0.1% SDS, 0.5% sodium deoxycholate) supplemented with cOmplete protease inhibitor cocktail (Roche), and the protein concentration was determined

using a BCA Protein Assay Kit (Thermo Scientific). To digest the genomic DNA and obtain RNA fragments of an optimal size range, each cell lysate was incubated with Turbo DNase (Invitrogen) and 0.4 U/ml of RNase I (Thermo Scientific) for exactly 3 min at 37 °C with shaking at 1100 rpm. After incubation on ice for 5 min, lysates were spun at 4 °C at 13,000 rpm for 10 min, and supernatants were incubated with antibody-conjugated protein A/G Dynabeads (Thermofisher scientific) overnight at 4 °C. The antibodies were pre-conjugated to Protein A/G Dynabeads by incubating 100 µl of beads with 5 µg of either mouse Anti-HA (16B12 clone, BioLegend) or mouse IgG2b isotype control (MPC-11 clone, Tonbo Biosciences) for 1 h at room temperature. On the next day, supernatants were discarded, and beads were washed 3x with high-salt wash buffer (50 mM Tris-HCl pH 7.4, 1 M NaCl, 1 mM EDTA, 1% Igepal, 0.1% SDS, 0.5% sodium deoxycholate) and 1x with PNK wash buffer (20 mM Tris-HCl pH 7.4, 10 mM $MgCl_2$, 0.2% Tween-20). Beads were then transferred to a new tube and the 3' end dephosphorylation was carried out: the magnetic beads were resuspended in a mixture containing T4 Polynucleotide Kinase (Thermo Scientific) and FastAP alkaline phosphatase (Thermo Scientific). Samples were incubated for 40 min at 37 °C with shaking at 1100 rpm; beads were washed once with 1x ligation buffer (50 mM Tris-HCl pH 7.5, 10 mM $MgCl_2$) and the on-bead ligation at room temperature (for 2 h) of the pre-adenylated adaptor L7-IR to the 3' ends of the RNAs was performed. Samples were then washed thrice with high-salt wash buffer and once with PNK wash buffer. To remove the excess of adaptor, beads were resuspended in a removal mix containing 5' deadenylase (NEB) and $RecJ_f$ exonuclease (NEB) and incubated for

30 min at 30 °C followed by 30 min at 37 °C whilst shaking at 1100 rpm. Beads were washed 3x with high-salt wash buffer and 1x with PNK wash buffer and the protein-RNA complexes were eluted in 1x NuPAGE loading buffer + 100 mM DTT at 70 °C for 1 min. The protein-RNA complexes were separated by SDS-PAGE in a 4-12% NuPAGE Bis-Tris gel (Invitrogen), transferred to a nitrocellulose membrane (Cytiva) for 2 h (at 30V) and detected using infrared light on a Chemidoc MP (Bio-Rad).

The protein-RNA complexes were excised from the membrane using the infrared image printout as a mask, treated with a mix of proteinase K (Sigma-Aldrich) and PK+SDS buffer (10 mM Tris-HCl pH 7.4, 100 mM NaCl, 1 mM EDTA, 0.2% SDS) for 1 h at 50 °C whilst shaking at 1100 rpm. The membrane pieces were removed, samples were mixed with phenol: chloroform: isoamyl alcohol (Sigma-Aldrich), moved to a pre-spun 2 ml Phase Lock Gel Heavy tube and incubated for 5 min at 30 °C with shaking at 1100 rpm and phases were separated by centrifugation for 5 min at 13000 rpm. Next, chloroform (VWR) was added to the top phase, tubes were inverted to mix, and spun for 5 min at 13000 rpm at 4 °C. The aqueous layer was transferred into a new tube and the RNA was precipitated by adding 3 M sodium acetate pH 5.2 (Thermo Scientific), glycoblue (Invitrogen) and absolute ethanol, overnight at - 20 °C. Samples were spun for 30 min at 15000 rpm at 4 °C, the supernatants were discarded, and RNA pellets were washed with 80% ethanol and resuspended in DEPC-treated water.

The RNAs were reversely transcribed into cDNAs using the Superscript IV (SSIV, Thermo Scientific), dNTP mix and barcoded RT primers (IDT) according to the manufacturer's instructions. Next,

1 M NaOH was added, and samples were incubated at 85 °C for 15 min for alkaline hydrolysis of the RNA. To neutralise the pH, the same amount of 1 M of HCl was added to the tubes. The cDNAs were purified using Mag-Bind Total Pure NGS beads (Omega Bio-Tek) following the manufacturer's instructions. The cDNAs were eluted in DEPC-treated water, circularized in a mixture containing CircLigase II ssDNA ligase with betaine additive (LGC Biosearch Technologies) for 2 h at 60 °C, and purified using the Mag-Bind Total Pure NGS beads.

The cDNAs were PCR amplified using an optimal number of cycles in a Phusion HF master mix (Thermo Scientific) containing P5/P7 Illumina sequencing primers. The amplified cDNA library was gel purified, the 150 – 400 bp fragments were incubated in crush-soak gel buffer (500 mM NaCl, 1 mM EDTA, 0.05% SDS) at 65 °C for 2h 15 min, with 15 sec of agitation at 1100 rpm and 45 sec of rest, transferred to Costar SpinX columns (Corning), and spun at 13000 rpm for 5 min. The amplified cDNA was ethanol precipitated as described above and resuspended in DEPC-treated water. Finally, the different (barcoded) cDNA libraries were mixed, purified using Mag-Bind Total Pure NGS beads, and sequenced at Genewiz (Azenta Life Sciences).

iCLIP data analysis

The iCLIP results were uploaded and analyzed on Flow bio (https://app.flow.bio) using the iCLIP pipeline as described https://docs.flow.bio/docs/clip-pipeline-1.0. In brief, 1) the demultiplexed reads were trimmed for the 3' end adapter sequence (AGATCGGAAGAGCACACGTCTGAA) by TrimGalore; 2) reads

were pre-mapped to an index of non-coding RNA sequences using Bowtie; and the resulting unmapped reads mapped to the *Drosophila* genome (BDGP6.32 annotation) using STAR; 3) the aligned reads were deduplicated based on the unique molecular identifiers (UMI) and start position; 4) the crosslink positions were defined as the cDNA start position minus one in uniquely mapped reads; 5) positionally-enriched k-mer analysis (Kuret *et al.*, 2022) as performed to determine enriched motifs in high-scoring crosslinks, using the following parameters: k-mer length as 5 nt (-k 5), proximal window as 20 nt (-w 20), distal window as 150 nt (-dw 150), and percentile parameter for assignment of "thresholded" crosslinks to 0.7 (-p 0.7). All Ataxin-2 iCLIP data files generated, including the .bedgraph files of Figure 4.5A, summary files of total crosslink counts in genes and RNA biotypes, and the parameters used in the iCLIP pipeline, are available on https://app.flow.bio/executions/562819420194487466. We selected the k-mers with highest PEKA scores and p value < 0.01 for Figure 4.5B. For the alignment of crosslinks at motif centers in the 3'UTR (Figure 4.5C), we normalized the crosslink counts at each meta position in the 3'UTR by the total number of crosslinks in the 3'UTR.

mRNA stability assay

For mRNA stability experiments, 3.0 x 10^6 cells were seeded in 25 cm^2 flasks and treated with 30 µg of Ataxin-2 dsRNA or LacZ dsRNA (control) for 10 days. S2 cells were then re-plated in 12-well plates (4.5 x 10^5 cells/well) and transfected with pUASTattb-Xbp1-HA-GFP$^{3'UTRspliced}$ (Cairrão *et al.*, 2022), pActinGal4 and pUAST plasmids. Three days after transfection, S2 cells were incubated

with 5 mM DTT (to induce UPR activation) for 4 h. Transcription was blocked with 5 µg/ml of actinomycin D (ActD, A9415, Sigma-Aldrich). Cells were incubated with ActD for 0, 1, 2 and 3 h and samples were collected at each indicated timepoint for RNA extraction using NZYtech Total RNA Isolation kit. RNA samples were treated with Turbo DNase (Thermo) to eliminate DNA contamination. Equal amounts of total RNA were retro-transcribed using RevertAid H Minus First Strand cDNA Synthesis Kit (Thermo/Fermentas). Each qPCR reaction was performed on 1/40 of the cDNA obtained, using SSoFast EvaGreen Supermix (Bio-Rad) according to the manufacturer's instructions and Bio-Rad CFX-96 as detection system. For each sample, the levels of mRNAs were normalized using rp49 as a loading control. Normalized data were then used to quantify the relative levels of mRNA using the $\Delta\Delta CT$ method.

Immunoblots

For Xbp1s-GFP immunoblot analysis, 3.0 x 10^6 cells were seeded in 25 cm^2 flasks and treated with 30 µg of Ataxin-2 dsRNA, Fbxo42 RNAi or LacZ dsRNA (control) for 10 days. S2 cells were then re-plated in 12-well plates (4.5 x 10^5 cells/well) and transfected with pUASTattb-Xbp1-HA-GFP$^{3'UTRspliced}$, pActinGal4 and empty pUAST plasmids. Three days after transfection, S2 cells were incubated with 5 mM DTT (to induce UPR activation) for 4 h and 8 h. Cell extracts were harvested at the indicated timepoints. Xbp1s-GFP protein levels were analysed by immunoblot with rat anti-GFP (1:1000, 3H9, Chromotek) and tubulin was used as loading control, being detected with mouse anti-alpha-Tubulin (1:500, AA4.3,

DSHB). Ataxin-2 mRNA depletion was confirmed by RT-PCR before further analysis. The knockdown of Ataxin-2 protein was also analysed by immunoblotting with guinea pig anti-Ataxin-2 (1:5000). Fbxo42 protein depletion was analysed by immunoblotting with rabbit anti-Fbxo42 (1:1000). iBright™ Analysis Software was used for densitometry.

Statistical analysis

Statistical analysis was carried out using GraphPad Prism 8 software. Two-way ANOVAs were performed as mentioned in the figure legends. *p* values refer to: ****$p < 0.0001$, ***$p < 0.001$, **$p < 0.01$ and *$p < 0.05$.

4.4 Results

Ataxin-2 co-localizes with Xbp1 mRNA during UPR activation in ring gland cells

To investigate the regulatory link between the RNA-binding protein Ataxin-2 and Xbp1 mRNA, we performed immunostaining with anti-Ataxin-2 and single molecule RNA fluorescence in situ hybridization (smFISH) for Xbp1 mRNA in ring gland cells of *Drosophila* larvae untreated or treated with DTT, to induce high levels of UPR activation. In untreated ring gland cells, Xbp1 mRNA is mostly located in the cytoplasm (Figure 4.1A), with little co-localization with Ataxin-2 protein (quantification in Figure 4.1C). In contrast, in DTT treated cells, Xbp1 mRNA colocalizes with cytoplasmic Ataxin-2 granules (arrows in Figure 4.1B and quantification in Figure 4.1C). Xbp1 mRNA is also detected in nuclear foci (arrowheads in Figure 4.1B), although Ataxin-2 is not present in these foci. The Xbp1 mRNA nuclear foci presumably correspond to Xbp1 transcription, since it is known that ER stress and UPR activation trigger Xbp1 transcription (Yoshida *et al.*, 2001). The quantification of the number of granules (Figure 4.1C) highlights the differences observed in Figures 4.1A and 4.1B. In the untreated condition, approximately 53.3% of the granules (average of two replicates) contain only Ataxin-2 protein, while 44.1% contain only Xbp1 mRNA. A small percentage of granules (2.6%) contain both Ataxin-2 protein and Xbp1 mRNA. In contrast, upon DTT treatment, the opposite is observed and most of the cytoplasmic granules contain both Ataxin-2 protein and Xbp1 mRNA (92%), with a small

percentage of granules containing only Ataxin-2 protein (3.9%) or only Xbp1 mRNA (4.1%) (average of two replicates).

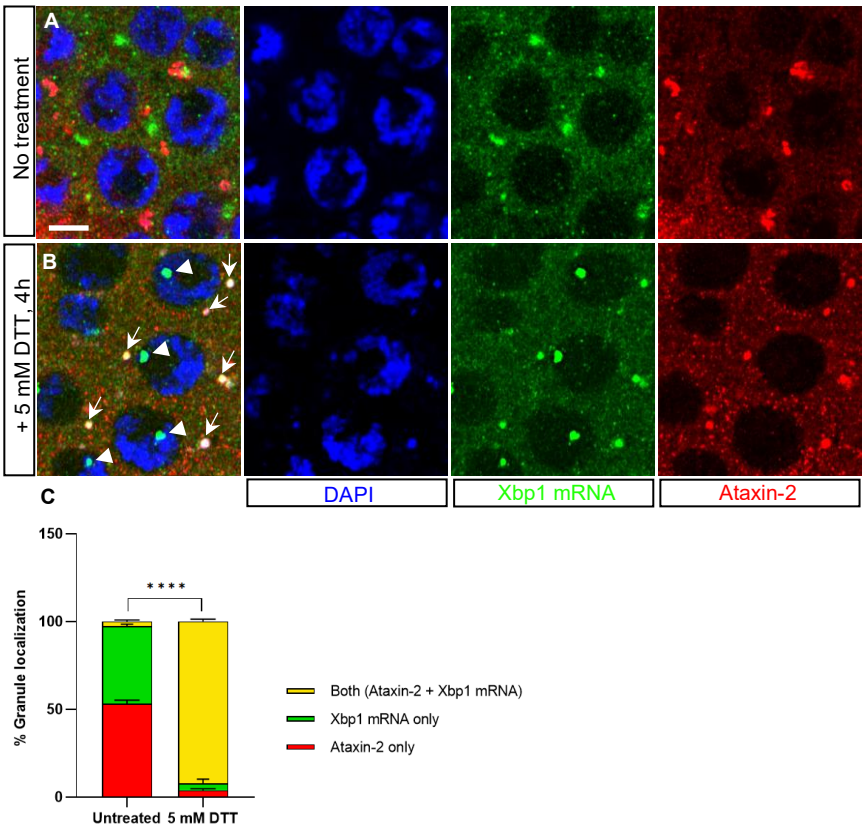

Figure 4.1: Ataxin-2 co-localizes with Xbp1 mRNA during UPR activation in ring gland cells (third instar larva). (A) Immunofluorescence (IF) and RNA-FISH of untreated ring gland cells. Endogenous Ataxin-2 is marked by anti-Ataxin-2 (red), Xbp1 mRNA is detected using Stellaris FISH probes against Xbp1, labelled with Quasar 670 dye (green), and DAPI marks the nuclei (blue). Scale bar = 10 µm. **(B)** Immunofluorescence and RNA FISH of ring gland cells, treated with 5 mM DTT for 4 hours. Endogenous Ataxin-2 is marked by anti-Ataxin-2 (red), Xbp1 mRNA is detected using Stellaris FISH probes against Xbp1, labelled with Quasar 670 dye (green), and DAPI marks the nuclei (blue). **(C)** Quantification of the number of granules of Ataxin-2 protein only (red bar), Xbp1 mRNA only (green bar) or both Ataxin-2 protein and Xbp1 mRNA (yellow bar) in untreated ring gland cells (shown in A) and in ring gland cells treated with 5 mM DTT for 4 h (shown in B). The quantification was

(Figure 4.1 continued):…performed in 2 biological replicates per condition and is presented in percentage (%) as mean + SD. Two-way ANOVA coupled with Sidak's multiple comparison test, ****$p < 0.0001$. The number of granules scored in untreated ring gland cells was n=125 (replicate 1) and n=150 (replicate 2). The number of granules scored in untreated ring gland cells was n=123 (replicate 1) and n=156 (replicate 2).

To assess the specificity of the Xbp1 mRNA FISH probes, we used eye imaginal discs of third instar larvae containing clones of Ex250 (Coelho *et al.*, 2013, 2014), a deletion of most of *Xbp1*. These eye discs show a strongly reduced FISH signal of Xbp1 mRNA in cells homozygous for Ex250, identified by the absence of ubiGFP, compared to wild-type cells (labelled by ubiGFP) (Figure 4.2).

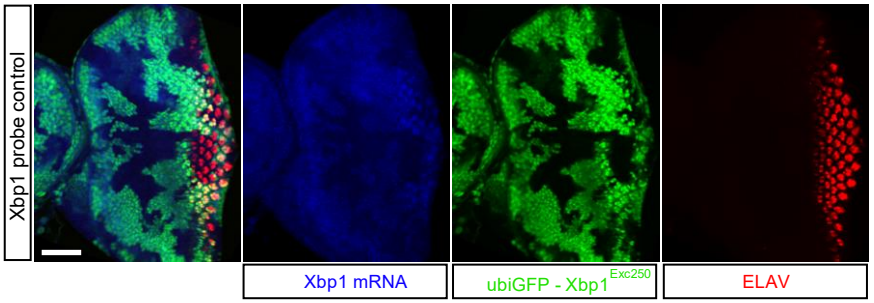

Figure 4.2: Xbp1 probe control. Immunofluorescence and RNA-FISH of third instar larval eye imaginal discs containing clones of cells homozygous for $Xbp1^{Exc250}$, a deletion of *Xbp1*. Xbp1 mRNA levels, detected with Stellaris RNA FISH probes (blue) are lower in $Xbp1^{Exc250}$ homozygous cells, labelled by the absence of ubiGFP (green). The photoreceptors are labelled with ELAV (red). Scale bar = 60 µm.

Ataxin-2 co-localizes with Xbp1 mRNA during UPR activation in human (HeLa) cells

To determine whether the IF-smFISH results observed in ring gland cells of *Drosophila* larvae were also seen in human cells, we combined smFISH and immunofluorescence to assess the co-localization of human Ataxin-2 and Xbp1 mRNA in HeLa cells. For this, cells were exposed to 1 µM thapsigargin (TG) for 3 hours to induce ER stress and activate the UPR, or left untreated. The HeLa cells were then incubated with FISH probes targeting the human Xbp1 mRNA and subsequently immunostained for human Ataxin-2. These experiments were carried out by our collaborators, Ming Yang and Franka Voight, from the University of Zurich. Consistent with the results obtained from DTT-treated ring gland cells of *Drosophila* larvae, thapsigargin treatment of HeLa cells led to a significant accumulation of Xbp1 mRNA in Ataxin-2 granules (Figure 4.3A and quantification in Figures 4.3B and 4.3C).

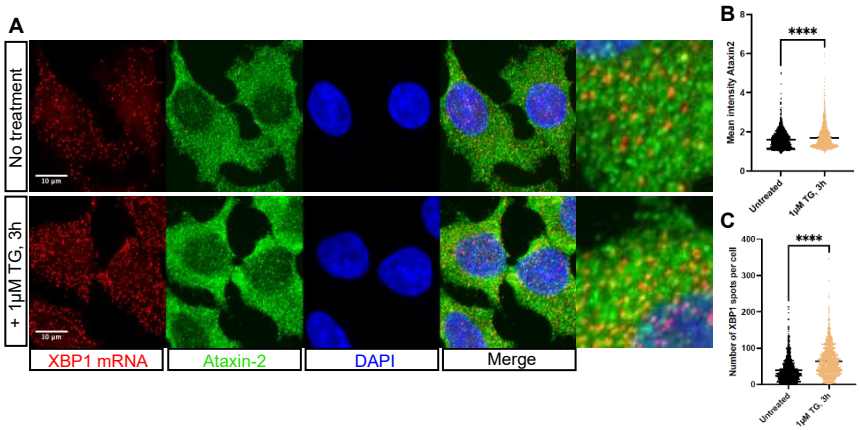

Figure 4.3: Ataxin-2 co-localizes with Xbp1 mRNA during UPR activation in human (HeLa) cells. (A) Combined smFISH and immunofluorescence (IF) analysis for co-localization of Ataxin-2 protein (green) and Xbp1 mRNA (red) in fixed HeLa cells with (or without) ER stress, induced by 1 µM thapsigargin (TG) for 3 h. DAPI marks the nuclei

(Figure 4.3 continued):… (blue). **(B)** and **(C)** Quantification of the data shown in (A). Depicted results were obtained from three biological replicates, including two technical replicates each. For each replicate and treatment, 10 images (approximately 200 cells) were analysed. **(B)** Plot showing mean (per pixel) Ataxin-2 IF signal intensities across all cytoplasmic Xbp1 mRNA spot positions (detected via smFISH) under control (untreated) and ER stress (1 µM TG, 3 h) conditions. Intensity values were normalized to the mean cytoplasmic background intensity per cell to correct for expression levels and ensure comparability in between replicates. Individual dots represent per-cell averages. Black bars show mean ± SEM. Statistical test: unpaired t-test, ****$p < 0.0001$. **(C)** Plot showing mean number of Xbp1 mRNA spots per cell, under the same conditions as in (B). Increased mRNA levels are indicative of Xbp1 upregulation in response to UPR induction. Black bars show mean ± SEM. Statistical test: unpaired t-test, ****$p < 0.0001$.

Ataxin-2 binds to Xbp1 mRNA during UPR activation in S2 *Drosophila* cells

The smFISH and IF results suggest that, during UPR activation, Ataxin-2 binds to Xbp1 mRNA, which is present in cytoplasmic Ataxin-2 granules. To identify the Ataxin-2 binding sites on Xbp1 mRNA, we performed iCLIP (individual-nucleotide resolution UV crosslinking and immunoprecipitation) experiments (König *et al.*, 2010), using S2 cells transfected with either wild-type (WT) Ataxin-2-HA or mutant Ataxin-2^{C244A}-HA (C244A). S2 cells were UV-irradiated (+UV) to crosslink Ataxin-2 with its target RNAs. As controls, we used non-UV-irradiated (no UV) cells and UV-exposed cells, whose lysates were not incubated with the antibody during the immunoprecipitation (IgG control). Cells from all conditions were treated with 5 mM DTT for 4 hours, to induce UPR activation. Afterwards, S2 cells were harvested, and lysates were treated with RNase I and DNase. Samples were then subjected to IP using beads pre-conjugated with anti-HA antibody (excluding the IgG control). The Ataxin-2–RNA complexes were purified by SDS-

PAGE and transferred to a nitrocellulose membrane, where they were detected by infrared (IR) light (Figure 4.4). Ataxin-2–RNA complexes (identified by a smear above the 150 kDa band in Figure 4.4) were detected in UV-irradiated WT and C244A samples. As expected, no such complexes were observed in the no UV or IgG controls (Figure 4.4). A band of approximately 150 kDa (marked with an asterisk in Figure 4.4) was observed in +UV and no UV samples, corresponding to the molecular weight of Ataxin-2-HA (135 kDa) along with the L7–IR adaptor (approximately 15 kDa). A band with a similar molecular weight (150 kDa) was also detected in IgG control sample, presumably due to non-specific interactions between IgG and proteins present in the cell lysate. Below the 150 kDa band, several non-specific bands were observed in all samples.

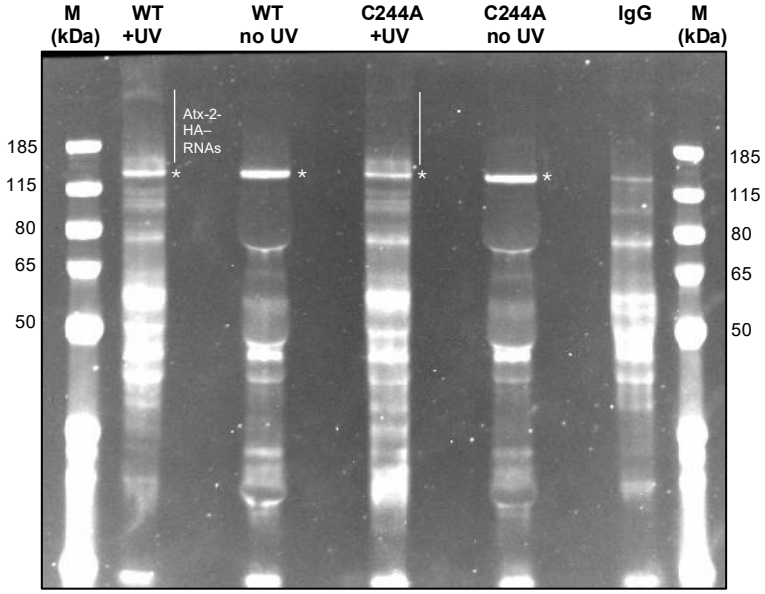

Figure 4.4: The Ataxin-2–RNA complexes were purified by SDS-PAGE and transferred to a nitrocellulose membrane, being detected by infrared light. These complexes are observed in UV-irradiated Ataxin-2-HA and Ataxin-2^{C244A}-HA samples, marked by a vertical line. (*) marks a band of 150 kDa, corresponding to adaptor L7–IR–Ataxin-2-HA.

The next step consisted of excising the protein-RNA complexes from the membrane, followed by treatment of the membrane pieces with proteinase K. RNA was then extracted, cDNA synthesized, and cDNA libraries generated for each condition. These cDNA libraries were sent for high-throughput sequencing and the iCLIP results were analysed bioinformatically. The iCLIP protocol was carried out in collaboration with Paulo Gameiro from CEDOC, who also analysed the iCLIP data.

The iCLIP results (Figure 4.5A) show that Ataxin-2 binds to the Xbp1 mRNA, especially to the 3' UTR, in a region containing an AU-rich motif. This is consistent with the binding-sites identified for human (Yokoshi *et al.*, 2014) and *Drosophila* (Singh *et al.*, 2021) Ataxin-2. Regarding the mutant Ataxin-2^{C244A}-HA, it still binds to Xbp1 mRNA, although there is a reduction in the number of iCLIP crosslink peaks. This reduction may be due to C244A being located within the LSM-AD domain, which is important for RNA-binding and essential to rescue the lethality of Ataxin-2 trans-heterozygous mutations.

The motif analysis around Ataxin-2 crosslink sites revealed that different AU-rich pentamers (with a "C" or a "G" or without) were enriched at the transcriptomic level in both WT and mutant Ataxin-2^{C244A}-HA UV-irradiated samples, but not in the non-UV crosslinked samples (Figure 4.5B). Furthermore, the iCLIP crosslink positions (the start positions of iCLIP cDNAs) were directly aligned with the motif centers at the metagene level (Figure 4.5C), including the GUUUC pentamer that was bound by Ataxin-2 on the Xbp1 3' UTR (Figure 4.5A, C).

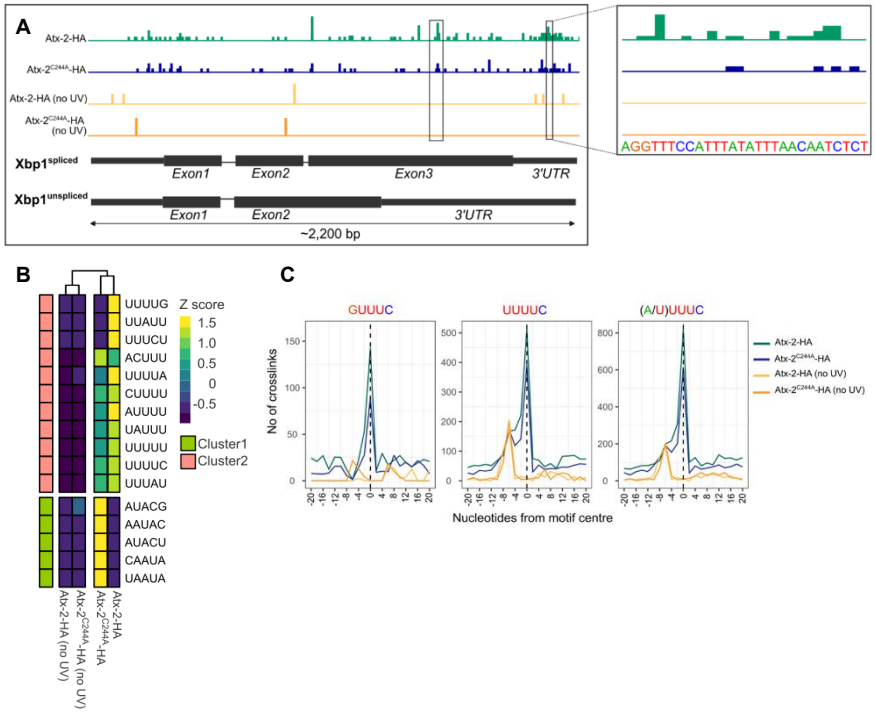

Figure 4.5: (A) iCLIP results for Xbp1 mRNA and WT Ataxin-2-HA or mutant Ataxin-2^{C244A}-HA. In green are depicted the peaks (sequencing reads) in *Xbp1* from UV-irradiated S2 cells transfected with Ataxin-2-HA. In blue are depicted the peaks in *Xbp1* of UV-irradiated cells transfected with Ataxin-2^{C244A}-HA. The non-UV irradiated controls for Ataxin-2-HA and Ataxin-2^{C244A}-HA samples are shown by the yellow and orange lines, respectively. To the right is a zoom of the *Xbp1* 3' UTR containing the AU-rich region. **(B)** Analysis of the motifs around the Ataxin-2-HA crosslink sites. The AU-rich pentamers identified in the transcripts of the UV-irradiated Ataxin-2-HA and Ataxin-2^{C244A}-HA samples are labelled with different colours according to their Z-scores. **(C)** iCLIP crosslink positions (i.e. start positions of iCLIP cDNAs) aligned with the motif centers at the metagene level.

Ataxin-2 regulates Xbp1 mRNA stability during UPR activation in S2 *Drosophila* cells

To test whether Ataxin-2 regulates the stability of Xbp1 mRNA, we performed actinomycin D (ActD) chase experiments in S2 cells, using the Xbp1 reporter for Ire1 activation, where the Xbp1s form is tagged by GFP (Ryoo *et al.*, 2007; Cairrão *et al.*, 2022). After ER stress induction with DTT (5 mM, for 4 h) and transcription inhibition with ActD, we analysed the decay of the Xbp1 reporter mRNA over time in S2 cells treated with either Ataxin-2 RNAi or control LacZ RNAi. We observe that, upon Ataxin-2 RNAi depletion, the stability of the Xbp1 reporter mRNA decreased compared to the LacZ RNAi control condition (Figure 4.6).

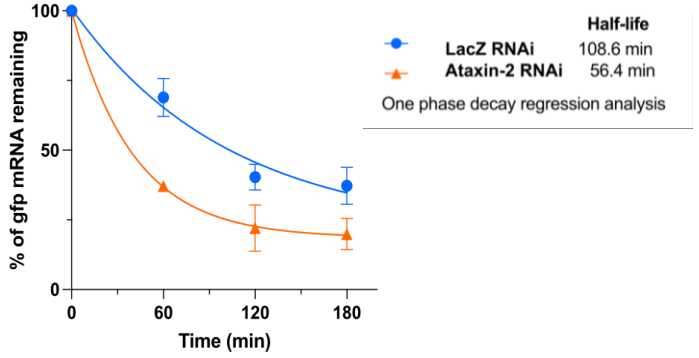

Figure 4.6: Ataxin-2 regulates Xbp1 mRNA stability during UPR activation in S2 *Drosophila* cells. Actinomycin D (ActD) chase experiments using S2 cells treated with Ataxin-2 RNAi or control LacZ RNAi and transfected with pUASTattb-Xbp1-HA-GFP. S2 cells were treated with 5 mM DTT for 4h and subsequently incubated with 5 µg/ml ActD until the indicated chase timepoints.

Ataxin-2 regulates Xbp1 mRNA translation during UPR activation in S2 *Drosophila* cells

The result obtained from the ActD experiments was further confirmed by immunoblotting experiments (Figure 4.7A, and quantification in Figure 4.7B) which shows that, upon Ataxin-2 depletion and after DTT treatment (5 mM, for 4 and 8 hours), the expression levels of Xbp1s-GFP protein are significantly decreased, compared to the LacZ RNAi control condition. Therefore, the ActD results, together with the protein expression data demonstrate that Ataxin-2 promotes Xbp1 mRNA stabilization and enhances the expression of Xbp1s protein during UPR activation. This is consistent with previous findings showing that human Ataxin-2 generally stabilizes its target mRNAs and increases the abundance of the corresponding proteins (Yokoshi *et al.*, 2014).

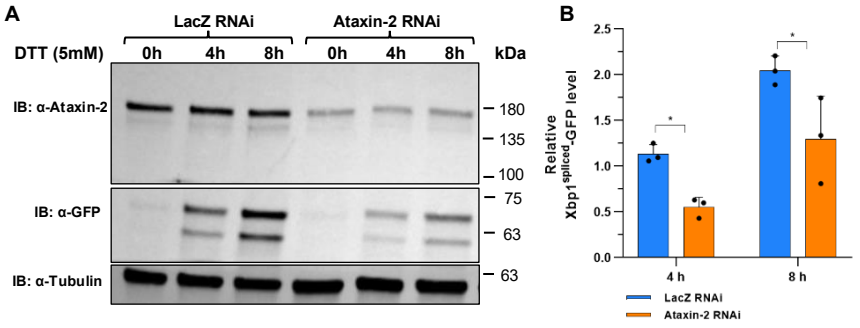

Figure 4.7: Ataxin-2 regulates Xbp1 mRNA translation during UPR activation in S2 *Drosophila* cells. (A) Immunoblots with anti-Ataxin-2, anti-GFP and anti-Tubulin of protein extracts from S2 cells treated with Ataxin-2 RNAi or LacZ RNAi, transfected with pUASTattb-Xbp1-HA-GFP, and incubated with 5 mM DTT for 4 and 8 h. Tubulin was used as loading control. **(B)** Quantification of the Xbp1s-GFP protein levels from (A) and 2 other independent experiments, is presented as mean + SD. Two-way ANOVA coupled with Sidak's multiple-comparison test, $*p < 0.05$.

Fbxo42 regulates Xbp1 mRNA translation during UPR activation in S2 *Drosophila* cells and in eye imaginal discs

Finally, we aimed to investigate whether the Fbxo42 protein influences Xbp1 mRNA translation. To assess this, S2 cells were transfected with pUASTattbXbp1-HA-GFP and incubated with 5 mM DTT (for 4 and 8 hours). S2 cells were harvested at the indicated timepoints, and protein was extracted for analysis by immunoblotting. The immunoblots probed with anti-GFP (Figure 4.8A and quantification in Figure 4.8B) show that, after RNAi depletion of Fbxo42, Xbp1s-GFP protein levels were significantly decreased compared to the LacZ RNAi control condition.

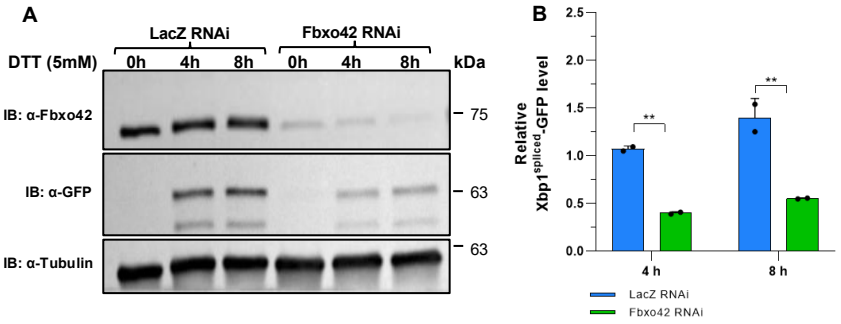

Figure 4.8: Fbxo42 regulates Xbp1 mRNA translation during UPR activation in S2 *Drosophila* cells. (A) Immunoblots with anti-Fbxo42, anti-GFP and anti-Tubulin of protein extracts from S2 cells treated with Fbxo42 RNAi or LacZ RNAi, transfected with pUASTattb-Xbp1-HA-GFP, and incubated with 5 mM DTT for 4 and 8 h. Tubulin was used as loading control. **(B)** Quantification of the Xbp1s-GFP protein levels from (A) and 1 other independent experiment is presented as mean + SD. Two-way ANOVA coupled with Sidak's multiple-comparison test, $^{**}p < 0.01$.

The results obtained for Fbxo42 in S2 *Drosophila* cells were further validated by immunofluorescence of eye imaginal discs of *Drosophila* third instar larvae, carrying Su218/ubiRFP clones and

the Xbp1-HA-GFP transgene. In these mosaic eye discs, cells homozygous for Su218 – Fbxo42^{N423*} are marked by the absence of red fluorescence. Upon treatment of the eye imaginal discs with 5 mM DTT for 4 hours, we observed that Xbp1s-GFP expression was reduced in clones of cells homozygous for Su218 (Figure 4.9).

Taken together, the results from S2 cells and eye imaginal discs suggest that Fbxo42-mediated degradation of Ataxin-2 is required for Xbp1 mRNA translation, which is consistent with the findings from our genetic screen, where loss-of-function mutations in Fbxo42 suppress the “glossy” eye phenotype caused by overexpression of XBP1s.

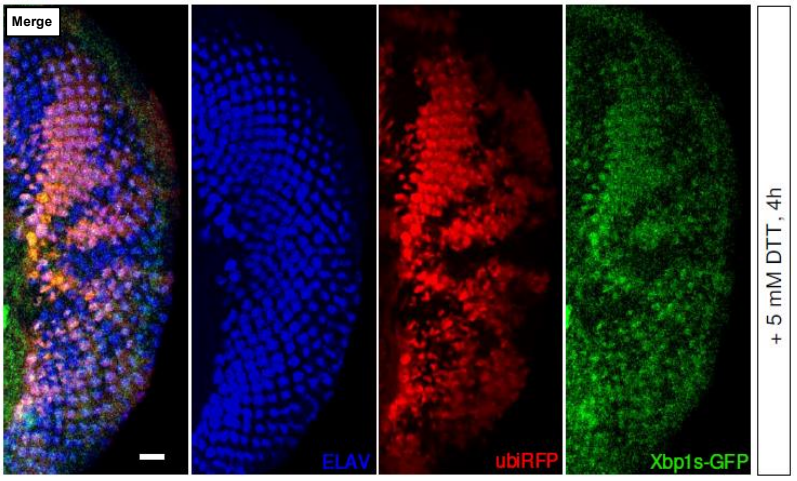

Figure 4.9: Immunofluorescence of *Drosophila* third instar larval eye imaginal discs containing Su218 (Fbxo42^{N423*})/ubiRFP clones and bearing the Xbp1-HA-GFP construct. Fbxo42 mutant clones are labelled by the absence of ubiRFP (red), Xbp1s-GFP is in green and photoreceptor marker ELAV is in blue. The larval discs were treated with 5 mM DTT for 4 hours, before fixation to activate Ire1 mediated splicing of Xbp1-HA-GFP. Scale bar = 10 μm. Genotype: eyFlpGMR-GAL4; FRT42D, Su218/ FRT42D, ubiRFP; UAS-Xbp1-HA-GFP.

4.5 Discussion

To investigate the regulatory link between Ataxin-2 and Xbp1 mRNA, we employed various experimental approaches. First, we aimed to study the interaction between Ataxin-2 protein and Xbp1 mRNA by combining immunofluorescence (IF) and single molecule RNA fluorescence in situ hybridization (smFISH) in ring gland cells of *Drosophila* larvae. We performed immunostaining of untreated or DTT-treated ring gland cells with anti-Ataxin-2 antibody, to detect the Ataxin-2 protein, followed by FISH to label Xbp1 mRNA. Through these experiments, we were able to observe that in untreated ring gland cells, Ataxin-2 and Xbp1 mRNA are predominantly located in the cytoplasm with little co-localization. In contrast, after 4 hours of DTT treatment, to induce ER stress and UPR activation, Xbp1 mRNA co-localizes with cytoplasmic Ataxin-2 granules. Notably, we also detected Xbp1 mRNA in nuclear foci, which may correspond to Xbp1 transcription, since it is known that ER stress and UPR activation induce Xbp1 mRNA transcription (Yoshida *et al.*, 2001). By quantifying cytoplasmic Ataxin-2 granules containing Xbp1 mRNA in DTT-treated cells, we found that the percentage of co-localization between Ataxin-2 granules and Xbp1 mRNA was approximately 92%, in contrast to the untreated condition, where the percentage of co-localization was very low, at only 2.6%. Taken together, these results suggest that during UPR activation, Ataxin-2 binds to Xbp1 mRNA, which is present in Ataxin-2 granules. In this way, Xbp1 mRNA is “stored” and protected from degradation. Consistent with these findings, we have shown that UPR activation (via thapsigargin treatment) in human HeLa cells

also leads to the accumulation of human Xbp1 mRNA in Ataxin-2 granules. These results demonstrate that this mechanism is conserved from fly to human, and that human Ataxin-2 probably binds to Xbp1 mRNA. This binding most likely occurs through the conserved RNA-binding domains, LSM/LSM-AD (Albrecht *et al.*, 2004).

To further show the binding between Ataxin-2 and Xbp1 mRNA, we performed the identification of Ataxin-2 binding sites on Xbp1 mRNA via iCLIP experiments in *Drosophila* S2 cells transfected with wild-type Ataxin-2 or mutant Ataxin-2^{C244A}-HA, and treated with 5 mM DTT for 4 hours, to induce ER stress. The iCLIP results confirmed that Ataxin-2 binds to Xbp1 mRNA. Several iCLIP crosslink peaks were identified throughout the *Xbp1* sequence, with a particularly high density of crosslink peaks (a cluster) observed in the 3' UTR of Xbp1, in a region containing an AU-rich motif. These results are consistent with the binding sites identified for human (Yokoshi *et al.*, 2014) and *Drosophila* Ataxin-2 (Singh *et al.*, 2021). Interestingly, in the studies by Yokoshi and Singh, Xbp1 mRNA was not detected, possibly because the experiments to identify Ataxin-2 target RNAs were not performed under ER stress conditions. Regarding the mutant Ataxin-2^{C244A}-HA, we observed that it still binds to Xbp1 mRNA; however, there is a decrease in the number of iCLIP crosslink peaks. As previously mentioned, the C244A mutation is located within the LSM-AD domain, and as such, it could impact the binding of Ataxin-2 to is target mRNAs, in this case, Xbp1 mRNA.

Our next goal was to assess the role of *Drosophila* Ataxin-2 in Xbp1 stability. Previous studies on the Ataxin-2 protein have shown antagonistic roles for this RNA-binding protein. Singh and collaborators showed that Ataxin-2 stabilizes the majority of its target mRNAs; however, a small percentage of these mRNAs increased after Ataxin-2 knockdown (Singh *et al.*, 2021). Thus, to determine the role of Ataxin-2 in Xbp1 mRNA stability under ER stress conditions, we used the Xbp1-HA-GFP reporter (Cairrão *et al.*, 2022), which allows the detection of the spliced form of Xbp1 (since it is tagged with GFP), and performed actinomycin D chase assays using S2 cells. Through these experiments, we observed that upon Ataxin-2 depletion, the stability of the Xbp1 reporter mRNA decreased in comparation with the control condition. Therefore, we can conclude that, during UPR activation, Ataxin-2 binds to the 3'UTR of Xbp1 mRNA, leading to its stabilization. In line with this, a recently study from our laboratory showed that the RNA-binding protein Pumilio binds to the 3' UTR of Xbp1s mRNA, in a different region from Ataxin-2, also stabilizing this mRNA (Cairrão *et al.*, 2022).

In order to assess the impact of Ataxin-2 depletion on Xbp1 mRNA translation, we performed the knockdown of Ataxin-2 in S2 cells, and upon DTT treatment (for 4 and 8 hours), we analysed the Xbp1 protein levels by immunoblotting. Consistent with the results obtained for Xbp1 mRNA, we observed that after RNAi depletion of Ataxin-2 and upon ER stress induction, Xbp1s-GFP protein levels decreased, compared to the control condition. This is also in accordance with the report by Yokoshi and collaborators (Yokoshi *et al.*, 2014), where the authors found that human Ataxin-2 promotes

the stabilization of target mRNAs and increases the expression of the corresponding proteins.

Finally, to determine the link between Fbxo42 and Xbp1 mRNA, we decided to deplete Fbxo42 in S2 cells and treat these cells for 4 and 8 hours with DTT, followed by the analysis of the Xbp1 protein levels by immunoblotting. We observed that after Fbxo42 RNAi depletion, the Xbp1s-GFP protein levels significantly decreased in comparation to the control condition. Furthermore, we observed that Xbp1s-GFP expression was also reduced in eye imaginal discs containing clones of cells mutant for Fbxo42. These results are consistent with our initial findings, showing that loss-of-function mutations in Fbxo42 lead to the suppression of the “glossy” eye phenotype caused by Xbp1s-overexpression. This result indicates that Fbxo42-mediated ubiquitylation and degradation of Ataxin-2 is required for Xbp1 mRNA translation.

Overall, our results indicate that upon ER stress, during the early phase of the UPR, Xbp1 mRNA is stabilized by the binding of Ataxin-2 within cytoplasmic Ataxin-2 granules. The storage of Xbp1 mRNA in Ataxin-2 granules is crucial for protecting Xbp1 mRNA from degradation, allowing it to be rapidly translated in the later stages of the ER stress response. Importantly, for Xbp1 mRNA translation to occur, Fbxo42 mediates Ataxin-2 degradation (this mechanism will be presented in further detail in the general discussion).

4.6 Acknowledgements

I would like to thank Fátima Cairrão, for providing the pUASTattbXbp1-HA-GFP reagent and for performing the mRNA stability/qPCR experiments. I express my gratitude to Paulo Gameiro, for teaching me the iCLIP technique, for hosting me in his lab for a few months, for supervising the iCLIP experiments and for analysing the iCLIP data. Furthermore, I acknowledge Zach Hensel for his guidance on smFISH experiments, for providing reagents and for his participation as a member of my PhD thesis committee. I am grateful to Ming Yang and Franka Voigt for performing smFISH+IF in HeLa cells, analysing data and for their willingness to participate in this project. Lastly, I am thankful to Pedro Domingos for supervising all this work.

4.7 References

Albrecht M, Golatta M, Wüllner U & Lengauer T (2004). Structural and functional analysis of ataxin-2 and ataxin-3. *Eur J Biochem* 271, 3155–3170.

Barreau C, Paillard L & Osborne HB (2005). AU-rich elements and associated factors: Are there unifying principles? *Nucleic Acids Res* 33, 7138–7150.

Berthold MR, Cebron N, Dill F, Gabriel TR, Meinl T, Ohl P, Thiel K & Wiswedel B (2009). KNIME:The Konstanz Information Miner, in: Studies in Classification, Data Analysis, and Knowledge Organization (GfKL 2007). 11, 26–31.

Cairrão F, Santos CC, Le Thomas A, Marsters S, Ashkenazi A & Domingos PM (2022). Pumilio protects Xbp1 mRNA from regulated Ire1-dependent decay. *Nat Commun* 13, 1–13.

Clemens JC, Worby CA, Simonson-Leff N, Muda M, Maehama T, Hemmings BA & Dixon JE (2000). Use of double-stranded RNA interference in Drosophila cell lines to dissect signal transduction pathways. *Proc Natl Acad Sci U S A* 97, 6499–6503.

Coelho DS, Cairrão F, Zeng X, Pires E, Coelho A V., Ron D, Ryoo HD & Domingos PM (2013). Xbp1-Independent Ire1 Signaling Is Required for Photoreceptor Differentiation and Rhabdomere Morphogenesis in Drosophila. *Cell Rep* 5, 791–801.

Coelho DS, Gaspar CJ & Domingos PM (2014). Ire1 mediated mRNA splicing in a C-terminus deletion mutant of drosophila Xbp1. *PLoS One* 9, 1–6.

Gómez-Puerta S, Ferrero R, Hochstoeger T, Zubiri I, Chao J, Aragón T & Voigt F (2022). Live imaging of the co-translational recruitment of XBP1 mRNA to the ER and its processing by diffuse, non-polarized IRE1α. *Elife* 11, 1–27.

Hollien J & Weissman JS (2006). Decay of Endoplasmic Reticulum-Localized mRNAs During the Unfolded Protein Response. *Science (80-)* 313, 104–107.

Huppertz I, Attig J, D'Ambrogio A, Easton LE, Sibley CR, Sugimoto Y, Tajnik M, König J & Ule J (2014). iCLIP: Protein-RNA interactions at nucleotide resolution. *Methods* 65, 274–287.

König J, Zarnack K, Rot G, Curk T, Kayikci M, Zupan B, Turner DJ, Luscombe NM & Ule J (2010). ICLIP reveals the function of hnRNP particles in splicing at individual nucleotide resolution. *Nat Struct Mol Biol* 17, 909–915.

Kuret K, Amalietti AG, Jones DM, Capitanchik C & Ule J (2022). Positional motif analysis reveals the extent of specificity of protein-RNA interactions observed by CLIP. *Genome Biol* 23, 1–34.

Lee FCY, Chakrabarti AM, Hänel H & Monzón-casanova E (2021). An improved iCLIP protocol We recently employed the iiCLIP protocol for the comparative studies of RBP binding upon changes. *bioRxiv*1–30.

Liu Y, Xu C, Gu R, Han R, Li Z & Xu X (2024). Endoplasmic reticulum stress in diseases. *MedComm* 5, 1–31.

Majumder M, Huang C, Snider MD, Komar AA, Tanaka J, Kaufman RJ, Krokowski D & Hatzoglou M (2012). A Novel Feedback Loop Regulates the Response to Endoplasmic Reticulum Stress via the Cooperation of Cytoplasmic Splicing and mRNA Translation. *Mol Cell Biol* 32, 992–1003.

Rasheva VI & Domingos PM (2009). Cellular responses to endoplasmic reticulum stress and apoptosis. *Apoptosis* 14, 996–1007.

Ryoo HD, Domingos PM, Kang MJ & Steller H (2007). Unfolded protein response in a Drosophila model for retinal degeneration. *EMBO J* 26, 242–252.

Singh A, Hulsmeier J, Kandi AR, Pothapragada SS, Hillebrand J, Petrauskas A, Agrawal K, Krishnan RT, Thiagarajan D, Jayaprakashappa D, Vijayraghavan K, Ramaswami M & Bakthavachalu B (2021). Antagonistic roles for ataxin-2 structured and disordered domains in rnp condensation. *Elife* 10, 1–25.

Tabas I & Ron D (2011). Integrating the mechanisms of apoptosis induced by endoplasmic reticulum stress. *Nat Cell Biol* 13, 184–190.

Voigt F, Gerbracht J V., Boehm V, Horvathova I, Eglinger J, Chao JA & Gehring NH (2019). *Detection and quantification of RNA decay intermediates using XRN1-resistant reporter transcripts*. Springer US. Available at: http://dx.doi.org/10.1038/s41596-019-0152-8.

Walter P & Ron D (2011). The Unfolded Protein Response: From Stress Pathway to Homeostatic Regulation. *Science (80-)* 334, 1081–1086.

Woehlbier U & Hetz C (2011). Modulating stress responses by the UPRosome: A matter of life and death. *Trends Biochem Sci* 36, 329–337.

Yokoshi M, Li Q, Yamamoto M, Okada H, Suzuki Y & Kawahara Y (2014). Direct binding of Ataxin-2 to distinct elements in 3' UTRs promotes mRNA stability and protein expression. 186–198.

Yoshida H, Matsui T, Yamamoto A, Okada T & Mori K (2001). XBP1 mRNA Is Induced by ATF6 and Spliced by IRE1 in Response to ER Stress to Produce a Highly Active Transcription Factor phorylation, the activated Ire1p specifically cleaves HAC1 precursor mRNA to remove an intron of 252 nucle-otides. The cleaved 5 and . *Cell* 107, 881–891.

Zarnegar BJ, Flynn RA, Shen Y, Do BT, Chang HY & Khavari PA (2016). irCLIP platform for efficient characterization of protein–RNA interactions. *Nat Methods* 13, 489–492.

CHAPTER V

General Discussion and Future Perspectives

5.1 Fbxo42 protein

The observation that overexpression of Xbp1 spliced, an important mediator of UPR, causes cell death and retinal degeneration in the *Drosophila* adult eye, leading to the "glossy" eye phenotype was the premise to this project. The first step was to conduct a genetic screen, to find mutations that could rescue the "glossy" eye phenotype. Through this screen, loss-of-function mutations in *Fbxo42* gene were identified, which suppressed the cell death induced by Xbp1s-overexpression.

Fbxo42 encodes a F-box protein. F-box proteins form complexes (SCF-complexes) with Skp-1, Cullin-1 and Rbx to mediate the ubiquitylation of specific substrates. Recently, it was found that Fbxo42 plays a role in the assembly of the synaptonemal complex during *Drosophila* female meiosis by down-regulating the protein levels of the phosphatase PP2A-B56 (Barbosa *et al.*, 2021). However, no other biological functions have been reported for this F-box protein, so far. In this way, to investigate the cellular and tissue localization of Fbxo42, we generated an antibody against this F-box protein. Using this antibody, we were able to detect Fbxo42 protein expression in different larval tissues, including the brain, ring gland and eye imaginal discs as well as in the adult brain, testis and ovary.

In contrast to *Drosophila* Fbxo42 protein, for human FBXO42, some substrates have been identified, specifically p53 (Sun *et al.*, 2009, 2011), ING4 (Yan *et al.*, 2015) and RBPJ (Jiang *et al.*, 2022). In the present study, to identify the specific substrates of the Fbxo42 protein, we employed two different proteomic approaches. The first approach involved mass spectrometry (MS)

using human HEK-293 cells transfected with several versions of *Drosophila* Fbxo42, while the second was performed with fly extracts. In the first mass spectrometry, several Fbxo42 interactors were identified, including the SCF components Skp-1, Cullin-1 and Rbx-1. However, when we tested these interactors by immunofluorescence, we found that most of them failed to accumulate in Fbxo42 homozygous mutant clones in the eye imaginal discs of the *Drosophila* larvae. In fact, the only positive result that we obtain was Lamin-B, when its immunostaining was performed with ADL84 antibody, which specifically recognizes Lamin-B when dephosphorylated at Serine 25 (Stuurman *et al.*, 1995). Based on this result, we hypothesized that a phosphatase might be a direct substrate of Fbxo42. We investigated whether the RNAi line for the fly phosphatase PP1-87B affected LaminB-ADL84 immunostaining. We found that eye imaginal discs from larvae containing Su218/ubiGFP clones along with PP1-87B RNAi expression, exhibited uniform LaminB-ADL84 immunostaining in wild-type and Fbxo42 mutant cells, suggesting that PP1-87B could be a substrate of Fbxo42. However, further studies are needed to confirm this result.

5.2 Ataxin-2 is a substrate of Fbxo42

As the first mass spectrometry was conducted using human cell extracts, we performed a second one, using fly extracts. This second proteomic approach was based on the ^{bio}Ub strategy (Franco *et al.*, 2011; Ramirez *et al.*, 2015), where a ubiquitin with a biotinylation site is expressed in cells to enable the pulldown and identification of proteins that are targets for ubiquitylation. In order

to use this approach, we generated flies expressing full-length Fbxo42 or the controls ΔFbxo42 and Fbxl7, along with a polyubiquitin tag containing a short biotinylatable motif and BirA. Through MS, we identified the RNA-binding protein Ataxin-2 as a substrate of Fbxo42.

We further confirmed biochemically that Ataxin-2 is indeed a bona fide substrate of Fbxo42. We conducted ubiquitylation assays in flies and in *Drosophila* S2 cells, followed by immunoblotting. Interestingly, the immunoblots from both assays revealed the presence of DTT-sensitive Ataxin-2/ubiquitin-conjugates, suggesting that Fbxo42 could mediate the ubiquitylation of Ataxin-2 on one or more cysteine residues.

Importantly, we also demonstrated that Ataxin-2 is a relevant substrate of Fbxo42 in the context of the original genetic screen, showing that RNAi depletion of Ataxin-2 abolished the suppression of the Xbp1s-induced "glossy" eye phenotype by Su218 ($Fbxo42^{N423*}$).

5.3 Fbxo42 interacts with Ataxin-2 protein

To further confirm the interaction between Fbxo42 and Ataxin-2, we performed immunoprecipitation experiments using fly head extracts and S2 cell lysates. Through these assays, we observed co-immunoprecipitation of both endogenous and overexpressed Fbxo42 with Ataxin-2 protein.

Our next aim was to investigate the intracellular localization and interaction between Fbxo42 and Ataxin-2 by immunofluorescence of ring gland cells of *Drosophila* larvae. Using this method, we observed the formation of Ataxin-2 granules

following DTT treatment of the tissues. Notably, these granules were located in close proximity to Fbxo42 foci, suggesting that Ataxin-2 and Fbxo42 interact. It is likely that Fbxo42 is not a constituent of the Ataxin-2 granules but is instead recruited to these granules during UPR activation.

We then asked whether Fbxo42-mediated ubiquitylation of Ataxin-2 regulates its activity or promotes its proteasomal degradation. To assess this, we performed cycloheximide (CHX)-chase experiments, demonstrating that overexpression of Fbxo42 accelerates the degradation of Ataxin-2, while knockdown of this F-box protein protects Ataxin-2 from degradation. Additionally, when CHX was combined with the proteasome inhibitor MG132, in S2 cells, Ataxin-2 was stabilized. Based on these experiments, we conclude that Fbxo42 promotes the proteasomal degradation of Ataxin-2.

Furthermore, using CHX-chase assays, we found that Ataxin-2^{C244A}-GFP mutant increased the stability of Ataxin-2 protein. Additionally, ubiquitylation assays followed by immunoblotting, revealed that protein extracts from S2 cells expressing Ataxin-2^{C244A}-GFP mutant did not present DTT-sensitive Ataxin-2/ubiquitin-conjugates. These results, lead us to conclude that Fbxo42 mediates the ubiquitylation of Ataxin-2 at cysteine 244.

The above-mentioned findings were further supported by an AlphaFold structural prediction of the Ataxin-2/Fbxo42/Cullin-1/Skp-1/Rbx1/E2/Ub complex, which showed the close proximity between cysteine 244, ubiquitin and the E2-conjugating enzyme.

From this part of the work, we conclude that Fbxo42 mediates the proteasomal degradation of Ataxin-2 at a cysteine

residue. Remarkably, our results revealed that during UPR activation, Fbxo42 is recruited to Ataxin-2 granules to mediate the degradation of Ataxin-2, ultimately leading to the degradation of the Ataxin-2 granules. A key signal in this pathway, which has not yet been identified, triggers the recruitment of Fbxo42 to Ataxin-2 granules. A possible mediator of this recruitment is the phosphorylation of Ataxin-2 following ER stress, a modification that may be catalysed by the kinase domain of Ire1. F-box proteins are known to recognize phosphorylated substrates (Ou *et al.*, 2003). Notably, FMRP, an interactor of Ataxin-2, is phosphorylated by Ire1 (Yildirim *et al.*, 2022). Furthermore, multiple phosphorylation sites have been identified in the Ataxin-2 protein (Asada *et al.*, 2014). Thus, upon ER stress, it is possible that Ataxin-2 is phosphorylated by Ire1, leading to the recruitment of Fbxo42 to Ataxin-2 granules. However, further experiments are required to validate this hypothesis.

5.4 Ataxin-2 binds to Xbp1 mRNA in Ataxin-2 granules, during UPR activation

The last part of this project focused on the role of Ataxin-2 in the regulation of Xbp1 mRNA stability and translation. By immunofluorescence and smFISH, we observed that upon ER stress induction and during UPR activation, Xbp1 mRNA co-localizes with Ataxin-2 granules in ring gland cells of *Drosophila* larvae, as well as in HeLa cells, suggesting that this mechanism is conserved from fly to human. Furthermore, using iCLIP

experiments, we demonstrated that Ataxin-2 binds to the 3'UTR of Xbp1 mRNA.

To assess the effect of Ataxin-2 on Xbp1 mRNA stability, we performed actinomycin D assays under ER stress conditions and during UPR activation, using a reporter to detect Xbp1 mRNA. These experiments revealed that, during UPR activation, Ataxin-2 promotes the stabilization of the Xbp1 reporter mRNA. Additionally, immunoblotting analysis showed that Ataxin-2 also enhances the expression of the Xbp1 spliced protein.

Finally, we showed that, upon Fbxo42 RNAi depletion and after ER stress induction, the levels of the Xbp1 spliced protein significantly decrease. Likewise, Xbp1 spliced expression levels were also reduced in Fbxo42 mutant clones. Therefore, Fbxo42-mediated ubiquitylation and degradation of Ataxin-2 are required to the translation of Xbp1 mRNA.

Altogether, our results are summarized in our working model (Figure 5.1). Upon ER stress induction, Xbp1 mRNA is spliced by the endoribonuclease activity of Ire1 and in the early phase of UPR activation, Xbp1 spliced mRNA is stabilized by Ataxin-2 within Ataxin-2 granules, being "stored" and protected from degradation. During this phase, Xbp1 is transcribed but not translated. This is supported by polysome profiling experiments which show that Ataxin-2 is mostly found in non-ribosomal fractions, indicating that Ataxin-2-bound mRNAs are predominantly non translated (Yokoshi *et al.*, 2014). In the late phase of UPR, Xbp1 spliced mRNA is translated. For this to occur, Fbxo42 is recruited to the Ataxin-2 granules, where it mediates the ubiquitylation and degradation of Ataxin-2, leaving Xbp1 mRNA free to be translated. In Fbxo42

knockdown or Fbxo42 mutant cells, Xbp1 mRNA remains untranslated within Ataxin-2 granules, resulting in reduced activation of downstream Xbp1 signalling (as in our initial genetic screen).

This model is based in our findings, specifically the Ataxin-2/Fbxo42 immunofluorescence results (Chapter III) and the Ataxin-2 immunofluorescence and Xbp1 mRNA FISH results (Chapter IV). Our biochemical data, including ubiquitylation assays and CHX-chase assay results (Chapter II and Chapter III) also contributed to the development of this model.

However, there are some important considerations regarding our model. Our smFISH probes cover the entire *Xbp1* sequence and do not distinguish between Xbp1 mRNA spliced and unspliced. Nonetheless, our IF+smFISH experiments were performed after 4 hours of DTT incubation, a time when most Xbp1 mRNA has already been spliced by Ire1, but its translation is still reduced (Majumder *et al.*, 2012). In mouse embryonic fibroblasts, it has been shown that Xbp1 mRNA is stabilized after 3 hours of UPR induction (with thapsigargin), while translation of the Xbp1 spliced occurs later. Xbp1 spliced protein expression progressively increases between 3 and 9 hours of thapsigargin treatment (Majumder *et al.*, 2012). This is also consistent with our studies using *Drosophila* S2 cells, where we observe the highest levels of Xbp1 spliced protein after 8 hours of DTT treatment [this work and (Cairrão *et al.*, 2022)]. Therefore, our results provide an explanation for the temporal delay observed between the availability of Xbp1 spliced mRNA (in the early phase of UPR) and the emergence of most of Xbp1 spliced protein (in the late phase of UPR). According

to our model, Xbp1 mRNA is “stored” and stabilized, but not translated, in Ataxin-2 granules during the first hours of ER stress and UPR activation.

Another consideration regarding our model relates to experiments using the ring glands. As shown in chapter III, in Figure 3.8., ring gland cells, even in the absence of strong ER stress induction by DTT, exhibit Xbp1s-GFP activation. Presumably, Ire1 signalling is physiologically activated in ring gland cells, perhaps as part of their developmental role in the biosynthesis of the ecdysone hormone. However, the strong co-localization of Xbp1 mRNA with Ataxin-2 granules in ring gland cells only occurs upon DTT treatment and is concomitant with the strong transcriptional activation of Xbp1 (Chapter III). This suggests that regulation of Xbp1 mRNA by Ataxin-2 must play a crucial role when UPR activation leads to high levels of Xbp1 transcription, as we demonstrated in our study by exposing cells to DTT or through Xbp1s-overexpression, as in our original genetic screen.

Cell death receptors (CD or DR) play a crucial role in ER-stress-induced cell death, including DR5 (Lu *et al.*, 2014) and CD95 (Pelizzari-Raymundo *et al.*, 2024). During the early adaptive pro-survival phase of the UPR (up to 6 hours of ER stress), the mRNAs of DR5 and CD95 are degraded by Ire1’s endoribonuclease activity. However, at later stages of UPR activation, the expression of DR5 and CD95 is upregulated, ultimately leading to cell death. Notably, a recent study has shown that overexpression of Xbp1s induces the transcription of CD95, thereby promoting cell death (Pelizzari-Raymundo *et al.*, 2024). This finding led us to hypothesise that the overexpression of Xbp1 spliced in the *Drosophila* eye, which

induces the “glossy” eye phenotype, might activate the transcription of cell death receptors, thus promoting cell death in the eye. However, further studies are required to confirm this hypothesis.

In our project, we uncovered a novel pathway, in which Xbp1 mRNA accumulates in Ataxin-2 granules during the early adaptive pro-survival phase of the UPR. This accumulation allows the rapid translation of Xbp1 mRNA at a later stage. A key player, Fbxo42, is recruited to the Ataxin-2 granules, where it mediates the degradation of Ataxin-2, during the late UPR phase. Ataxin-2 degradation is essential for the translation of the Xbp1 mRNA. The Xbp1 spliced protein, in turn, can activate the transcription of cell death receptors, ultimately promoting cell death.

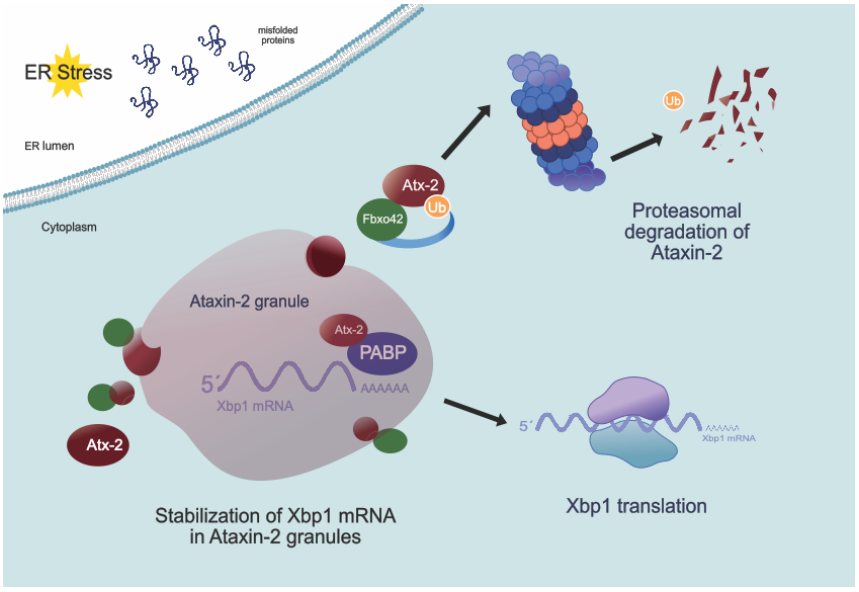

Figure 5.1: Working model. Upon ER stress, Xbp1 mRNA is transcribed and progressively accumulates in Ataxin-2 granules, where it is protected from degradation. Ataxin-2 (Atx-2) binds to the 3’ UTR of Xbp1 mRNA, together with PABP. At later stage of UPR activation, Fbxo42 is recruited to Ataxin-2 granules, promoting Ataxin-2 ubiquitylation and its degradation by the proteasome. Xbp1 mRNA is released from Ataxin-2 and is translated.

Concluding remarks

Our main aim was to understand the mechanism behind the Fbxo42 suppression of the retinal degeneration and cell death ("glossy" eye phenotype) induced by Xbp1s-overexpression.

With this work, we unveiled a new mechanism in which, during early stages of UPR activation, Xbp1 mRNA is stabilized by Ataxin-2 binding, within Ataxin-2 granules. Xbp1 mRNA is "stored" and protected from degradation in these granules. At later stages of UPR activation, Fbxo42 is recruited to the Ataxin-2 granules, where it mediates the ubiquitylation (on Cysteine 244) and degradation of Ataxin-2, ultimately leading to the degradation of these granules. As a result, Xbp1 mRNA is released from Ataxin-2 and is translated.

To sum up, we identified Fbxo42-mediated degradation of Ataxin-2 as a key mechanism regulating the levels of Xbp1 mRNA and protein, triggering cell death in later stages of UPR activation. This mechanism was identified in *Drosophila* tissues and in S2 *Drosophila* cells. But the accumulation of Xbp1 mRNA in Ataxin-2 granules was also detected in HeLa cells, highlighting the conservation of this pathway.

Future perspectives

In the future, it will be relevant to determine whether Ire1 promotes the phosphorylation of Ataxin-2 under ER stress conditions, and whether this phosphorylation functions as a signal for the recruitment of Fbxo42.

Furthermore, it will be important to confirm whether Xbp1s activates cell death receptors in S2 *Drosophila* cells or fly tissues, to trigger cell death.

Additionally, while this study shows that Ataxin-2 granules in human cells also accumulate Xbp1 mRNA, it would be valuable to test whether human Ataxin-2 is also a substrate of FBXO42, and whether FBXO42 can promote the degradation of human Ataxin-2, including the pathogenic forms of Ataxin-2, involved in diseases such as SCA2, ALS and Parkinson's disease.

References

Asada A, Yamazaki R, Kino Y, Saito T, Kimura T, Miyake M, Hasegawa M, Nukina N & Hisanaga S ichi (2014). Cyclin-dependent kinase 5 phosphorylates and induces the degradation of ataxin-2. *Neurosci Lett* **563,** 112–117.

Barbosa P, Zhaunova L, Debilio S, Steccanella V, Kelly V, Ly T & Ohkura H (2021). SCF-Fbxo42 promotes synaptonemal complex assembly by downregulating PP2A-B56. *J Cell Biol*; DOI: 10.1083/JCB.202009167.

Cairrão F, Santos CC, Le Thomas A, Marsters S, Ashkenazi A & Domingos PM (2022). Pumilio protects Xbp1 mRNA from regulated Ire1-dependent decay. *Nat Commun* **13,** 1–13.

Franco M, Seyfried NT, Brand AH, Peng J & Mayor U (2011). A novel strategy to isolate ubiquitin conjugates reveals wide role for ubiquitination during neural development. *Mol Cell Proteomics* **10,** 1–15.

Jiang H, Bian W, Sui Y, Li H, Zhao H, Wang W & Li X (2022). FBXO42 facilitates Notch signaling activation and global chromatin relaxation by promoting K63-linked polyubiquitination of RBPJ. *Sci Adv* **8,** 1–18.

Lu M, Lawrence DA, Marsters S, Acosta-Alvear D, Kimmig P, Mendez AS, Paton AW, Paton JC, Walter P & Ashkenazi A (2014). Opposing unfolded-protein-response signals converge on death receptor 5 to control apoptosis. *Science (80-)* **345,** 98–101.

Majumder M, Huang C, Snider MD, Komar AA, Tanaka J, Kaufman RJ, Krokowski D & Hatzoglou M (2012). A Novel Feedback Loop Regulates the Response to Endoplasmic Reticulum Stress via the Cooperation of Cytoplasmic Splicing and mRNA Translation. *Mol Cell Biol* **32,** 992–1003.

Ou CY, Pi H & Chien CT (2003). Control of protein degradation by E3 ubiquitin ligases in Drosophila eye development. *Trends Genet* **19,** 382–389.

Pelizzari-Raymundo D, Maltret V, Nivet M, Pineau R, Papaioannou A, Zhou X, Caradec F, Martin S, Le Gallo M, Avril T, Chevet E & Lafont E (2024). IRE1 RNase controls CD95-mediated cell death. *EMBO Rep* **25,** 1792–1813.

Ramirez J, Martinez A, Lectez B, Lee SY, Franco M, Barrio R, Dittmar G & Mayor U (2015). Proteomic analysis of the ubiquitin landscape in the Drosophila embryonic nervous system and the adult photoreceptor cells. *PLoS One* **10,** 1–24.

Stuurman N, Maus N & Fisher PA (1995). Interphase phosphorylation of the Drosophila nuclear lamin: Site-mapping using a monoclonal antibody. *J Cell Sci* **108,** 3137–3144.

Sun L, Shi L, Li W, Yu W, Liang J, Zhang H, Yang X, Wang Y, Li R, Yao X, Yi X & Shang Y (2009). JFK, a Kelch domain-containing F-box protein, links the SCF complex to p53 regulation. *Proc Natl Acad Sci U S A* **106,** 10195–10200.

Sun L, Shi L, Wang F, Huangyang P, Si W, Yang J, Yao Z & Shang Y (2011). Substrate phosphorylation and feedback regulation in JFK-promoted p53 destabilization. *J Biol Chem* **286,** 4226–4235.

Yan R, He L, Li Z, Han X, Liang J, Si W, Chen Z, Li L, Xie G, Li W, Wang P, Lei L, Zhang H, Pei F, Cao D, Sun L & Shang Y (2015). SCFJFK is a bona fide e3 ligase for ING4 and a potent promoter of the angiogenesis and metastasis of breast cancer. *Genes Dev* **29,** 672–685.

Yildirim Z, Baboo S, Hamid SM, Dogan AE, Tufanli O, Robichaud S, Emerton C, Diedrich JK, Vatandaslar H, Nikolos F, Gu Y, Iwawaki T, Tarling E, Ouimet M, Nelson DL, Yates JR, Walter P & Erbay E (2022). Intercepting IRE1 kinase-FMRP signaling prevents atherosclerosis progression. *EMBO Mol Med* **14,** 1–22.

Yokoshi M, Li Q, Yamamoto M, Okada H, Suzuki Y & Kawahara Y (2014). Direct binding of Ataxin-2 to distinct elements in 3' UTRs promotes mRNA stability and protein expression. 186–198.

Appendix

Table S1: List of primers used in the present study.

Primer´s application	Primer's designation	Sequence
Generation of pTWG-Fbxo42 (Gateway protocol)	Forward primer FP-GWS-C-Fbox	GGGGACAAGTTTGTACAAAAAAGCAGGCTTCACCATGGACGCGAGCAGATACAAGG
	Reverse primer RP-GWS-C-Fbox	GGGGACCACTTTGTACAAGAAAGCTGGGTCGATAATATCACGTGGCACACTCAGG
Generation of pTFHW-Fbxo42 (Gateway protocol)	Forward primer FP-GWS-N-Fbox	GGGGACAAGTTTGTACAAAAAAGCAGGCTTCGACGCGAGCAGATACAAGG
	Reverse primer RP-GWS-N-Fbox	GGGGACCACTTTGTACAAGAAAGCTGGGTCCTAGATAATATCACGTGGCACACTCAGG
Generation of pTFHW-deltaFbxo42 (Gateway protocol)	FP-GWS-FboxdeltaF-N	GGGGACAAGTTTGTACAAAAAAGCAGGCTTCCACAATCTCGAGAAGGGC
Construction of pUAST-Ataxin-2-GFP	Primer Ataxin2-GFP FW	GCATTTTATTTTTTTTGTGAGCAAGGGCGAG
	Primer Ataxin2-GFP Rev	CTCGCCCTTGCTCACAAAAAAAATAAAATGC
	Primer Fw with BglII_Gibson	GAATTGGGAATTCGTTAACAGATCTATGCACTCGGCCACGGCG
	Primer Rev with XhoI_Gibson	GATCCTCTAGAGGTACCCTCGAGCTACTTGTACAGCTCGTCCATG
Generation of pUAST-Ataxin-2-HA	Rev-XhoI-HA_GIBSON	GATCCTCTAGAGGTACCCTCGAGCTAAGCGTAATCTGGAACGTC
Anti-Fbxo42 antibody generation	FW_CG6758 fragmentinpetm-30RIGHT	CTTTATTTTCAGGGCGCCATGGATCGTCGACTAGGTGGAG
	Rev_CG6758 fragmentinpetm-30RIGHT	GTGGTGGTGGTGCTCGAGCTAGTGATGGTGATGGTGATGGATAATATCACGTGGCAC
Generation of the Ataxin-2 mutants	Primer_FW_mutC103A	GCACTGGAGCTACCGGCGGCCATTAAGTCCAAGAATCTG
	Primer_Rev_mutC103A	CAGATTCTTGGACTTAATGGCCGCCGGTAGCTCCAGTGC
	Primer_FW_mutC154A	GGCGCCATTTCTGACAAGGCCAACGGTGCGCGTCCGGAC
	Primer_Rev_mutC154A	GTCCGGACGCGCACCGTTGGCCTTGTCAGAAATGGCGCC
	Primer_FW_mutC244A	GAGATCGAAAATAATCCGACGGCCCGGGACCGTCTGGACTTG
	Primer_Rev_mutC244A	CAAGTCCAGACGGTCCCGGGCCGTCGGATTATTTTCGATCTC
Knockdown of Fbxo42 in S2 cells	T7-FWCG6758	TAATACGACTCACTATAGGGAGGAGCAGCGCTGGTGGC
	T7-RevCG6758	TAATACGACTCACTATAGGGATGCAGCTGCTGCACCTCC
Knockdown of Ataxin-2 in S2 cells	PFW-T7-Atx-2_RNAi - 5´UTR	TAATACGACTCACTATAGGGATTCGATACCGAACACTGTGG
	Prev -T7-Atx-2_RNAi - 5´UTR	TAATACGACTCACTATAGGGACGGATTTACCAACTTTCCGA
Control RNAi used in CHX chase assays in S2 cells	primerctrl_Fw	TAATACGACTCACTATAGGGACTAATCAAGTTTTTTGGGGTC
	primerctrl_Rev	TAATACGACTCACTATAGGGAATGACCATGATTACGCCAAG
LacZ RNAi (control) used in mRNA stability assay	T7-RNAi LacZ Fw	GGATCCTAATACGACTCACTATAGGGTGACGTCTCGTTGCTGCATAAAC
	T7-RNAi LacZ Rev	GGATCCTAATACGACTCACTATAGGGGGCGTTAAAGTTGTTCTGCTTCATC
qRT-PCR primers to check Ataxin-2 mRNA depletion	PrimerFW_Atx-2_qPCR	CAACGGTGCCTACAGGAAC
	PRev_atx2End	GACTTACGTAATTACTACGG
qRT-PCR primers - mRNA stability assay ($Xbp1^{uORF}$-GFP target)	GFP-FW1	GGCTACGTCCAGGAGCGCACCATCTT
	GFP-Rev	CGCTTCTCGTTGGGGTCT
qRT-PCR primers - mRNA stability assay (RP49 target)	RP49-Fc1	AGATCGTGAAGAAGCGCACCAAGC
	RP49-Fc2	GCACCAGGAACTTCTTGAATCCGG
RT primers - iCLIP	i7CLIP_ddRT_17 (iCLIP barcoded primer used for Atx-2-HA +UV)	/5Phos/WWWNNNAATGNNNNAGATCGGAAGAGCGTCGTGATIiSp18/GGATCCiSp18/CAGACGTGTGC
	i7CLIP_ddRT_18 (iCLIP barcoded primer used for Atx-2-HA no UV)	/5Phos/WWWNNNAAGTNNNNAGATCGGAAGAGCGTCGTGATIiSp18/GGATCCiSp18/CAGACGTGTGC
	i7CLIP_ddRT_19 (iCLIP barcoded primer used for Atx-2^{C244A}-HA +UV)	/5Phos/WWWNNNAATACNNNNAGATCGGAAGAGCGTCGTGATIiSp18/GGATCCiSp18/CAGACGTGTGC
	i7CLIP_ddRT_20 (iCLIP barcoded primer used for Atx-2^{C244A}-HA no UV)	/5Phos/WWWNNNACGCANNNNAGATCGGAAGAGCGTCGTGATIiSp18/GGATCCiSp18/CAGACGTGTGC
	i7CLIP_ddRT_21 (iCLIP barcoded primer used for IgG control)	/5Phos/WWWNNNACTTGNNNNAGATCGGAAGAGCGTCGTGATIiSp18/GGATCCiSp18/CAGACGTGTGC
PCR primers - iCLIP	iiCLIP_P5_1	AATGATACGGCGACCACCGAGATCTACACGTGTAGAAACACTCTTTCCCTACACGACGCTCTTCCGATCT
	iiCLIP_P7_1	CAAGCAGAAGACGGCATACGAGATGGACATCAGTGACTGGAGTTCAGACGTGTGCTCTTCCGA*T*C*T

Table S2: List of antibodies used in the present study.

Designation	Source or reference	Identifiers	Additional information
Anti-alpha-Tubulin (Mouse monoclonal)	Developmental Studies Hybridoma Bank (DSHB)	DSHB Cat#: AA4.3; RRID: AB_579793	WB (1:500)
Anti-Ataxin-2 (Guinea-pig polyclonal)	kind gift from Patrick Emery (Zhang *et al.*, 2013)	N/A	IF (1:200) WB (1:5000)
Anti-biotin HRP-linked (Goat polyclonal)	Cell Signaling Technology	Cat#: 7075; RRID: N/A	WB (1:1000)
Anti-ELAV (Rat monoclonal)	DSHB	DSHB Cat#: Rat-Elav-7E8A10; RRID: AB_528218	IF (1:200)
Anti-ELAV (Mouse monoclonal)	DSHB	DSHB Cat#: Elav-9F8A9 RRID: AB_528217	IF (1:200)
Anti-Fbxo42 (rabbit polyclonal)	This paper (homemade)	N/A	IF (1:50 or 1:100) WB (1:1000)
Anti-FLAG (Mouse monoclonal)	Sigma-Aldrich, M2 clone	Cat#: F1804; RRID: N/A	WB (1:1000)
Anti-GFP (Rat monoclonal)	Chromotek, 3H9 clone	3h9-150; RRID: AB_10773374	WB (1:1000)
Anti-HA (Mouse monoclonal)	BioLegend, 16B12 clone (Previously Covance)	Cat#: 901501; RRID: AB_2565006 (Covance Cat# MMS-101P)	IF (1:200) WB (1:1000)
Anti-HA (Rat monoclonal)	Chromotek, 7C9 clone	7c9-100; RRID: AB_2631399	WB (1:1000)
Anti-Myc (Rat monoclonal)	Chromotek, 9E1 clone	9e1-100; RRID: AB_2631398	WB (1:2000)
Goat anti-Rabbit IgG (H&L) HRP-conjugated	Agrisera	product#: AS10 668; RRID: N/A	WB (1:5000)
Goat anti-Guinea Pig IgG HRP-conjugated	Thermo Scientific	Cat#: PA128679; RRID: N/A	WB (1:5000)
Goat anti-Rat IgG (H+L) HRP-conjugated	Advansta	Cat#: R-05075-500; RRID: N/A	WB (1:2000)
Sheep anti-Mouse IgG HRP-linked	Cytiva	Cat#: NXA931; RRID: AB_772209	WB (1:10 000)
Cy™3-conjugated AffiniPure™ Donkey Anti-Rabbit IgG (H+L)	Jackson ImmunoResearch Laboratories	Code: 711-165-152; RRID: AB_2307443	IF (1:400)
Alexa Fluor® 647 AffiniPure™ Donkey Anti-Rat IgG (H+L)	Jackson ImmunoResearch Laboratories	Code: 712-605-153; RRID: AB_2340694	IF (1:200)
Cy™5 AffiniPure™ Donkey Anti-Guinea Pig IgG (H+L)	Jackson ImmunoResearch Laboratories	Code: 706-175-148; RRID: AB_2340462	IF (1:200)
Cy™3 AffiniPure™ Donkey Anti-Mouse IgG (H+L)	Jackson ImmunoResearch Laboratories	Code: 715-165-150; RRID: AB_2340813	IF (1:200)

Table S3: List of smFISH probes to detect human XBP1 mRNA.

1	cagactacgcaccgcgcaccgcgcg
2	gcgcggctgccaccaccaccatagc
3	ctttaggggtcccgtcggccgggtt
4	aggcgggctgccccgacagaagcag
5	ccatgagcggcagggcctggccggc
6	ccgggctggcccctctctgggctgg
7	ctgtcgcttgcgcgcctggggcagc
8	ctcctcggggctcaggtgcgtgagg
9	tggcagtctgagctgctactctgtttt
10	gctcactcattcgagccttctttcgatc
11	ggttctcttcttctaaatctaccacttgctgttc
12	tgagttttctctcgtaaaagctgattttctagcaa
13	tgtcttaactcctggttctcaactacaaggc
14	gcaaccagggcatccatccccaagc
15	ttccccttggcttccgcctcctctt
16	gcagacccggccactggcctcactt
17	gtgacaactgggcctgcacctgctg
18	ccagaatccatggggagatgttctggag
19	catgactgggtccaagttgtccagaatg
20	aggctctggggaagggcatttgaag
21	tggtaaggaactgggtccttctggg
22	ggggcttggtatatatgtggtcaaaacgaatt
23	ggctctctgtctcagagggtatctctaagac
24	ggtgatcattctctgaggggctgaga

25	cccagctccggaacgaggtcatctt
26	cagtggctggatgaaagcagatttgaga
27	tcactgaatggggaaagggaacccc
28	agaatggtttacaccaagcagagaggaca
29	ggaaagagttcattggcaaaagtgtcctcc
30	ggggtcatctatgagatctgaacaaatagaggaa
31	ctggaggcaagccaggatgccaaaa
32	acttgaagtatacatgagggaaagagcccc